NORTHWESTERN UNIVERSITY

Enhancing Sensitivity of an Atomic Interferometer to the Heisenberg Limit Using Increased Quantum Noise

A DISSERTATION

SUBMITTED TO THE GRADUATE SCHOOL
IN PARTIAL FULFILLMENT OF THE REQUIREMENTS

for the degree

DOCTOR OF PHILOSOPHY

Field of Physics And Anstronomy

By

Renpeng Fang

EVANSTON, ILLINOIS

August 2018

ABSTRACT

Enhancing Sensitivity of an Atomic Interferometer to the Heisenberg Limit Using Increased Quantum Noise

Renpeng Fang

Quantum metrology has been among the most vigorous branches of quantum technology. It involves using quantum effects to achieve better estimation of parameters of a physical system. Conventionally the system consists of an ensemble of N non-interacting atoms and the measurements are done on individual atomic states, such as a conventional Raman atomic interferometer (CRAIN) or a Raman-Ramsey atomic clock (RRAC). The measurement sensitivity of such a system is restricted by the standard quantum limit (SQL), which scales as $\sim \sqrt{N}$ (this is known as the shot-noise scaling). Introducing quantum entanglement in the system, it is possible to surpass the SQL, and a key goal in this context is to achieve the Heisenberg limit (HL), which scales as $\sim N$ (this is know as the Heisenberg scaling), representing an improvement by a factor of $\sqrt{N}$. In this thesis, we propose a protocol that can enhance the measurement sensitivity of an atomic interferometer (or an atomic clock) to the HL, while at the same time make it substantially robust against excess noise present in the system. Specifically, the protocol employs critically tuned one-axis-twist (OAT) spin squeezing to generate maximially-entangled states among the atoms, known as Schrödinger

cat (SC) states, in combination with the conventional detection (CD) scheme (measurements of individual atomic states). Since the interferometer makes use of Schrödinger cat states, we name it as Schrödinger cat atomic interferometer (SCAIN).

A SCAIN relies on the collective behavior of the atomic ensemble, so as a first step, we investigate the behavior of an ensemble of N non-interacting, identical, two-level atoms, excited by the same laser field. Traditionally, the ensemble would be described using direct product states as the basis. In his seminal paper, R. H. Dicke proposed an alternative basis known as collective states, and showed that under ideal conditions, the dynamics of the system can be confined within the $N+1$ sysmmetric collective states (also known as Dicke collective states), labeled as $\{|E_0\rangle, |E_1\rangle, \ldots, |E_N\rangle\}$, with all the other $2^N - (N+1)$ asymmetric collective states decoupled from the system. This simplifies greatly the descriptions of the ensemble. Furthermore, the collective state descriptions suggest a new detection scheme for the ensemble, named as collective state detection (CSD), in addition to the conventional detection scheme. The CSD can be applied to both an atomic interferometer, referred to as collective state atomic interferometer (COSAIN), and an atomic clock, referred to as collective state atomic clock (COSAC). We show that the fringe widths of a COSAIN and a COSAC are narrowed by a factor of $\sqrt{N}$ compared to their conventional counterparts, CRAIN and RRAC, respectively, despite the fact that the measurement sensitivity remains the same at the SQL for both cases.

With the model of collective state descriptions in place, we move to the key part of the protocol for realizing a SCAIN and review the concepts of spin squeezing. We first present the spin representation of the ensemble, where collective spins are defined for the system. We then introduce the coherent spin states (CSSs), which are direct product states of individual coherent states and which turn out to be equivalent to the Dicke collective

states in this picture. Lastly based on CSSs, we define the spin squeezed states (SSSs) using the definitions proposed by Kitagawa and Ueda, and summarize the two approaches for generating squeezed spin states: one-axis-twist (OAT) and two-axis-counter-twist (TACT) spin squeezing.

Before we get to the formal descriptions of the protocol for a SCAIN, we revisit the Sagnac effect that is essential for using the SCAIN for rotation sensing. We propose two alternative models for deriving and interpreting the Sagnac effect. The first one is based on Lorentz transformation of special relativity and can be generalized to an interferometer of an arbitrary shape, while the second one is a quantum-mechanical model which shows that the total effect can be split equally during each of the two dark zones of the interferometer.

Finally, we present the detailed protocol for implementing a SCAIN. The core components of the protocol are the four pulses employed to implement the squeezing, rotation, inverse-rotation and unsqueezing operations, in addition to the usual $\pi/2$-dark-π-dark-$\pi/2$ pulse sequence of its conventional counterpart. The squeezing effect is controlled by the squeezing parameter μ, which indicates the length of interaction of the squeezing Hamiltonian. A squeezing pulse with $\mu = \pi/2$ will split an initial CSS into equal superpositions of two extremal collective states. A rotation pulse is then applied to rotate the mean spin directions of those extremal collective states and align them with the z-axis, generating the SC state. After the second dark zone, an inverse-rotation pulse and an unsqueezing pulse are applied sequentially to undo the previous rotation and squeezing effects in order to extract the phase imprinted during the dark zones. One difficulty of this protocol is that the splitting of the CSS after the squeezing pulse depends on the parity of N, which requires rotation around different axes to produce the SC state. This leads to two equivalent versions of the protocol (protocol A and protocol B), depending on the axis around which the rotation pulse

is applied. At the end of the interferometer, the signal can be measured using either the collective state detection scheme, or the conventional detection scheme, where the former is referred to as CSD-SCAIN, while the latter as CD-SCAIN. For each detection scheme, we examine the signal fringes and the measurement sensitivity for different values of the squeezing parameter μ. We show that for both detection schemes, when $\mu = \pi/2$, the signal fringes are narrowed by a factor of N for one of the two parities, and the measurement sensitivity reaches the HL for that same parity of N. When averaged over the two parities, the overall sensitivity is below the HL by a factor of $\sqrt{2}$. Despite the fact that both schemes can reach the HL, the CD-SCAIN can provide additional robustness against excess noise, due to the increase in the standard deviation of the signal. We compare and summarize the robustness against excess noise of different protocols proposed for atomic interferometers (and clocks) in the last chapter of the thesis. Lastly, we note that the core components of the protocol for SCAIN consisting of squeezing, rotation, inverse-rotation and unsqueezing operations can also be applied to atomic clocks and atomic accelerometers, which leads to similar results as SCAIN.

Acknowledgments

I couldn't imagine I would have come so far if I had to work all alone for my PhD study. Fortunately that was not the case and I'm so lucky to have so many people who stand behind me throughout the past six years and to whom I owe a great debt of gratitude.

First of all, I would like to express my deepest gratitude to my adviser, Professor Selim Shahriar, for his continued support and guidance throughout the research. He introduced me to the field of atomic, molecular and optical physics, explained to me the fundamental theories of interaction between atoms and lasers, and fully trusted me to carry out all sort of experiments. Whenever I was stuck on the experiments, he would be able to sort out the problems and point me to the right direction.

I would also like to extend my appreciation to my committee members, Professor John Ketterson and Professor Brian Odom, for their insights and advice on my research. I still remembered those "unexpected" questions raised by John and Brian during our joint weekly meetings, which turned out to be very inspiring. I was also impressed by their comments during my prospectus presentation, which prompted me to think deeper into my experiments.

In terms of the actual lab work, I am most grateful to my labmates May Kim and Yanfei Tu, both of whom are excellent experimentalists. When I first started working in the atomic lab, I was like a blank piece of paper. They had to teach me everything from scratch. It was May who showed me how to align a laser beam with two mirrors (which intrigued me at the beginning by the way), how to plug and unplug BNC cables and how to operate acousto-optic

modulators (AOM). It was Yanfei who showed me how to tune half wave-plates to control laser powers, how to measure the power and wavelength of the beam and how to use lenses to expand or reduce the beam size. Later when I understood all the basics, May introduced me to the saturated absorption setup for scanning and locking lasers; Yanfei demonstrated to me the principles for aligning and transporting lasers through fibers. Thanks to their hands-on instructions, I was able to master all the necessary techniques to conduct my own experiments.

My first project was to build and charaterize a Zeeman slower which was meant to pre-cool Rubidium (Rb) atoms to eventually obtain Bose-Einstein condensates (BEC). May shared with me her coil design for the slower. Later both she and Mohamed Fouda helped me wind the coils, transport and mount the slower on the optical bench. Jonathan Trossman from Professor Ketterson's group kindly lent me his ion pump and controllers. My colleagues Ye Wang, Shih Tseng and Subramanian Krishnamurthy spent a fair amount of time resolving the issues with the Ti-Sapphire laser. Mohamed also assisted me with the simulation of the slowing effects using Matlab code.

My second project was to investigate the collective state effects on atomic clock. May and Yanfei built three magneto-optical traps (MOT) from scratch, the third of which was committed to this project. Shih made two servo boxes for locking the repump and MOT lasers which worked like a charm. May and Yanfei set up the 1.5GHz AOMs, all the necessary electronics (switches and amplifiers), designed and implemented the pulses for driving the Raman transitions. Daniel Villalon developed most part of the LabView programs for collecting the experimental data. Later the whole system was transitioned into a new one with digital pulses and automatic data acquisition, which couldn't have been done without guidance from one of our collaborators, Dr. Frank A. Narducci at Naval Air Systems

Command. Frank generously shared with me their LabView programs for controlling the data acquisition board (DAQ) and set aside half an hour or so every week talking with me (phone, skype or teamviewer) to debug the programs, analyze the experimental results and offer suggestions and solutions to all sort of problems I ran into.

My sincere thanks also goes to Professor Phil Hemmer at Texas A&M who visited us periodically to check up on our progress and to lend us his hand in the lab; to Resham Sarkar for her efforts into developing and explaining the theoretical work of collective state effects and spin squeezing; to Joshua Yablon for showing me his homemade spatial filter; to Zifan Zhou for helping me out with the soldering; to Nicholas Condon and Devin Hileman at Digital Optics Technologies for putting together all the pieces of the DBR lasers; to Mehjabin Sultana Monjur for allowing me to use some apparatus from her setup; and to Minchuan Zhou for her cooperation with my role as a teaching assitant.

As for financial support, I would like to thank NSF IGERT and the Materials Research Science and Engineering Center for over four years of fellowships. All my tuitions, expenses and experimental instruments were financed by these fellowships.

Lastly but most importantly, I would like to thank my family and my four best friends from high school who have been my staunch supporters and seen me through graduate school. They shared my joy, my tears, those high and low moments. It was them who encouraged and motivated me to keep going forward till eventually I become who I am today, and surely this journey will be continued to a new chapter.

Dedication

This thesis is dedicated to my beloved parents who have always been a source of great comfort during my seven years of PhD study abroad.

Table of Contents

List of Figures

CHAPTER 1

Introduction

1.1. Brief Review of Quantum Metrology

Metrology plays a central role in science and engineering. In short, it is concerned with the highest achievable precision in various parameter estimation tasks, and with finding measurement schemes that reach that precision. Originally, metrology was focusing on measurements using classical or semiclassical systems, such as mechanical systems described by classical physics or optical systems modeled by classical wave optics. In the last decades, it has become possible to observe the dynamics of many-body quantum systems. If such systems are used for metrology, the quantum nature of the problem plays an essential role in the metrological setup. Examples of the case above are phase measurements with trapped ions [**1**], interferometry with photons [**2, 3, 4, 5**] and magnetometry with cold atomic ensembles [**6, 7, 8, 9, 10, 11**].

One important technique for pushing towards high-precision quantum metrology is spin squeezing [**12, 13, 14, 15, 16**], which has attracted considerable attention, both theoretically and experimentally in the past two decades. The notion of spin squeezing has arisen mainly from two considerations: the study of particle correlations and entanglement [**17, 18, 19**], as well as the improvement of measurement precision in experiments [**13, 14, 20, 21, 22, 23, 24**]. One application of spin squeezing is to detect quantum entanglement [**19, 25, 26**], which plays a key role in both the foundations of quantum physics and also in quantum-information processing [**27, 28**]. Another application of spin squeezing, especially in experiments, is to

improve the precision of measurements, e.g., in Ramsey spectroscopy [**13, 14, 21, 29, 30, 31, 32, 33, 34, 35**], as well as in making more precise atomic clocks [**14, 18, 20, 36, 37, 38, 39, 40, 41**] and gravitational-wave interferometers [**42, 43, 44**].

1.2. Organization of the Thesis

The rest of the thesis is organized as follows. Chapter 2 presents a review of the fundamental concepts in quantum optics and atomic physics. It develops physical models for describing the interaction between atoms and external fields (laser fields and static magnetic fields in particular), and introduces notations that will be used throughout this thesis.

Chapter 3 investigates the collective behavior of an ensemble of non-interacting atoms. We will derive the mathematical model for describing collective states (Dicke Collective States, in particular) and discuss briefly their applications to atomic clocks and interferometers.

Chapter 4 reviews the basics of spin squeezing effects. We start with the spin representation of an atomic ensemble, followed by descriptions of coherent spin states, then transition to the mathematical model of squeezed spin states, and lastly introduce two approaches for generating squeezed spin states.

Chapter 5 reviews the Sagnac effect and presents a generalized model for deriving the Sagnac effect that is applicable to an interferometer of an arbitrary shape.

Chapter 6 reviews the Schrödinger cat states and shows their applications to atomic interferometers and clocks. In particular, we propose two protocols for making a Schrödinger Cat Atomic Interferometer (and Clock), which, in combination with collective state detection or conventional detection schemes, can achieve a metrological sensitivity that is equivalent to the Heisenberg Limit, within a factor of $\sqrt{2}$. For the conventional detection scheme, the

interferometer (or clock) will also be significantly more robust against excess noise (by as much as a factor of $\sqrt{N}$).

CHAPTER 2

Fundamentals of Atomic Interaction with External Fields

This chapter is a review of the basic concepts and properties of atomic interactions with external fields, such as laser field and static magnetic field. We will begin with atom-light interactions where the atoms are first modeled by a two-level system. We will derive an expression for the interaction Hamiltonian and perform necessary approximations and transformations to solve for the time evolution of the wave function of the atomic system. We will then introduce the density matrix method and Bloch vector representation of the atomic state, which will be employed to study the state evolution in the separated field Ramsey fringe experiments. We will next generalize the atomic model to a three-level system and apply the results to the off-resonant Raman-Rabi excitation and again to the Ramsey fringes experiments, which will form the starting point for the collective state description of an atomic ensemble. The other half of this chapter will deal with atomic interaction with external magnetic field, where we will first briefly review the fine and hyperfine structures of the atoms and then describe the effects of the external magnetic field on the atoms such as the Zeeman splitting of the atomic levels and coupling of the Zeeman sublevels. Most of the materials can be found in such sources as [**45, 46, 47, 48, 49, 50**].

2.1. Atomic Interaction with Laser Fields

2.1.1. Two-level Atomic System

2.1.1.1. Time Evolution of the State Vector. From the postulates of quantum mechanics, the state of an atom is represented by a vector $|\Psi(t)\rangle$ in a Hilbert space. The time evolution of this state vector is governed by the time-dependent Schrödinger equation given by

$$i\hbar\frac{\partial\,|\Psi(t)\rangle}{\partial t} = H\,|\Psi(t)\rangle \tag{2.1}$$

where H is the Hamiltonian for the atom and $\hbar$ is the reduced Planck constant.

Without presence of any external fields, the total Hamiltonian H is the same as the so-called unperturbed Hamiltonian, denoted by H_0. In this case, we assume all the relevant information is known such that H_0 has eigenvalues $E_n = \hbar\omega_n$ with eigenstates $|\phi_n\rangle$ and therefore $H_0\,|\phi_n\rangle = E_n\,|\phi_n\rangle$.

With the presence of the laser field, apart from H_0, the total Hamiltonian H also has the interaction part which is described by $H'(t)$, and thus $H(t) = H_0 + H'(t)$. Note the interaction Hamiltonian is usually time-dependent, which renders the total Hamiltonian also time-dependent. In this case, the normal approach for solving the Schrödinger equation would be expanding $|\Psi(t)\rangle$ in terms of $|\phi_n\rangle$ since the latter form a complete set, and then making appropriate approximations on the coefficients based on perturbation theory. However, this approach is not applicable to narrow-band laser excitation of atoms, where large excited-state populations are possible. Instead, a different approximation [**47**] is made by retaining only two states out of the complete set, the single ground and excited state that are connected by the laser frequency. We then end up with this two-level model for the atomic

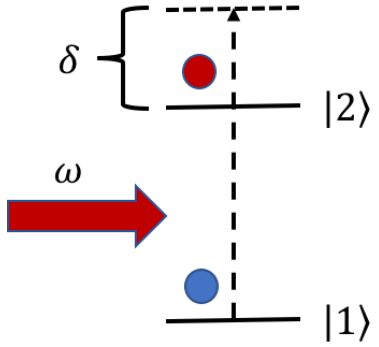

Figure 2.1. A two-level atom driven by a classical laser field.

system as shown in Fig. 2.1, where the ground and excited states are denoted as $|1\rangle$ and $|2\rangle$ with corresponding energies of $E_1 = \hbar\omega_1$ and $E_2 = \hbar\omega_2$, respectively.

With other states left out, $|1\rangle$ and $|2\rangle$ are now a complete set, indicating we can use them as a basis and write

$$|1\rangle = \begin{bmatrix} 1 \\ 0 \end{bmatrix}, \quad |2\rangle = \begin{bmatrix} 0 \\ 1 \end{bmatrix} \tag{2.2}$$

In this basis, the state vector $|\Psi(t)\rangle$ can be written as

$$|\Psi(t)\rangle = c_1(t)\,|1\rangle + c_2(t)\,|2\rangle = \begin{bmatrix} c_1(t) \\ c_2(t) \end{bmatrix} \tag{2.3}$$

where the two coefficients $c_1(t)$ and $c_2(t)$ are generally time-dependent complex numbers with normalization condition $\langle\Psi(t)|\Psi(t)\rangle = |c_1(t)|^2 + |c_2(t)|^2 = 1$. The Hamiltonian is given by

$$H = \sum_{i,j=1}^{2} H_{ij}\,|i\rangle\,\langle j| = \begin{bmatrix} H_{11} & H_{12} \\ H_{21} & H_{22} \end{bmatrix} \tag{2.4}$$

where the matrix element $H_{ij} = \langle i|H|j\rangle$. The Schrödinger equation then becomes

$$i\hbar \begin{bmatrix} \dot{c}_1(t) \\ \dot{c}_2(t) \end{bmatrix} = \begin{bmatrix} H_{11} & H_{12} \\ H_{21} & H_{22} \end{bmatrix} \begin{bmatrix} c_1(t) \\ c_2(t) \end{bmatrix} \tag{2.5}$$

To solve for Eq. (2.5), we need to know the matrix elements of the total Hamiltonian, which consists of two parts: the unperturbed Hamiltonian H_0 and the interaction Hamiltonian $H'(t)$. The former is readily known since the two basis states $|1\rangle$ and $|2\rangle$ are its eigenstates

$$H_0 = \sum_{i,j=1}^{2} \hbar\omega_i \delta_{ij} \, |i\rangle \, \langle j| = \begin{bmatrix} \hbar\omega_1 & 0 \\ 0 & \hbar\omega_2 \end{bmatrix} \tag{2.6}$$

where δ_{ij} is the Kronecker delta function. Obtaining the expression for the latter is not so straightforward. A formal approach [**48**] would begin by writing down the full Hamiltonian of the atom in a quantized laser field and then transition to a classical description of the field with some proper gauge transformation until the expression

$$H'(t) = -e \, \mathbf{E}(\mathbf{r}, t) \cdot \mathbf{r} \tag{2.7}$$

emerges, where e is the electron charge, $\mathbf{E}(\mathbf{r}, t)$ is the classical electric field and $\mathbf{r}$ is the position operator of the electron. Eq. (2.7) represents the interaction between the atomic electric dipole moment and the external laser field. For a plane wave traveling in the positive z direction, the electric field is given by

$$\mathbf{E}(\mathbf{r}, t) = \hat{\mathbf{e}} \, E_0 \, cos(kz - \omega t) = \hat{\mathbf{e}} \, E_0 \, \frac{e^{i(kz-\omega t)} + e^{-i(kz-\omega t)}}{2} \tag{2.8}$$

where $\hat{\mathbf{e}}$ is the unit polarization vector, E_0 is the amplitude of the light field, ω is the laser frequency and k is the wave number. The matrix form of $H'(t)$ for this case will be

$$H' = \begin{bmatrix} H'_{11} & H'_{12} \\ H'_{21} & H'_{22} \end{bmatrix} = \begin{bmatrix} 0 & \frac{\hbar\Omega^*}{2}(e^{i(kz-\omega t)} + e^{-i(kz-\omega t)}) \\ \frac{\hbar\Omega}{2}(e^{i(kz-\omega t)} + e^{-i(kz-\omega t)}) & 0 \end{bmatrix} \tag{2.9}$$

where the diagonal terms are zero due to the fact that the position operator $\mathbf{r}$ is odd, Ω is the Rabi frequency defined by

$$\Omega = \frac{-eE_0}{\hbar} \langle 2|\hat{\mathbf{e}} \cdot \mathbf{r}|1\rangle \tag{2.10}$$

and Ω^* is the complex conjugate of Ω. Combining Eq. (2.6) and Eq. (2.9), we have

$$H = \begin{bmatrix} \hbar\omega_1 & \frac{\hbar\Omega^*}{2}(e^{i(kz-\omega t)} + e^{-i(kz-\omega t)}) \\ \frac{\hbar\Omega}{2}(e^{i(kz-\omega t)} + e^{-i(kz-\omega t)}) & \hbar\omega_2 \end{bmatrix} \tag{2.11}$$

and Eq. (2.5) becomes

$$i\hbar \begin{bmatrix} \dot{c}_1(t) \\ \dot{c}_2(t) \end{bmatrix} = \begin{bmatrix} \hbar\omega_1 & \frac{\hbar\Omega^*}{2}(e^{i(kz-\omega t)} + e^{-i(kz-\omega t)}) \\ \frac{\hbar\Omega}{2}(e^{i(kz-\omega t)} + e^{-i(kz-\omega t)}) & \hbar\omega_2 \end{bmatrix} \begin{bmatrix} c_1(t) \\ c_2(t) \end{bmatrix} \tag{2.12}$$

Solving Eq. (2.12) for the case of two-level atomic system requires the use of two very well-known approximations. The first of these approximations is the electric dipole approximation (EDA), which consists of neglecting the spatial variation of $\mathbf{E}(\mathbf{r}, t)$ over the region of the atom because the optical wavelength λ is typically several hundred nm whereas the radius of the atom is typically $< 1nm$. This allows us to set $z = 0$. The second approximation is the rotating wave approximation (RWA), which consists of neglecting the rapid varying terms

in the Hamiltonian that are assumed to average away very quickly and thus make a small contribution to the final solution [**45, 48, 49**].

Applying the electric dipole approximation is straightward. To see how the rotating wave approximation works, we need to transform to the rotating frame by applying the so-called rotating wave transformation (RWT). The basis states in this rotating frame, $|\widetilde{1}\rangle$ and $|\widetilde{2}\rangle$, are related to $|1\rangle$ and $|2\rangle$ by

$$\begin{bmatrix} |\widetilde{1}\rangle & |\widetilde{2}\rangle \end{bmatrix} = \begin{bmatrix} |1\rangle & |2\rangle \end{bmatrix} Q^{-1}(t) \tag{2.13}$$

where $Q(t)$ is the transformation matrix given by

$$Q(t) = \begin{bmatrix} e^{i\theta_1 t} & 0 \\ 0 & e^{i\theta_2 t} \end{bmatrix} \tag{2.14}$$

and $Q^{-1}(t)$ is the inverse of $Q(t)$. Here θ_1 and θ_2 are two parameters to be determined. The state vector in this new basis is

$$|\widetilde{\Psi}(t)\rangle = \begin{bmatrix} \widetilde{c}_1(t) \\ \widetilde{c}_2(t) \end{bmatrix} = Q(t)\,|\Psi(t)\rangle = \begin{bmatrix} c_1(t)e^{i\theta_1 t} \\ c_2(t)e^{i\theta_2 t} \end{bmatrix} \tag{2.15}$$

The Schrödinger equation for $|\widetilde{\Psi}(t)\rangle$ will be

$$i\hbar \begin{bmatrix} \dot{\widetilde{c}}_1(t) \\ \dot{\widetilde{c}}_2(t) \end{bmatrix} = \widetilde{H} \begin{bmatrix} \widetilde{c}_1(t) \\ \widetilde{c}_2(t) \end{bmatrix} \tag{2.16}$$

where $\widetilde{H}$ is the transformed Hamiltonian given by (with EDA applied)

(2.17)

$$\widetilde{H} = i\hbar\dot{Q}Q^{-1} + QHQ^{-1} = \hbar \begin{bmatrix} \omega_1 - \theta_1 & \frac{\Omega^*}{2}(e^{i(\omega+\theta_1-\theta_2)t} + e^{i(-\omega+\theta_1-\theta_2)t}) \\ \frac{\Omega}{2}(e^{i(-\omega-\theta_1+\theta_2)t} + e^{i(\omega-\theta_1+\theta_2)t}) & \omega_2 - \theta_2 \end{bmatrix}$$

The parameters θ_1 and θ_2 will now be chosen to eliminate as much time-dependence in $\widetilde{H}$ and render it as simple as possible, which by convention are $\theta_1 = \omega_1$ and $\theta_2 = \omega_1 + \omega$. Then Eq. (2.17) simplifies to

(2.18)
$$\widetilde{H} = \hbar \begin{bmatrix} 0 & \frac{\Omega^*}{2}(1 + e^{-i2\omega t}) \\ \frac{\Omega}{2}(1 + e^{i2\omega t}) & -\delta \end{bmatrix}$$

where $\delta \equiv \omega - \omega_0$, is the laser detuning from the atomic resonance frequency $\omega_0 = \omega_2 - \omega_1$. The rotating wave approximation says now the fast oscillating terms $e^{\pm i2\omega t}$ can be dropped so Eq. (2.18) is further reduced to

(2.19)
$$\widetilde{H} = \hbar \begin{bmatrix} 0 & \frac{\Omega^*}{2} \\ \frac{\Omega}{2} & -\delta \end{bmatrix}$$

Plugging Eq. (2.19) back to Eq. (2.16) yields the following coupled differential equations for the two coefficients

(2.20a)
$$i\hbar\,\dot{\widetilde{c}}_1(t) = \frac{\hbar\Omega^*}{2}\,\widetilde{c}_2(t)$$

(2.20b)
$$i\hbar\,\dot{\widetilde{c}}_2(t) = \frac{\hbar\Omega}{2}\,\widetilde{c}_1(t) - \hbar\delta\,\widetilde{c}_2(t)$$

which can be solved for arbitrary initial conditions $\tilde{c}_1(0) = A$ and $\tilde{c}_2(0) = B$ as

$$\widetilde{c}_1(t) = e^{\frac{i\delta t}{2}}(Acos(\frac{\Omega' t}{2}) + i\frac{A\delta - B\Omega^*}{\Omega'}sin(\frac{\Omega' t}{2})) \tag{2.21a}$$

$$\widetilde{c}_2(t) = e^{\frac{i\delta t}{2}}(Bcos(\frac{\Omega' t}{2}) + i\frac{B\delta - A\Omega}{\Omega'}sin(\frac{\Omega' t}{2})) \tag{2.21b}$$

where $\Omega' = \sqrt{|\Omega|^2 + \delta^2}$ is the generalized Rabi frequency. Using Eq. (2.15), we obtain for the same initial conditions

$$c_1(t) = e^{-i\omega_1 t}e^{-i\frac{\delta}{2}t}(Acos(\frac{\Omega' t}{2}) + i\frac{A\delta - B\Omega^*}{\Omega'}sin(\frac{\Omega' t}{2})) \tag{2.22a}$$

$$c_2(t) = e^{-i\omega_2 t}e^{i\frac{\delta}{2}t}(Bcos(\frac{\Omega' t}{2}) + i\frac{B\delta - A\Omega}{\Omega'}sin(\frac{\Omega' t}{2})) \tag{2.22b}$$

As an example, we consider the case where all the atoms start from the ground state $|1\rangle$, i.e., $A = 1$ and $B = 0$. At time t, the probability of finding an atom in the excited state $|2\rangle$ is given by $P_2(t) = |c_2(t)|^2 = \left|\frac{\Omega}{\Omega'}\right|^2 sin^2(\frac{\Omega' t}{2})$, which oscillates back and forth between 0 and $\left|\frac{\Omega}{\Omega'}\right|^2$. This phenomenon is called Rabi oscillation. Fig. 2.2 shows the oscillations for various detunings, with larger detunings oscillating at greater frequencies but with smaller amplitudes.

Before moving onto the next section, we consider another example for completeness. The Hamiltonian dropped from RWA is given by

$$\widetilde{H}' = \hbar \begin{bmatrix} 0 & \frac{\Omega^*}{2}e^{-i2\omega t} \\ \frac{\Omega}{2}e^{i2\omega t} & -\delta \end{bmatrix} \tag{2.23}$$

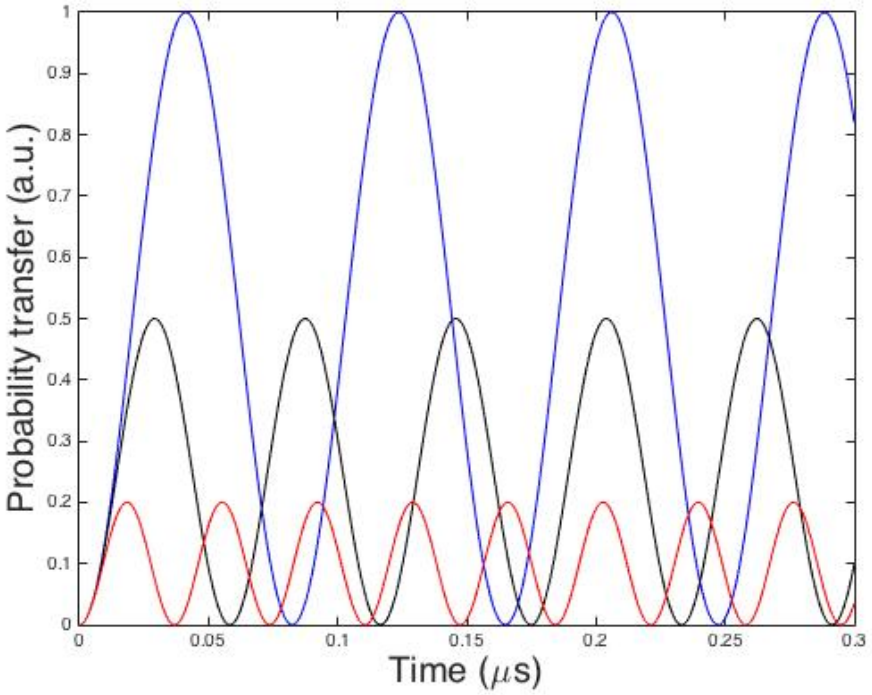

Figure 2.2. Probability $|c_2(t)|^2$ for the atom to be in the excited state for $\Omega = \Gamma$ and $\delta = 0$ (blue), $\delta = \Gamma$ (black), and $\delta = 2\Gamma$ (red), where $\Gamma = 2\pi * 6.066\,\mathrm{MHz}$.

To solve for the probability transfer resulted from this Hamiltonian, we can apply another RWT and choose the parameters properly to get rid of the time dependence which yields

$$\widetilde{H}' = \hbar \begin{bmatrix} 0 & \frac{\Omega^*}{2} \\ \frac{\Omega}{2} & 2\omega - \delta \end{bmatrix} \tag{2.24}$$

If the atoms were initialized to the ground state, from our calculations above, the maximum probability transfer will be $\frac{|\Omega|^2}{(2\omega-\delta)^2+|\Omega|^2}$. Compared with the maximum probability obtained above $\frac{|\Omega|^2}{\delta^2+|\Omega|^2}$, we get a ratio of $\frac{\delta^2+|\Omega|^2}{(2\omega-\delta)^2+|\Omega|^2}$. With typical values $\Omega \simeq \delta \simeq 2\pi \cdot 10^6 sec^{-1}$ and $\omega \simeq 2\pi \cdot 10^{14} sec^{-1}$, this ratio is $\simeq 10^{-16}$, which is negligible, justifying the RWA.

2.1.1.2. Bloch Vector Representation. When we write the state vector as a linear combination of the basis states, $|\widetilde{\Psi}(t)\rangle = \widetilde{c}_1(t)\,|\widetilde{1}\rangle + \widetilde{c}_2(t)\,|\widetilde{2}\rangle$, it looks like there are four free parameters since the two coefficients are complex numbers. Because the overall phase of the state vector has no physical meaning, there are really only three free parameters which can be constructed from the real and imaginary parts of $\widetilde{c}_1(t)$ and $\widetilde{c}_2(t)$ as follows [**51**]

$$R_1 \equiv \widetilde{c}_1\widetilde{c}_2^* + \widetilde{c}_1^*\widetilde{c}_2 \tag{2.25a}$$

$$R_2 \equiv i(\widetilde{c}_1\widetilde{c}_2^* - \widetilde{c}_1^*\widetilde{c}_2) \tag{2.25b}$$

$$R_3 \equiv \widetilde{c}_1\widetilde{c}_1^* - \widetilde{c}_2^*\widetilde{c}_2 \tag{2.25c}$$

From Eq. (2.16) it can be shown that

$$\dot{R}_1 = \frac{\widetilde{H}_{22} - \widetilde{H}_{11}}{\hbar} R_2 - \frac{\widetilde{H}_{12} - \widetilde{H}_{21}}{i\hbar} R_3 \tag{2.26a}$$

$$\dot{R}_2 = \frac{\widetilde{H}_{12} + \widetilde{H}_{21}}{-\hbar} R_3 - \frac{\widetilde{H}_{22} - \widetilde{H}_{11}}{\hbar} R_1 \tag{2.26b}$$

$$\dot{R}_3 = \frac{\widetilde{H}_{12} - \widetilde{H}_{21}}{i\hbar} R_1 - \frac{\widetilde{H}_{12} + \widetilde{H}_{21}}{-\hbar} R_2 \tag{2.26c}$$

If we group R_1, R_2 and R_3 into a vector called Bloch vector, $\mathbf{R} = [R_1,\, R_2,\, R_3]^T$, Eqs. (2.26) indicates that the time evolution of this vector will obey

$$\dot{\mathbf{R}} = \mathbf{R} \times \mathbf{D} \tag{2.27}$$

where $\mathbf{D}$ is a another vector given by

$$\mathbf{D} = \Big[\frac{\widetilde{H}_{12} + \widetilde{H}_{21}}{-\hbar},\, \frac{\widetilde{H}_{12} - \widetilde{H}_{21}}{i\hbar},\, \frac{\widetilde{H}_{22} - \widetilde{H}_{11}}{\hbar}\Big]^T \tag{2.28}$$

Note that the components of **R** (and **D**) are arranged to form a column vector but written as the transpose of the corresponding row vector to save space. The Hamiltonian after EDA, RWA and RWT is given by Eq. (2.19), which leads to $\mathbf{D} = [-\mathrm{Re}(\Omega), -\mathrm{Im}(\Omega), -\delta]^T$, with Ω the Rabi frequency and δ the laser detuning. The Rabi frequency is usually taken to be real and the components of **D** become $[-\Omega, 0, -\delta]^T$. The probabilities of finding the atoms in the ground and excited states are related to the Bloch vector by $P_1 = (1 + R_3)/2$ and $P_2 = (1 - R_3)/2$, respectively, which can be derived from the normalization condition and Eq. (2.25c).

Eq. (2.27) shows that the Bloch vector **R** precesses with time without changing length and its motion is confined to the surface of a sphere. The north (south) poles of this sphere correspond to the ground (excited) states of the atom, and equatorial points correspond to equal superpositions with various phases. When $\delta \gg \Omega$, the precession axis (determined by **D**) passes very nearly through the poles. In this case, an atom initially in the ground state undergoes rapid precessions on a small circle near the north pole and thus has a small excitation probability, as shown in Eq. (2.22) and Fig. 2.2. By constrast, for $\delta = 0$, the precession axis passes through the equator so an atom initially in the ground state is described by a Bloch vector **R** undergoing slow, full-circle oscillations through the poles, which are the Rabi oscillations mentioned above.

2.1.1.3. Density Matrix and the Optical Bloch Equations. Until now we have presented the equations for the coherent evolution of the amplitudes of a two-level atom in a radiation field. However, we have left out an important phenomenon, spontaneous emission of the excited states resulting from their interaction with the vacuum modes of the electromagnetic field. The effects of spontaneous emission cannot be described in terms of such

coherent evolution of the state vector. Instead, they will be most readily handled by the density matrix, which is detailed below.

The density matrix is the matrix representation of the density operator ρ which is used to characterize the state of an ensemble of similarly prepared quantum systems (we do not need to refer to a concrete set of systems that coexist in space as long as they could have been prepared in principle). We have the following constraints imposed on ρ:

– ρ is self-adjoint: $\rho = \rho^\dagger$.

– ρ is non-negative: $\langle u|\rho|u\rangle \geq 0$ for $\forall u$.

– ρ has trace of 1: $\mathrm{Tr}\{\rho\} = 1$.

The expectation value of any dynamical variable X over the ensemble represented by the density operator ρ is given by

$$\langle X\rangle = \mathrm{Tr}\{\rho X\} = \sum_i \langle i|\rho X|i\rangle \tag{2.29}$$

where $\{i\}$ is some complete set of basis states and $\langle X\rangle$ is guaranteed to be real due to the first constraint above. From Eq. (2.29), we can derive an expression of the density operator in terms of the state vector. If all the systems in the ensemble can be described by the same state $|\Psi\rangle$, the expectation value of X is

$$\langle X\rangle = \langle\Psi|X|\Psi\rangle = \sum_i \langle\Psi|X|i\rangle\langle i|\Psi\rangle = \sum_i \langle i|(|\Psi\rangle\langle\Psi|)X|i\rangle \tag{2.30}$$

Comparing with Eq. (2.29), we have

$$\rho = |\Psi\rangle\langle\Psi| \tag{2.31}$$

If now the ensemble is actually a statistical mixture of a set of states where the portition of the ensemble being in the state $|\Psi_k\rangle$ is given by p_k, the expectation value $\langle X\rangle$ will be

$$\sum_k p_k \langle\Psi_k|X|\Psi_k\rangle = \sum_i \sum_k p_k \langle\Psi_k|X|i\rangle \langle i|\Psi_k\rangle = \sum_i \langle i|(\sum_k p_k |\Psi_k\rangle\langle\Psi_k|)X|i\rangle \tag{2.32}$$

and the density operator is identified as

$$\rho = \sum_k p_k |\Psi_k\rangle \langle\Psi_k| \tag{2.33}$$

where $0 < p_k < 1$ and $\sum_k p_k = 1$. By convention, if the density operator can be writen in the form of Eq. (2.31), the ensemble is said in a pure state; otherwise it is in a mixed state. Mixed states arise in situations where the system undergoes an uncertain preparation history or it is a subsystem entangled with other subsystems. The density operator for pure and mixed states can be combined into one expression

$$\rho = \sum_k p_k |\Psi_k\rangle \langle\Psi_k| \tag{2.34}$$

where now $0 \leq p_k \leq 1$ and $\sum_k p_k = 1$.

Using Eq. (2.1) and Eq. (2.34), it can be shown that the time dependence of the density operator depends on the total Hamiltonian simply as

$$i\hbar\frac{\mathrm{d}\rho}{\mathrm{d}t} = [H, \rho] \tag{2.35}$$

where $[H, \rho] = H\rho - \rho H$ is the commutator of the Hamiltonian and the density operator. For a two-level atomic system without spontaneous emission, the density operator is describing a pure state. In the basis after RWT, its matrix elements are related to the two coefficients $\widetilde{c}_1$ and $\widetilde{c}_2$ by $\rho_{ij} = \widetilde{c}_i\widetilde{c}_j^*$ where $i, j = 1, 2$. The components of the Bloch vector in Eq. (2.25)

can be rewritten in terms of the density matrix elements and Eq. (2.27) can be recovered following Eq. (2.35). In the presence of spontaneous emission, the atomic system is coupled with the vacuum modes of the electromagnetic field. The density operator describing the whole system has two parts: the atom and the spontaneously emitted light. If observation is done only for the atomic system, a partial trace has to be taken over the spontaneously emitted light field and the atomic system is now left in a mixed state. In this case there is no simple relation between the density matrix elements and the state vector coefficients, but the effects of spontaneous emission can be added independently in terms of the decay rate Γ of the excited state [**52**]. On the one hand, the excited state population is diminishing due to the spontaneous emission. This can be accounted for by adding an imaginary term to the total Hamiltonian. On the other hand, the ground state population will increase since we have a closed two-level system. This can be accounted for by adding a source term to Eq. (2.35). Putting everything together, we arrive at

$$\frac{\mathrm{d}\rho}{\mathrm{d}t} = \frac{1}{i\hbar}(H\rho - \rho H^{\dagger}) + L \tag{2.36}$$

where in the basis of Eq. (2.2), the density operator is represented by the following density matrix

$$\rho = \begin{bmatrix} \rho_{11} & \rho_{12} \\ \rho_{21} & \rho_{22} \end{bmatrix} \tag{2.37}$$

the Hamiltonian now will be

$$H = \begin{bmatrix} \hbar\omega_1 & \frac{\hbar\Omega^*}{2}(e^{i(kz-\omega t)} + e^{-i(kz-\omega t)}) \\ \frac{\hbar\Omega}{2}(e^{i(kz-\omega t)} + e^{-i(kz-\omega t)}) & \hbar\omega_2 - \frac{i\hbar\Gamma}{2} \end{bmatrix} \tag{2.38}$$

$H^\dagger$ is the Hermitian conjugate of H, and L is the source terms given by

$$L = \begin{bmatrix} \Gamma\rho_{22} & 0 \\ 0 & 0 \end{bmatrix} \tag{2.39}$$

Solving for Eq. (2.36) again requires EDA, RWA and then applying RWT to transform to the rotating basis of Eq. (2.13), after which we have the following counterparts corresponding to Eqs. (2.36), (2.37), (2.38) and (2.39)

$$\frac{\mathrm{d}\widetilde{\rho}}{\mathrm{d}t} = \frac{1}{i\hbar}(\widetilde{H}\widetilde{\rho} - \widetilde{\rho}\widetilde{H}^\dagger) + \widetilde{L} \tag{2.40}$$

$$\widetilde{\rho} = \begin{bmatrix} \widetilde{\rho}_{11} & \widetilde{\rho}_{12} \\ \widetilde{\rho}_{21} & \widetilde{\rho}_{22} \end{bmatrix} \tag{2.41}$$

$$\widetilde{H} = \begin{bmatrix} 0 & \frac{\hbar\Omega^*}{2} \\ \frac{\hbar\Omega}{2} & -\hbar\delta - \frac{i\hbar\Gamma}{2} \end{bmatrix} \tag{2.42}$$

$$\widetilde{L} = \begin{bmatrix} \Gamma\widetilde{\rho}_{22} & 0 \\ 0 & 0 \end{bmatrix} \tag{2.43}$$

Substitution of Eqs. (2.41), (2.42) and (2.43) back into Eq. (2.40) and writting explicitly in component forms leads to the following equations for the two-level atomic system, including

spontaneous emission:

$$\frac{\mathrm{d}\widetilde{\rho}_{11}}{\mathrm{d}t} = \Gamma\widetilde{\rho}_{22} + \frac{i}{2}(\Omega^*\widetilde{\rho}_{21} - \Omega\widetilde{\rho}_{12}) \tag{2.44a}$$

$$\frac{\mathrm{d}\widetilde{\rho}_{22}}{\mathrm{d}t} = -\Gamma\widetilde{\rho}_{22} + \frac{i}{2}(\Omega\widetilde{\rho}_{12} - \Omega^*\widetilde{\rho}_{21}) \tag{2.44b}$$

$$\frac{\mathrm{d}\widetilde{\rho}_{12}}{\mathrm{d}t} = -(\frac{\Gamma}{2} + i\delta)\widetilde{\rho}_{12} + \frac{i}{2}\Omega^*(\widetilde{\rho}_{22} - \widetilde{\rho}_{11}) \tag{2.44c}$$

$$\frac{\mathrm{d}\widetilde{\rho}_{21}}{\mathrm{d}t} = -(\frac{\Gamma}{2} - i\delta)\widetilde{\rho}_{21} + \frac{i}{2}\Omega(\widetilde{\rho}_{11} - \widetilde{\rho}_{22}) \tag{2.44d}$$

These equations are called the optical Bloch equations (OBE). Note that $\mathrm{d}\widetilde{\rho}_{22}/\mathrm{d}t = -\,\mathrm{d}\widetilde{\rho}_{11}/\mathrm{d}t$, in accordance with the requirement of a closed two-level system where the total population $\widetilde{\rho}_{11} + \widetilde{\rho}_{22} = 1$ is conserved.

The steady state solutions of the OBE can be found by setting $\mathrm{d}\widetilde{\rho}/\mathrm{d}t = 0$ and exploiting certain relationships among the four components of the density matrix for a two-level system, such as $\widetilde{\rho}_{11} + \widetilde{\rho}_{22} = 1$ from conservation of the total population and $\widetilde{\rho}_{12} = \widetilde{\rho}_{21}^*$ from the hermiticity of ρ. The results are

$$\widetilde{\rho}_{11} = \frac{\Gamma^2 + |\Omega|^2 + 4\delta^2}{\Gamma^2 + 2|\Omega|^2 + 4\delta^2} \tag{2.45a}$$

$$\widetilde{\rho}_{22} = \frac{|\Omega|^2}{\Gamma^2 + 2|\Omega|^2 + 4\delta^2} \tag{2.45b}$$

$$\widetilde{\rho}_{21} = \frac{\Omega(i\Gamma - 2\delta)}{\Gamma^2 + 2|\Omega|^2 + 4\delta^2} \tag{2.45c}$$

$$\widetilde{\rho}_{12} = \frac{\Omega^*(-i\Gamma - 2\delta)}{\Gamma^2 + 2|\Omega|^2 + 4\delta^2} \tag{2.45d}$$

Eqs. (2.45) shows that when the decay rate Γ is large compared to the other terms ($\Gamma \gg \Omega, \delta$) or the detuning is large compared to the other terms ($\delta \gg \Gamma, \Omega$), the steady state solution is $\rho_{11} \sim 1, \rho_{22} \sim 0$, i.e., the atom ends up in the ground state; when the Rabi frequency Ω

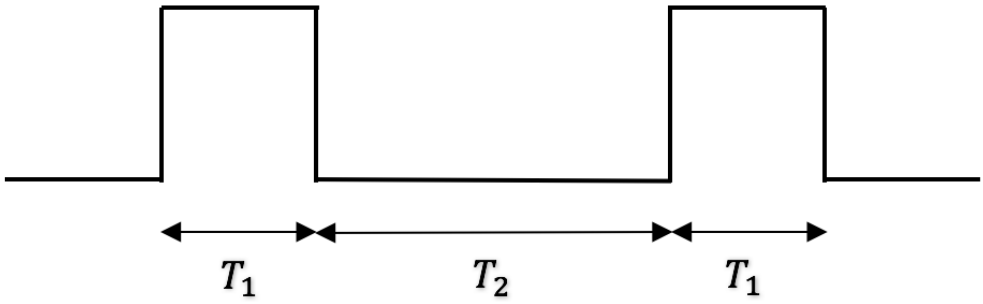

Figure 2.3. Laser pulses for separated oscillating field experiment.

is large compared to the other terms ($\Omega \gg \Gamma, \delta$), we find $\rho_{11} = \rho_{22} \sim \frac{1}{2}$, i.e., the atom has equal chance of occupying either state at the end.

2.1.1.4. Separated Oscillating Field Experiment and Ramsey Fringes. With the theory for two-level atomic system in place, we now consider its application to the separated oscillating field experiment consisting of three zones where in the first and third zones the atom interacts with the laser field for time duration of T_1 while in the second zone the atom is left in dark for time duration of T_2, as shown in Fig. 2.3. The atom is initialized in the ground state right before the first zone and we want to know the population distribution of the atom right after the third zone. For simplicity, we ignore spontaneous emission of the excited state (this will be justified for the three-level atomic system case). The final population distribution can be found either by solving the evolution of the state vector directly using Eqs. (2.20) along with proper initial conditions for each zone, or by examining the rotation of the Bloch vector described by Eq. (2.27). The computation of the latter is much simpler and clearer than the former and thus will be employed here.

We assume $t = 0$ right before the first zone. Since the atom is initialized in the ground state, we have $\mathbf{R}(0) = [0,\, 0,\, 1]^T$. During the first zone, the Bloch vector will precess along

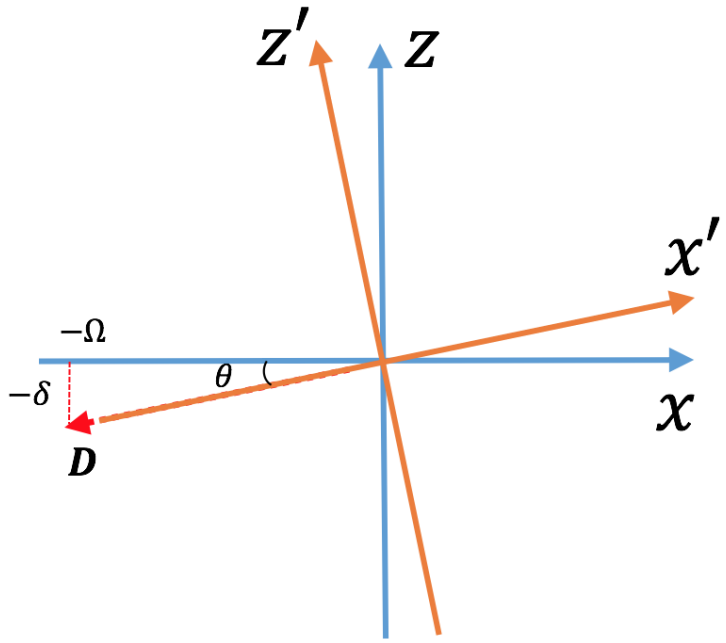

Figure 2.4. Construction of the new coordinate system O' from the original coordinate system O. The y axis shared by both systems is pointing into the page and not shown here. θ is the angle made between $\mathbf{D}$ and the negative-x axis where $\sin(\theta) = \delta/\Omega'$ and $\cos(\theta) = \Omega/\Omega'$ with $\Omega' = \sqrt{\Omega^2 + \delta^2}$ being the generalized Rabi frequency.

the axis aligned with $\mathbf{D} = [-\Omega,\, 0,\, -\delta]^T$. Assume the current coordinate system is O with coordinate axes of x, y and z. Since the precession axis does not coincide with any of the coordinate axes, it will be awkward if we still work in current coordinate system. Instead, we will construct a new coordinate system O' with axes of x', y and z', where now the precession axis $\mathbf{D}$ is aligned with negative-x' axis, as shown in Fig. 2.4. To work in the new coordinate system O', we need to rewrite the initial conditions in reference to x', y and z'. Note that O' can be obtained from O by a rotation around the positive-y axis. The matrix describing

such a rotation with an arbitrary angle α is given by

$$A = \begin{bmatrix} cos(\alpha) & 0 & sin(\alpha) \\ 0 & 1 & 0 \\ -sin(\alpha) & 0 & cos(\alpha) \end{bmatrix} \tag{2.46}$$

where now $\alpha = -\theta$ as is easily seen from Fig. 2.4. The initial Bloch vector can be rewritten in the new coordinate system O' as $\mathbf{R}'(0) = A^{-1}\mathbf{R}(0)$, where A^{-1} is the inverse of A and equal to A^T as A is orthonormal ($AA^T = A^TA = I$ where I is the 3-by-3 identity matrix). Note we have matrix multiplications here as the components of the Bloch vector have been arranged into column form. Since the precession axis is aligned with the negative-x' axis, the evolution of the Bloch vector in the new coordinate system O' can be described by another rotation matrix

$$B = \begin{bmatrix} 1 & 0 & 0 \\ 0 & cos(\beta) & -sin(\beta) \\ 0 & sin(\beta) & cos(\beta) \end{bmatrix} \tag{2.47}$$

where $\beta = -\Omega' T_1$ is the total precession angle of the Bloch vector in the first zone and $\Omega' = \sqrt{\Omega^2 + \delta^2}$ is the generalized Rabi frequency. The Bloch vector at the end of this zone written in the new coordinate system O' will be $\mathbf{R}'(T_1) = B\mathbf{R}'(0)$. Transforming back to the original coordinate system O, we have $\mathbf{R}(T_1) = A\mathbf{R}'(T_1)$, which becomes the initial condition for the second zone.

In the second zone, the atom is left in dark so we have $\mathbf{D} = [0,\, 0,\, -\delta]^T$, which is aligned with the negative-z axis. This means we can work directly in the original coordinate system O and similarly have the following rotation matrix to describe the evolution of the Bloch

vector

$$C = \begin{bmatrix} cos(\gamma) & -sin(\gamma) & 0 \\ sin(\gamma) & cos(\gamma) & 0 \\ 0 & 0 & 1 \end{bmatrix} \tag{2.48}$$

where $\gamma = -\delta T_2$ is the total precession angle of the Bloch vector in the second zone. The Bloch vector at the end of this zone written in the coordinate system O will be $\mathbf{R}(T_1+T_2) = C\mathbf{R}(T_1)$, which now serves as the initial condition for the third zone.

During the third zone, the atom will undergo the same interaction with the laser field as in the first one, therefore we can simply repeat what has been done in the first zone, i.e., transforming the initial condition $\mathbf{R}(T_1+T_2)$ into the new coordinate system O', applying effects of the rotation matrix A and then transforming back to the original coordinate system O, to obtain the Bloch vector at the end of this zone as $\mathbf{R}(2T_1+T_2) = ABA^{-1}\mathbf{R}(T_1+T_2)$.

Piecing everything together, we find the final expression of the Bloch vector at the end of the third zone to be $\mathbf{R}(2T_1+T_2) = ABA^{-1}CABA^{-1}\mathbf{R}(0) = ABA^{T}CABA^{T}\mathbf{R}(0)$. Carrying out the complicated yet straightforward matrix multiplications yields

$$P_2 = \frac{4\Omega^2}{\Omega'^2}\sin^2\left(\frac{\Omega' T_1}{2}\right)\left[\cos\left(\frac{\Omega' T_1}{2}\right)\cos\left(\frac{\delta T_2}{2}\right) - \frac{\delta}{\Omega'}\sin\left(\frac{\Omega' T_1}{2}\right)\sin\left(\frac{\delta T_2}{2}\right)\right]^2 \tag{2.49}$$

where P_2 is the probability of finding the atom in the excited state at the end of the third zone. Fig. 2.5 plots P_2 in terms of the laser detuning δ for two different dark zone durations. The blue trace is for $T_2 = 0$, i.e., there is no dark zone and the first and last zones are essentially merged into a single one. It's easy to show that the results for single zone interaction, Eq. (2.22b), is recovered for this case. A very interesting point shows up when the dark zone duration becomes non-zero: the width of the center peak begins to decrease with

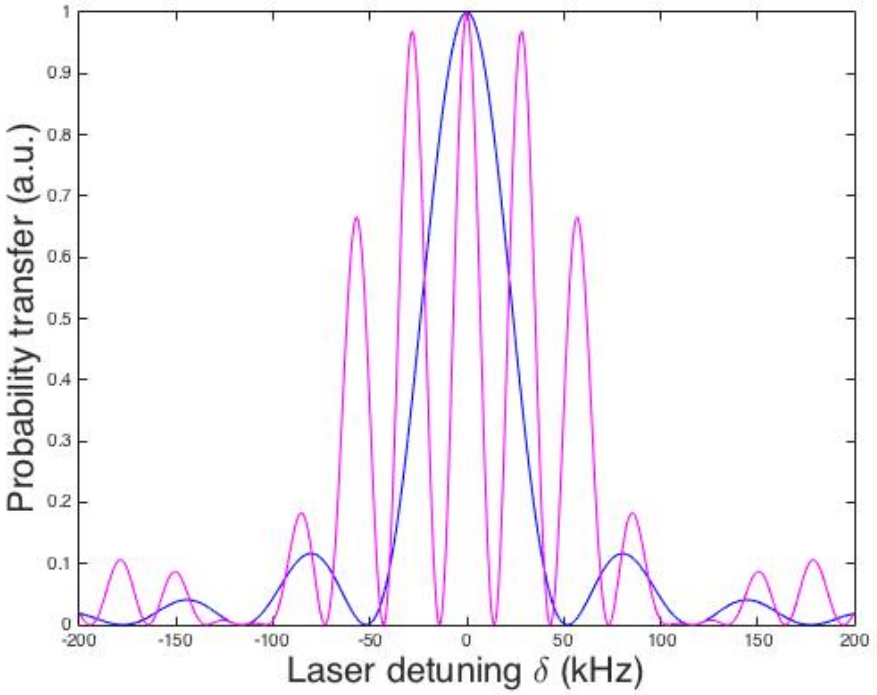

Figure 2.5. Probability P_2 for the atom to be in the excited state at the end of the third zone in terms of the laser detuning δ for $\Omega = 2\pi * 30\,\mathrm{kHz}$, $\Omega T_1 = \pi/2$, $T_2 = 0$ (blue) and $T_2 = 3T_1$ (magenta).

increasing dark zone time, as is demonstrated by the magenta trace where $T_2 = 3T_1$. The narrower peaks contained in the central envelope are called the Ramsey fringes, named after Norman Ramsey who invented this separated oscillating fields method. Since the dark zone duration can be made very large compared to the two interaction zones, the Ramsey fringes can become much narrower than its single-zone counterpart, which renders this method extremely useful in applications for measuring atomic transition frequencies, in particular for building atomic clocks.

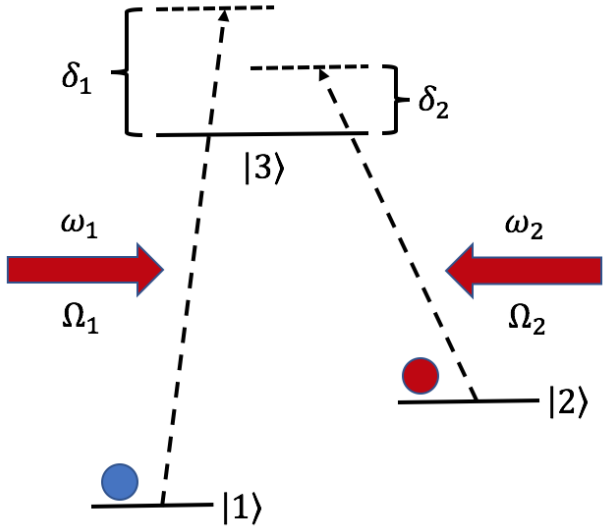

Figure 2.6. A three-level atom driven by two classical laser fields.

2.1.2. Three-level Atomic System

Despite a two-level atomic system sounds simple enough, in practice it is hard to construct such a system due to the fact that atoms in general have many levels and normally more than two of them get coupled to the ligh field at the same time. Even if we do succeed in isolating two levels to form a pure two-level atomic system, its applications are limited by effects like spontaneous emission from the upper state which is detrimental to maintaining coherence between the two states. To deal with these situations, it's necessary to extend the system to include multiple levels, the simplest of which would be a three-level atomic system in the Λ-configuration (two lower states and one upper state), as shown in Fig. 2.6 and will be investigated here.

2.1.2.1. Hamiltonian of the Three-level Atomic System. Similar to the two-level case, the three basis states can be written as

$$|1\rangle = \begin{bmatrix} 1 \\ 0 \\ 0 \end{bmatrix}, \quad |2\rangle = \begin{bmatrix} 0 \\ 1 \\ 0 \end{bmatrix}, \quad |3\rangle = \begin{bmatrix} 0 \\ 0 \\ 1 \end{bmatrix} \tag{2.50}$$

with corresponding energies of $E_1 = \hbar\omega_{a1}$, $E_2 = \hbar\omega_{a2}$ and $E_2 = \hbar\omega_{a3}$, respectively (the notations of frequencies are different here to distinguish from those of the lasers). In contrast to the two-level case where there is only one laser involved in driving the atom, we now have two lasers coupling the two lower states to the upper state while there is no direct coupling between the two lower ones (this type of interaction is called Raman excitation). The total Hamiltonian of the system H will again have two parts, $H = H_0 + H'(t)$ where H_0 is the unperturbed Hamiltonian and $H'(t)$ is the interaction Hamiltonian. Assuming the two laser fields are co-propogating plane waves traveling in the positive z direction

$$\mathbf{E}_1(\mathbf{r},t) = \hat{\mathbf{e}}_1 \, E_{01} \, cos(k_1 z - \omega_1 t) = \hat{\mathbf{e}}_1 \, E_{01} \, \frac{e^{i(k_1 z - \omega_1 t)} + e^{-i(k_1 z - \omega_1 t)}}{2} \tag{2.51a}$$

$$\mathbf{E}_2(\mathbf{r},t) = \hat{\mathbf{e}}_2 \, E_{02} \, cos(k_2 z - \omega_2 t) = \hat{\mathbf{e}}_2 \, E_{02} \, \frac{e^{i(k_2 z - \omega_2 t)} + e^{-i(k_2 z - \omega_2 t)}}{2} \tag{2.51b}$$

where $\hat{\mathbf{e}}_1$ and $\hat{\mathbf{e}}_2$ are the unit polarization vectors, E_{01} and E_{02} are the amplitudes, ω_1 and ω_2 are the angular frequencies, k_1 and k_2 are the wave numbers for the two laser fields, respectively. The three Hamiltonians, H_0, H' and H can be written of matrix form in the

given basis as

$$H_0 = \begin{bmatrix} \hbar\omega_{a1} & 0 & 0 \\ 0 & \hbar\omega_{a2} & 0 \\ 0 & 0 & \hbar\omega_{a3} \end{bmatrix} \tag{2.52}$$

(2.53)

$$H' = \begin{bmatrix} 0 & 0 & \frac{\hbar\Omega_1^*}{2}\left(e^{i(k_1 z-\omega_1 t)} + e^{-i(k_1 z-\omega_1 t)}\right) \\ 0 & 0 & \frac{\hbar\Omega_2^*}{2}\left(e^{i(k_2 z-\omega_2 t)} + e^{-i(k_2 z-\omega_2 t)}\right) \\ \frac{\hbar\Omega_1}{2}\left(e^{i(k_1 z-\omega_1 t)} + e^{-i(k_1 z-\omega_1 t)}\right) & \frac{\hbar\Omega_2}{2}\left(e^{i(k_2 z-\omega_2 t)} + e^{-i(k_2 z-\omega_2 t)}\right) & 0 \end{bmatrix}$$

(2.54)

$$H = \begin{bmatrix} \hbar\omega_{a1} & 0 & \frac{\hbar\Omega_1^*}{2}\left(e^{i(k_1 z-\omega_1 t)} + e^{-i(k_1 z-\omega_1 t)}\right) \\ 0 & \hbar\omega_{a2} & \frac{\hbar\Omega_2^*}{2}\left(e^{i(k_2 z-\omega_2 t)} + e^{-i(k_2 z-\omega_2 t)}\right) \\ \frac{\hbar\Omega_1}{2}\left(e^{i(k_1 z-\omega_1 t)} + e^{-i(k_1 z-\omega_1 t)}\right) & \frac{\hbar\Omega_2}{2}\left(e^{i(k_2 z-\omega_2 t)} + e^{-i(k_2 z-\omega_2 t)}\right) & \hbar\omega_{a3} \end{bmatrix}$$

where again we have defined the Rabi frequencies for the two transitions

$$\Omega_1 = \frac{-eE_{01}}{\hbar}\langle 3|\hat{\mathbf{e}}_1 \cdot \mathbf{r}|1\rangle \tag{2.55a}$$

$$\Omega_2 = \frac{-eE_{02}}{\hbar}\langle 3|\hat{\mathbf{e}}_2 \cdot \mathbf{r}|2\rangle \tag{2.55b}$$

As usual, we can apply EDA and RWA then RWT to transform to the rotating basis, after which (with proper choices of the parameters of the transformation matrix) the total

Hamiltonian can be simplified to

$$\widetilde{H} = \hbar \begin{bmatrix} \frac{\Delta}{2} & 0 & \frac{\Omega_1^*}{2} \\ 0 & -\frac{\Delta}{2} & \frac{\Omega_2^*}{2} \\ \frac{\Omega_1}{2} & \frac{\Omega_2}{2} & -\delta \end{bmatrix} \tag{2.56}$$

where the laser detunings $\delta_1 = \omega_1 - (\omega_{a3} - \omega_{a1})$ and $\delta_2 = \omega_2 - (\omega_{a3} - \omega_{a2})$ have been used to define the difference detuning $\Delta \equiv \delta_1 - \delta_2$ and the average detuning $\delta \equiv (\delta_1 + \delta_2)/2$.

2.1.2.2. Off-resonant Raman Excitations and Reduction to an Effective Two-level System. The above Hamiltonian in Eq. (2.56) can be used to solve for the evolution of the state vector or the density matrix of the three-level system in the rotating basis, as is done for the two-level case. However, here we will not deal with the general cases but instead choose the laser detunings such that they are of the same sign and much greater than the two Rabi frequencies and the decay rate of the upper state, i.e., $|\delta_1|, |\delta_2| \gg |\Omega_1|, |\Omega_2|, \Gamma$, which implies $|\delta| \gg |\Omega_1|, |\Omega_2|, \Gamma$. Under these conditions it can be shown that the probability of finding the atom in the upper state is very low if the atom starts in one of the lower states. Therefore the upper state can be adiabatically eliminated [**53, 54**] from the basis set and we end up with the following reduced Hamiltonian corresponding to an effective two-level atomic system formed by the two lower states

$$\widetilde{H}_{red} = \hbar \begin{bmatrix} \frac{\Delta}{2} + \frac{\varepsilon_1}{\hbar} & \frac{\Omega^*}{2} \\ \frac{\Omega}{2} & -\frac{\Delta}{2} + \frac{\varepsilon_2}{\hbar} \end{bmatrix} \tag{2.57}$$

where $\Omega = \frac{\Omega_1 \Omega_2^*}{2\delta}$ is the Raman-Rabi frequency, $\varepsilon_1 = \frac{\hbar|\Omega_1|^2}{4\delta}$ and $\varepsilon_2 = \frac{\hbar|\Omega_2|^2}{4\delta}$ are the light shifts induced by the two lasers to the two lower states $|1\rangle$ and $|2\rangle$, respectively. A simple rotating wave transformation specified by Eq. (2.14) with the two parameters chosen as

$\theta_1 = \theta_2 = \frac{\Delta}{2} + \frac{\varepsilon_1}{\hbar}$ will bring the Hamiltonian in Eq. (2.57) to a more familiar form

$$\widetilde{H}_{red} = \hbar \begin{bmatrix} 0 & \frac{\Omega^*}{2} \\ \frac{\Omega}{2} & -(\Delta - \frac{\varepsilon_2 - \varepsilon_1}{\hbar}) \end{bmatrix} \tag{2.58}$$

where compared with Eq. (2.19), the Raman-Rabi frequency Ω will take the role of the Rabi frequency (hence the name), while $(\Delta - \frac{\varepsilon_2 - \varepsilon_1}{\hbar})$ will be the effective laser detuning (hence Δ is also called two-photon detuning).

Since the reduced Hamiltonian in Eq. (2.58) corresponds to an effective two-level atomic system, all the theoretical analyses developed in the previous section are equally applicable here. We expect Rabi oscillations between the two states, single peaks for single zone interaction and Ramsey fringes for separated oscillating field experiment. In the context of Raman excitations, these are called Raman-Rabi oscillations, Raman peaks and Raman-Ramsey fringes, respectively. One advantage of this effective two-level atomic system is that there is no direct coupling between the two states so we do not have to worry about spontaneous emission. The acutal decay from the eliminated upper state is largely suppressed by the large laser detunings and thus transparent to the reduced two-level system.

Lastly for completeness, we will look at some typical experimental values for the parameters involved in the Raman excitations. For our experiments with ^{85}Rb, the two lower levels are chosen to be the two hyperfine ground states ($F = 2$ and $F = 3$ of $5\,^2S_{1/2}$) and the upper level to be the two middle hyperfine states of the D_2 transitions ($F = 2$ and $F = 3$ of $5\,^2P_{3/2}$), as shown in Fig. 2.7 [**55**]. More information about the energy levels can be found in the next section. The two laser detunings are set to be $\delta_1 \sim \delta_2 \sim 2\pi * 1.5\,\text{GHz}$, while the two Raman-Rabi frequencies are $\Omega_1 \sim \Omega_2 \sim 2\pi * 9.5\,\text{MHz}$ and the decay rate of the excited state

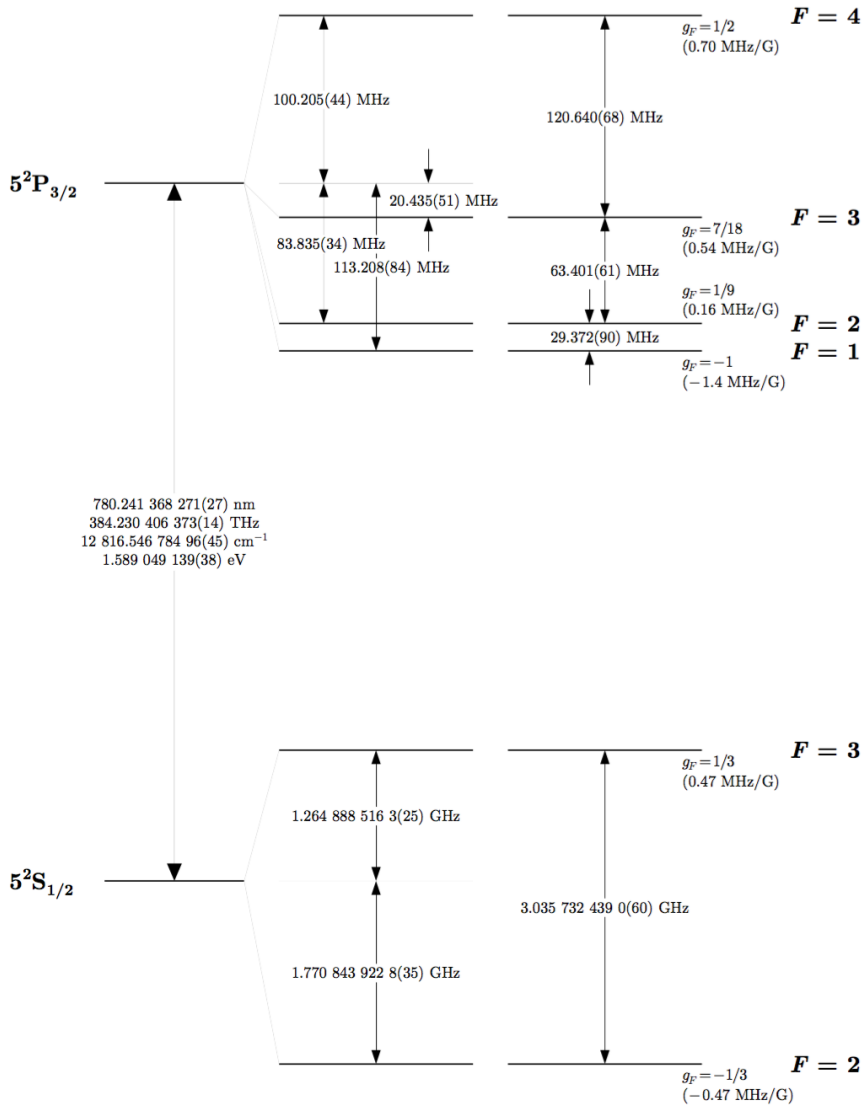

Figure 2.7. Rubidium 85 D_2 transition hyperfine structure, with frequency splittings between the hyperfine energy levels.

is $\Gamma = 2\pi * 6.066\,\text{MHz}$. The conditions $|\delta_1|, |\delta_2| \gg |\Omega_1|, |\Omega_2|, \Gamma$ are easily met. The Raman-Rabi frequency for the reduced system is $\Omega \sim 2\pi * 30\,\text{kHz}$. I shall say all the aforementioned phenomena, Raman-Rabi oscillations, Raman peaks and Raman-Ramsey fringes have been

observed. The results are in good agreement with predictions (Eq. (2.22) and Eq. (2.49)) derived in the previous section and will be presented in the following chapters.

2.2. Atomic Interaction with Static Magnetic Fields

2.2.1. Atomic Fine and Hyperfine Structures

From quantum mechanics, the electron state in an atom is described by a set of quantum numbers, which are the principal quantum number n, the azimuthal quantum number l, the magnetic quantum number m and the spin quantum number s. The principal quantum number n represents the relative overall energy of the electron orbital. The sets of orbitals with the same n value are often referred to as electron shells. The azimuthal quantum number l determines the angular momentum and describes the shape of the electron orbital. The sets of orbitals with the same n and l values are referred to as subshells. The magnetic quantum number m distinguishes the orbitals available within a subshell and is used to calculate the azimuthal component of the orientation of the orbital in space. Lastly the spin quantum number s is used to parameterize the intrinsic angular momentum (or spin) of the electron.

The energy levels described by the above quantum numbers are called the gross structure of the atom. It turns out that these energy levels are split to form the fine structure as a result of the coupling between the orbital angular momtemum $\mathbf{L}$ of the outer electron and its spin angular momentum $\mathbf{S}$. The total electron angular momentum will be given by $\mathbf{J} = \mathbf{L}+\mathbf{S}$ and the corresponding quantum number J must lie in the range $|L - S| \leq J \leq L + S$. Here we use the convention that the magnitude of L, S and J are $\sqrt{L(L+1)}\hbar$, $\sqrt{S(S+1)}\hbar$ and $\sqrt{J(J+1)}\hbar$, respectively. For the ground state in ^{85}Rb, $L = 0$ and $S = 1/2$, so $J = 1/2$; for the first excited state, $L = 1$, so $J = 1/2$ or $J = 3/2$. The energy of any particular level is

shifted according to the value of J, so the $L = 0 \longrightarrow L = 1$ (D line) transition is split into two components, the D_1 line ($5\,^2S_{1/2} \longrightarrow 5\,^2P_{1/2}$) and the D_2 line ($5\,^2S_{1/2} \longrightarrow 5\,^2P_{3/2}$). The energy levels are labeled according to the following rules: the first number is the principal quantum number n of the outer electron, the superscript is $2S + 1$, the letter refers to L (i.e., $S \leftrightarrow L = 0$, $P \leftrightarrow L = 1$, etc.), and the subscript gives the value of J. The D_2 line is shown in Fig. 2.7 and the D_1 line in Fig. 2.8. If we now take into account the coupling of the total electron angular momentum $\mathbf{J}$ with the total nuclear angular momentum $\mathbf{I}$, the energy levels will be split further to form the hyperfine structure. The total atomic angular momentum $\mathbf{F}$ is then given by $\mathbf{F} = \mathbf{J} + \mathbf{I}$ and as before, the magnitude of $\mathbf{F}$ can take the values $|J - I| \leq F \leq J + I$. For the ^{85}Rb ground state, $J = 1/2$ and $I = 5/2$, so $F = 2$ or $F = 3$. For the excited state of the D_2 line ($5\,^2P_{3/2}$), F can take any of the values 1, 2, 3, or 4, and for the D_1 excited state ($5\,^2P_{1/2}$), F is either 2 or 3. Again, the atomic energy levels are shifted according to the value of F. These hyperfine levels can be seen in Fig. 2.7 and Fig. 2.8.

2.2.2. Zeeman Effect and Zeeman Sublevels

Each of the hyperfine (F) energy levels contains $2F + 1$ magnetic sublevels that determine the angular distribution of the electron wave function. In the absence of external magnetic fields, these sublevels are degenerate. However, when an external magnetic field is applied, their degeneracy is broken. The Hamiltonian describing the atomic interaction with the magnetic field is

$$H_B = \frac{\mu_B}{\hbar}(g_S\mathbf{S} + g_L\mathbf{L} + g_I\mathbf{I}) \cdot \mathbf{B} \tag{2.59}$$

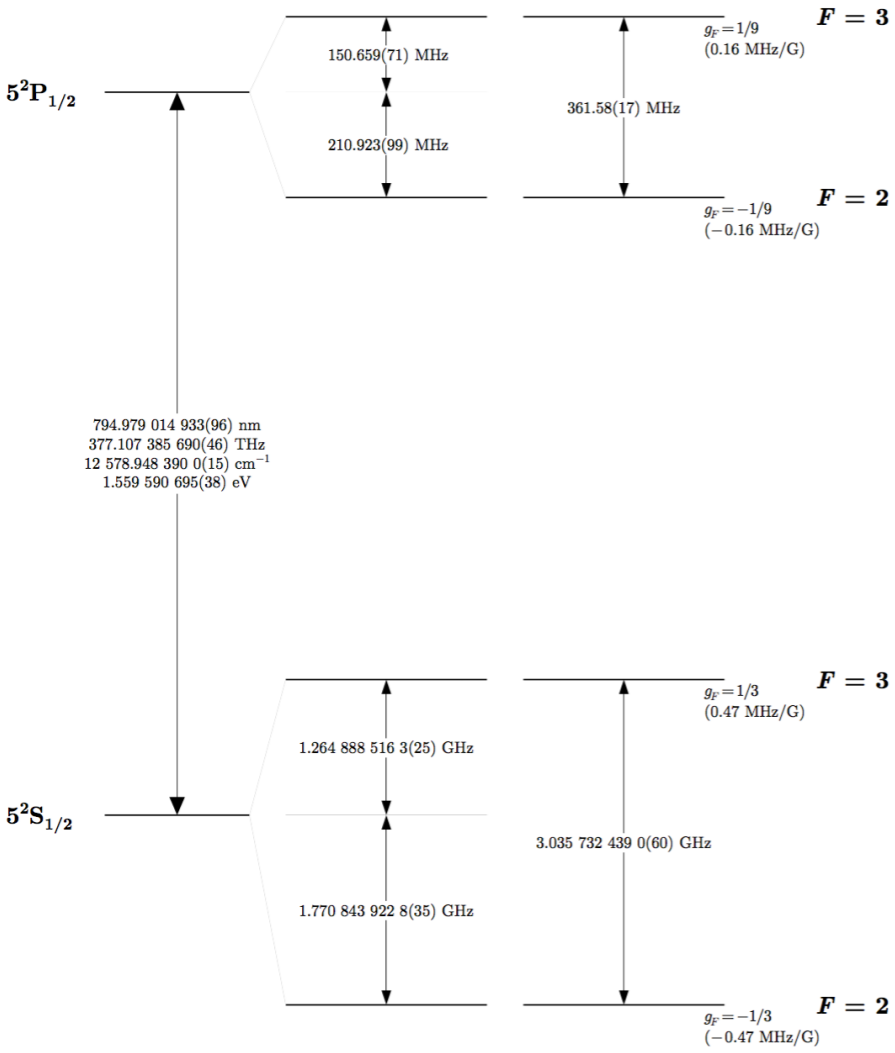

Figure 2.8. Rubidium 85 D_1 transition hyperfine structure, with frequency splittings between the hyperfine energy levels.

where μ_B is the Bohr magneton and the quantities g_S, g_L, and g_I are respectively the electron spin, electron orbital, and nuclear "g-factors" that account for various modifications to the corresponding magnetic dipole moments. Eq. (2.59) represents the interaction between the atomic magnetic dipole moment and the external magnetic field.

If the energy shift due to the magnetic field is small compared to the fine-structure splitting, the fine-structure Hamiltonian H_{fs} describing the coupling of $\mathbf{L}$ and $\mathbf{S}$ dominates H_B and J will be a good quantum number. In this case, H_B can be rewritten as

$$H_B = \frac{\mu_B}{\hbar}(g_J\mathbf{J} + g_I\mathbf{I}) \cdot \mathbf{B} \tag{2.60}$$

where $g_J = g_L\frac{J(J+1)-S(S+1)+L(L+1)}{2J(J+1)} + g_S\frac{J(J+1)-L(L+1)+S(S+1)}{2J(J+1)}$ is the "g-factor" for the total electron angular momentum.

If the energy shift due to the magnetic field is small compared to the hyperfine-structure splitting, then the hyperfine-structure Hamiltonian H_{hfs} describing the coupling of $\mathbf{J}$ and $\mathbf{I}$ dominates H_B and similarly F will be a good quantum number. In this case, H_B becomes

$$H_B = \frac{\mu_B}{\hbar}g_F\mathbf{F} \cdot \mathbf{B} = \frac{\mu_B}{\hbar}g_F(F_xB_x + F_yB_y + F_zB_z) \tag{2.61}$$

where $g_F = g_J\frac{F(F+1)-I(I+1)+J(J+1)}{2F(F+1)} + g_I\frac{F(F+1)-J(J+1)+I(I+1)}{2F(F+1)}$ is the "g-factor" for the total atomic angular momentum.

Here we assume the magnetic fields are weak such that the interaction Hamiltonian H_B perturbs the zero-field eigenstates of H_{hfs}. To lowest order, the levels split linearly according to [**56**]

$$\Delta E_{|F,m_F\rangle} = \mu_B g_F m_F B_z \tag{2.62}$$

where m_F is the magnetic quantum number corresponding to F_z and we have taken the magnetic field to be along the z-direction (i.e., along the atomic quantization axis). The splitting in this regime is called the Zeeman effect and the split levels are referred to as Zeeman sublevels. For ^{85}Rb, the corresponding splittings between adjacent magnetic sublevels

of the ground state, the D_1 excited state and the D_2 excited state are given in Fig. 2.9, Fig. 2.10 and Fig. 2.11, respectively.

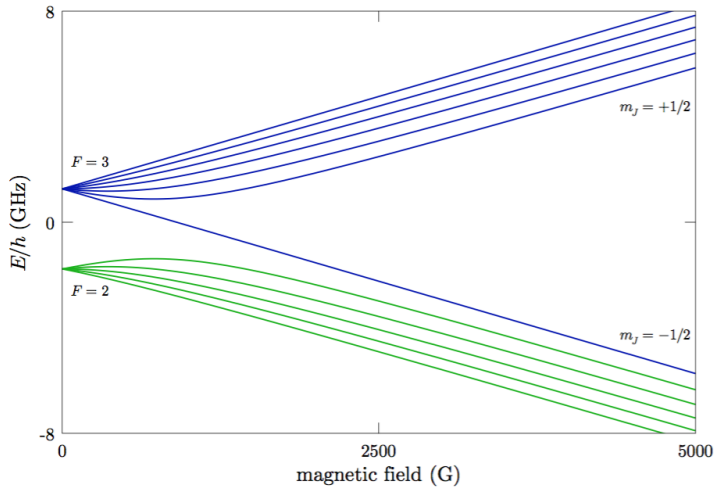

Figure 2.9. Rubidium 85 $5\,^2S_{1/2}$ (ground) level hyperfine structure in an external magnetic field.

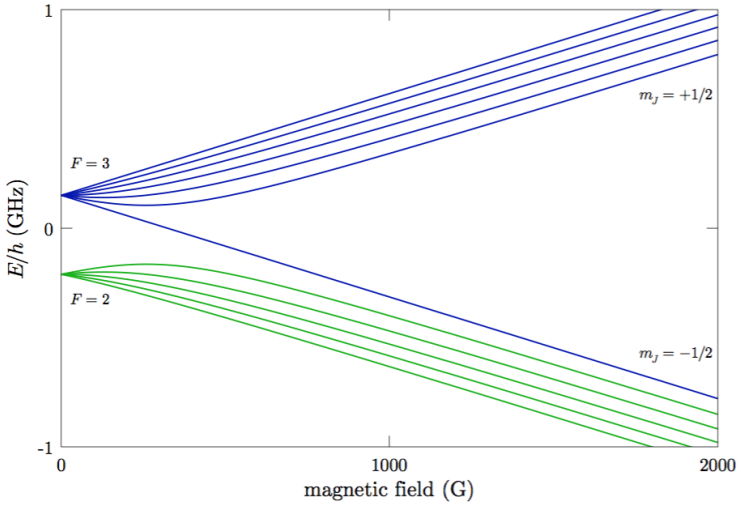

Figure 2.10. Rubidium 85 $5\,^2P_{1/2}$ (D_1 excited) level hyperfine structure in an external magnetic field.

In the more general case when the direction of the magnetic field is not necessarily aligned with the atomic quantization axis, the interaction Hamiltonian H_B is given by Eq. (2.61).

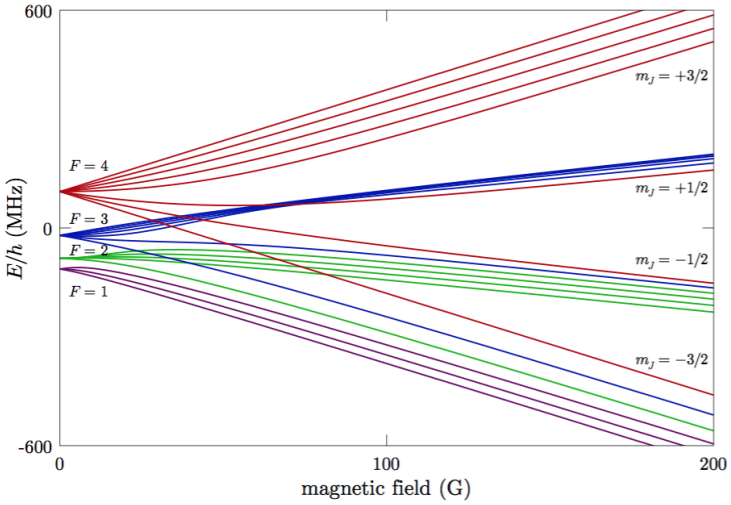

Figure 2.11. Rubidium 85 $5\,^2P_{3/2}$ (D_2 excited) level hyperfine structure in an external magnetic field.

In the basis formed by the Zeeman sublevels $|F, m_F\rangle$, the matrix elements of H_B will be

(2.63)

$$\langle F, m_F^{'}|H_B|F, m_F\rangle = \frac{\mu_B}{\hbar} g_F \Big(B_x \langle F, m_F^{'}|F_x|F, m_F\rangle + B_y \langle F, m_F^{'}|F_y|F, m_F\rangle + B_z \langle F, m_F^{'}|F_z|F, m_F\rangle \Big)$$

Since $F_z |F, m_F\rangle = \hbar m_F |F, m_F\rangle$, the last term can be written as

$$\langle F, m_F^{'}|F_z|F, m_F\rangle = \hbar m_F \delta_{m_F^{'}, m_F} \tag{2.64}$$

To evaluate the first two terms, we refer to the raising and lowering operators

$$F_+ |F, m_F\rangle = \hbar\sqrt{F(F+1) - m_F(m_F+1)}\,|F, m_F+1\rangle \tag{2.65a}$$

$$F_- |F, m_F\rangle = \hbar\sqrt{F(F+1) - m_F(m_F-1)}\,|F, m_F-1\rangle \tag{2.65b}$$

where $F_+ \equiv F_x + iF_y$ and $F_- \equiv F_x - iF_y$. Rearranging the terms, $F_x = (F_+ + F_-)/2$ and $F_- = (F_+ - F_-)/(2i)$. Using these expressions, we can get

(2.66a)

$$\langle F, m_F^{'}|F_x|F, m_F\rangle = \frac{\hbar}{2}\sqrt{F(F+1) - m_F(m_F+1)}\delta_{m_F^{'},m_F+1} + \frac{\hbar}{2}\sqrt{F(F+1) - m_F(m_F-1)}\delta_{m_F^{'},m_F-1}$$

(2.66b)

$$\langle F, m_F^{'}|F_y|F, m_F\rangle = -\frac{i\hbar}{2}\sqrt{F(F+1) - m_F(m_F+1)}\delta_{m_F^{'},m_F+1} + \frac{i\hbar}{2}\sqrt{F(F+1) - m_F(m_F-1)}\delta_{m_F^{'},m_F-1}$$

Substituting Eqs. (2.64), (2.66a) and (2.66b) into Eq. (2.63) yields

(2.67)

$$\begin{aligned}\langle F, m_F^{'}|H_B|F, m_F\rangle = \mu_B g_F\Big(&B_z m_F \delta_{m_F^{'},m_F} + \\ &B_x\Big(\frac{1}{2}\sqrt{F(F+1) - m_F(m_F+1)}\delta_{m_F^{'},m_F+1} + \frac{1}{2}\sqrt{F(F+1) - m_F(m_F-1)}\delta_{m_F^{'},m_F-1}\Big) + \\ &B_y\Big(\frac{-i}{2}\sqrt{F(F+1) - m_F(m_F+1)}\delta_{m_F^{'},m_F+1} + \frac{i}{2}\sqrt{F(F+1) - m_F(m_F-1)}\delta_{m_F^{'},m_F-1}\Big)\Big)\end{aligned}$$

2.3. Summary

In this chapter, we have reviewed the fundamentals of interactions between atomic systems and external fields. In particular, we have introduced two-level and three-level atomic systems, for which we derived the Hamiltonian and studied their dynamics. These two atomic models will be used extensively in the following chapters when we discuss collective states and spin squeezing, as well as their applications to atomic clocks and atomic interferometers.

CHAPTER 3

Collective State Effects and Its Applications to Atomic Clocks and Interferometers

3.1. Introduction

One important factor for measuring the performance of atomic metrological devices, such as atomic clocks, atomic magnetometers or atomic interferometers, is their sensitivity, which is characterized by the quantum phase fluctuation (QPF). Generally speaking, the QPF will depend on the line width of the signal, ϱ, and the signal to noise ratio (SNR). The smaller ϱ and the larger the SNR is, the smaller the QPF will be, and correspondingly the better the device will be. Though it is possible to improve the sensitivity by reducing the line width ϱ (such as switching from single-zone Raman interaction to three-zone Ramsey interaction for an atomic clock), the more traditional way would be using an ensemble of non-interacting atoms to enhance the SNR due to its simple experimental implementation. However, the optimal QPF obtainable by this method is constrained by the standard quantum limit (SQL), under which the QPF scales as $1/\sqrt{N}$ [**22**], with N being the number of atoms in the ensemble. To surpass the SQL, one has to introduce entanglement among the atoms, and a key goal in this context is to achieve the Heisenberg Limit (HL), under which the QPF scales as $1/N$, representing an improvement by a factor of $\sqrt{N}$.

There are two approaches for generating entanglement within a large ensemble of atoms: one-axis-twist (OAT) spin squeezing [**12**] and two-axis-counter-twist (TACT) spin squeezing [**12**]. Both will turn the ensemble into a spin squeezed state (SSS) [**12**]. Since the SSS

is a collective effect of all atoms within the ensemble, the system is best described by the so-called collective states [**57**]. In this chapter, we present the mathematical descriptions of the collective states, then discuss its applications to atomic clocks. In particular, we show that by switching the detection scheme from individual atomic states to collective states, the line width of the signal can be reduced by a factor of $\sqrt{N}$ [**58**], strongly violating the conventional transit time limit of spectroscopic resolution, though the sensitivity remains the same (at SQL). In the next chapter, we will show that OATS in combination with collective state detection can eventually enhance the sensitivity to the HL.

3.2. Mathematical Descriptions of the Collective States

3.2.1. Hamiltonian of the Atomic Ensemble

The system considered here consists of a collection of non-interacting identical atoms that interact with a laser field of uniform intensity over the atomic ensemble. Each atom is modeled as having two energy levels, $|1\rangle$ and $|2\rangle$, as detailed in Sec. 2.1.1. The Hamiltonian for the l-th atom under the electric dipole and rotating wave approximations, and the rotating wave transformation, can be written as

$$H_l = \hbar \begin{bmatrix} \frac{\delta}{2} & \frac{\Omega}{2} \\ \frac{\Omega}{2} & \frac{-\delta}{2} \end{bmatrix} = H_{0l} + H_{1l} \tag{3.1}$$

where Ω is the Rabi frequency and δ is the laser detuning. Note that the Hamiltonian H_l can be broken up into two parts such that $H_l = H_{0l} + H_{1l}$, where we have defined

$$H_{0l} \equiv \frac{\hbar\delta}{2}\begin{bmatrix} 1 & 0 \\ 0 & -1 \end{bmatrix} = \hbar\delta\frac{\sigma_{zl}}{2} = \hbar\delta j_{zl} \tag{3.2a}$$

$$H_{1l} \equiv \frac{\hbar\Omega}{2}\begin{bmatrix} 0 & 1 \\ 1 & 0 \end{bmatrix} = \hbar\Omega\frac{\sigma_{xl}}{2} = \hbar\Omega j_{xl} \tag{3.2b}$$

where $\mathbf{j}_l \equiv (j_{xl}, j_{yl}, j_{zl}) = \frac{1}{2}(\sigma_{xl}, \sigma_{yl}, \sigma_{zl})$, with $\{\sigma_{xl}, \sigma_{yl}, \sigma_{zl}\}$ being the Pauli matrices for the l-th atom. The total Hamiltonian of the system consisting of N atoms then is given by

$$H = \sum_{l=1}^{N} H_l = \sum_{l=1}^{N}(H_{0l} + H_{1l}) = H_0 + H_1 \tag{3.3}$$

where we have defined

$$H_0 = \sum_{l=1}^{N} H_{0l} = \sum_{l=1}^{N} \hbar\delta j_{zl} = \hbar\delta J_z \tag{3.4a}$$

$$H_1 = \sum_{l=1}^{N} H_{1l} = \sum_{l=1}^{N} \hbar\Omega j_{xl} = \hbar\Omega J_x \tag{3.4b}$$

where $\mathbf{J} \equiv (J_x, J_y, J_z) = (\sum_{l=1}^{N} j_{xl}, \sum_{l=1}^{N} j_{yl}, \sum_{l=1}^{N} j_{zl}) = \sum_{l=1}^{N} \mathbf{j}_l$. The J_x, J_y and J_z operators are known as collective spin operations. If we define the total spin operator $J^2 = {J_x}^2 + {J_y}^2 + {J_z}^2$ and the ladder operators $J_\pm = J_x \pm iJ_y$, then the following commutation rules hold true

$$[J_\alpha, J_\beta] = i\epsilon_{\alpha\beta\gamma}J_\gamma \tag{3.5a}$$

$$[J^2, J_\alpha] = 0 \tag{3.5b}$$

$$[J_z, J_\pm] = \pm J_\pm \tag{3.5c}$$

where α, β, γ denote the components in any three orthogonal directions, $\epsilon_{\alpha\beta\gamma}$ is the Levi-Civita symbol, and the i in the right hand side of Eq. (3.5a) is the imaginary unit.

3.2.2. Direct Product State As Basis

To solve for the time evolutions of the states of the atomic ensemble, the natural choice of basis would be the eigenstates of the H_0 operator, which are referred to as direct product states. Note that the eigenstates of the H_{0i} operator are given by $|1\rangle$ and $|2\rangle$ with eigenvalues $\hbar\delta/2$ and $-\hbar\delta/2$, resepectively, then the direct product states can be arranged as follows

$$
\begin{aligned}
&m = 0 : |2\rangle \otimes |2\rangle \otimes \ldots \otimes |2\rangle \\
&m = 1 : |1\rangle \otimes |2\rangle \otimes |2\rangle \otimes \ldots \otimes |2\rangle \,; |2\rangle \otimes |1\rangle \otimes |2\rangle \otimes \ldots \otimes |2\rangle \,; \ldots \\
&m = 2 : |1\rangle \otimes |1\rangle \otimes |2\rangle \otimes |2\rangle \otimes \ldots \otimes |2\rangle \,; |1\rangle \otimes |2\rangle \otimes |1\rangle \otimes |2\rangle \otimes \ldots \otimes |2\rangle \,; \ldots \\
&\ldots \\
&m = N : |1\rangle \otimes |1\rangle \otimes \ldots \otimes |1\rangle
\end{aligned}
\tag{3.6}
$$

where m is the number of atoms that are in state $|1\rangle$. Since each atom can be in either state $|1\rangle$ or state $|2\rangle$, and we have N atoms, the total number of direct product states is 2^N. It's easy to show that those direct product states with the same m value are degenerate, with energy level given by $E_m = (m - N/2)\hbar\delta$ and degeneracy given by $D_m = \binom{N}{m} = \frac{N!}{m!(N-m)!}$. These direct product states form a subspace with dimensionality of D_m.

If the system is initially prepared in the state where all atoms are in state $|2\rangle$ (i.e., $m = 0$), then the interaction Hamiltonian H_1 will couple the state with $m = 0$ to those with $m = 1$, and then couple those with $m = 1$ to those with $m = 2$, and so on. Eventually the system can evolve into any state with all possible m values, which renders it intractable to solve for

the dynamics of the system due to the large number of states involved. Therefore, though the direct product states are conceptually simple to understand, they are not suitable for ensembles with large number of atoms.

3.2.3. Collective State As Basis

As mentioned in the previous subsection, direct product states are not suitable for solving the dynamics of ensembles with large number of atoms. A more useful basis consists of the so-called collective states [**59**], which are common eigenstates of the J^2 and J_z operators. Since the J_x, J_y and J_z operators follow the same commutation rules as angular momentum operators, we can label these eigenstates as $|J, M\rangle$, where $J = N/2, N/2-1, \ldots, (J \geq 0)$, $M = -J, -J+1, \ldots, J$, and the J^2 and J_z operators have eignevalues of $J(J+1)$ and M, respectively.

Note that the interaction Hamiltonian $H_1 = \hbar\Omega J_x$ commutes with J^2, therefore, if the system is initially prepared in one of the subspaces with some particular J value, it will stay in that subspace. Moreover, H_1 can be rewritten as $H_1 = \hbar\Omega(J_+ + J_-)/2$, so only states with adjacent M values in this subspace will be coupled by the interaction Hamiltonian. Since the dimension of the subspace with specific J value can be much smaller than that of the whole Hilbert space, this can simplify the descriptions of the ensemble substantially and make it possible to study the time evolutions of the whole system.

The collective states can be expressed as linear combinations of the direct product states. First, for each subspace with some particular J value, if we can obtain the maximally polarized state, then all other states within that same subspace can be generated by applying the lowering operator J_- repeatedly. Second, the eigenstate $|J, M\rangle$ has an energy level of $\hbar\delta M$, then it must belong to the subspace of $m = N/2 + M$ in terms of direct product states (see

Eq. (3.6)), which implies $|J, M\rangle$ can be written as linear combinations of the basis for the $m = N/2 + M$ subspace. Following these two rules, the collective states for the $J = N/2$ subspace are found as follows

$$
\begin{aligned}
&|E_0\rangle \equiv |2, 2, \ldots, 2, 2\rangle \\
&\ldots \\
&|E_n\rangle \equiv \binom{N}{n}^{-\frac{1}{2}} \sum_{k=1}^{\binom{N}{n}} \mathcal{P}_k \left| 2^{\otimes(N-n)} \bigotimes 1^{\otimes n} \right\rangle \\
&\ldots \\
&|E_N\rangle \equiv |1, 1, \ldots, 1, 1\rangle
\end{aligned}
\tag{3.7}
$$

corresponding to $M = -N/2, -N/2+1, -N/2+2, \ldots, N/2-1, N/2$, respectively. Here $\mathcal{P}_k$ is the permutation operator [**57**], and the summation is done over all the different permutations of $(N - n)$ 2's and n 1's, so that $|E_n\rangle$ is a normalized equal superposition all direct product states within the $m = n$ subspace ($n = 0, 1, \ldots, N$). These collective states are known as Dicke Collective States (DCS's). They are also referred to as symmetric collective states (SCS's), since they are totally symmetric under permutations of any pair of atoms. All other collective states are referred to as asymmetric collective states (ACS's) and there are $2^N - (N + 1)$ of them. These ACS's can be obtained by applying either the Gram-Schmidt Orthogonalization process or a series of rotations within each of the direct product state subspaces of different m values [**57, 60**].

Usually the system is initially prepared with all atoms in state $|1\rangle$, corresponding to collective state $|E_N\rangle$ within the $J = N/2$ subspace. Thus under ideal conditions (homogeneous laser field, negligible center of mass motion, etc.), the interaction Hamiltonian H_1 will not

couple SCS's to ACS's, and solving the dynamics of the whole system can be done using the SCS's as basis states. For all the following discussions in this thesis, we assume this is the case unless explicitly specified otherwise. However, it should be noted that it is possible for SCS's to evolve into ACS's and the readers are referred to [**57, 60**] for more detailed discussions.

3.3. Applications to Atomic Clocks

In the previous section, we have presented a brief mathematical description of the collective states (symmetric collective states in particular). In this section, we will show how they can be applied to atomic clocks to produce fringes that are narrowed by a factor of $\sim \sqrt{N}$ compared to that of a conventional atomic clock, which strongly violates the conventional transit time limit of spectroscopic resolution. In the next section, we show the same effects can be observed for an atomic interferometer.

3.3.1. Conventional Raman-Ramsey Atomic Clocks

Here we consider an ensemble consisting of N non-interacting three-level atoms, where the ground states, $|1\rangle$ and $|2\rangle$ interact with an excited state $|3\rangle$ via two co-propagating laser beams, as shown in Fig. 2.6. One of the two laser beams is detuned from resonance by δ_1 and has a Rabi frequency Ω_1; this couples state $|1\rangle$ to state $|3\rangle$. The other beam is detuned from resonance by δ_2 and has a Rabi frequency Ω_2; this couples state $|2\rangle$ to state $|3\rangle$. For $\delta \gg \Omega_1, \Omega_2, \Gamma$, where $\delta = (\delta_1 + \delta_2)/2$ and Γ is the excited state decay rate, each atom can be modeled as an effective two-level system, consisting of states $|1\rangle$ and $|2\rangle$, excited by a traveling wave with a Rabi frequency $\Omega = \Omega_1\Omega_2/(2\delta)$, and detuning $\Delta = \delta_1 - \delta_2$, so that the ensemble can be seen as a collection of N non-interacting two-level atoms.

The ensemble is initially prepared in the state where all atoms are in state $|2\rangle$. Then it undergoes a sequence of $\pi/2$-dark-$\pi/2$ pulses similar to Fig. 2.3. The final state of the ensemble can be written as

$$|\psi\rangle = \bigotimes_{i=1}^{N} \frac{1}{2}\Big[(1 - e^{i\phi})\,|2\rangle - i(1 + e^{i\phi})\,|1\rangle\Big] \tag{3.8}$$

where $\phi = \Delta T_D = 2\pi f T_D$ is the phase accumulated in the dark zone, $f = \Delta/2\pi$ is the (two-photon) detuning of the clock in Hertz, and T_D is the dark zone duration. For a conventional Raman-Ramsey atomic clock (RRAC), the population of atoms in state $|1\rangle$ is measured. Note that for each atom, the probabilty of finding it in state $|1\rangle$ is given by $P_1 = \cos^2(\phi/2)$. Since all the atoms are independent from each other, the signal for a Raman-Ramsey atomic clock is then given by

$$S_{RRAC} = \sum_{i=1}^{N}(P_1) = N\cos^2(\phi/2) \tag{3.9}$$

The signal S_{RRAC} as a function of f for the case of $N = 1$ is shown in Fig. 3.1 by the blue trace. For other values of N, the shape of the signal will be similar except for the amplitude, which is proportional to N.

3.3.2. Collective State Atomic Clocks

A collective state atomic clock (COSAC) is exactly the same as a conventional Raman-Ramsey atomic clock except for the detection scheme. That is, we still have an ensemble of N non-interacting effective two-level atoms. The atoms are all initialized in state $|2\rangle$ and will undergo the usual $\pi/2$-dark-$\pi/2$ pulse sequence. The final state of the system is again given by Eq.(3.8). But now instead of measuring the population of atoms in state $|1\rangle$, we

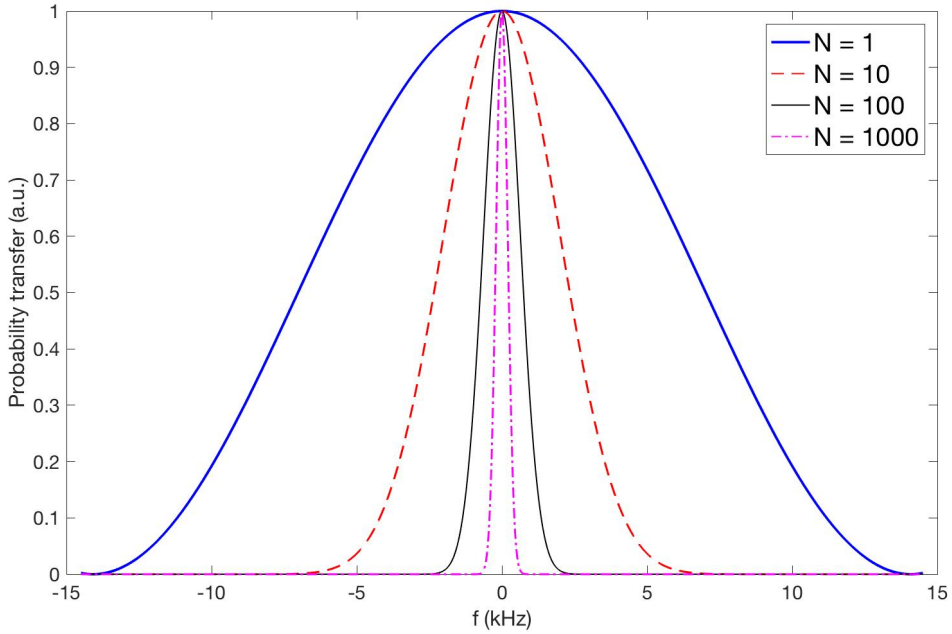

Figure 3.1. Signal of a collective state atomic clock as a function of f for different values of N, where $\Omega = 2\pi * 30\,\mathrm{kHz}, \Omega T_{\pi/2} = \pi/2, T_D = 3T_{\pi/2}$.

will measure the population of the collective state $|E_N\rangle$, corresponding to the direct product state where all atoms are in state $|1\rangle$. Note that the probability of finding the ensemble in state $|E_N\rangle$ can be obtained by simple projection: $|\langle E_N|\psi\rangle|^2$, therefore we have

$$S_{COSAC} = |\langle E_N|\psi\rangle|^2 = [\cos^2(\phi/2)]^N = (P_1)^N \tag{3.10}$$

The signal S_{COSAC} is plotted as a function of f in Fig. 3.1 for different values of N. We can clearly see that the linewidth of the fringe as a function of f decreases as N increases. The value of the linewidth, defined as the full width half maximum (FWHM), is given by $\varrho(N) = 2\arccos\left(2^{-1/(2N)}\right)$ [**58**]. The derivative of $[\varrho(1)/\varrho(N)]^2$ with respect to N, for $N \gg 1$, approaches the value of $0.8899 + O(N^{-3/2})$, which can be verified with a linear fit

to $[\varrho(1)/\varrho(N)]^2$. To a good approximation, $\varrho(N)/\varrho(1) \approx 1/\sqrt{N}$. Note that $\varrho(1) \simeq 1/T_D$ is understood to be the transit time limited linewidth, then $\varrho(N) = \varrho(1)/\sqrt{N}$ implies a strong violation of the transit time limit when $N \gg 1$.

3.3.3. Detection Scheme for Collective States

While measuring the population of atoms in state $|1\rangle$ can be as straightforward as first using a probe laser coupling it to some higher energy state and then collecting fluorescence from that higher level, detecting the population of the collective state $|E_N\rangle$ is very different and more difficult. The signature of the collective state $|E_N\rangle$ is that all atoms are in state $|1\rangle$. The usual detection scheme using a probe to couple state $|1\rangle$ to higher energy state won't work anymore since the probe will also see other collective states where only a fraction of atoms are in state $|1\rangle$, such as $|E_{N-1}\rangle, |E_{N-2}\rangle, \ldots, |E_1\rangle$, etc. Fortunately there is an alternative way viewing the collective state $|E_N\rangle$: absence of atoms in state $|2\rangle$. Therefore for a given collective state, if we cannot detect the presence of any atom in state $|2\rangle$, then we can say for sure the given collective state is $|E_N\rangle$. This leads to the following null detection scheme [**58**] for measuring the population of $|E_N\rangle$, as shown in Fig. 3.2.

For the null detection scheme, the probe is the one of the two Raman beams used to drive the transition from state $|2\rangle$ to state $|3\rangle$. If the atomic ensemble is not in the desired collective state (that is, $|E_N\rangle$), then the probe will induce Raman transitions within the ensemble. As a result, there will be photons emitted corresponding to the other leg of the Raman transition. In the bad cavity limit, the emitted photons will not be reabsorbed by the atomic system. The beam consisting of the probe and the emitted photons is then sent to a high speed detector, which produces a dc voltage as well as a beat signal with frequency matching the energy difference between states $|1\rangle$ and $|2\rangle$ (divided by the Planck constant).

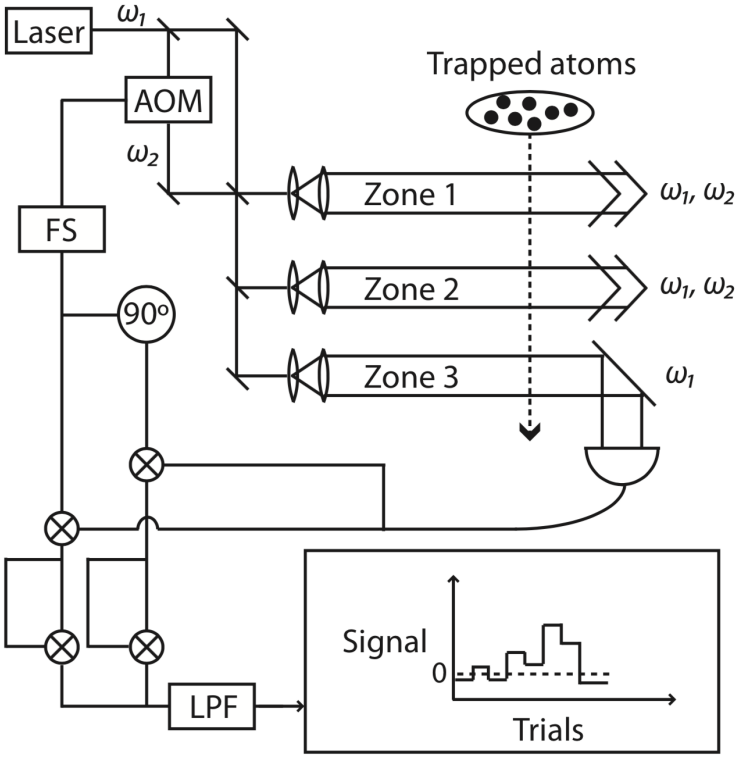

Figure 3.2. Raman-Ramsey fringe experiment for an ensemble of Λ-type atoms for the detection of collective state $|E_N\rangle$. Atoms are released from the trap, and the experiment is performed while they are free falling inside the vacuum chamber. They interact with two $\pi/2$ pulses (each pulse consisting of two co-propagating Raman beams), which are separated in time by T_D, and are probed by one of the two Raman beams. The probe induces a unidirectional Raman transition in the atoms while producing photons in the direction of the probe. The combined signal from the probe and emitted photons are multiplied with the frequency produced by the frequency synthesizer in such a way that the resulting signal will be proportional to the number of photons detected. Determining the threshold of the zero emission signal, and counting how many trials result in zero emission, the histogram can be built to produce signals in Fig. 3.1.

The phase of this beat signal is unknown. As such, the total signal is sent in two different paths, one to be multiplied by the frequency synthesizer (FS) signal and another to be multiplied by the FS signal shifted in phase by 90° (note that the two beams used to drive

the Raman transition are generated from the same laser source using frequency synthesizers). Each of these signals is squared, then combined and sent through a low pass filter (LPF) to extract the dc voltage that is proportional to the number of scattered photons. A voltage reading above a predetermined threshold value will indicate the presence of emitted photons during the interrogation period. If no photon emission occurs and the voltage reads below the threshold, this indicates that the atoms are all in state $|1\rangle$ and the collective state of the system is $|E_N\rangle$. For any other collective state, at least one photon will be emitted. For a given value of f (or Δ), this process is repeated m times (where the choice of m would depend on the temporal granularity of interest). The fraction of events corresponding to detection of no photons would represent the signal for this value of f. The process is now repeated for a different value of f, thus enabling one to produce the clock signal as a function of f. Usual techniques of modulating the detuning and demodulating the signal can be used to produce the error signal for stabilizing the FS, thus realizing the COSAC.

3.4. Applications to Atomic Interferometers

In this section, we will show how collective states can be applied to atomic interferometers to produce fringes that are narrowed by a factor of $\sim \sqrt{N}$ compared to that of a conventional atomic interferometer.

3.4.1. Conventional Raman Atomic Interferometers

The building block of a conventional Raman atom interferometer (CRAIN) is a three-level atom, with two metastable states $|g, p_z = 0\rangle \equiv |g, 0\rangle$ and $|e, p_z = \hbar(k_1 + k2)\rangle \equiv |e, \hbar k\rangle$ and an excited state $|a, p_z = \hbar k_1\rangle \equiv |a, \hbar k_1\rangle$ coupled by two counterpropagating beams (with wavevectors k_1 and k_2, respectively), with a single-photon detuning δ, as shown in Fig. 3.3(a).

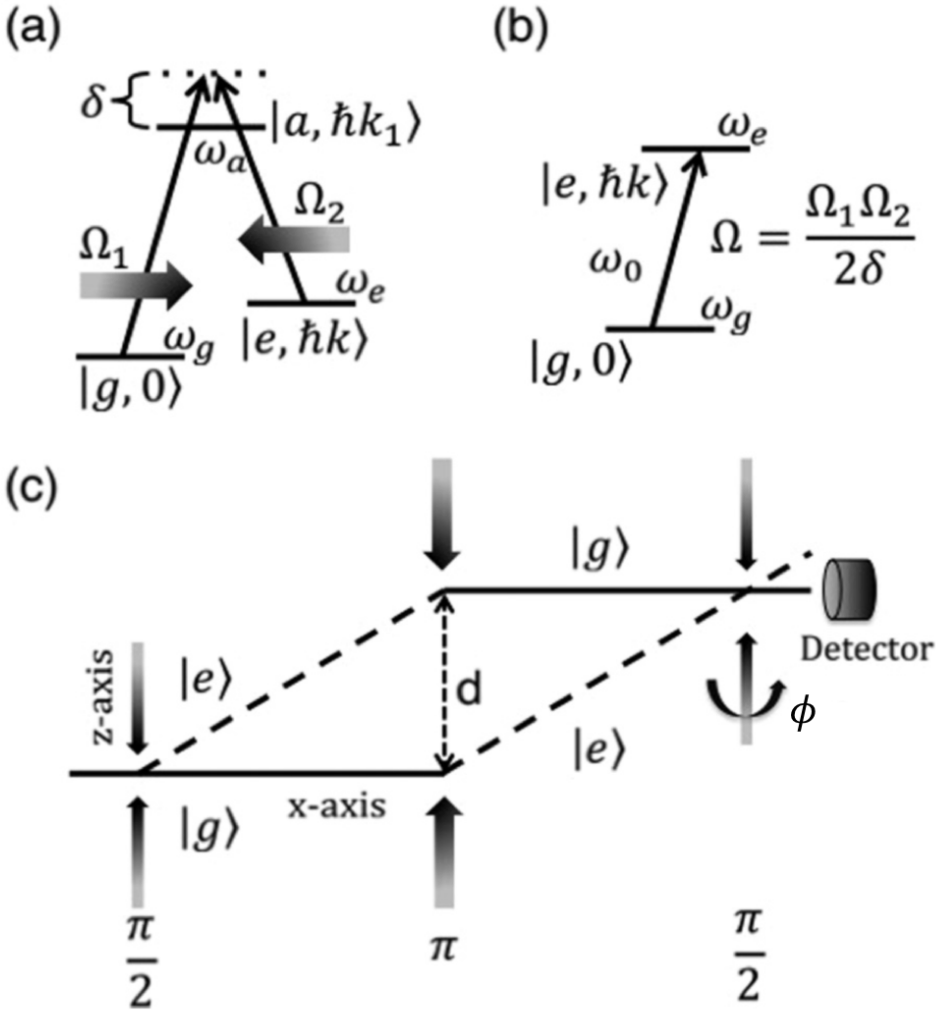

Figure 3.3. Schematic diagram for a conventional atomic interferometer. (a) A three-level atom. (b) An equivalent reduced two-level atom model. (c) A CRAIN produced via $\pi/2$-dark-π-dark-$\pi/2$ sequence of excitation.

One of the beams, with Rabi frequency Ω_1, couples $|g,0\rangle$ to $|a,\hbar k_1\rangle$, while the other beam, with Rabi frequency Ω_2, couples $|a,\hbar k_1\rangle$ to $|e,\hbar k\rangle$. For $\delta \gg \Omega_1, \Omega_2$, the interaction can be described as an effective two-level system excited by an effective traveling wave with a momentum $\hbar k = \hbar(k_1 + k_2)$, with a Rabi frequency $\Omega = \Omega_1\Omega_2/(2\delta)$ [**61, 62**], as shown in

Fig. 3.3(b). We assume that $\delta \gg \Gamma$, where Γ is the decay rate of the excited state $|a\rangle$, so that the effect of Γ can be neglected. Under a sequence of $\pi/2$-dark-π-dark-$\pi/2$ pulses, the wave packet first separates into two components, then gets redirected, and finally recombines to produce an interference which is sensitive to any phase difference ϕ between the two paths, as shown in Fig. 3.3(c).

The ensemble is initially prepared in the state where all atoms are in state $|g,0\rangle$. After it undergoes the $\pi/2$-dark-π-dark-$\pi/2$ pulse sequence, the final state of the ensemble can be written as [**54, 63**]

$$|\psi\rangle = \bigotimes_{i=1}^{N} -\frac{1}{2} e^{-i\phi/2}\Big[(1+e^{i\phi})\,|g,0\rangle + i(1-e^{i\phi})\,|e,\hbar k\rangle\Big] \tag{3.11}$$

For a CRAIN, the population of atoms in state $|g,0\rangle$ is measured. Note that for each atom, the probabilty of finding it in state $|g,0\rangle$ is given by $P_g = \cos^2(\phi/2)$. Since all the atoms are independent from each other, the signal for a CRAIN is then given by

$$S_{CRAIN} = \sum_{i=1}^{N} (P_g) = N\cos^2(\phi/2) \tag{3.12}$$

The signal S_{CRAIN} as a function of ϕ for the case of $N = 1$ is shown in Fig. 3.4 by the blue trace. For other values of N, the shape of the signal will be similar except for the amplitude, which is proportional to N.

3.4.2. Collective State Atomic Interferometer

Similar to the case of an atomic clock, a collective state atomic interferometer (COSAIN) is exactly the same as a conventional Raman atomic interferometer except for the detection scheme. That is, we still have an ensemble of N non-interacting effective two-level atoms.

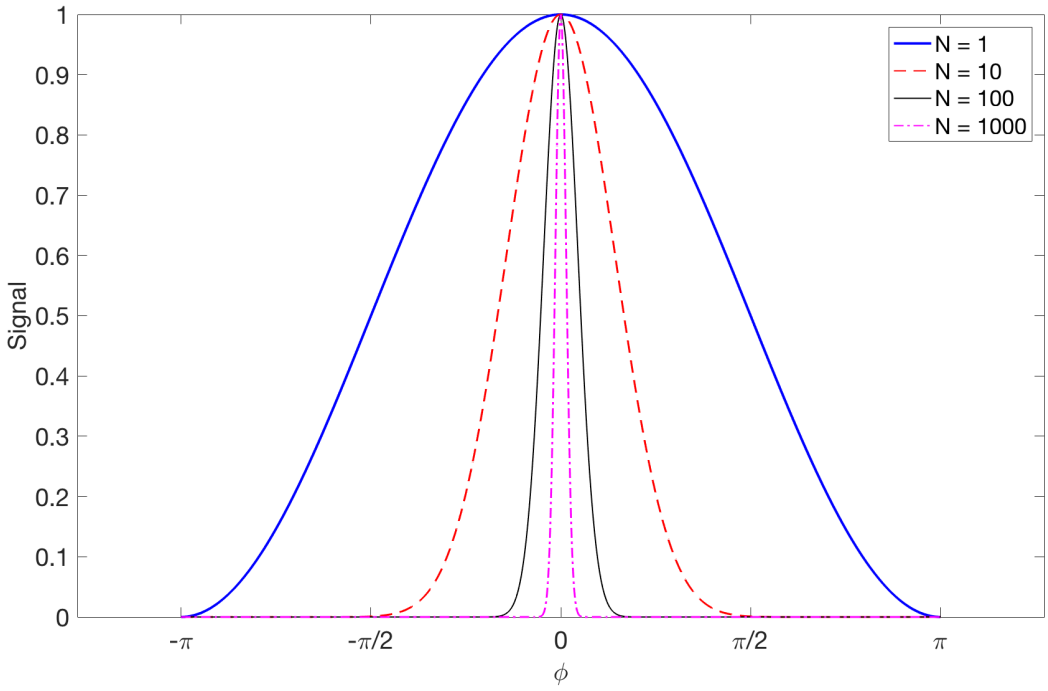

Figure 3.4. Signal of a collective state atomic interferometer (amplitude of $|E_0\rangle$) as a function of ϕ for different values of N.

The atoms are all initialized in state $|g,0\rangle$ and will undergo the usual $\pi/2$-dark-π-dark-$\pi/2$ pulse sequence. The final state of the system is again given by Eq.(3.11). But now instead of measuring the population of atoms in state $|g,0\rangle$, we will measure the population of the collective state $|E_0\rangle$, corresponding to the direct product state where all atoms are in state $|g,0\rangle$. Note that the probability of finding the ensemble in state $|E_0\rangle$ can be obtained by simple projection: $|\langle E_0|\psi\rangle|^2$, therefore we have

$$S_{COSAIN} = |\langle E_N|\psi\rangle|^2 = [\cos^2(\phi/2)]^N = (P_g)^N \tag{3.13}$$

The signal S_{COSAIN} is plotted as a function of ϕ in Fig. 3.4 for different values of N. We can clearly see that the fringe linewidth as a function of ϕ decreases with increasing N. We define this linewidth as the full width at half maximum (FWHM) of the signal fringe $\varrho(N) = 2\arccos\left(2^{-1/(2N)}\right)$ [**64**]. As is the case of atomic clock, we have verified that $\varrho(1)/\varrho(N) \approx \sqrt{N}$ for $N \gg 1$. Lastly, we point out that the signal measurements for a COSAIN can be done in a similar way as a COSAC, where a null detection scheme can be used to determine the population of atoms in the state $|E_0\rangle$.

3.5. Summary

In this chapter, we have presented a brief mathematical description of the collective states (Dicke collective states in particular), and shown their applications to a Raman-Ramsey atomic clock and a conventional Raman atomic interferometer, which produces signals with significant reduction in the fringe linewidth (by a factor of $\sqrt{N}$, with N the number of atoms in the ensemble). The signal is detected by measuring the amplitude of a collective state with a null detection scheme. Note that this chapter is only meant to introduce the basic concepts of collective states. For more thorough discussions of collective states, please refer to Refs. [**59, 57, 60**]; for more detailed dicussions of collective state atomic clocks, please refer to Refs. [**58, 65**]; for more detailed dicussions of collective state atomic interferometers, please refer to Refs. [**64, 60**].

CHAPTER 4

Review of Spin Squeezing

4.1. Introduction

As mentioned in the last chapter, one-axis-twist (OAT) spin squeezing [**12**] and two-axis-counter-twist (TACT) spin squeezing [**12**] can be used to suppress the quantum phase fluctuation beyond the standard quantum limit (SQL). In this chapter, we present an overview of the concepts of spin squeezing, which starts with a brief review of spin-1/2 systems and collective spin operators introduced in the previous chapter, then follows with descriptions of coherent spin states (CSS), and lastly transtions to discussions of spin squeezed states (SSS) and the two approaches used to generate SSS: OAT and TACT spin squeezings. A comprehensive review of the theoretical and experimental advancements in spin squeezing is given in [**66**].

4.2. Spin Representation of Atomic Ensembles

4.2.1. Spin-$\frac{1}{2}$ System

As demonstrated in Sec. 3.2.1, any two-level quantum system, regardless of its physical manifestations, can be modeled as a (pseudo) spin-1/2 particle, with states $\{|\uparrow\rangle, |\downarrow\rangle\}$. Any operator acting on this system can be expanded in the set of angular momentum operators

$\mathbf{j} = (j_x, j_y, j_z)$, as well as the identity matrix I_2 associated with the two-level system, where

$$j_x = \frac{(|\downarrow\rangle\langle\uparrow| + |\uparrow\rangle\langle\downarrow|)}{2} = \frac{\sigma_x}{2} \tag{4.1a}$$

$$j_y = \frac{i(|\downarrow\rangle\langle\uparrow| - |\uparrow\rangle\langle\downarrow|)}{2} = \frac{\sigma_y}{2} \tag{4.1b}$$

$$j_z = \frac{(|\uparrow\rangle\langle\uparrow| - |\downarrow\rangle\langle\downarrow|)}{2} = \frac{\sigma_z}{2} \tag{4.1c}$$

$$I_2 = (|\uparrow\rangle\langle\uparrow| + |\downarrow\rangle\langle\downarrow|) \tag{4.1d}$$

with $\{\sigma_x, \sigma_y, \sigma_z\}$ being Pauli matrices, and the states, $|\uparrow\rangle$ and $|\downarrow\rangle$, being eigenstates of the j_z operator. We define, for this spin-1/2 system, the atomic population operators for the spin-up and spin-down states, the ladder operators (raising and lowering operators), and the total spin operator as follows

$$n_\uparrow = |\uparrow\rangle\langle\uparrow| \tag{4.2a}$$

$$n_\downarrow = |\downarrow\rangle\langle\downarrow| \tag{4.2b}$$

$$j_\pm = j_x \pm i j_y \tag{4.2c}$$

$$j^2 = j_x^2 + j_y^2 + j_z^2 \tag{4.2d}$$

And the usual commutation rules for angualr momentum operators follow

$$[j_\alpha, j_\beta] = i\epsilon_{\alpha\beta\gamma} j_\gamma \tag{4.3a}$$

$$[j^2, j_\alpha] = 0 \tag{4.3b}$$

$$[j_z, j_\pm] = \pm j_\pm \tag{4.3c}$$

where α, β, γ denote the components in any three orthogonal directions, and $\epsilon_{\alpha\beta\gamma}$ is the Levi-Civita symbol.

4.2.2. Collective Spins

The discussion above can be generalized to an N-particle system where each particle can be modeled as a (pseudo) spin-1/2 system. The collective spin of the ensemble is the sum of individual spins, $\mathbf{J} = \sum_{l=1}^{N} \mathbf{j}_l = (J_x, J_y, J_z)$, where

$$J_x = \sum_{l=1}^{N} j_{xl} \tag{4.4a}$$

$$J_y = \sum_{l=1}^{N} j_{yl} \tag{4.4b}$$

$$J_z = \sum_{l=1}^{N} j_{zl} \tag{4.4c}$$

are the collective spin operators. Similarly we define the corresponding operators for the ensemble as follows

$$N_\uparrow = \sum_{l=1}^{N} (n_\uparrow)_l = \sum_{l=1}^{N} |\uparrow_l\rangle\langle\uparrow_l| \tag{4.5a}$$

$$N_\downarrow = \sum_{l=1}^{N} (n_\downarrow)_l = \sum_{l=1}^{N} |\downarrow_l\rangle\langle\downarrow_l| \tag{4.5b}$$

$$J_\pm = \sum_{l=1}^{N} (j_\pm)_l = \sum_{l=1}^{N} (j_{xl} \pm i j_{yl}) \tag{4.5c}$$

$$J^2 = \sum_{l=1}^{N} (j^2)_l = \sum_{l=1}^{N} (j_{xl}^2 + j_{yl}^2 + j_{zl}^2) \equiv J_x^2 + J_y^2 + J_z^2 \tag{4.5d}$$

And the usual commutation rules follow

$$[J_\alpha, J_\beta] = i\epsilon_{\alpha\beta\gamma} J_\gamma \tag{4.6a}$$

$$[J^2, J_\alpha] = 0 \tag{4.6b}$$

$$[J_z, J_\pm] = \pm J_\pm \tag{4.6c}$$

These commutation rules give rise to the Heisenberg uncertainty relation

$$\left\langle \Delta J_\alpha^2 \right\rangle \left\langle \Delta J_\beta^2 \right\rangle \geq \frac{1}{4} |\langle J_\gamma \rangle|^2 \tag{4.7}$$

where $\Delta J_\alpha^2 = \langle J_\alpha^2 \rangle - \langle J_\alpha \rangle^2$ is the variance of the measurement of the spin projection J_α for numerous iterations of identical preparations and measurements.

4.2.3. Direct Product States and Collective States As Basis

As discussed in Sec. 3.2, for an atomic ensemble interacting with homogeneous external laser fields, there are two sets of basis states we can choose for solving the dynamics of the system: direct product states and collective states. The latter is shown to be more appropriate under certain conditions when the asymmetric collective states are decoupled from the symmetric ones. In the following discussions, we will assume this is the case and focus exclusively on the symmetric collective states (also known as Dicke collective states). For convenience, we

redefine here the symmetric collective states in terms of direct product states

$$
\begin{aligned}
|E_0\rangle &\equiv \bigotimes_{k=1}^{N} |{\downarrow_k}\rangle = |{\downarrow},{\downarrow},\ldots,{\downarrow},{\downarrow}\rangle \\
&\ldots \\
|E_n\rangle &\equiv \binom{N}{n}^{-\frac{1}{2}\binom{N}{n}} \sum_{k=1} \mathcal{P}_k \left| {\downarrow}^{\otimes(N-n)} \bigotimes {\uparrow}^{\otimes n} \right\rangle \\
&\ldots \\
|E_N\rangle &\equiv \bigotimes_{k=1}^{N} |{\uparrow_k}\rangle = |{\uparrow},{\uparrow},\ldots,{\uparrow},{\uparrow}\rangle
\end{aligned}
\tag{4.8}
$$

where $\mathcal{P}_k$ is the permutation operator, and the summation is done over all the different permutations of $(N-n)$ $\downarrow$'s and n $\uparrow$'s.

Using the symmetric collective states as basis, the dynamics of the atomic ensemble can be expressed as unitary transformations related to the collective spin operators. For example, when the system interact with a laser field of uniform intensity over the atomic ensemble, the interaction Hamiltonian is given by $H_1 = \hbar\Omega J_x$, as shown in Eq. (3.4b). The corresponding unitary transformation will be $U(t) = \exp(-iH_1 t/\hbar) = \exp(-i\Omega t J_x)$. For a $\pi/2$-pulse, we have $\Omega t = \pi/2$, and the effective unitary transformation will be $\exp(-i\frac{\pi}{2}J_x)$; for a π-pulse, we have $\Omega t = \pi$, and the effective unitary transformation will be $\exp(-i\pi J_x)$. However, when the system is left in dark (no laser interaction), the Hamiltonian will be proportional to the J_z operator, and the corresponding unitary transformation can be written as $\exp(-i\phi J_z)$, where ϕ is the phase accumulated by the ensemble in the dark zone. We can even impose non-linear Hamiltonian on the ensemble, in which case the dynamics of the system can still be written as unitary transformations of the corresponding collective spin operators.

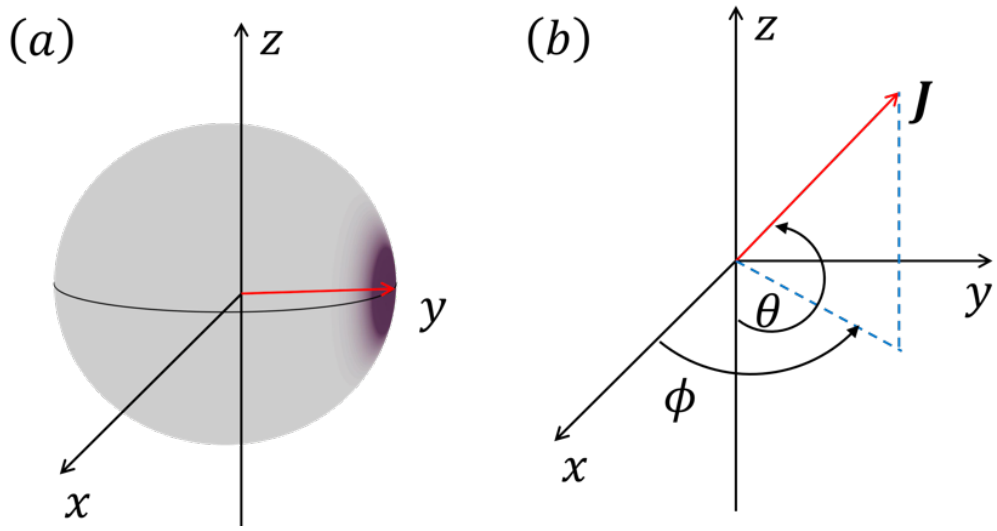

Figure 4.1. (a) Bloch sphere representation of a CSS. In this illustration, the CSS is prepared along the $\hat{\mathbf{y}}$-axis. The Husimi Quasi Probablity Distributions (QPDs) for the CSS noise in J_x and J_z (coordinate system defined in (b)) is shown as a noise blob (purple disc) at the tip of the collective spin **J** (red arrow). (b) Coordinate system defining the collective spin polar angle θ and azimuthal angle ϕ. The Cartesian components of the collective spin **J** in the x, y and z directions are J_x, J_y and J_z.

4.2.4. Coherent Spin States

For an ensemble of N spin-1/2 particles, the coherent spin state (CSS) is defined as a direct product of individual spin states, where each individual spin state itself is a minimum uncertainty state

$$|\theta,\phi\rangle = \bigotimes_{l=1}^{N}\left(\cos\left(\frac{\theta}{2}\right)|\downarrow_l\rangle - e^{-i\phi}\sin\left(\frac{\theta}{2}\right)|\uparrow_l\rangle\right) \tag{4.9}$$

where the angles θ and ϕ describe the direction (θ, ϕ) along which the mean spin vector is pointed, as illustrated in Fig. 4.1. Using the following operator identity

$$\exp[i(\xi j_+ + \eta j_-)] = \cos\Big(\sqrt{\xi\eta}\Big) + i\frac{\sin\big(\sqrt{\xi\eta}\big)}{\sqrt{\xi\eta}}(\xi j_+ + \eta j_-) \tag{4.10}$$

One can write the CSS in the following form

$$|\theta, \phi\rangle = \bigotimes_{l=1}^{N} R_l(\theta, \phi)\,|{\downarrow_l}\rangle = \bigotimes_{l=1}^{N} \exp[\zeta (j_+)_l - \zeta^* (j_-)_l]\,|{\downarrow_l}\rangle \tag{4.11}$$

where $\zeta = -\frac{\theta}{2}e^{-i\phi}$. Using Eq. (4.5c), this state can be further written as

$$|\theta, \phi\rangle = R(\theta, \phi)\,|{\downarrow_l}\rangle = \exp(\zeta J_+ - \zeta^* J_-)\,|J, -J\rangle \tag{4.12}$$

where $|J, -J\rangle = \bigotimes_{l=1}^{N} |{\downarrow_l}\rangle$ is the eigenstate of the J_z operator with eigenvalue $M = -J = -N/2$ (this is also the symmetric collective state $|E_0\rangle$ defined above), $R(\theta, \phi)$ is the rotation operator, which can also be written as

$$R(\theta, \phi) = \exp(\zeta J_+ - \zeta^* J_-) = \exp(\tau J_+)\exp[\ln\big(1 + |\tau|^2\big) J_z]\exp(-\tau^* J_-) \tag{4.13}$$

where $\tau = -\tan\big(\frac{\theta}{2}\big)e^{-i\phi}$. Combining Eq. (4.12) and Eq. (4.13), we obtain

$$\begin{aligned} |\theta, \phi\rangle &= \exp(\tau J_+)\exp[\ln\big(1 + |\tau|^2\big) J_z]\exp(-\tau^* J_-)\,|J, -J\rangle \\ &= \left(\cos\frac{\theta}{2}\right)^{2J} \sum_{l=0}^{2J} \sqrt{\binom{2J}{l}} \left(e^{i\phi}\tan\frac{\theta}{2}\right)^{l} |J, J-l\rangle \end{aligned} \tag{4.14}$$

For clarity, we consider an example of the CSS: $|\pi/2, \pi/2\rangle = \bigotimes_{l=1}^{N}(|{\downarrow_l}\rangle - i\,|{\uparrow_l}\rangle)/\sqrt{2}$, which corresponds to the state of the ensemble after the first $\pi/2$-pulse in Ramsey spectroscopy, discussed in Sec. 3.3. Essentially, this state is a result of rotating $|J, -J\rangle$ about the $\hat{\mathbf{x}}$-axis.

Substituting $\theta = \pi/2$, $\phi = \pi/2$ into Eq. (4.14), we get

$$\begin{aligned} \left|\frac{\pi}{2}, \frac{\pi}{2}\right\rangle &= \exp(iJ_+)\exp[\ln(2)J_z]\exp(iJ_-)\,|J,-J\rangle \\ &= 2^{-J}\sum_{l=0}^{2J} i^l \sqrt{\binom{2J}{l}}\,|J, J-l\rangle \end{aligned} \tag{4.15}$$

Each individual spin in the CSS is aligned along the $\hat{\mathbf{y}}$ axis. The mean collective spin that represents this CSS is, therefore $\mathbf{J} = \frac{N}{2}\hat{\mathbf{y}}$. Due to quantum mechanics, an uncertainty is introduced in the spin projections, governed by the Heisenberg uncertainty relationships given in Eq. (4.7). Therefore, the quantum projection noise in $|\pi/2, \pi/2\rangle$ is $\Delta J_z = \Delta J_x = \sqrt{N}/2$. The quantum fluctuations in a CSS is, therefore, isotropic in the plane orthogonal to the direction of the mean spin.

Using Eq. (4.14), we can also define the Husimi Quasi Probablity Distributions (QPDs) which is expressed as a function $Q_H(\theta, \phi)$ of the angles in spherical coordinates that span the surface of the Bloch sphere. For a given quantum state $|\Psi\rangle$, it is given by $Q_H(\theta, \phi) \equiv |\langle\Psi|\Phi(\theta, \phi)\rangle|^2$. In the rest of the thesis, we will use QPDs to illustrate the dynamics of the atomic ensemble extensively.

4.3. Spin Squeezing for Atomic Ensembles

The definition of spin squeezing is not unique, and it depends on the context where squeezing is considered. The most popular definitions were proposed by Kitagawa and Ueda [**12**], in analogy to photon squeezing, and by Wineland et al. [**13, 14**], in Ramsey experiments. In addition to these two widely studied definitions, there are some other definitions of spin squeezing, which were introduced for certain considerations. Here I will focus on the definitions proposed by Kitagawa and Ueda.

4.3.1. Spin-squeezing Parameter Given by Kitagawa and Ueda

Unlike bosonic systems, where the variance is equal in any direction for a bosonic coherent state [**67, 68, 69, 70, 71**], for a CSS the variance of spin operators depends on $\mathbf{n}$, and there exists a prior direction: the mean-spin direction (MSD)

$$\mathbf{n}_0 = \frac{\langle \mathbf{J} \rangle}{|\langle \mathbf{J} \rangle|} = \frac{(\langle J_x \rangle, \langle J_y \rangle, \langle J_z \rangle)}{|\langle \mathbf{J} \rangle|} \tag{4.16}$$

Below we use $\mathbf{n}_\perp$ to denote any direction perpendicular to the MSD. For a CSS, we have $(\Delta J_{\mathbf{n}_\perp})^2 = J/2$, where $J = N/2$. The spin-squeezing parameter is then defined in reference to $(\Delta J_{\mathbf{n}_\perp})^2$ of a CSS

$$\xi_{KU} = \frac{\min\left(\Delta J^2_{\mathbf{n}_\perp}\right)}{J/2} = \frac{4\min(\Delta J^2_{\mathbf{n}_\perp})}{N} \tag{4.17}$$

where the minimization is done over all directions $\mathbf{n}_\perp$. It is desirable that the spin-squeezing parameter ξ_{KU} is equal to 1 for the CSS.

To calculate the parameter ξ_{KU}, the first step is to compute the MSD determined by the expectation values $\langle J_\alpha \rangle$, with $\alpha \in \{x, y, z\}$. The MSD $\mathbf{n}_0$ can be written in spherical coordinates as

$$\mathbf{n}_0 = (\sin\theta\cos\phi,\ \sin\theta\sin\phi,\ \cos\theta) \tag{4.18}$$

where θ and ϕ are polar and azimuthal angles, respectively. The angles θ and ϕ are given by [**72**]

$$\theta = \arccos\left(\frac{\langle J_z\rangle}{|\mathbf{J}|}\right) \tag{4.19a}$$

$$\phi = \begin{cases} \arccos\left(\frac{\langle J_x\rangle}{|\mathbf{J}|\sin(\theta)}\right) & \text{if } \langle J_y\rangle > 0, \\ 2\pi - \arccos\left(\frac{\langle J_x\rangle}{|\mathbf{J}|\sin(\theta)}\right) & \text{if } \langle J_y\rangle \leq 0, \end{cases} \tag{4.19b}$$

where $|\mathbf{J}| = \sqrt{\langle J_x\rangle^2 + \langle J_y\rangle^2 + \langle J_z\rangle^2}$ is the magnitude of the mean spin. With respect to $\mathbf{n}_0$, the other two orthogonal bases are given by

$$\mathbf{n}_1 = (-\sin\phi,\, \cos\phi,\, 0) \tag{4.20a}$$

$$\mathbf{n}_2 = (\cos\theta\cos\phi,\, \cos\theta\sin\phi,\, -\sin\theta) \tag{4.20b}$$

The above expressions are valid for $\theta \neq 0, \pi$. For $\theta = 0, \pi$, the mean spin is along the $\pm\hat{\mathbf{z}}$ direction, and the possible choices of ϕ can be either 0 or π.

The second step now is to find the minimal variance of $\mathbf{J}_{\mathbf{n}_\perp} = \mathbf{J}\cdot\mathbf{n}_\perp$. The direction $\mathbf{n}_\perp$ can be represented as

$$\mathbf{n}_\perp = \mathbf{n}_1 O^T = \mathbf{n}_1\cos\nu + \mathbf{n}_2\sin\nu \tag{4.21}$$

where O is a 2×2 orthogonal matrix that performs rotations in the normal plane. The variance $\Delta J^2_{\mathbf{n}_\perp}$ can be written as

$$\Delta J^2_{\mathbf{n}_\perp} = \left\langle J^2_{\mathbf{n}_\perp}\right\rangle = \mathbf{n}_\perp \Gamma \mathbf{n}_\perp^T \tag{4.22}$$

where the symmetric matrix

$$\Gamma = \begin{bmatrix} \left\langle J^2_{\mathbf{n}_1} \right\rangle & \mathrm{Cov}(J_{\mathbf{n}_1}, J_{\mathbf{n}_2}) \\ \mathrm{Cov}(J_{\mathbf{n}_1}, J_{\mathbf{n}_2}) & \left\langle J^2_{\mathbf{n}_2} \right\rangle \end{bmatrix} \tag{4.23}$$

with

$$\mathrm{Cov}(J_{\mathbf{n}_1}, J_{\mathbf{n}_2}) = \frac{1}{2} \left\langle [J_{\mathbf{n}_1}, J_{\mathbf{n}_2}]_+ \right\rangle - \left\langle J_{\mathbf{n}_1} \right\rangle \left\langle J_{\mathbf{n}_2} \right\rangle = \frac{1}{2} \left\langle [J_{\mathbf{n}_1}, J_{\mathbf{n}_2}]_+ \right\rangle \tag{4.24}$$

is the covariance between $J_{\mathbf{n}_1}$ and $J_{\mathbf{n}_2}$, and $[X, Y]_+ = XY + YX$ is the anti-commutator. In the above equation, $\langle J_{\mathbf{n}_1} \rangle = \langle J_{\mathbf{n}_2} \rangle = 0$, since $\mathbf{n}_1$ and $\mathbf{n}_2$ are perpendicular to the MSD. The variance can be written as

$$\Delta J^2_{\mathbf{n}_\perp} = \mathbf{n}_1 O^T \Gamma O \mathbf{n}_1^T \tag{4.25}$$

and the matrix O can be chosen such that

$$O^T \Gamma O = \mathrm{diag}\{\lambda_-, \lambda_+\} \tag{4.26}$$

where the eigenvalues

$$\lambda_\pm = \frac{1}{2} \left[\left\langle J^2_{\mathbf{n}_1} + J^2_{\mathbf{n}_2} \right\rangle \pm \sqrt{\left(\left\langle J^2_{\mathbf{n}_1} - J^2_{\mathbf{n}_2} \right\rangle \right)^2 + 4\,\mathrm{Cov}(J_{\mathbf{n}_1}, J_{\mathbf{n}_2})^2} \right] \tag{4.27}$$

and $\min(\Delta J^2_{\mathbf{n}_\perp}) = \lambda_-$. Thus the squeezing parameter becomes

$$\xi_{KU} = \frac{4}{N} \lambda_- = \frac{2}{N} \left[\left\langle J^2_{\mathbf{n}_1} + J^2_{\mathbf{n}_2} \right\rangle - \sqrt{\left(\left\langle J^2_{\mathbf{n}_1} - J^2_{\mathbf{n}_2} \right\rangle \right)^2 + 4\,\mathrm{Cov}(J_{\mathbf{n}_1}, J_{\mathbf{n}_2})^2} \right] \tag{4.28}$$

The optimal squeezing angle in Eq. (4.21) is given by

$$\nu = \begin{cases} \frac{1}{2}\arccos\left(\frac{-A}{\sqrt{A^2+B^2}}\right) & \text{if } B \leq 0, \\ \pi - \frac{1}{2}\arccos\left(\frac{-A}{\sqrt{A^2+B^2}}\right) & \text{if } B > 0, \end{cases} \tag{4.29}$$

where we define

$$A \equiv \left\langle J_{\mathbf{n}_1}^2 - J_{\mathbf{n}_2}^2 \right\rangle \tag{4.30a}$$

$$B \equiv 2\,\mathrm{Cov}(J_{\mathbf{n}_1}, J_{\mathbf{n}_2}) \tag{4.30b}$$

4.3.2. Squeezed Spin States

It is known that $\xi_{KU} = 1$ for the uncorrelated pure CSS $|\theta, \phi\rangle$ in Eq. (4.9). However, if there are certain quantum correlations among the elementary spins, we may have $\xi_{KU} < 1$. Here, we regard spin as squeezed only if $\xi_{KU} < 1$, that is, the variance of one spin component normal to the MSD is smaller than the standard quantum limit of $J/2$. The corresponding states are then named as squeezed spin states (SSS's), which are demonstrated in Fig. 4.2.

From the above definition, spin squeezing can be achieved by introducing correlations among the elementary spins, which requires a nonlinear interaction because a linear Hamiltonian merely rotates the individual spins and does not establish quantum correlations among them. In the following subsections, we will focus primarily on the two approaches of generating squeezed spin states: One-Axis-Twist (OAT) and Two-Axis-Counter-Twist (TACT) spin squeezing.

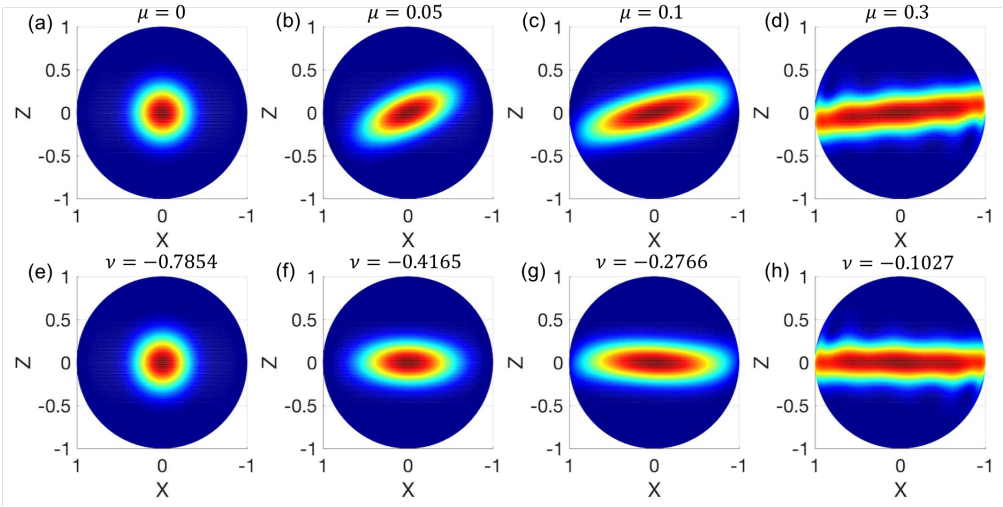

Figure 4.2. The QPDs of the squeezed spin states generated from H_{OAT} for $J = 20$. (a) is the starting CSS: $|\pi/2, \pi/2\rangle$; (b)-(d) represent the SSS's generated with increasing squeezing parameters μ; (e)-(h) are the corresponding states after the corrective rotation with different angles ν to minimize the variance along the $\hat{\mathbf{z}}$ axis. Note that (b) and (f) correspond to under-squeezed states; (c) and (g) correspond to optimally squeezed states; (d) and (h) correspond to excessively squeezed states.

4.3.3. One-Axis-Twist Spin Squeezing

One-Axis-Twist (OAT) spin squeezing is realized by applying the following nonlinear Hamiltonian

$$H_{OAT} = \hbar\chi J_z^2 \tag{4.31}$$

on a coherent spin state, say $|CSS\rangle = |\pi/2, \pi/2\rangle$, for which the MSD is along the direction given by $+\hat{\mathbf{y}}$. The dynamics of the ensemble can be expressed as a unitary transformation given by $\exp(-iH_{OAT}t/\hbar)$ and the resulting squeezed spin state can be written as

$$|SSS\rangle = \exp\left(\frac{-iH_{OAT}t}{\hbar}\right)|CSS\rangle = \exp\left(-i\mu J_z^2\right)|CSS\rangle \tag{4.32}$$

where $\mu = \chi t$ is the squeezing parameter, and t is the time duration of the squeezing interaction. The deformation of variances in the normal plane (x-z plane) by *twisting* with increasing μ is shown in Fig. 4.2 (a)-(d). Here we are plotting the QPDs for the state right after the squeezing interaction.

It is clear that variances are redistributed between certain orthogonal components in the x-z plane. A corrective rotation of angle ν along the MSD can be applied to bring the two orthogonal components to be aligned with x and z axes, such that the variance along the z-axis is minimized, as shown in Fig. 4.2 (e)-(h). The maximum and minimum variances can be found as

$$\lambda_{\pm} = \frac{J}{2}\left[1 + \frac{1}{2}\left(J - \frac{1}{2}\right)\left(A \pm \sqrt{A^2 + B^2}\right)\right] \tag{4.33}$$

the optimal squeezing angle as

$$\nu = -\frac{1}{2}\arctan\left(\frac{B}{A}\right) \tag{4.34}$$

and the spin-squeezing parameter as

$$\xi_{KU} = \frac{\lambda_-}{J/2} = 1 + \frac{1}{2}\left(J - \frac{1}{2}\right)\left(A - \sqrt{A^2 + B^2}\right) \tag{4.35}$$

where we have

$$A = 1 - \cos^{2J-2}(2\mu) \tag{4.36a}$$

$$B = 4\sin(\mu)\cos^{2J-2}(\mu) \tag{4.36b}$$

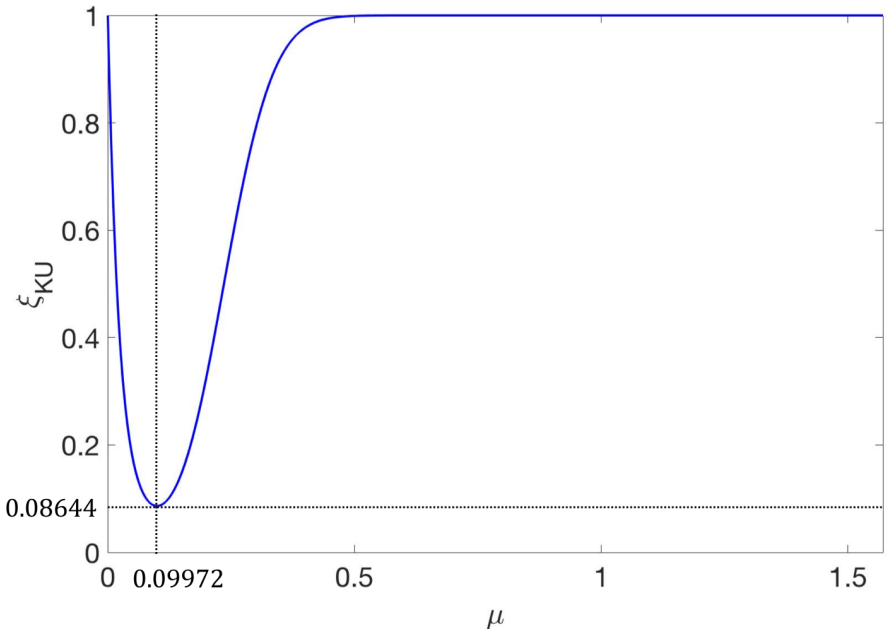

Figure 4.3. The spin-squeezing parameter ξ_{KU} as a function of the squeezing parameter μ for $J = 20$. The minimum $\xi_{KU} \approx 0.08644$ is achieved at $\mu \approx 0.09972$.

The spin-squeezing parameter ξ_{KU} depends on the squeezing parameter μ, which is shown in Fig. 4.3. For every J value, there is an optimal value of the squeezing parameter μ for which ξ_{KU} is minimized. For $J \gg 1$, these values can be approximated by

$$\mu_{opt} \simeq 24^{\frac{1}{6}} J^{-\frac{2}{3}} \tag{4.37a}$$

$$(\xi_{KU})_{min} \simeq 3^{-\frac{1}{6}} J^{-\frac{2}{3}} \tag{4.37b}$$

In addition to QPDs, spin squeezing can also be visualized using Collective-state Population Distributions (CPDs). Using Eq. (4.15), the SSS after applying H_{OAT} can be written

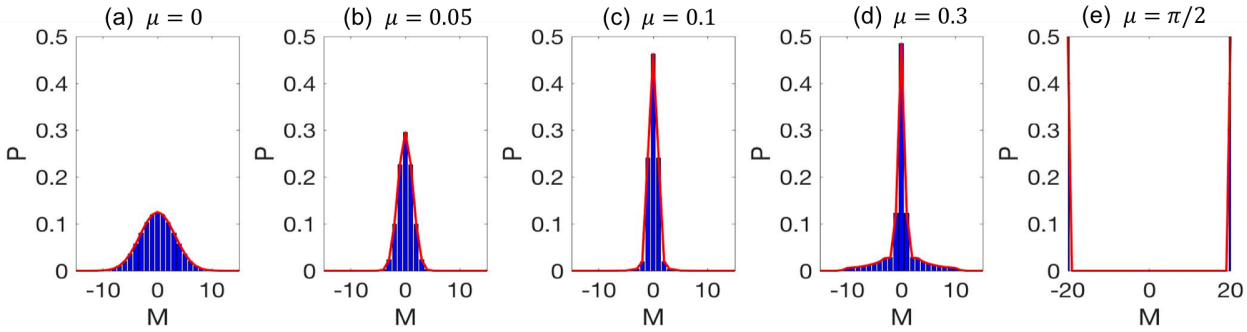

Figure 4.4. The CPDs of the squeezed spin states generated from H_{OAT} for $J = 20$. (a) is the starting CSS: $|\pi/2, \pi/2\rangle$; (b)-(d) represent the SSS's after corrective rotation, corresponding to those in Fig. 4.2 (f)-(h); (e) represent the SSS after corrective rotation for $\mu = \pi/2$.

in terms of the Dicke collective states as follows

$$
\begin{aligned}
|SSS\rangle &= \exp\Big(-i\frac{\mu}{2}J_z^2\Big)\Big|\frac{\pi}{2}, \frac{\pi}{2}\Big\rangle \\
&= 2^{-J}\sum_{l=0}^{2J}(-i)^l\sqrt{\binom{2J}{l}}\exp\Big(-i\frac{\mu}{2}(-J+l)^2\Big)|J, -J+l\rangle
\end{aligned}
\tag{4.38}
$$

The population in the collective state $|E_{M+J}\rangle = |J, M\rangle$ can be obtained by projection: $|\langle J, M|SSS\rangle|^2$. The CPD for the SSS's of various μ values are shown in Fig. 4.4. For a CSS, the CPD is characterized by a binomial distribution, while for an SSS, the CPD is not binomial and the width of the distribution becomes smaller as μ increases. For a critical value of $\mu = \pi/2$, the SSS after the corrective rotation becomes an equal superposition of the two extremal collective states: $(|E_0\rangle + |E_N\rangle)/\sqrt{2}$, which is referred to as a Schrödinger Cat (SC) state [**73**]. The SC state can be employed to enhance the measurement sensitivities of an atomic interferometer (clock) to the Heisenberg limit [**60, 74, 75**], which will be detailed in the following chapters.

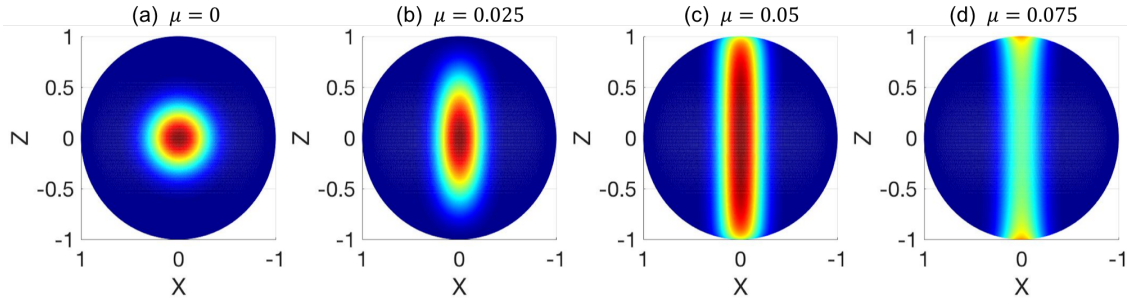

Figure 4.5. The QPDs of the squeezed spin states generated from H_{TACT} for $J = 20$. (a) is the starting CSS: $|\pi/2, \pi/2\rangle$; (b)-(d) represent the SSS's generated with increasing squeezing parameters μ. Note that (b) corresponds to under-squeezed states; (c) corresponds to optimally squeezed states; (d) corresponds to excessively squeezed states. As μ increases, the QPDs distorts and eventually splits into two.

4.3.4. Two-Axis-Counter-Twist Spin Squeezing

Two-Axis-Counter-Twist (TACT) spin squeezing is realized by applying the following nonlinear Hamiltonian

$$H_{TACT} = \frac{\hbar\chi}{2i}\Big((J_x + iJ_z)^2 - (J_x - iJ_z)^2\Big) \tag{4.39}$$

on a coherent spin state, say $|CSS\rangle = |\pi/2, \pi/2\rangle$. The resulting squeezed spin state can be written as

$$|SSS\rangle = \exp\left(\frac{-iH_{TACT}t}{\hbar}\right)|CSS\rangle = \exp\left(-\frac{\mu}{2}\Big((J_x + iJ_z)^2 - (J_x - iJ_z)^2\Big)\right)|CSS\rangle \tag{4.40}$$

where again $\mu = \chi t$ is the squeezing parameter, and t is the time duration of the squeezing interaction. The deformation of variances in the normal plane (x-z plane) by *counter-twisting* with increasing μ is shown in Fig. 4.5 (a)-(d). Again here we are plotting the QPDs for the state right after the squeezing interaction.

Similar to OAT, the spin-squeezing parameter ξ_{KU} depends on the squeezing parameter μ, and for every J value, there is an optimal value of μ for which ξ_{KU} is minimized. However, the action of H_{TACT} on the CSS $|\pi/2, \pi/2\rangle$ does not have analytical solutions. For $J \gg 1$, the minimum attainable variance for TACT squeezing asymptotically approaches $1/2$, which implies $(\xi_{KU})_{min}$ scales as $\propto J^{-1}$. Therefore, for large J (or N), TACT squeezing can achieve better noise reduction compared to OAT squeezing.

4.4. Summary

In this chapter, we have reviewed the collective model of an atomic ensemble using collective spins, presented mathematical descriptions of coherent spin states and squeezed spin states, and lastly introduced two approaches (OAT and TACT) for generating squeezed spin states. The OAT spin squeezing with critically-tuned squeezing parameter can be used to produce Schrödinger Cat state, which in turn can be employed to make a Schrödinger Cat atomic interferometer (SCAIN). Later we will show that a SCAIN in combination with collective state detection (CSD) or conventional detection (CD) can achieve a metrological sensitivity equivalent to the Heisenberg Limit (HL), within a factor of $\sqrt{2}$ [**74, 75**]. Furthermore, CD-SCAIN (Schrödinger Cat atomic interferometer with conventional detection) are more robust against excess noise by as much as $\sim \sqrt{N}$ [**75**], with N being the number of atoms in the ensemble. We also show that the same technique can be applied to an atomic clock, which increases the effective base frequency by a factor of N, and again yields a metrological sensitivity equivalent to the HL, within a factor of $\sqrt{2}$ [**74, 75**].

CHAPTER 5

Review of Sagnac Effect

5.1. Introduction

For a gyrosocope based on a planar Mach-Zehnder interferometer, a rotation normal to its plane causes a phase shift $\Delta\phi$ that is proportional to the rotation rate Ω. This is known as the Sagnac effect [**76, 77**]. In this chapter, we present two models for deriving the effect. The first model is based on special relativity and can be generalized to an interferometer of an arbitrary shape, while the second is a quantum-mechanical model which shows that the total effect can be split equally during each of the two dark zones.

5.2. Relativistic Model for the Sagnac Effect

In this section, we derive the Sagnac effect using the relativistic model. This is done first for a circular loop using relativistic laws of addition of velocities. Then it is done for the same loop but using Lorentz transformations. Lastly we generalize the model using Lorentz transformations to an interferometer of an arbitrary shape.

5.2.1. Deriving the Sagnac Effects for a Circular Loop Using Relativistic Laws of Addition of Velocities

We first review the conventional ways for deriving the Sagnac effects of a circular interferometer, which is shown in Fig. 5.1. The interferometer is rotating with angular frequency Ω and trangential velocity $v = \Omega R$. The phase velocity of the counter-clockwise (CCW) and

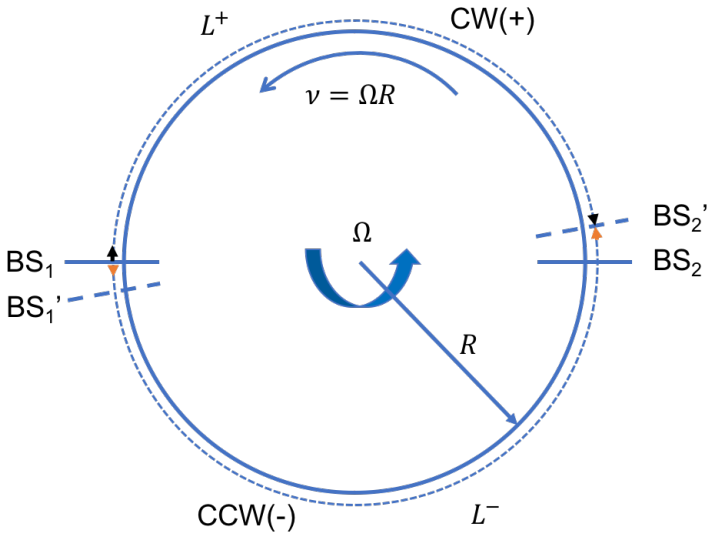

Figure 5.1. Schematic illustration for a circular interferometer.

clockwise (CW) waves without rotation is given by v_p. We use $v_R^{\pm}$ to denote the relativistic phase velocities of the CW(+) and CCW(-) waves as seen from the rest frame, $L^{\pm}$ to denote the distances travelled by the CW(+) and CCW(-) waves from BS_1 to BS_2' (BS short for beam splitter; BS_2' is defined as the position of the second beam splitter, i.e., BS_2, during detection of interference), $T_{\pm}$ to denote the time elapsed, as seen in the rest frame, for the CW(+) and the CCW(-) waves to reach BS_2'. We assume both waves (CW and CCW) have the same phase when they are split at BS_1. Our goal is to determine the difference in the phase of these two waves when the arrive at the detector at BS_2'.

We define $\beta \equiv v/c_0$, $\beta_p \equiv v_p/c_0$, where c_0 is the speed of light in vacuum, and assume $\beta \ll 1$. According to the relativistic laws of addition of velocities, we have:

$$v_R^+ = \frac{v_p - v}{1 - v_p v/c_0^2} = \frac{v_p - v}{1 - \beta\beta_p} \simeq (v_p - v)(1 + \beta\beta_p) \tag{5.1a}$$

$$v_R^- = \frac{v_p + v}{1 + v_p v/c_0^2} = \frac{v_p + v}{1 + \beta\beta_p} \simeq (v_p + v)(1 - \beta\beta_p) \tag{5.1b}$$

Note that the distances $L^\pm$ are related to the travel times $T^\pm$ as follows

$$L^+ = \pi R - vT^+ \tag{5.2a}$$

$$L^- = \pi R + vT^- \tag{5.2b}$$

$$T^+ = L^+/V_R^+ \tag{5.2c}$$

$$T^- = L^-/V_R^- \tag{5.2d}$$

we then obtain

$$T^+ = \frac{\pi R}{v_R^+ + v} \simeq \frac{\pi R}{(v_p - v)(1 + \beta\beta_p) + v} = \frac{\pi R}{v_p + v_p\beta\beta_p - v\beta\beta_p} \tag{5.3a}$$

$$T^- = \frac{\pi R}{v_R^- - v} \simeq \frac{\pi R}{(v_p + v)(1 - \beta\beta_p) - v} = \frac{\pi R}{v_p - v_p\beta\beta_p - v\beta\beta_p} \tag{5.3b}$$

Since $v \ll v_p$ for any waves under consideration, including optical waves and matter waves, we can write

$$T^+ \simeq \frac{\pi R}{v_p + v_p\beta\beta_p} \simeq \frac{\pi R}{v_p}(1 - \beta\beta_p) \tag{5.4a}$$

$$T^- \simeq \frac{\pi R}{v_p - v_p\beta\beta_p} \simeq \frac{\pi R}{v_p}(1 + \beta\beta_p) \tag{5.4b}$$

Thus, the time difference between the two waves is

$$\begin{aligned} \Delta t = T^- - T^+ &= \frac{\pi R}{v_p} 2\beta\beta_p \\ &= \frac{2\pi R v}{c_0^2} = \frac{2\pi\Omega R^2}{c_0^2} = \frac{2\Omega A}{c_0^2} \end{aligned} \tag{5.5}$$

where $A = \pi R^2$ is the area enclosed by the interferometer. Therefore, the phase shift is given by

$$\Delta\phi = \omega\Delta t = \frac{2\Omega A}{c_0^2} \cdot \omega \tag{5.6}$$

where ω is the radial frequency of the wave. Note that the time delay found above is a purely geometric effect, and the parameter c_0 appears in it because of the use of the relativistic laws of addition of velocities. Next we apply Eq. (5.6) to two special types of waves: optical wave and matter wave.

For optical wave, we have $\omega = 2\pi f$, where f is the temporal frequency of the wave. Then Eq. (5.6) can be rewritten as

$$\Delta\phi = \frac{4\pi\Omega A f}{c_0^2} \tag{5.7}$$

Note that the index of refraction of the medium through which the optical wave propagate does not show up in this result. If the index of refraction is n, then $v_p = c_0/n$. However, the expression for Δt does not depend on v_p. Hence, there is no dependence on n. This is verified experimentally. As such, the Sagnac effect phase shift is considered a key experimental evidence of special relativity.

For matter wave (such as by splitting atomic states quantum mechanically and recombining them), the relavant frequency of the wave is given by

$$\omega = \frac{mc_0^2}{\hbar} \tag{5.8}$$

where m is the mass of the atom, and we have used the result that the energy of the atom is $E = mc_0^2$. Using this, we get

$$\Delta\phi = \frac{2\Omega A}{c_0^2} \cdot \frac{mc_0^2}{\hbar} = \frac{2\Omega A m}{\hbar} \tag{5.9}$$

This result has also been verified experimentally.

Though the application of addition of velocities gives the right result for the time delay, the interpretation of Δt is not straightforward, nor can it be generalized to an interferometer with arbitrary shape. In the following two sections, we will develop a generic way for deriving the time delay using Lorentz transformations.

5.2.2. Deriving the Sagnac Effects for a Circular Loop Using Lorentz Transformations

The interpretation of Δt can be seen more transparently by carrying out an alternative derivation that uses Lorentz transformations directly, rather than addition of velocities, as follows.

Since the velocity of the interferometer is $v = \Omega R$ at every point locally (i.e., tangential velocity), the time delay in going from BS_1 to BS_2' can be equivalently calculated assuming linear motion, as illustrated in Fig. 5.2.

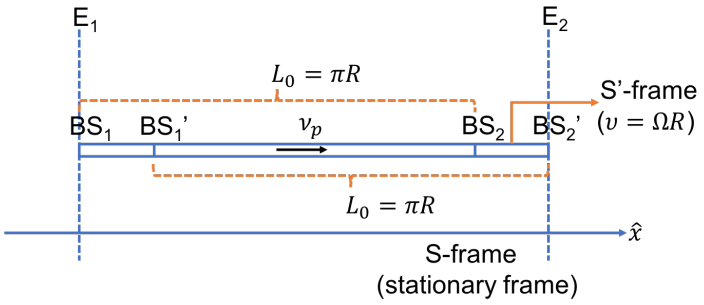

Figure 5.2. Equivalent linear-motion model of a circular interferometer.

We define two events: E_1 represents the event when the wavefront leaves BS_1; E_2 represents the event when the wavefront arrives at BS_2'. The S′ frame is defined as the one in which the slab is stationary, while the S frame is the stationary reference frame. As seen from S, S′ is moving in the $\hat{x}$ direction at velocity v, with $v = \Omega R$. In the S′ frame, the wave is moving with velocity v_p. We assume, as above, that $v \ll v_p$ and $v \ll c_0$.

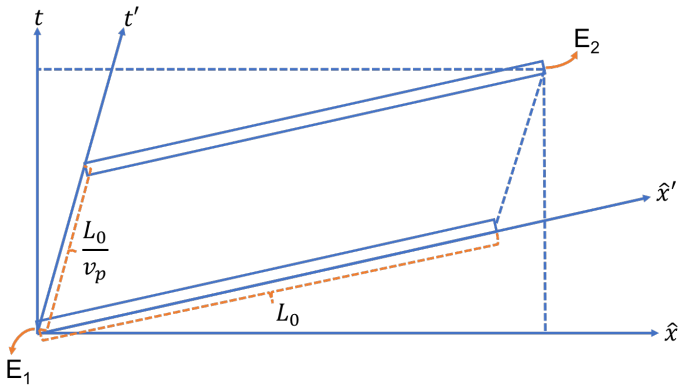

Figure 5.3. Coordinates of the two events for the CCW wave in the S and S′ frames.

For the CCW wave, the coordinates of the event E_1 in the two frames are denoted as (x_1^-, t_1^-) and $(x_1^{-'}, t_1^{-'})$, respectively; the coordinates of the event E_2 in the two frames are denoted as (x_2^-, t_2^-) and $(x_2^{-'}, t_2^{-'})$, respectively. As shown in Fig. 5.3, in the S′ frame, we

have

$$x_2^{-\prime} - x_1^{-\prime} = L_0 \tag{5.10a}$$

$$t_2^{-\prime} - t_1^{-\prime} = \frac{L_0}{v_p} \tag{5.10b}$$

Then in the S frame, by applying Lorentz transformations, we obtain

$$\begin{aligned} t_2^- - t_1^- &= \gamma(t_2^{-\prime} - t_1^{-\prime}) + \gamma\frac{v}{c_0^2}(x_2^{-\prime} - x_1^{-\prime}) \\ &= \gamma\frac{L_0}{v_p} + \gamma\frac{vL_0}{c_0^2} \end{aligned} \tag{5.11}$$

where $\gamma = 1/\sqrt{1-\beta^2}$ is the Lorentz factor.

For the CW wave, the coordinates of the event E_1 in the two frames are denoted as (x_1^+, t_1^+) and $(x_1^{+\prime}, t_1^{+\prime})$, respectively; the coordinates of the event E_2 in the two frames are denoted as (x_2^+, t_2^+) and $(x_2^{+\prime}, t_2^{+\prime})$, respectively. Carrying out the same calculations yields

$$x_2^{+\prime} - x_1^{+\prime} = -L_0 \tag{5.12a}$$

$$t_2^{+\prime} - t_1^{+\prime} = \frac{L_0}{v_p} \tag{5.12b}$$

and

$$\begin{aligned} t_2^+ - t_1^+ &= \gamma(t_2^{+\prime} - t_1^{+\prime}) + \gamma\frac{v}{c_0^2}(x_2^{+\prime} - x_1^{+\prime}) \\ &= \gamma\frac{L_0}{v_p} + \gamma\frac{-vL_0}{c_0^2} \end{aligned} \tag{5.13}$$

Note the negative sign at the right-hand side of Eq. (5.12a), since in the S′ frame, the CW wave is travelling equivalently in the $-\hat{x}'$ direction.

The time delay of the two paths in the S frame is then given by

$$\begin{aligned}\Delta t &= (t_2^- - t_1^-) - (t_2^+ - t_1^+) \\ &= \gamma\frac{2vL_0}{c_0^2} = \gamma\frac{2\Omega R\pi R}{c_0^2} = \gamma\frac{2\Omega A}{c_0^2} \\ &\simeq \frac{2\Omega A}{c_0^2}\end{aligned} \tag{5.14}$$

where we have made use of the approximation $\gamma \simeq 1$, giving that $\beta = v/c_0 \ll 1$.

Now the meaning of the time delay is clear: it is a manifestation of relativity of simultaneity. In the S′ frame, the two wavefronts travel at the same speed, and since the second beam splitter is located the same distance from the first beam splitter, the two wavefronts will reach the second beam splitter simultaneouly. However, because the second beam splitter is spatially separated for the two wavefronts in the linear-motion model, the two wavefronts will not reach the second beam splitter at the same time when observed in the S frame. This manifests itself as the time delay, and eventually leads to the phase shift of the two wavefronts.

5.2.3. Deriving the Sagnac Effects for an Interferometer of Arbitrary Shape Using Lorentz Transformations

Assume we have an interferometer of arbitrary shape as shown in Fig. 5.4. The interferometer lies in a plane that is normal to the rotation axis. In the rotating frame S_R in which the interferometer is stationary, the origin O' of the coordinates is chosen to be the intersection point (which we define as the pivot point) of the rotation axis and the interferometer plane. The wavefronts are split at point A, then follow the two paths (denoted as C and D) until they meet at point B. Note that now we cannot apply the linear-motion model to the whole

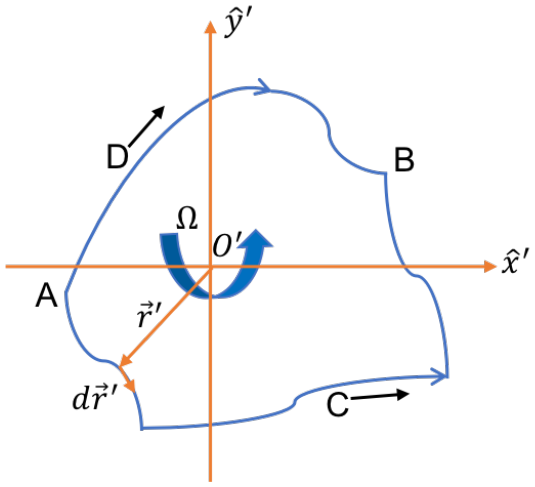

Figure 5.4. Schematic illustration for an interferometer of arbitrary shape.

path (C or D) directly, since the tangential velocity at each point along the path may be different. Instead, we will break down the path into infinitesimal segments and apply the linear-motion model to each of them sequentially.

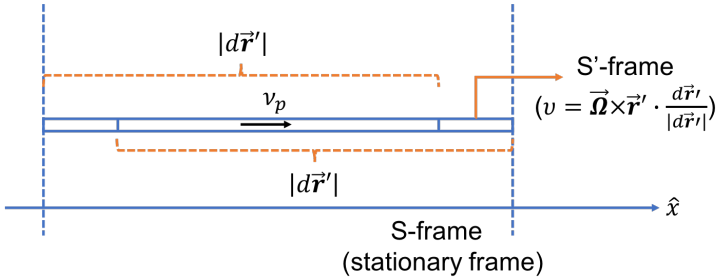

Figure 5.5. Equivalent linear-motion model for the chosen segment.

Take the segment $d\mathbf{r}'$ located at position $\mathbf{r}' = (x', y', 0)$ along path C as an example. The tangential speed of this segment is given by

$$v = (\mathbf{\Omega} \times \mathbf{r}') \cdot \frac{d\mathbf{r}'}{|d\mathbf{r}'|} \tag{5.15}$$

where $\mathbf{\Omega} = (0, 0, \Omega)$ is the angular velocity vector of the interferometer. The equivalent linear-motion model for this segment is shown in Fig. 5.5. In the S′ frame, the time it takes for the wavefront to travel from the start to the end of the segment, denoted as dt'_C, is given by $dt'_C = |d\mathbf{r}'|/v_p$. The corresponding time, dt_C, as seen in the S frame, then can be found using Lorentz transformations

$$\begin{aligned} dt_C &= \gamma dt'_C + \gamma \frac{v|d\mathbf{r}'|}{c_0^2} \\ &= \gamma \frac{|d\mathbf{r}'|}{v_p} + \gamma \frac{(\mathbf{\Omega} \times \mathbf{r}') \cdot d\mathbf{r}'}{c_0^2} \end{aligned} \tag{5.16}$$

where $\gamma = \sqrt{1 - (v/c_0)^2}$ is the Lorentz factor for the chosen segment (note now γ is a function of $\mathbf{r}'$). The total time it takes for the wavefront to travel from point A to point B along path C, denoted as Δt_C, as seen in the S frame, will be

$$\begin{aligned} \Delta t_C &= \int_C dt_C \\ &= \int_C \left\{ \gamma \frac{|d\mathbf{r}'|}{v_p} + \gamma \frac{(\mathbf{\Omega} \times \mathbf{r}') \cdot d\mathbf{r}'}{c_0^2} \right\} \\ &= I_1 + I_2 \end{aligned} \tag{5.17}$$

where we have defined

$$I_1 \equiv \int_C \gamma \frac{|d\mathbf{r}'|}{v_p} \tag{5.18a}$$

$$I_2 \equiv \int_C \gamma \frac{(\mathbf{\Omega} \times \mathbf{r}') \cdot d\mathbf{r}'}{c_0^2} \tag{5.18b}$$

Similarly we can obtain the corresponding results for path D

$$\begin{aligned} dt_D &= \gamma dt'_D + \gamma \frac{v|d\mathbf{r}'|}{c_0^2} \\ &= \gamma \frac{|d\mathbf{r}'|}{v_p} + \gamma \frac{(\mathbf{\Omega} \times \mathbf{r}') \cdot d\mathbf{r}'}{c_0^2} \end{aligned} \tag{5.19}$$

and

$$\begin{aligned} \Delta t_D &= \int_D dt_D \\ &= \int_D \left\{ \gamma \frac{|d\mathbf{r}'|}{v_p} + \gamma \frac{(\mathbf{\Omega} \times \mathbf{r}') \cdot d\mathbf{r}'}{c_0^2} \right\} \\ &= I_3 + I_4 \end{aligned} \tag{5.20}$$

where we have defined

$$I_3 \equiv \int_D \gamma \frac{|d\mathbf{r}'|}{v_p} \tag{5.21a}$$

$$I_4 \equiv \int_D \gamma \frac{(\mathbf{\Omega} \times \mathbf{r}') \cdot d\mathbf{r}'}{c_0^2} \tag{5.21b}$$

Then the time delay of the wavefronts along the two paths, denoted as Δt, is given by

$$\Delta t = \Delta t_C - \Delta t_D = (I_1 + I_2) - (I_3 + I_4) \tag{5.22}$$

To evaluate these integrals, we assume $v \ll c_0$ for all segments along the two paths so that $\gamma \simeq 1$. Then we get

$$I_1 \simeq \int_C \frac{|d\mathbf{r}'|}{v_p} = \frac{L_C}{v_p} \tag{5.23a}$$

$$I_3 \simeq \int_D \frac{|d\mathbf{r}'|}{v_p} = \frac{L_D}{v_p} \tag{5.23b}$$

where L_C and L_D are respectively the length of path C and D, as well as

$$\begin{aligned} I_2 - I_4 &\simeq \int_C \frac{(\mathbf{\Omega} \times \mathbf{r}') \cdot d\mathbf{r}'}{c_0^2} - \int_D \frac{(\mathbf{\Omega} \times \mathbf{r}') \cdot d\mathbf{r}'}{c_0^2} \\ &= \oint_{A \to A} \frac{(\mathbf{\Omega} \times \mathbf{r}') \cdot d\mathbf{r}'}{c_0^2} \end{aligned} \tag{5.24}$$

where now the integral is to be done on the closed-loop: A $\to$ B $\to$ A, by first following path C then following path D but in reverse direction.

Using Stokes$'$ theorem, the line integral on the right-hand side of Eq. (5.24) can be converted into a surface integral

$$\begin{aligned} I_2 - I_4 &\simeq \oint_{A \to A} \frac{(\mathbf{\Omega} \times \mathbf{r}') \cdot d\mathbf{r}'}{c_0^2} \\ &= \iint_S \frac{\boldsymbol{\nabla} \times (\mathbf{\Omega} \times \mathbf{r}') \cdot d\mathbf{S}}{c_0^2} \end{aligned} \tag{5.25}$$

where $\boldsymbol{\nabla} = (\partial/\partial x', \partial/\partial y', \partial/\partial z')$ is the differential operator, $d\mathbf{S} = (0, 0, dS)$ is the differential surface vector, and the surface integral is to be done over the area enclosed by the interferometer. Using the following vector identity

$$\begin{aligned} \boldsymbol{\nabla} \times (\mathbf{A} \times \mathbf{B}) =& \mathbf{A}(\boldsymbol{\nabla} \cdot \mathbf{B}) - \mathbf{B}(\boldsymbol{\nabla} \cdot \mathbf{A}) + \\ & (\mathbf{B} \cdot \boldsymbol{\nabla})\mathbf{A} - (\mathbf{A} \cdot \boldsymbol{\nabla})\mathbf{B} \end{aligned} \tag{5.26}$$

and the following equations

$$\boldsymbol{\Omega}(\boldsymbol{\nabla}\cdot\mathbf{r}') = 2\boldsymbol{\Omega} \tag{5.27a}$$

$$\mathbf{r}'(\boldsymbol{\nabla}\cdot\boldsymbol{\Omega}) = 0 \tag{5.27b}$$

$$(\mathbf{r}'\cdot\boldsymbol{\nabla})\boldsymbol{\Omega} = 0 \tag{5.27c}$$

$$(\boldsymbol{\Omega}\cdot\boldsymbol{\nabla})\mathbf{r}' = 0 \tag{5.27d}$$

we arrive at

$$\begin{aligned} I_2 - I_4 &\simeq \iint_S \frac{\boldsymbol{\nabla}\times(\boldsymbol{\Omega}\times\mathbf{r}')\cdot d\mathbf{S}}{c_0^2} \\ &= \frac{2\Omega}{c_0^2}\iint_S dS = \frac{2\Omega A}{c_0^2} \end{aligned} \tag{5.28}$$

where again A is the area enclosed by the interferometer. The time delay Δt now can be written as

$$\Delta t \simeq \frac{L_C - L_D}{v_p} + \frac{2\Omega A}{c_0^2} \tag{5.29}$$

For symmetric interferometers, the first term on the right-hand side goes to zero, and we obtain

$$\Delta t \simeq \frac{2\Omega A}{c_0^2} \tag{5.30}$$

It should be noted that the integrals in Eqs. (5.18a), (5.18b), (5.21a), (5.21b) can be generalized to arbitrary direction of $\boldsymbol{\Omega}$ and arbitrary pivot point for the rotation, therefore Eq. (5.22) also holds for those general cases. Since the time delay in Eq. (5.30) does not depend on the pivot point of rotation, the signals of the interferometer are not expected to

depend on the pivot point, either (this is true even for asymmetric interferometers). However, the time delay for each half loop does depend on the location of the pivot point, as shown in Eqs. (5.17), (5.20). Furthermore, for asymmetric interferometers, the signals will also depend on the length difference between the two paths, as can be seen from Eq. (5.30).

5.3. Quantum-mechanical Model for the Sagnac Effect

In this section, we derive the Sagnac effect using the quantum-mechanical model. We show that though the Sagnac effect is uniformly spread throughout the interferometric sequence, we can introduce it in two equal parts during each of the two dark zones.

5.3.1. Derivation of the Sagnac Effects Using Rotation Hamiltonian

The atomic interferometer (AI) considered here makes use of N non-interacting identical two-level atoms, all interacting with the same laser field, as shown in Fig. 5.6. The lower state is defined as $|1\rangle \equiv |g, p_x = mv_x, p_y = 0\rangle$ and the upper state as $|2\rangle \equiv |e, p_x = mv_x, p_y = mv_y\rangle$, where p_x and p_y are respectively the x- and y-components of the linear momentum of the center of mass (COM) motion of the atom, and m is the mass of the atom.

The ensemble is initially prepared in a state where all atoms are in state $|1\rangle$, then undergoes a pulse sequence of $\pi/2-$dark$-\pi-$dark$-\pi/2$, during which each atom's wavepacket first separates into two components, then gets redirected and finally recombined to produce an interference that is sensitive to any phase-difference, ϕ, between the two paths. The schematic diagram for the AI is shown in Fig. 5.7. The trajectory of the AI forms a closed loop with an area A in the x-y plane, and the system is rotating around the $\hat{\mathbf{z}}$-axis with angular frequency $\mathbf{\Omega} = \Omega\hat{\mathbf{z}}$.

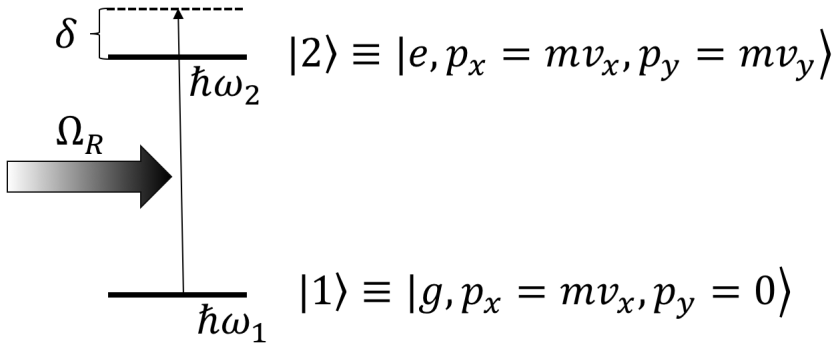

Figure 5.6. Schematic diagram for a two-level atomic system. The energies associated with the two levels are denoted as $\hbar\omega_1$ and $\hbar\omega_2$, respectively. δ is the laser detuning and Ω_R is the Rabi frequency. Here we assume resonant excitations, hence $\delta = 0$. Each level consists of internal states characterizing the electron motion, as well as external states characterizing the center of mass (COM) motion of the atom.

For each atom, the Hamiltonian due to rotation is given by

$$H_\Omega = -\mathbf{\Omega} \cdot (\mathbf{r} \times \mathbf{p}) = -\Omega(x\, p_y - y\, p_x) \tag{5.31}$$

where $\mathbf{r} = (x,\, y,\, 0)$ and $\mathbf{p} = (p_x,\, p_y,\, 0)$ are respectively the position and momentum operators of the COM motion of the atom. Next we will derive the phase factors imparted to the two channels in the two dark zones using the rotation Hamiltonian H_Ω given in Eq.(5.31).

During the first dark zone, the lower arm (channel 1) is in state $|1\rangle$ while the upper arm (channel 2) is in state $|2\rangle$. Note that in the two-level atomic model, each atom can be represented by a pseudospin-1/2 operator, $\mathbf{j} = (j_x,\, j_y,\, j_z)$. The spin-up and spin-down states are defined as $|\uparrow\rangle \equiv |2\rangle$, $|\downarrow\rangle \equiv |1\rangle$, respectively. In this representation, the matrix elements

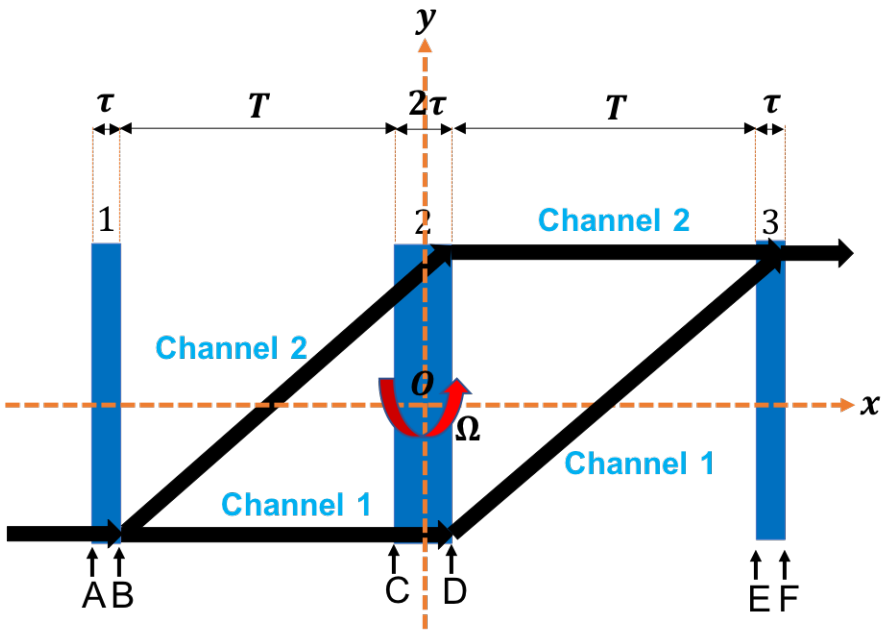

Figure 5.7. Schematic illustration of an atomic interferometer for rotation sensing. 1 and 3 are the two $\pi/2$-pulses, while 2 is the π-pulse. The duration for the $\pi/2$-pulse, the π-pulse and the dark zone are τ, 2τ and T, respectively, where we assume $\tau \ll T$. The system is rotating around the $\hat{\mathbf{z}}$-axis with angular frequency $\mathbf{\Omega}$, which will induce phase difference between the two arms of the interferometer.

of H_Ω are given by

$$(H_\Omega)_{\downarrow\downarrow} = \langle\downarrow|H_\Omega|\downarrow\rangle = -\Omega(\langle 1|x\,p_y|1\rangle - \langle 1|y\,p_x|1\rangle) \tag{5.32a}$$

$$(H_\Omega)_{\uparrow\uparrow} = \langle\uparrow|H_\Omega|\uparrow\rangle = -\Omega(\langle 2|x\,p_y|2\rangle - \langle 2|y\,p_x|2\rangle) \tag{5.32b}$$

$$(H_\Omega)_{\downarrow\uparrow} = \langle\downarrow|H_\Omega|\uparrow\rangle = 0 \tag{5.32c}$$

$$(H_\Omega)_{\uparrow\downarrow} = \langle\uparrow|H_\Omega|\downarrow\rangle = 0 \tag{5.32d}$$

Note that the last two equations, Eqs. (5.32c) and (5.32d), are results of the fact that the rotation Hamiltonian H_Ω operates only on the external states of the atomic system and that the internal states of the two basis states are orthogonal to each other. Also note that $|1\rangle$ and $|2\rangle$ are eigenstates of the p_x and p_y operators, where for p_x, the corresponding eigenvalue is mv_x for both states, while for p_y, the corresponding eigenvalues are 0 and mv_y, respectively. Then using the following equations

(5.33a) $$\langle 1|x|1\rangle = -x_0 + v_x(t - t_B)$$

(5.33b) $$\langle 2|x|2\rangle = -y_0 + v_x(t - t_B)$$

(5.33c) $$\langle 1|y|1\rangle = -y_0$$

(5.33d) $$\langle 2|y|2\rangle = -y_0 + v_y(t - t_B)$$

with t_B being the time when the atomic system enters the first dark zone (time point B), and $(-x_0, -y_0)$ being the coordinate of the COM of the atomic system at t_B, we can write H_Ω in matrix form as

(5.34)
$$\begin{aligned} H_\Omega &= \begin{bmatrix} (H_\Omega)_{\uparrow\uparrow} & (H_\Omega)_{\uparrow\downarrow} \\ (H_\Omega)_{\downarrow\uparrow} & (H_\Omega)_{\downarrow\downarrow} \end{bmatrix} \\ &= \begin{bmatrix} -\Omega(mv_x y_0 - mv_y x_0) & 0 \\ 0 & -\Omega m v_x y_0 \end{bmatrix} \\ &= \begin{bmatrix} \Omega m v_x y_0 & 0 \\ 0 & -\Omega m v_x y_0 \end{bmatrix} \end{aligned}$$

where we have made use of the following identities according to the geometry of the AI

$$x_0 = v_x T \tag{5.35a}$$

$$2y_0 = v_y T \tag{5.35b}$$

$$v_y x_0 = 2 v_x y_0 \tag{5.35c}$$

$$A = 2 x_0 y_0 \tag{5.35d}$$

Also note that in the same representation, the j_z operator is given by

$$j_z = \frac{1}{2} \begin{bmatrix} 1 & 0 \\ 0 & -1 \end{bmatrix} \tag{5.36}$$

Then the rotation Hamiltonian H_Ω can be written in terms of the j_z operator as $H_\Omega = 2\Omega m v_x y_0 j_z$. Thus, the propagator for the first dark zone can be expressed as

$$\begin{aligned} U(t) &= e^{-\frac{i}{\hbar}\int_{t_B}^{t} H_\Omega(t')dt'} \\ &= e^{-\frac{i}{\hbar} 2\Omega m v_x y_0 (t - t_B) j_z} \end{aligned} \tag{5.37}$$

Then at $t = t_C$, the end of the first dark zone (time point C), we have

$$\begin{aligned} U(t_C) &= e^{-\frac{i}{\hbar} 2\Omega m v_x y_0 (t_C - t_B) j_z} \\ &= e^{-\frac{i}{\hbar} 2\Omega m v_x y_0 T j_z} \\ &= e^{-\frac{i}{\hbar} \Omega m A j_z} \\ &= e^{-\frac{i\phi}{2} j_z} \end{aligned} \tag{5.38}$$

where we have defined $\phi = \frac{2mA\Omega}{\hbar}$. Eq. (5.38) implies, during the first dark zone, the upper and lower arms will pick up a phase factor of $e^{-i\phi/4}$ and $e^{i\phi/4}$, respectively, resulting in a phase difference of $\phi/2$ between the two channels.

During the second dark zone, the states of the two arms are reversed due to the effects of the π-pulse. Now the upper arm is in state $|1\rangle$, while the lower arm is in state $|2\rangle$. Following the same convention as in the first dark zone, the spin-up and spin-down states are defined as $|\uparrow\rangle \equiv |2\rangle$, $|\downarrow\rangle \equiv |1\rangle$, respectively. The matrix elements of H_Ω are then given by

$$(H_\Omega)_{\downarrow\downarrow} = \langle\downarrow|H_\Omega|\downarrow\rangle = -\Omega(\langle 1|x\, p_y|1\rangle - \langle 1|y\, p_x|1\rangle) \tag{5.39a}$$

$$(H_\Omega)_{\uparrow\uparrow} = \langle\uparrow|H_\Omega|\uparrow\rangle = -\Omega(\langle 2|x\, p_y|2\rangle - \langle 2|y\, p_x|2\rangle) \tag{5.39b}$$

$$(H_\Omega)_{\downarrow\uparrow} = \langle\downarrow|H_\Omega|\uparrow\rangle = 0 \tag{5.39c}$$

$$(H_\Omega)_{\uparrow\downarrow} = \langle\uparrow|H_\Omega|\downarrow\rangle = 0 \tag{5.39d}$$

Similarly using the following equations for the second dark zone

$$\langle 1|x|1\rangle = v_x(t - t_D) \tag{5.40a}$$

$$\langle 2|x|2\rangle = v_x(t - t_D) \tag{5.40b}$$

$$\langle 1|y|1\rangle = y_0 \tag{5.40c}$$

$$\langle 2|y|2\rangle = -y_0 + v_y(t - t_D) \tag{5.40d}$$

and the identities in Eq.(5.35), we obtain

$$
\begin{aligned}
H_\Omega &= \begin{bmatrix} (H_\Omega)_{\uparrow\uparrow} & (H_\Omega)_{\uparrow\downarrow} \\ (H_\Omega)_{\downarrow\uparrow} & (H_\Omega)_{\downarrow\downarrow} \end{bmatrix} \\
&= \begin{bmatrix} -\Omega m v_x y_0 & 0 \\ 0 & \Omega m v_x y_0 \end{bmatrix}
\end{aligned} \tag{5.41}
$$

which can be written in terms of the j_z operator as $H_\Omega = -2\Omega m v_x y_0 j_z$. Thus the propagator for the second dark zone can be expressed as

$$
\begin{aligned}
U(t) &= e^{-\frac{i}{\hbar}\int_{t_D}^{t} H_\Omega(t')dt'} \\
&= e^{\frac{i}{\hbar}2\Omega m v_x y_0 (t-t_D) j_z}
\end{aligned} \tag{5.42}
$$

Then at $t = t_E$, the end of the second dark zone (time point E), we have

$$
\begin{aligned}
U(t_C) &= e^{\frac{i}{\hbar}2\Omega m v_x y_0 (t_E-t_D) j_z} \\
&= e^{\frac{i}{\hbar}2\Omega m v_x y_0 T j_z} \\
&= e^{\frac{i}{\hbar}\Omega m A j_z} \\
&= e^{\frac{i\phi}{2} j_z}
\end{aligned} \tag{5.43}
$$

which implies, during the second dark zone, the upper and lower arms will again pick up a phase factor of $e^{-i\phi/4}$ and $e^{i\phi/4}$, respectively, resulting in a phase difference of $\phi/2$ between the two channels.

Therefore, though the effect of the overall phase shift $\phi = \frac{2mA\Omega}{\hbar}$ due to rotation is uniformly spread throughout the interferometric sequence, we can introduce it in two equal

parts during each of the two dark zones, where the propagators for the first and second dark zones are given by $e^{-i\phi j_z/2}$ and $e^{i\phi j_z/2}$, respectively.

Note that the above results are for each individual atomic system. For the atomic ensemble, the total Hamiltonian due to rotation in the two dark zones can be obtained by summing up the rotation Hamiltonian for each individual atom, which are

$$H_\Omega^{1st} = 2\Omega m v_x y_0 \sum_{i=1}^{N} (j_z)_i = 2\Omega m v_x y_0 J_z \tag{5.44a}$$

$$H_\Omega^{2nd} = -2\Omega m v_x y_0 \sum_{i=1}^{N} (j_z)_i = -2\Omega m v_x y_0 J_z \tag{5.44b}$$

where we have defined the collective spin operators: $\mathbf{J} = (J_x,\, J_y,\, J_z) = \sum_{i=1}^{N} (\mathbf{j})_i$. The propagators for the two dark zones are then given by $e^{-i\phi J_z/2}$ and $e^{i\phi J_z/2}$, respectively, with $\phi = \frac{2mA\Omega}{\hbar}$. Hence, for the ensemble, the effect of the overall phase shift $\phi = \frac{2mA\Omega}{\hbar}$ due to rotation can still be introduced in two equal parts during each of the two dark zones.

5.4. Summary

In this chapter, we presented two models for deriving the Sagnac effect. For the relativistic model, we showed that the Sagnac effect can be viewed as a geometric time delay due to non-simultaneity of events under Lorentz transformation. This approach yields a differential form of the time delay, which in turn can be be used to derive easily the Sagnac phase shift for an interferometer of an arbitrary shape. For the quantum-mechanical mode, we showed that despite the fact that the Sagnac effect is uniformly spread throughout the interferometric sequence, we can introduce it in two equal parts during each of the two dark zones.

CHAPTER 6

Schrödinger Cat Atomic Interferometers and Clocks

6.1. Introduction

In the previous chapters, we briefly mentioned that critical tuning of the one-axis-twist (OAT) spin squeezing can be used to generate Schrödinger Cat (SC) states [**73**]. In this chapter, we will investigate their applications to atomic interferometers and clocks. In particular, we propose an experimentally-realizable protocol for implementing an atomic interferometer (or clock) using SC states, which, in combination with particular detection schemes (collective state detection or conventional detection), can enhance the measurement sensitivity of the interferometer (or clock) from Standard Quantum Limit (SQL) up to the Heisenberg Limit (HL), where the sensitivity scales $\propto 1/N$, with N being the number of atoms in the ensemble. We also show that for the conventional detection scheme, the proposed protocol can make the interferometer (or clock) more robust against excess noise, by as much as $\sqrt{N}$, compared to other protocols proposed for atomic interferometers [**22, 78**].

6.2. Schrödinger Cat Atomic Interferometer

In order to illustrate clearly the mechanism for realizing the Schrödinger Cat Atomic Interferometer (SCAIN), and the characteristics thereof, as well as to establish the notations employed in the rest of this chapter, it is useful to recall briefly the relevant features of a Conventional Raman Atomic Interferometer (CRAIN) and a Collective State Atomic Interferometer (COSAIN). In particular, we will describe them using the spin representation

model of atomic ensembles developed in the previous chapter, instead of using direct product states, as was done in Sec. 3.4. Furthermore, we will also evaluate the performance of the interferometers as metrological devices by examining the phase fluctuations (PF) as well as the measurement sensitivities Λ (where $\Lambda = \mathrm{PF}^{-1}$).

6.2.1. CRAIN and COSAIN in Spin Representation

A CRAIN makes use of N non-interacting identical three-level atoms with metastable hyperfine states $|\downarrow, p_z = 0\rangle$ and $|\uparrow, p_z = \hbar k\rangle$, (where $k = k_1 + k_2$, with k_1 and k_2 being the wave numbers for the two counter-propagating beams, and p_z being the z-component of the linear momentum), and an excited state $|e\rangle$, in the Λ-configuration, reduced to an equivalent two-level model [**61, 62**], as shown in Fig. 3.3. Using the spin representation model developed in Sec. 4.2, we can describe these atoms by a collective spin $\mathbf{J} = \sum_{l=1}^{N} \mathbf{j}_l = (J_x, J_y, J_z)$, where $\mathbf{j}_l = (j_{xl}, j_{yl}, j_{zl})$ represents the pseudospin-1/2 operator for each atom.

The ensemble is initially prepared in a CSS

$$|-\hat{\mathbf{z}}\rangle \equiv |E_0\rangle = \bigotimes_{l=1}^{N} |\downarrow_l\rangle \tag{6.1}$$

where we have employed the notation that $|\hat{\mathbf{w}}\rangle$ represents a CSS where the pseudo-spin of each atom is aligned in the direction of the unit vector $\hat{\mathbf{w}}$. Note that here the state $|E_0\rangle$ corresponds to all pseudospins in the $-\hat{\mathbf{z}}$ direction. As such, we will refer to the collective state basis containing $|E_0\rangle$ as the Z-directed Dicke Collective States (ZDCSs). As needed, we will also refer to XDCSs (YDCSs) for which $|E_0\rangle$ corresponds to all pseudospins in the $-\hat{\mathbf{x}}$ ($-\hat{\mathbf{y}}$) direction. Under a pulse sequence of $\pi/2-$dark$-\pi-$dark$-\pi/2$, each atom's wavepacket first separates into two components, then gets redirected and finally recombined to produce

an interference which is sensitive to any phase difference, ϕ, between the two paths, as demonstrated in Fig. 3.3.

As an example, we consider the case where an atomic interferometer is rotating at a rate Ω_G about an axis normal to the area Θ enclosed by the two paths. From our analyses in Chapter 5, the interferometer will accrue a phase difference of

$$\phi = 2\omega_c \Theta \Omega_G / c^2 \tag{6.2}$$

between its trajectories due to the Sagnac effect [**76, 77**], where $\omega_c = mc^2/\hbar$ is the Compton frequency of the atom, m is the rest mass of the atom, c is the speed of light in vacuum and $\hbar$ is the reduced Planck constant. It should be noted that the effects of the overall phase shift ϕ due to rotation is uniformly spread throughout the interferometric sequence. However, for theoretical convenience, we introduce it in two equal parts during each of the dark zones (a rigorous justification of this approach can be found in Ref. [**75**]). The final state of the atoms can be written as a series of unitary transformations related to the corresponding collective spins

$$\begin{aligned} |\psi\rangle &= e^{-i\frac{\pi}{2}J_x} e^{i\frac{\phi}{2}J_z} e^{-i\pi J_x} e^{-i\frac{\phi}{2}J_z} e^{-i\frac{\pi}{2}J_x} |-\hat{\mathbf{z}}\rangle \\ &= \bigotimes_{l=1}^{N} -\frac{1}{2} e^{-i\phi/2} \{(1+e^{i\phi}) |\downarrow_l\rangle + i(1-e^{i\phi}) |\uparrow_l\rangle\} \end{aligned} \tag{6.3}$$

In a CRAIN, the phase difference ϕ is measured by mapping it onto the operator representing the difference in spin-up and spin-down populations: $J_z = (N_\uparrow - N_\downarrow)/2$, where $N_\uparrow = \Sigma_{l=1}^{N} |\uparrow_l\rangle \langle\uparrow_l|$ and $N_\downarrow = \Sigma_{l=1}^{N} |\downarrow_l\rangle \langle\downarrow_l|$. The signal, which is a measure of the population

of the $|\downarrow\rangle$ state is, therefore, $S_{CRAIN} = J + \langle -J_z \rangle = N\cos^2(\phi/2)$, where $J = N/2$. The corresponding fringe linewidth is given by $\varrho = c^2/(2\omega_c\Theta)$. The measurement process causes wavefunction collapse of the individual spins from the superposition state to $|\downarrow\rangle$, resulting in quantum projection noise in the measure of the signal [**79**], $\Delta S_{CRAIN} = \Delta(J_z) = \sqrt{N/4}\sin(\phi)$, where ΔJ_z is the standard deviation of J_z. Assuming ideal quantum efficiency, the Quantum Fluctuation in Rotation (QFR) is given by $\Delta\Omega_G\big|_{CRAIN} = |\Delta(J_z)/\partial_{\Omega_G}\langle J_z\rangle| = c^2/2\omega_C\Theta\sqrt{N}$, where $\partial_{\Omega_G} \equiv \partial/\partial\Omega_G$.

The COSAIN differs from a CRAIN in that the measurement of the signal is done on a Dicke collective state of the ensemble, instead of a single atomic state [**64**]. The Dicke collective states are eigenstates of J_z and can be represented as $|E_n, p_z = n\hbar k\rangle = \Sigma_{l=1}^{\binom{N}{n}}\mathcal{P}_k\left|\downarrow^{N-n}\otimes\uparrow^n\right\rangle/\sqrt{\binom{N}{n}}$, where $\mathcal{P}_k$ is the permutation operator [**57**]. As a result of the first $\pi/2$-pulse, the initial state $|E_0, p_z = 0\rangle$ is coupled to $|E_1, p_z = \hbar k\rangle$, which in turn is coupled to $|E_2, p_z = 2\hbar k\rangle$, and so on, all the way up to $|E_N, p_z = N\hbar k\rangle$. This causes the ensemble to split into $N + 1$ trajectories. The dark zone that immediately follows imparts a phase $e^{in\phi/2}$ to $|E_n\rangle$. At this point, the π-pulse generates a flip in the individual spins, causing $|E_n\rangle$ to become $|E_{N-n}\rangle$, and vice versa. The second dark-zone lends a phase $e^{i(0.5N-n)\phi}$ to $|E_n\rangle$. The mathematical derivation of this mechanism is discussed in detail in Ref. [**64**]. The last $\pi/2$-pulse causes each of the collective states to interfere with the rest of the states. The COSAIN can, thus, be viewed as an aggregation of interference patterns due to $\binom{N+1}{2}$ interferometers working simultaneously. The narrowest constituent signal fringes are derived from interferences between states with the largest difference in phase, i.e. $|E_0\rangle$ and $|E_N\rangle$. The width of this fringe is ϱ/N. The widths of the rest of the signal components range from ϱ to $\varrho/(N-1)$. The signal, which is the measure of population of $|E_0\rangle$, is the result of the weighted sum of all the pairwise interferences with this

state. This is detected by projecting the final state of the ensemble, $|\psi\rangle$ on $|E_0\rangle$. Thus, $S_{COSAIN} = \langle G\rangle = \cos^{2N}(\phi/2)$, where $G \equiv |E_0\rangle\langle E_0|$. The quantum projection noise is the standard deviation of G, given by $\Delta S_{COSAIN} = \cos^{N}(\phi/2)\sqrt{1-\cos^{2N}(\phi/2)}$. The QFR of the COSAIN is thus, $\Delta\Omega_G\big|_{COSAIN} = |\Delta G/\partial_{\Omega_G}\langle G\rangle|$. Under quantum noise limited operation, this equals $(\Delta\Omega_G\big|_{CRAIN}/\sqrt{N})|\sqrt{\sec^{4J}(\phi/2)-1}/\tan(\phi/2)|$. Therefore, for $\Omega_G \to 0$, the rotation sensitivity of the COSAIN is same as that of a CRAIN, which is the standard quantum limit (SQL), assuming all the other factors remain the same.

6.2.2. Protocols for Realizing the SCAIN

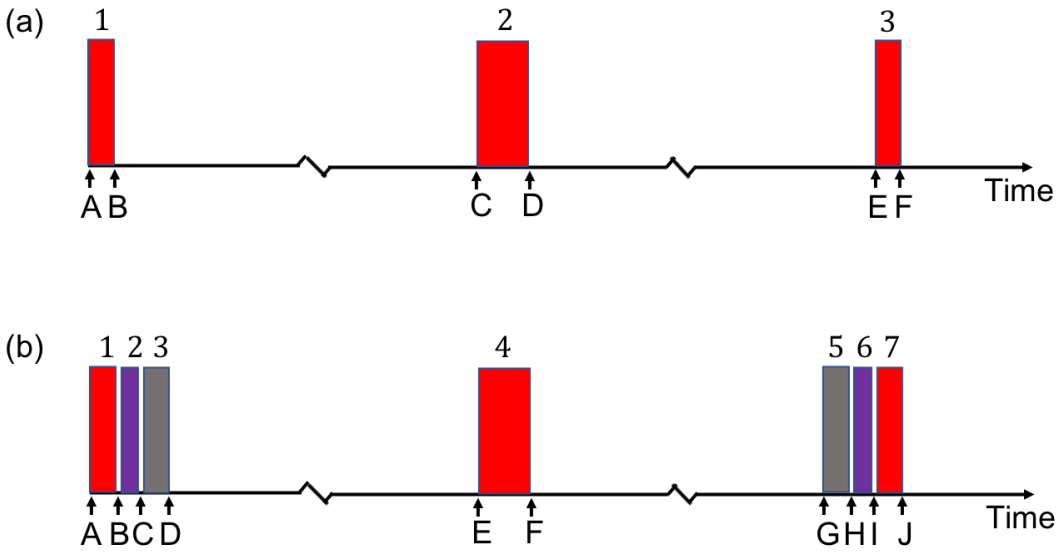

Figure 6.1. (a) Schematic illustration of the pulse sequence employed for a CRAIN. (b) Schematic illustration of the pulse sequence employed for a SCAIN. In addition to the usual $\pi/2$-π-$\pi/2$ pulses (colored in red for both (a) and (b)), a SCAIN employs four more pulses compared to a CRAIN, labeled as 2, 3, 5, 6 in (b), corresponding to the squeezing, rotation, inverse rotation and unsqueezing operations in the protocols for realizing the SCAIN.

The analyses for the COSAIN above implies that one way of surpassing the SQL is to suppress the contribution of the constituent fringes broader than ϱ/N. This is precisely what

happens in a SCAIN, which employs critically-tuned one-axis-twist (OAT) spin squeezing and a rotation to generate a Schrödinger Cat state corresponding to an equal superposition of $|E_0\rangle$ and $|E_N\rangle$ [**80**], such that interferences happen only between these two extremal collective states leading to the largest phase difference and the narrowest signal fringes.

The complete pulse sequence employed for a SCAIN is illustrated in Fig. 6.1, along with that for a CRAIN. Explicitly, we apply OAT spin squeezing around the $\hat{\mathbf{z}}$ axis (defined as the spin-up direction) immediately following the first $\pi/2$-pulse in a CRAIN, which aligns the mean spin vector along the $\hat{\mathbf{y}}$ axis. Prior to the application of the squeezing interaction, the population of the collective states follow a binomial distribution, corresponding to a Coherent Spin State (CSS). As the strength of squeezing is increased, the distribution begins to flatten out, eventually generating a Schrödinger cat state corresponding to an equal superposition of $|E_0\rangle$ and $|E_N\rangle$ when the OAT is followed by an auxiliary rotation of $\pi/2$ around the $\hat{\mathbf{x}}$ or $\hat{\mathbf{y}}$ axis, depending on the parity of N. The usual dark-π-dark sequence follows, at the end of which we apply a corrective rotation of $\pi/2$ around the same axis as the previous auxiliary rotation, and then apply a corrective reverse-OAT interaction about the $\hat{\mathbf{z}}$ axis. Finally, the last $\pi/2$ pulse effectuates interference between the collective states, and the signal is detected by measuring the population of either one of the collective states or one of the individual atomic states. Since the process makes use of a superposition of two mesoscopic quantum states, we name this a Schrödinger Cat Atomic Interferometer (SCAIN).

Due to the exotic behaviors of the states after the OAT squeezing, the SCAIN can be operated under two different protocols, which differ by the choice of the axis around which we apply the auxiliary rotation (and the following corrective rotation) that maximizes the degree of observed squeezing. In one case (Protocol A), the rotation is around the $\hat{\mathbf{x}}$ axis while in the other (Protocol B), the rotation is around the $\hat{\mathbf{y}}$ axis. Protocol A will be optimal

when N is even while Protocl B will be optimal when N is odd. For both protocols, the exact state evolutions of the atomic ensemble depend on the choices of a set of parameters, including the value (and parity) of N, the squeezing parameter μ for the OAT squeezing, the auxiliary rotation axis (ARA, $\hat{\mathbf{x}}$ axis for Protocol A, $\hat{\mathbf{y}}$ axis for Protocol B) around which to implement the rotation, the corrective rotation sign ξ which can take values of ± 1 corresponding to redoing or undoing the first auxiliary rotation, and lastly the dark zone phase shift ϕ. Next we will demonstrate the state evolutions of the atomic ensemble at each stage of the two protocols using Husimi Quasi Probability Distributions (QPDs).

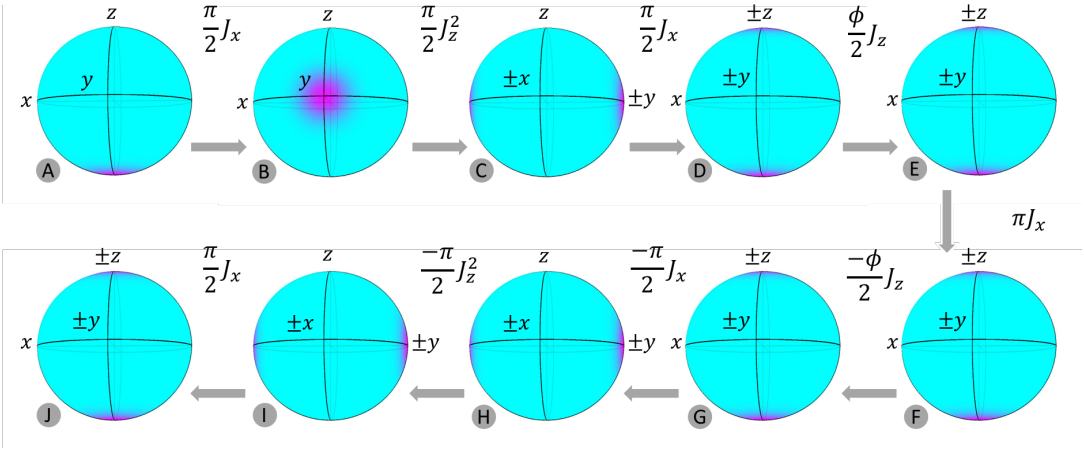

Figure 6.2. The QPDs at different stages of Protocol A, for even $N = 40$, $\mu = \pi/2$, ARA $= \hat{\mathbf{x}}$, $\xi = -1$ and $\phi = 0.5\pi/N$.

6.2.2.1. Protocol A. We distinguish the two cases when N is even and when N is odd. For either case, in illustrating the nature of the QPDs at various stages, we have used different orientations of the Bloch sphere as suited, and added $\pm$ symbols in front of two axes to indicate that the picture looks the same when it is rotated by 180° around the third axis.

The even case is shown in Fig. 6.2, where we have $N = 40$, $\mu = \pi/2$, ARA $= \hat{\mathbf{x}}$, $\xi = -1$ and $\phi = \pi/80$. At the start (point A), the system is in state $|-\hat{\mathbf{z}}\rangle$. After the first $\pi/2$ pulse (point B), the state rotates around the $\hat{\mathbf{x}}$ axis to reach state $|\hat{\mathbf{y}}\rangle$. We then apply a

squeezing Hamiltonian of the form $H_{OAT} = \chi J_z^2$ for a duration of τ such that $\mu = \chi\tau$. After the squeezing pulse (point C), the state is split equally between two CSSs, and can be expressed as $(|\hat{\mathbf{y}}\rangle - \eta\,|-\hat{\mathbf{y}}\rangle)/\sqrt{2}$ [**1, 81**], where $\eta = i(-1)^{N/2}$, representing a phase factor with unity amplitude. This is a SC state, but as a superposition of the two extremal states of the YDCS manifold, which cannot be used to achieve phase magnification, since the phase difference between the two arms corresponds to rotation around the $\hat{\mathbf{z}}$ axis. This problem is solved by applying an auxiliary rotation of $\pi/2$ around the $\hat{\mathbf{x}}$ axis, which transforms this state to $(|-\hat{\mathbf{z}}\rangle + \eta\,|\hat{\mathbf{z}}\rangle)/\sqrt{2}$. This (point D) represents the desired SC state, as a superposition of the two extremal states of the ZDCS manifold: $(|E_0\rangle + \eta\,|E_N\rangle)/\sqrt{2}$. After the first dark zone (point E), the state is $e^{-i\phi J_z/2}(|E_0\rangle_L + \eta\,|E_N\rangle_U)/\sqrt{2}$, where the subscript L (U) is for the lower (upper) arm of the interferometer (the total phase shift ϕ is split equally in the two dark zones [**75**]). Since both $|E_0\rangle$ and $|E_N\rangle$ are eigenstates of J_z, with eigenvalues of $-N/2$ and $N/2$ respectively ($\hbar = 1$), this state can be simplified to $\left(e^{i\phi N/4}\,|E_0\rangle_L + e^{-i\phi N/4}\eta\,|E_N\rangle_U\right)/\sqrt{2}$. The resulting QPD remains unchanged but the quantum state incorporates these phase accumulations. After the π-pulse (point F), $|E_0\rangle_L$ becomes $-i\,|E_N\rangle_L$ while $|E_N\rangle_U$ becomes $-i\,|E_0\rangle_U$. After the second dark zone (point G), the state is $\left(e^{i\phi N/2}\eta\,|E_N\rangle_L + e^{-i\phi N/2}\,|E_0\rangle_U\right)/\sqrt{2}$, so that the net phase difference between the two paths is $N\phi$, thus magnifying the rotation induced phase by a factor of N. To reveal the phase magnification, we apply another auxiliary rotation (i.e., the corrective rotation) by an angle of $-\pi/2$ around the $\hat{\mathbf{x}}$ axis (point H), followed by the unsqueezing Hamiltonian $-H_{OAT}$ (point I). After the second $\pi/2$ pulse (point J) the state is $|\Psi\rangle_f = \cos(N\phi/2)\,|E_0\rangle - \eta\sin(N\phi/2)\,|E_N\rangle$.

The odd case is shown in Fig. 6.3, where we have $N = 41$, $\mu = \pi/2$, ARA $= \hat{\mathbf{x}}$, $\xi = -1$ and $\phi = \pi/4$. The state evolutions from A to B will be the same as the even case. However, the state after the OAT squeezing is drastically different. Since N is odd, H_{OAT} transforms

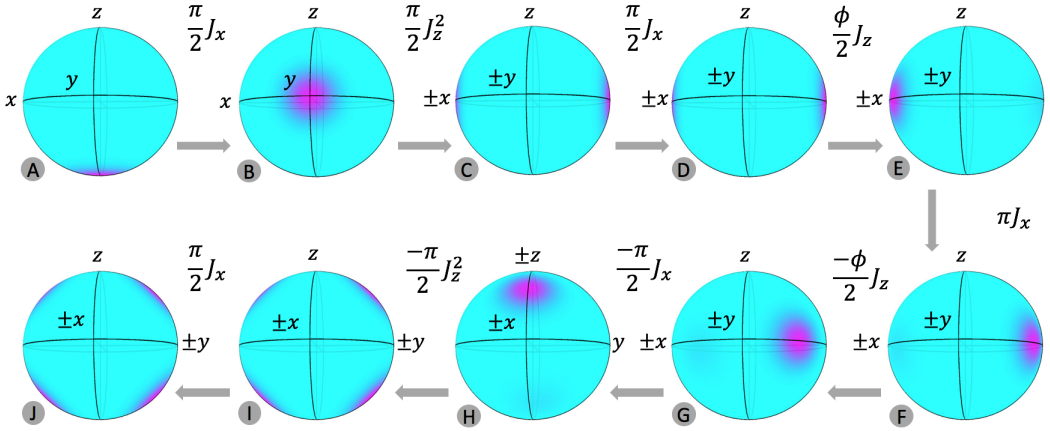

Figure 6.3. The QPDs at different stages of Protocol A, for odd $N = 41$, $\mu = \pi/2$, ARA $= \hat{\mathbf{x}}$, $\xi = -1$ and $\phi = \pi/4$.

$|\hat{\mathbf{y}}\rangle$ to $(|\hat{\mathbf{x}}\rangle + \eta\,|-\hat{\mathbf{x}}\rangle)/\sqrt{2}$, where $\eta = i(-1)^{(N+1)/2}$, representing a phase factor with unity amplitude. This state, illustrated in the QPDs at time point C, also represents an SC state, as a superposition of two extremal collective states, but in terms of the XDCSs. Now the application of the auxiliary rotation by $\pi/2$ around the $\hat{\mathbf{x}}$ axis from C to D leaves the QPD unchanged. The rotation in the first dark zone by an angle of $\phi/2$ around the $\hat{\mathbf{z}}$ axis (D to E) moves the QPD in the x-y plane on both sides, as shown at time point E. This rotation is inverted by the π pulse from E to F. The rotation in the second dark zone by an angle of $-\phi/2$ around the $\hat{\mathbf{z}}$ axis (F to G) moves the QPD in the x-y plane further on both sides, as shown at time point G. This is followed by a rotation of $-\pi/2$ around the $\hat{\mathbf{x}}$ axis from G to H. The unsqueezing pulse turns the QPD distribution into four lobes in the y-z plane, as shown at time point I. The final $\pi/2$ pulse rotates this pattern by 90°, but still with a four-lobed pattern in the y-z plane, as shown at time point J.

For both cases, the whole protocol can be represented as a series of unitary transformations

$$|\Psi\rangle_{f,A} = e^{-i\frac{\pi}{2}J_x} e^{i\mu J_z^2} e^{-i\xi\frac{\pi}{2}J_x} e^{i\frac{\phi}{2}J_z} e^{-i\pi J_x} e^{-i\frac{\phi}{2}J_z} e^{-i\frac{\pi}{2}J_x} e^{-i\mu J_z^2} e^{-i\frac{\pi}{2}J_x} |-\hat{\mathbf{z}}\rangle \tag{6.4}$$

which can be used to numerically compute the state evolutions for an arbitrary value of ϕ.

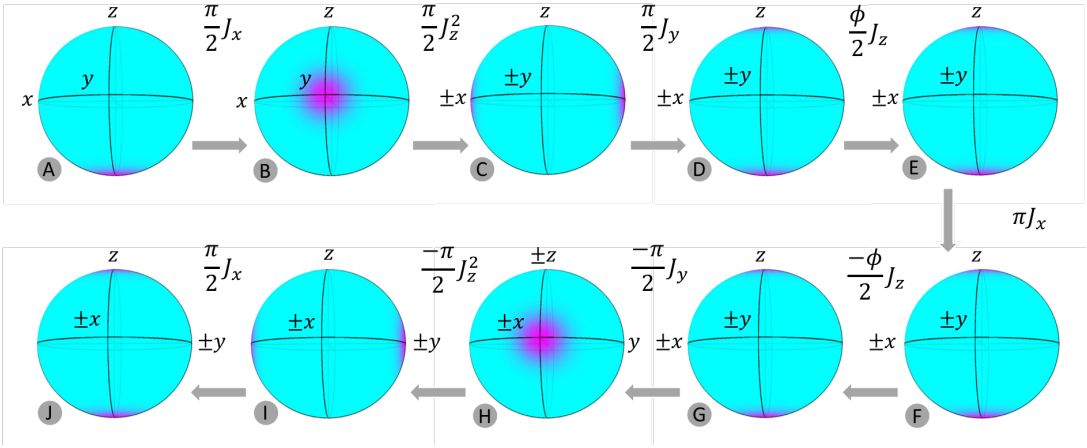

Figure 6.4. The QPDs at different stages of Protocol B, for odd $N = 41$, $\mu = \pi/2$, ARA $= \hat{\mathbf{y}}$, $\xi = -1$ and $\phi = 0.5\pi/N$.

6.2.2.2. Protocol B. Here again we distinguish the two cases when N is even and when N is odd. The odd case is shown in Fig. 6.4, where we have $N = 41$, $\mu = \pi/2$, ARA $= \hat{\mathbf{y}}$, $\xi = -1$ and $\phi = \pi/82$. The state evolutions from A to C resemble that of the odd case for Protocol A. From C to D, with ARA $= \hat{\mathbf{y}}$, the auxiliary rotation now will take the SC state from the XDCS manifold to the ZDCS manifold, yielding the desired SC state at time point D. The evolutions from D to G will be the similar to that of the even case for Protocol A. From G to H, the corrective rotation transforms the SC state from ZDCS manifold to the XDCS manifold, and then the unsqueezing interaction transforms it to the YDCS manifold. After that, the evolution again will be similar to that of the even case for Protocol A.

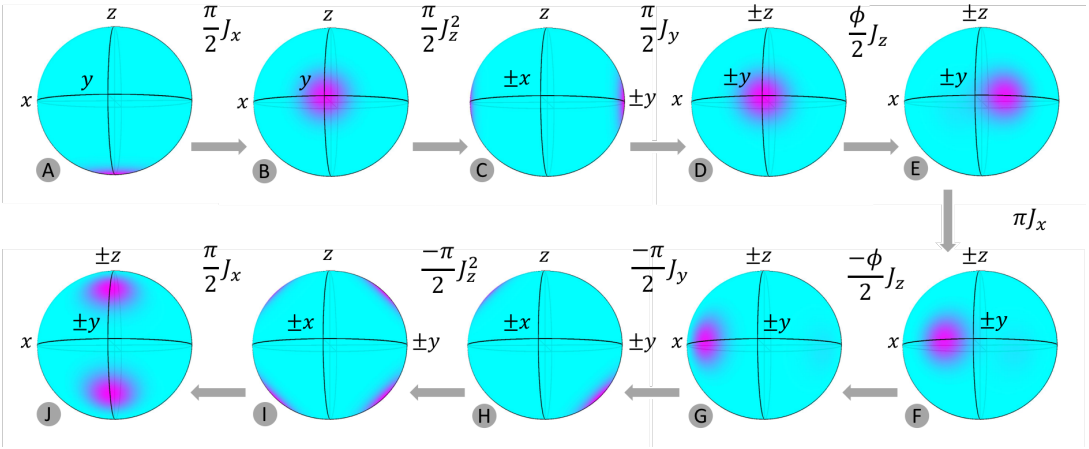

Figure 6.5. The QPDs at different stages of Protocol B, for even $N = 40$, $\mu = \pi/2$, ARA $= \hat{\mathbf{y}}$, $\xi = -1$ and $\phi = \pi/4$.

The even case is shown in Fig. 6.5, where we have $N = 40$, $\mu = \pi/2$, ARA $= \hat{\mathbf{y}}$, $\xi = -1$ and $\phi = \pi/4$. The state evolutions from A to C resemble that of the even case for Protocol A. From C to D, with ARA $= \hat{\mathbf{y}}$, the auxiliary rotation now will leave the SC state unchanged. The rest part of the evolutions will be the similar to that of the odd case for Protocol A, where the QPD will develop into into four lobes at the end of the protocol.

Again for both cases, the whole protocol can be represented as a series of unitary transformations

$$|\Psi\rangle_{f,B} = e^{-i\frac{\pi}{2}J_x} e^{i\mu J_z^2} e^{-i\xi\frac{\pi}{2}J_y} e^{i\frac{\phi}{2}J_z} e^{-i\pi J_x} e^{-i\frac{\phi}{2}J_z} e^{-i\frac{\pi}{2}J_y} e^{-i\mu J_z^2} e^{-i\frac{\pi}{2}J_x} |-\hat{\mathbf{z}}\rangle \tag{6.5}$$

which can be used to numerically compute the state evolutions for an arbitrary value of ϕ.

6.2.3. Detection Scheme for the SCAIN

As mentioned ealier, there are two detection schemes for the SCAIN. We can measure either the population of the collective state $|E_0\rangle$, corresponding to detection of $\langle G\rangle = \langle |E_0\rangle\langle E_0|\rangle$,

or the population of individual atomic states, corresponding to detection of $\langle J_z/\hbar \rangle$. The former is referred as collective state detection (CSD) scheme while the latter is referred to as conventional detection (CD) scheme. The SCAIN in combination with CSD scheme is then referred to as CSD-SCAIN, and the SCAIN in combination with CD scheme is referred to as CD-SCAIN. Next we will show the signal finges for these two detection schemes for various scenarios.

6.2.3.1. Signal Fringes for CSD-SCAIN with $\mu = \pi/2$. We first look at the signals for the CSD-SCAIN and focus on the special case where the squeezing parameter $\mu = \pi/2$ (this is the condition for generating SC states after the OAT squeezing operation). The signals for this case can be obtained by directly taking the expectation value of the operator $G = |E_0\rangle\langle E_0|$ with respect to $|\Psi\rangle_{f,A}$ for Protocol A, or $|\Psi\rangle_{f,B}$ for Protocol B. The final expression depends on the parity of N. For Protocol A, the result is found to be $\langle \Psi_{f,A}|G|\Psi_{f,A}\rangle = \sin^2(N\phi/2)$ when N is even, and vanishes when N is odd (the exact reasons for that are not manifestly obvious due to the complexity of the states, but can be verified via simulations). The results of this case for both parities are illustrated in the left subplots of Fig. 6.6. For Protocol B, the result is found to be $\langle \Psi_{f,B}|G|\Psi_{f,B}\rangle = \sin^2(N\phi/2)$ when N is odd, and will be similar to that of a COSAIN when N is even. The results of this case for both parities are shown in the right subplots of Fig. 6.6. For both protocols, it can be seen clearly that the fringes will be narrowed by a factor of N for one of the parities compared to that of a CRAIN ($\sqrt{N}$ narrower than that of a COSAIN).

6.2.3.2. Fringe shapes for CSD-SCAIN with various μ values. We next look at the signals for the CSD-SCAIN for various values of the squeezing parameter μ ranging from 0 up to $\pi/2$. Again the signals for this case can be obtained by directly taking the expectation value of the operator $G = |E_0\rangle\langle E_0|$ with respect to $|\Psi\rangle_{f,A}$ for Protocol A, or $|\Psi\rangle_{f,B}$ for

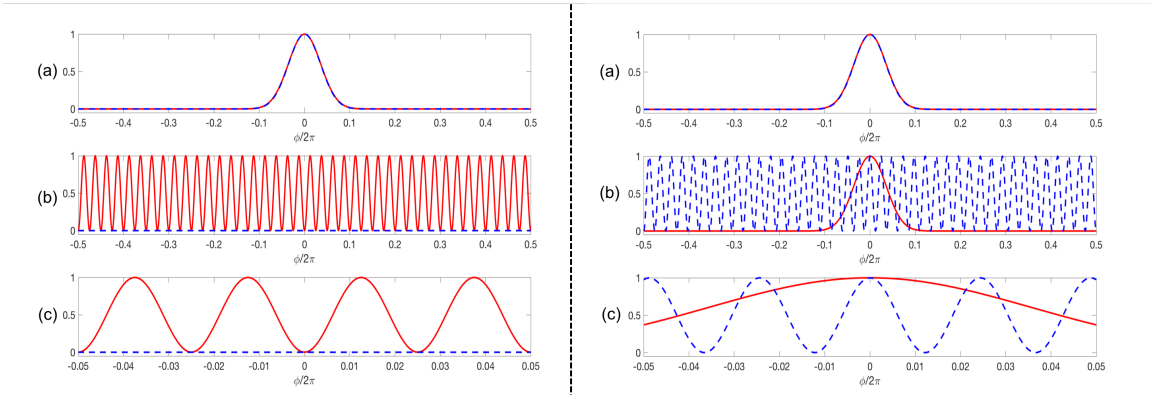

Figure 6.6. Signals for CSD-SCAIN corresponding to detection of $\langle G\rangle = \langle |E_0\rangle\langle E_0|\rangle$, as a function of ϕ, for $\mu = \pi/2$ and $\xi = +1$. Left subplots are for protocol A with ARA $= \hat{\mathbf{x}}$ and right subplots are for protocol B with ARA $= \hat{\mathbf{y}}$. In each subplots, $N = 40$ is red while $N = 41$ is dashed-blue. (a) Fringes for COSAIN for comparison; (b) Fringes for CSD-SCAIN; (c) Zoomed-in fringes for CSD-SCAIN. The horizontal span in (c) is 10 times smaller than those in (a) and (b).

Protocol B. Unlike the special case discussed above, we don't have an analytical expression for the final results, but they can be simulated numerically. The results for Protocal A and for both parities are illustrated in the left subplots of Fig. 6.7, while those for Protocol B are shown in the right subplots of Fig. 6.7. It can be seen that for both protocols, the central fringes shrink as the squeezing parameter increases.

6.2.3.3. Signal Fringes for CD-SCAIN with $\mu = \pi/2$. We now turn to the signals for the CD-SCAIN and again first focus on the special case where the squeezing parameter $\mu = \pi/2$. The signals for this case can be obtained by directly taking the expectation value of the operator $J_z/\hbar$ with respect to $|\Psi\rangle_{f,A}$ for Protocol A, or $|\Psi\rangle_{f,B}$ for Protocol B. The final expression again depends on the parity of N. For Protocol A, the result is found to be $\langle\Psi_{f,A}|J_z/\hbar|\Psi_{f,A}\rangle = -N/2\cos(N\phi)$ when N is even, and will be similar to that of a COSAIN when N is odd. The results of this case for both parities are illustrated in the left subplots

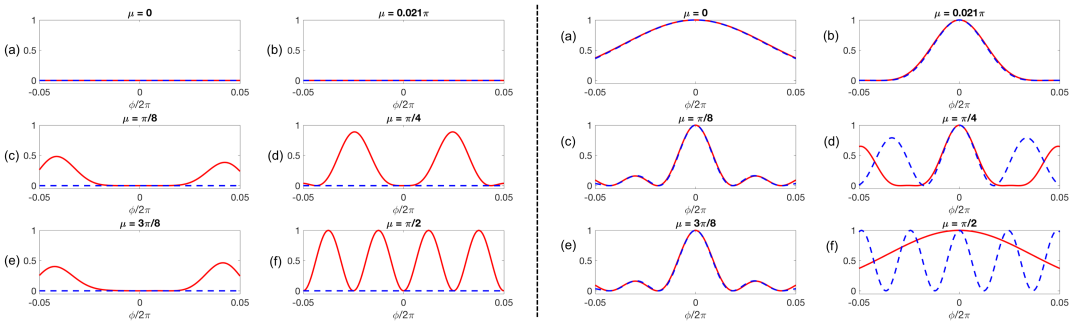

Figure 6.7. Fringe shapes for CSD-SCAIN for different values of the squeezing parameter μ with $\xi = +1$. Left subplots are for protocol A with ARA $= \hat{\mathbf{x}}$ and right subplots are for protocol B with ARA $= \hat{\mathbf{y}}$. In each subplots, $N = 40$ is red while $N = 41$ is dashed-blue. (a) $\mu = 0$; (b) $\mu = 0.021\pi$; (c) $\mu = \pi/8$; (d) $\mu = \pi/4$; (e) $\mu = 3\pi/8$; (f) $\mu = \pi/2$.

of Fig. 6.8. For Protocol B, the result is found to be $\langle \Psi_{f,B}|J_z/\hbar|\Psi_{f,B}\rangle = -N/2\cos(N\phi)$ when N is odd, and will be similar to that of a COSAIN when N is even. The results of this case for both parities are shown in the right subplots of Fig. 6.8. For both protocols, it can be seen clearly that the fringes will be narrowed by a factor of N for one of the parities compared to that of a CRAIN ($\sqrt{N}$ narrower than that of a COSAIN).

6.2.3.4. Fringe shapes for CD-SCAIN with various μ values. Lastly we look at the signals for the CD-SCAIN for various values of the squeezing parameter μ ranging from 0 up to $\pi/2$. Again the signals for this case can be obtained by directly taking the expectation value of the operator $\langle J_z/\hbar\rangle$, with respect to $|\Psi\rangle_{f,A}$ for Protocol A, or $|\Psi\rangle_{f,B}$ for Protocol B. Unlike the special case discussed above, we don't have an analytical expression for the final results, but they can be simulated numerically. The results for Protocal A and for both parities are illustrated in the left subplots of Fig. 6.9, while those for Protocol B are shown in the right subplots of Fig. 6.9. It can be seen that for both protocols, the central fringes shrink as the squeezing parameter increases.

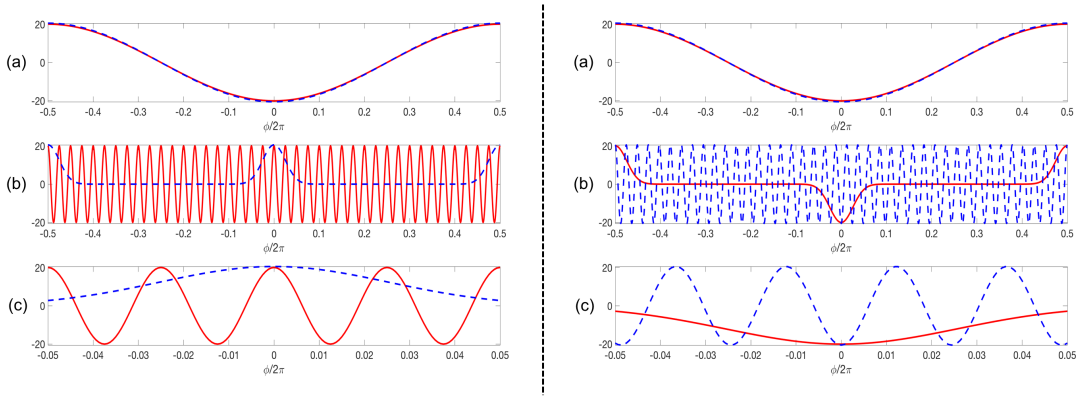

Figure 6.8. Signals for CD-SCAIN corresponding to detection of $\langle J_z/\hbar \rangle$, as a function of ϕ, for $\mu = \pi/2$ and $\xi = +1$. Left subplots are for protocol A with ARA $= \hat{\mathbf{x}}$ and right subplots are for protocol B with ARA $= \hat{\mathbf{y}}$. In each subplots, $N = 40$ is red while $N = 41$ is dashed-blue. (a) Fringes for CRAIN for comparison; (b) Fringes for CD-SCAIN; (c) Zoomed-in fringes for CD-SCAIN. The horizontal span in (c) is 10 times smaller than those in (a) and (b).

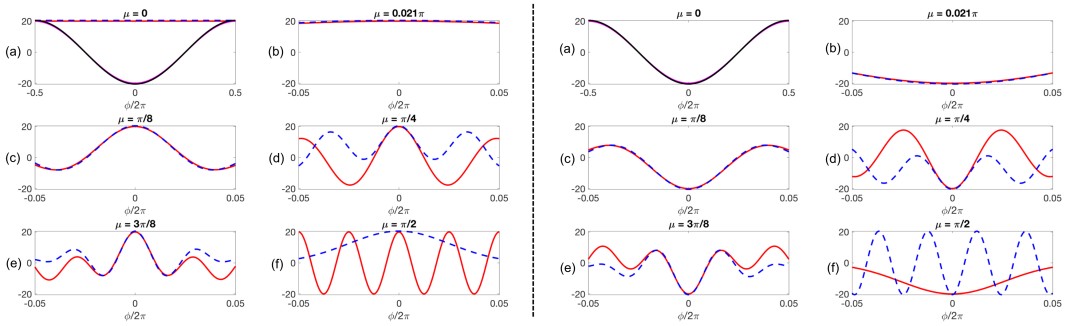

Figure 6.9. Fringe shapes for CSD-SCAIN for different values of the squeezing parameter μ with $\xi = +1$. Left subplots are for protocol A with ARA $= \hat{\mathbf{x}}$ and right subplots are for protocol B with ARA $= \hat{\mathbf{y}}$. In each subplots, $N = 40$ is red while $N = 41$ is dashed-blue. (a) $\mu = 0$; (b) $\mu = 0.021\pi$; (c) $\mu = \pi/8$; (d) $\mu = \pi/4$; (e) $\mu = 3\pi/8$; (f) $\mu = \pi/2$.

6.2.4. Measurement Sensitivities for the SCAIN

After examining the signals of the SCAIN for various cases, we now switch to the measurement sensitivities of the two protocols. In Fig. 6.10, we show the $\mathrm{QFR}^{-1} \equiv |\partial_{\Omega_G} \langle J_z \rangle / \Delta(J_z)|$ of the SCAIN as a function of the squeezing parameter μ, normalized to the HL. The top two subplots are for Protocol A, while the bottom two subplots are for Protocol B. And again we distinguish between the two cases when N is even and odd. The left two subplots are for even N while the right two subplots are for odd N. Within each subplot, we compare results for both the CSD and CD detection schemes.

For Protocol A, when N is even, the measurement sensitivities of both detection schemes tend to increase with increasing squeezing parameter μ, and both eventually reach the HL when $\mu = \pi/2$. When N is odd, however, the measurement sensitivity of CSD scheme vanishes (due to null signal for this case), and that of CD scheme first increases and then plummets to SQL when $\mu = \pi/2$. Therefore, Protocol A is optimal for the case when N is even. In scenarios where N fluctuates randomly between even and odd (such as atoms released from a MOT), the averaged measurement sensitivities (over the even and odd cases) for both detection schemes at $\mu = \pi/2$ will be lower than the HL by a factor of $\sqrt{2}$.

For Protocol B, we have almost the opposite effects. when N is odd, the measurement sensitivities of both detection schemes tend to increase with increasing squeezing parameter μ, and both eventually reach the HL when $\mu = \pi/2$. When N is even, however, the measurement sensitivity of both schemes first increase and then plummet to SQL when $\mu = \pi/2$. Therefore, Protocol B is optimal for the case when N is odd, and in scenarios where N fluctuates randomly between even and odd, the averaged measurement sensitivities for both detection schemes at $\mu = \pi/2$ again will be lower than the HL by a factor of $\sqrt{2}$.

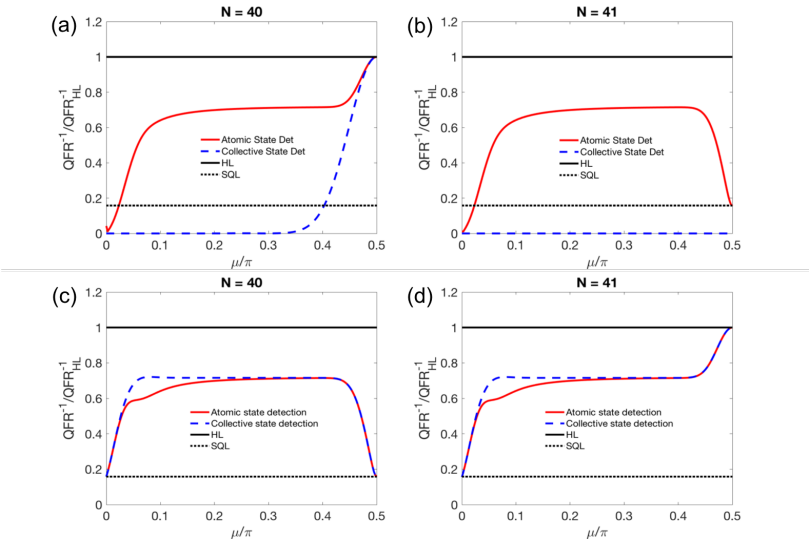

Figure 6.10. Illustration of QFR^{-1} for different cases, as a function of the squeezing parameter μ, normalized to the HL (solid black line), for $\xi = +1$. (a) and (b) are for Protocol A with $N = 40$ and $N = 41$, respectively, in which red is for CD-SCAIN and dashed-blue for CSD-SCAIN; (c) and (d) are for Protocol B with $N = 40$ and $N = 41$, respectively, in which red is for CD-SCAIN and dashed-blue for CSD-SCAIN. The dotted black line shows the SQL.

So far, we have presented the value of QFR^{-1} separately for odd and even values of N. In certain cases, such as for a magnetometer using NVD, where it is possible to operate with a fixed parity of N, the values of QFR^{-1} for a given parity is relevant. For other situation, such as a clock using atoms cooled in a magneto-optical trap (MOT) and released for interrogation, it is necessary to consider the effect of averaging over the two parities. In this case the average value is given by $\mathrm{QFR}^{-1}_{AVE} = \left[(\mathrm{QFR}^{-1}_{EVEN})^2/2 + (\mathrm{QFR}^{-1}_{ODD})^2/2\right]^{1/2}$. Using this result, we can reach the following conclusions, assuming $N \gg 1$. If $\mathrm{QFR}^{-1}_{EVEN} = \mathrm{QFR}^{-1}_{HL}$ and $\mathrm{QFR}^{-1}_{ODD} = 0$, then $\mathrm{QFR}^{-1}_{AVG} = \mathrm{QFR}^{-1}_{QHL}$, where we define $\mathrm{QFR}^{-1}_{QHL} \equiv \mathrm{QFR}^{-1}_{HL}/\sqrt{2}$. Similarly, if $\mathrm{QFR}^{-1}_{EVEN} = \mathrm{QFR}^{-1}_{HL}$ and $\mathrm{QFR}^{-1}_{ODD} = \mathrm{QFR}^{-1}_{SQL}$, then $\mathrm{QFR}^{-1}_{AVG} \cong \mathrm{QFR}^{-1}_{QHL}$. Finally, if $\mathrm{QFR}^{-1}_{EVEN} = \mathrm{QFR}^{-1}_{QHL}$ and $\mathrm{QFR}^{-1}_{ODD} = \mathrm{QFR}^{-1}_{QHL}$, then $\mathrm{QFR}^{-1}_{AVG} = \mathrm{QFR}^{-1}_{QHL}$.

6.3. Schrödinger Cat Atomic Clock

As mentioned in the beginning of this chapter, the protocol consisting of one-axis-twist (OAT) spin squeezing, rotation, unrotation, unsqueezing operations can also be used to realize a Schrödinger Cat Atomic Clock (SCAC) with HL sensitivity. Again the protocol can be combined with collective state detection or conventional detection schemes, where the former is referred to as CSD-SCAC while the latter is referred to as CD-SCAC. In this section, we will first review the features of a conventional Raman Ramsey Atomic Clock (RRAC) and a Collective State Atomic Clock (COSAC) [**58**], then present the results obtained for SCAC for both detection schemes.

6.3.1. Raman Ramsey Atomic Clock and Collective State Atomic Clock

Here we consider a system where the ground states, $|1\rangle$ and $|2\rangle$ of a three-level atom interact with an excited state $|3\rangle$ via two copropagating laser beams (see Fig. 2.6). One of the beams is detuned from resonance by δ_1 and has a Rabi frequency Ω_1; this couples $|1\rangle$ to $|3\rangle$. The second beam is detuned from resonance by δ_2 and has a Rabi frequency Ω_2; this couples $|2\rangle$ to $|3\rangle$. For $\delta \gg \Omega_1,\ \Omega_2,\ \Gamma$, where $\delta \equiv (\delta_1 + \delta_2)/2$ and Γ is the excited state decay rate, the system can be modeled as an effective two level system, consisting of states $|1\rangle$ and $|2\rangle$, excited by a traveling wave with a Rabi frequency $\Omega = \Omega_1\Omega_2/(2\delta)$, and detuning $\Delta \equiv \delta_1 - \delta_2$. For simplicity, we assume $\Omega_1 = \Omega_2$, and $\Delta \ll \delta$, so that $\delta_1 \simeq \delta_2$. Under this condition, the light-shifts experienced by states $|1\rangle$ and $|2\rangle$ are essentially the same, and do not affect the equation of motion [**82**]. For more general cases, it is possible to incorporate any differences in the light shifts into the definition of Δ.

As in the case of the SCAIN discussed in the previous section, we denote states $|1\rangle$ and $|2\rangle$ as being the pseudo-spin states $|\downarrow\rangle$ and $|\uparrow\rangle$, respectively. In a conventional Raman Ramsey atomic clock, an ensemble of N effective two-level atoms is first prepared in a coherent spin state (CSS) where all spins are in the spin-down state, as shown in Eq. (6.1). The first $\pi/2$ pulse produces a rotation about the $\hat{\mathbf{x}}$ axis. During the dark zone with a duration of T_D, each atom acquires a phase $\phi = 2\pi f T_D$, where $f = \Delta/2\pi$ is the (two-photon) detuning of the clock (in Hertz). Application of the second $\pi/2$ pulse around the $\hat{\mathbf{x}}$ axis produces the final state, which, for each atom, can be expressed, ignoring an overall phase-factor, as:

$$\begin{aligned} |\Psi\rangle &= e^{-i\frac{\pi}{2}J_x} e^{-i\phi J_z} e^{-i\frac{\pi}{2}J_x} |-\hat{\mathbf{z}}\rangle \\ &= \bigotimes_{l=1}^{N} \frac{1}{2}\{(1-e^{i\phi})\,|\downarrow_l\rangle - i(1+e^{i\phi})\,|\uparrow_l\rangle\} \end{aligned} \tag{6.6}$$

In a RRAC, typically the signal is a measure of the population of $|\uparrow\rangle$, given by $S_{RRAC} = J + \langle J_z\rangle = N\cos^2(\phi/2)$. The associated quantum projection noise is $\Delta S_{RRAC} = \Delta J_z = \sqrt{N/4}|\sin\phi|$. The stability of the clock is attributed to the quantum fluctuation in frequency (QFF), analogous to the QFR described in the previous section. This can be expressed as $\mathrm{QFF} = \Delta f|_{RRAC} = |\Delta(J_z)/\partial_f \langle J_z\rangle| = (2\pi T_D\sqrt{N})^{-1}$, where $\partial_f \equiv \partial/\partial f$. This can also be expressed as $\Delta f|_{RRAC} = \gamma/\sqrt{N}$, where $\gamma = 1/(2\pi T_D)$ is the effective linewidth. This is, of course, the SQL value of the QFF.

In a COSAC, however, the signal is a measure of the population of one of the extremal collective states and is given by $S_{COSAC} = \langle\hat{Q}\rangle = \cos^{2N}(\phi/2)$, where $\hat{Q} \equiv |E_N\rangle\langle E_N|$. This signal shows a $\sqrt{N}$-fold reduction in fringes compared to that of a RRAC, which can be explained as follows. The first $\pi/2$ pulse couples the initial state $|E_0\rangle$ to $|E_1\rangle$, which in turn is coupled to $|E_2\rangle$ and so on, effectively causing the ensemble to split into $N+1$ states. During

the dark zone, the *n-th* collective state $|E_n\rangle$ picks up a phase $e^{-in\phi}$. When the ensemble interacts with the last $\pi/2$ pulse, each of the collective states interferes with the rest of the collective states. The COSAC can thus be viewed as the aggregation of interference patterns due $\binom{N+1}{2}$ RRAC's working simultaneously [**58**]. The narrowest constituent signal fringes are derived from interferences between states with the largest difference in phase, i.e. $|E_0\rangle$ and $|E_N\rangle$; the width of this fringe is γ/N. The width of the rest of the signal components range from γ to $\gamma/(N-1)$. The signal, which is the measure of population of $|E_N\rangle$, is the result of the weighted sum of all the pairwise interferences, with a width of $\gamma/\sqrt{N}$. However, the system acts as a single particle, which reduces the effective SNR by the factor of $\sqrt{N}$. As a result, we have shown that the QFF for the COSAC is essentially the same as that for the RRAC [**58**].

From the analyses above, if the evolution of the system could be restricted to just the two extremal Dicke states (namely, $|E_0\rangle$ and $|E_N\rangle$) during the dark zone evolution, the fringes would be narrowed by a factor of N compared to those of the RRAC. In that case, the QFF would be enhanced by a factor of $\sqrt{N}$, thus reaching the HL sensitivity. As noted at the beginning of this chapter, the process of OAT squeezing indeed can be used to create just such a Schrödinger Cat (SC) state if the degree of squeezing is chosen to be $\mu = \pi/2$, and an auxiliary rotation of $\pi/2$ is applied along a particular axis after the squeezing pulse. The resulting clock is then referred to as the SCAC.

6.3.2. The Complete Protocol for Realizing the SCAC

The complete pulse sequence employed for a SCAC is illustrated in Fig. 6.11. Everything else is the same as that used for a RRAC, except for the four additional pulses necessary for implementing the OAT spin squeezing effects. The process starts by applying a $\pi/2$ pulse

around the $\hat{\mathbf{x}}$ axis. This is followed by the application of OAT, corresponding to a rotation around the $\hat{\mathbf{z}}$ axis by an angle of μJ_z, with $\mu = \pi/2$. The next step is an auxiliary rotation of $\pi/2$ around the $\hat{\mathbf{x}}$ axis. The ensuing evolution in the dark zone corresponds to a rotation by ϕ around the $\hat{\mathbf{z}}$ axis, where $\phi = 2\pi f T_D$. This is now followed by another auxiliary rotation around the $\hat{\mathbf{x}}$ axis, by an angle of $\xi\pi/2$. This is followed by an unsqueezing pulse, which corresponds to a rotation around the $\hat{\mathbf{z}}$ axis by an angle of $-\mu J_z$, with $\mu = \pi/2$. Finally, the process ends with the application of the final $\pi/2$ pulse around the $\hat{\mathbf{x}}$ axis. Mathematically, the whole process can thus be expressed as:

$$|\Psi\rangle_f = e^{-i\frac{\pi}{2}J_x} e^{i\mu J_z^2} e^{-i\xi\frac{\pi}{2}J_x} e^{-i\phi J_z} e^{-i\frac{\pi}{2}J_x} e^{-i\mu J_z^2} e^{-i\frac{\pi}{2}J_x} |-\hat{\mathbf{z}}\rangle \tag{6.7}$$

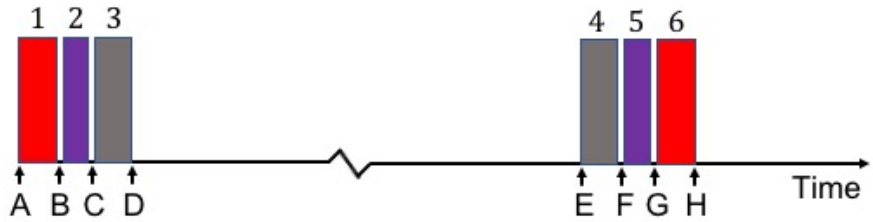

Figure 6.11. Schematic illustration of the pulse sequence employed for a SCAC. In addition to the usual two $\pi/2$ pulses (labeled as 1, 6) used in a RRAC, a SCAC employs four more pulses, labeled as 2, 3, 4, 5, corresponding to the squeezing, rotation, inverse rotation and unsqueezing operations.

As in the case of the SCAIN, there are two equivalent protocols for SCAC, where for Protocol A, the auxiliary rotation is done around $\hat{\mathbf{x}}$ axis while for Protocol B, the auxiliary rotation is done around $\hat{\mathbf{y}}$ axis. Again the exact effects of the protocol depend on a set of parameters such as the value (and parity) of N, the squeezing parameter μ for the OAT spin squeezing, the auxiliary rotation axis (ARA, can be $\hat{\mathbf{x}}$ or $\hat{\mathbf{y}}$ axes), the corrective rotation sign ξ which can take values of ± 1 corresponding to redoing or undoing the first auxiliary rotation,

and lastly the dark zone phase shift ϕ. Since the two protocols are essentially equivalent, here we are only showing the results for Protocol A. The evolution of the quantum states on a Bloch sphere, using the QPDs, is illustrated in Fig. 6.12. The upper subplot is for even $N = 40$, while the lower subplot is for odd $N = 41$.

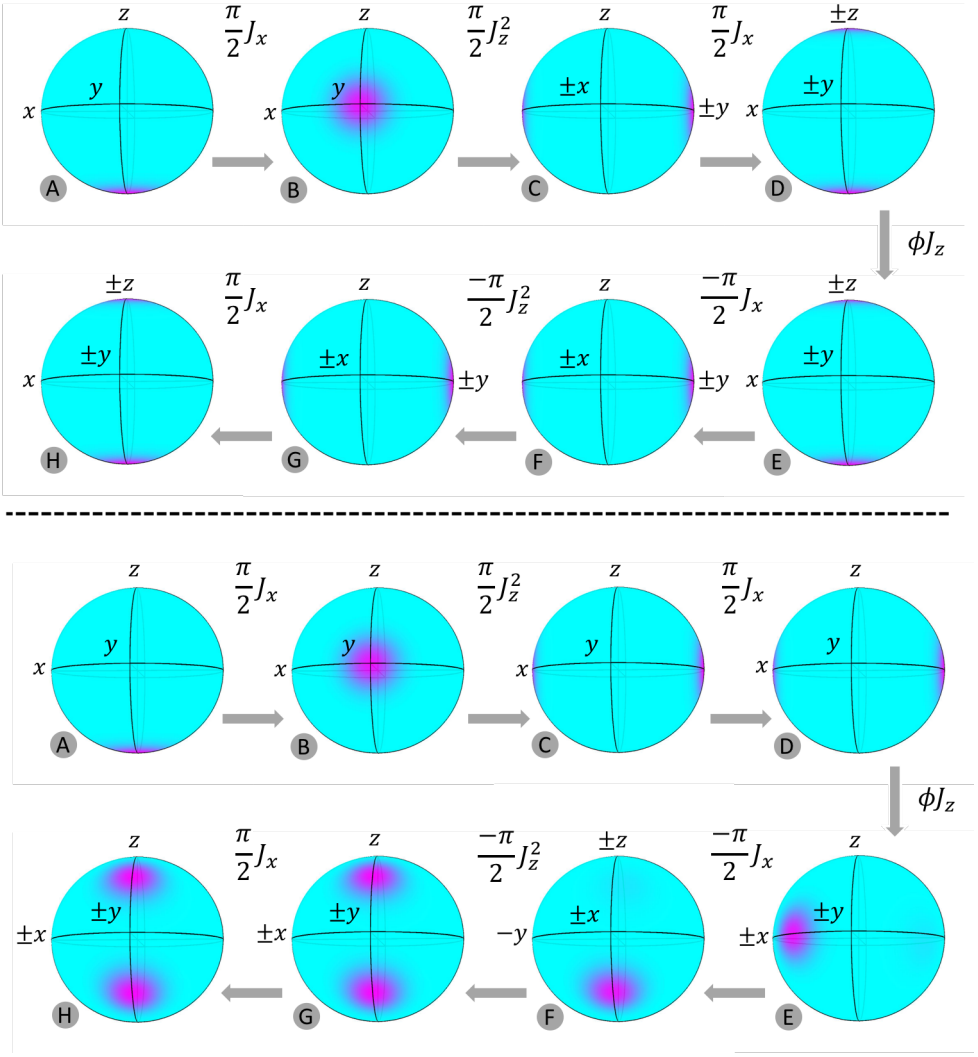

Figure 6.12. The QPDs at different stages of Protocol A. The upper subplots are for $N = 40$, $\mu = \pi/2$, ARA $= \hat{\mathbf{x}}$, $\xi = -1$ and $\phi = 0.5\pi/N$, while the lower subplots are for $N = 41$, $\mu = \pi/2$, ARA $= \hat{\mathbf{x}}$, $\xi = -1$ and $\phi = \pi/4$.

We first detail the evolution for the even case (upper subplot). At the onset of the process (time point A), the system is assumed to be in the state $|E_0\rangle = |-\hat{\mathbf{z}}\rangle$, which is a CSS. After the first $\pi/2$ rotation around the $\hat{\mathbf{x}}$ axis (time point B), it is in state $|\hat{\mathbf{y}}\rangle$. After the squeezing pulse, the state (time point C) is split between two CSSs, and can be expressed as $(|\hat{\mathbf{y}}\rangle - \eta\,|-\hat{\mathbf{y}}\rangle)/\sqrt{2}$, , where $\eta = i(-1)^{N/2}$, representing a phase factor with unity amplitude. This factor depends on the super even parity (SEP). However, the shapes of the fringes, as well as the values of QFF^{-1}, for both CSD and CD protocols, are not expected to depend on the value of the SEP, as we have verified explicitly. Application of the auxiliary rotation of $\pi/2$ around the $\hat{\mathbf{x}}$ axis transforms this state to $(|-\hat{\mathbf{z}}\rangle + \eta\,|\hat{\mathbf{z}}\rangle)/\sqrt{2}$. This (time point D) represents the desired SC state, as a superposition of the two extremal states of the ZDCS manifold: $(|E_0\rangle + \eta\,|E_N\rangle)/\sqrt{2}$. During the dark zone, the phase shift causes a rotation by an angle of ϕ around the $\hat{\mathbf{z}}$ axis, for each atom. The state after the dark zone can be expressed as $e^{-i\phi J_z}(|E_0\rangle + \eta\,|E_N\rangle)/\sqrt{2}$. Since both $|E_0\rangle$ and $|E_N\rangle$ are eigenstates of the J_z operator, with eigenvalues (assuming $\hbar = 1$) of $-N/2$ and $N/2$ respectively, this state can be expressed as $\left(e^{i\phi N/2}\,|E_0\rangle + e^{-i\phi N/2}\eta\,|E_N\rangle\right)/\sqrt{2}$. The resulting QPD, shown at time point E of Fig. 6.12, remains unchanged, but the quantum state incorporates these phase accumulations. In order to reveal the interference magnified by the factor of N, it is necessary to apply first another auxiliary rotation, by an angle of $\xi\pi/2$ around the $\hat{\mathbf{x}}$ axis. The QPD resulting from the case for $\xi = -1$ is shown at time point F. It is then necessary to apply the unsqueezing pulse, by an angle of $-\mu J_z$, with $\mu = \pi/2$. The QPD of the resulting state is shown at time point G. Finally, it is necessary to apply one more rotation around the $\hat{\mathbf{x}}$ axis, by an angle of $\pi/2$. The QPD for the final state is shown at time point H.

For this case, the final state can be expressed as $|\Psi\rangle_f = \eta\cos(N\phi/2)\,|E_N\rangle + \sin(N\phi/2)\,|E_0\rangle$. For the particular value of ϕ (which is $0.5\pi/N$) used in generating the QPDs, the final state is

$(\eta\,|E_N\rangle + |E_0\rangle)/\sqrt{2}$. If the population of $|E_N\rangle$ were detected, the signal would be expressed as $\cos^2(N\phi/2)$, with fringes that are a factor of N narrower than that for the RRAC. This is referred to as CSD-SCAC, which is discussed in Ref. [**74**]. If we choose to measure the expected value of the operator $J_z/\hbar$, the same results hold, and the corresponding type of SCAC is referred to as CD-SCAC.

We then look at the evolution for the odd case (lower subplot). The state after the OAT squeezing is found to be very different, which is SC state as a superposition of two extremal collective states, but in terms of the XDCSs. Now the application of the auxiliary rotation by $\pi/2$ around the $\hat{\mathbf{x}}$ axis from C to D leaves the QPD unchanged. The rest evolutions then will be drastically different, as can be seen from time point D to H.

6.3.3. Signal Fringes for the SCAC

In Fig. 6.13, the signal fringes for the SCAC using Protocol A are plotted as a function of ϕ. Left subplots are for Collective State Detection scheme, while right subplots are for Conventional Detection scheme. For both detection schemes, we can clearly see the N-fold reduction in fringe width.

6.3.4. QFF^{-1} for the SCAC

In Fig. 6.14, we illustrate the behavior of $\mathrm{QFF}^{-1} \equiv |\partial_f \langle J_z/\Delta(J_z)\rangle|$, as a function of μ, for Protocol A with $\xi = +1$, along with comparison with the Echo Scueezing Protocol (ESP) [**22, 24**]. In each case, the QFF^{-1} is normalized to the QFF^{-1}_{HL} for $N = 40$, indicated as the solid black line. The dashed black line shows the QFF^{-1}_{SQL} for $N = 40$.

Fig. 6.14 (a) corresponds to $N = 40$. Here, the red line corresponds to the CD-SCAC, and the dashed-blue line is for the CSD-SCAC. For $\mu = \pi/2$, we see that the sensitivity for

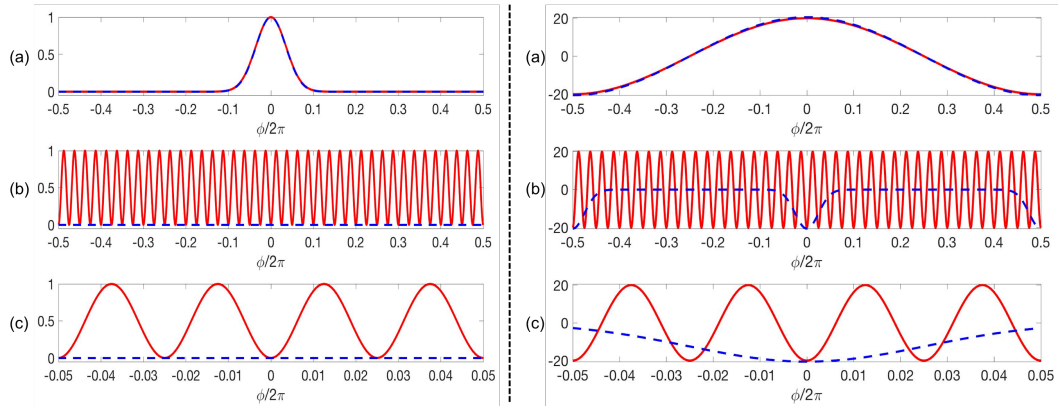

Figure 6.13. Signals corresponding to detection of $\langle J_z/\hbar \rangle$, as a function of ϕ for Protocol A with $\mu = \pi/2$ and $\xi = +1$. Left subplots are for Collective State Detection scheme, while right subplots are for Conventional Detection scheme. In each subplots, $N = 40$ is red while $N = 41$ is dashed-blue. For left subplots: (a) Fringes for COSAC for comparison; (b) Fringes for CSD-SCAIN; (c) Zoomed-in fringes for CSD-SCAIN. For right subplots: (a) Fringes for RRAC for comparison; (b) Fringes for CD-SCAIN; (c) Zoomed-in fringes for CD-SCAIN. For both detection schemes, the horizontal span in (c) is 10 times smaller than those in (a) and (b).

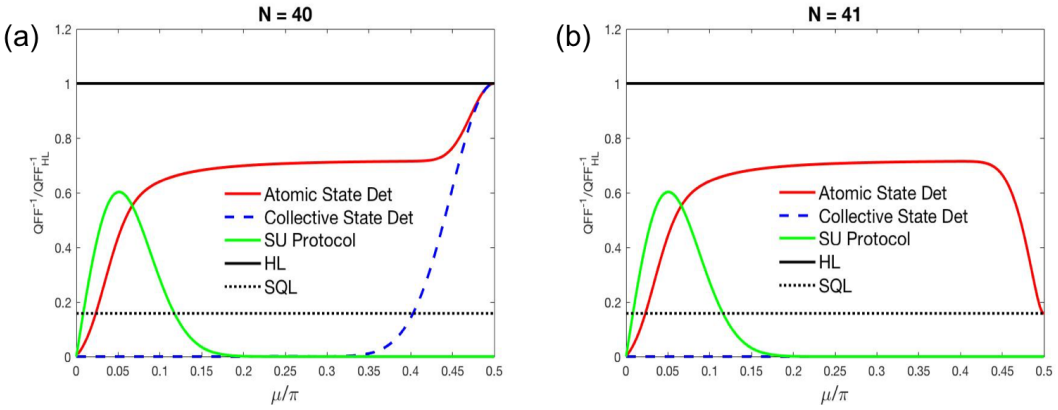

Figure 6.14. Illustration of QFF^{-1} for Protocol A, as a function of the squeezing parameter μ, normalized to the HL (solid black line). (a) The case for even $N = 40$; (b) The case for odd $N = 41$. The dotted black line shows the SQL. Red is for CD-SCAC, dashed-blue for CSD-SCAC and green for the ESP case. For all cases shown, $\xi = +1$.

both CD and CSD protocols yield the HL sensitivity. This sensitivity is reached due to an amplification of phase by a factor of N, and a concomitant increase in the SD by a factor of $\sqrt{N}$. Fig. 6.14 (b) is the same as Fig. 6.14 (a), except that $N = 41$. In this case, $\mu = \pi/2$, for the CD-SCAC, there is a phase amplification, manifested as a Fabry-Perot like fringe around $\phi = 0$ which is narrowed by a factor of $\sqrt{N}$, along with an increase in the square-root of the variance by a factor of $\sqrt{N}$. The difference between the even and odd cases disappears when the value of μ is reduced below a threshold value of $\sim 0.45\pi$. There is a range of values of the squeezing parameter ($0.2\pi \leq \mu \leq 0.45\pi$) over which the normalized value of QFF^{-1} is ~ 0.71 for the CD-SCAC. We have verified that this plateau ratio between QFF^{-1} and QFF^{-1}_{HL} remains unchanged when N is increased or decreased. We also see that, for this choice of the ARA, the behavior of the CSD-SCAC is drastically different. Specifically, for odd values of N, the QFF^{-1} is strictly zero for all values of the squeezing parameter, and for even value of N, the QFF^{-1} drops to zero quickly for $\mu < \pi/2$.

So far, we have presented the value of QFF^{-1} separately for odd and even values of N. For certain situations, such as a clock using atoms cooled in a magneto-optical trap (MOT) and released for interrogation, it is necessary to consider the effect of averaging over the two parities. In this case the average value is given by $\mathrm{QFF}^{-1}_{AVE} = \left[(\mathrm{QFF}^{-1}_{EVEN})^2/2 + (\mathrm{QFF}^{-1}_{ODD})^2/2\right]^{1/2}$. Using this result, we can reach the following conclusions, assuming $N \gg 1$. If $\mathrm{QFF}^{-1}_{EVEN} = \mathrm{QFF}^{-1}_{HL}$ and $\mathrm{QFF}^{-1}_{ODD} = 0$, then $\mathrm{QFF}^{-1}_{AVG} = \mathrm{QFF}^{-1}_{QHL}$, where we define $\mathrm{QFF}^{-1}_{QHL} \equiv \mathrm{QFF}^{-1}_{HL}/\sqrt{2}$. Similarly, if $\mathrm{QFF}^{-1}_{EVEN} = \mathrm{QFF}^{-1}_{HL}$ and $\mathrm{QFF}^{-1}_{ODD} = \mathrm{QFF}^{-1}_{SQL}$, then $\mathrm{QFF}^{-1}_{AVG} \cong \mathrm{QFF}^{-1}_{QHL}$. Finally, if $\mathrm{QFF}^{-1}_{EVEN} = \mathrm{QFF}^{-1}_{QHL}$ and $\mathrm{QFF}^{-1}_{ODD} = \mathrm{QFF}^{-1}_{QHL}$, then $\mathrm{QFF}^{-1}_{AVG} = \mathrm{QFF}^{-1}_{QHL}$.

6.4. Comparison of Measurement Sensitivities for Various Protocols

In this section, we briefly review and compare the various protocols proposed for improving the measurement sensitivities of an atomic interferometer (AI). For an AI, the signal S can be expressed as a function of the phase difference ϕ between the two arms. The measurement sensitivity, Λ, can be expressed as the inverse of the phase fluctuation (PF): $\Lambda = \mathrm{PF}^{-1} = |\partial_\phi S/\Delta S|$, where $\partial_\phi \equiv \partial/\partial\phi$. Here, $\partial_\phi S$ is the phase gradient of the signal (PGS), and ΔS is the standard deviation of the signal (SDS). When excess noise (EN) is suppressed sufficiently, Λ is limited by the quantum projection noise (QPN) [**79**], and is given by the inverse of the quantum phase fluctuation (QPF^{-1}). Therefore, to enhance Λ, one can either increase the PGS or decrease the SDS.

For a conventional AI, the sensitivity is at the Standard Quantum Limit (SQL): $\Lambda = \mathrm{QPF}^{-1} = \sqrt{N}$, which will serve as the baseline for other protocols. As we have shown, using spin-squeezing, it is possible to surpass the SQL, and a key goal in this context is to achieve the Heisenberg Limit (HL), under which $\Lambda = N$, representing an improvement by a factor of $\sqrt{N}$.

In a conventional approach for spin squeezing, one minimizes the SDS. For example, using optimal one-axis-twist (OAT) spin squeezing and two-axis-counter-twist (TACT) spin squeezing [**12**], the SDS can be reduced respectively by a factor of $N^{1/3}$ and $\sqrt{N/2}$, while the PGS remains essentially unchanged, compared to those of a conventional AI. As such, $\Lambda = N^{5/6}$ for the former and $\Lambda = N/\sqrt{2}$ for the latter. Though the TACT squeezing can yield a better sensitivity, it is experimentally more complicated than the OAT squeezing [**15, 16, 24, 83, 84, 85, 86, 87**].

Recently [**22, 24**], it was shown that it is also possible to reach sensitivity at or near the HL using variants of the OAT. Ref. [**22**] proposed and Ref. [**24**] demonstrated the echo squeezing protocol (ESP), which can increase the PGS by a factor of $\sim \sqrt{N/2}$, while leaving the SDS unchanged, thus producing $\Lambda \approx N/\sqrt{2}$.

In the previous sections, we introduced the CSD-SCAIN [**74**] that makes use of critically tuned OAT, rotation, inverse rotation and unsqueezing operations, in combination with collective state detection scheme. The CSD-SCAIN reduces the SDS by a factor of $\sqrt{N}$, while leaving the PGS unchanged, yielding $\Lambda = N$.

We also described the CD-SCAIN protocol, which employs the conventional detection scheme by measuring directly the populations of the spin-up or spin-down states of individual atoms. Under this protocol, the PGS is increased by a factor of N, while the SDS is also increased by a factor of $\sqrt{N}$. The net enhancement in Λ is by a factor of $\sqrt{N}$, reaching the HL. However, because of the increase in noise (i.e., SDS), this is now significantly more robust against excess noise than all the protocols described above. *Specifically, for this protocol, it should be possible to achieve $\Lambda = N/\sqrt{2}$ even when the excess noise is greater than the QPN for a conventional AI by a factor of $\sqrt{N}$.*

The degree of suppression of excess noise for different protocols is illustrated in Fig. 6.15. Here, we consider a situation where excess noise contributes an additional variance, ΔS^2_{EN}, to the signal. The sensitivity is then given by $\Lambda = \left|\mathrm{PGS}/\sqrt{\Delta S^2_{\mathrm{QPN}} + \Delta S^2_{\mathrm{EN}}}\right| = \Lambda_{\mathrm{QPN}}/\sqrt{1+\rho^2}$, where $\rho \equiv \Delta S_{\mathrm{EN}}/\Delta S_{\mathrm{QPN}}$. One way to characterize the degree of robustness against excess noise is by determining the value of ΔS_{EN} for which $\rho = 1$. As can be seen, for TACT, this value is 1, making it particularly vulnerable to excess noise. In contrast, for ESP (as well as for the conventional AI), this value is $\sqrt{N}$, making it a factor of $\sqrt{N}$ more robust than TACT. For CD-SCAIN, this value is N, making it a factor of $\sqrt{N}$ (N) more robust

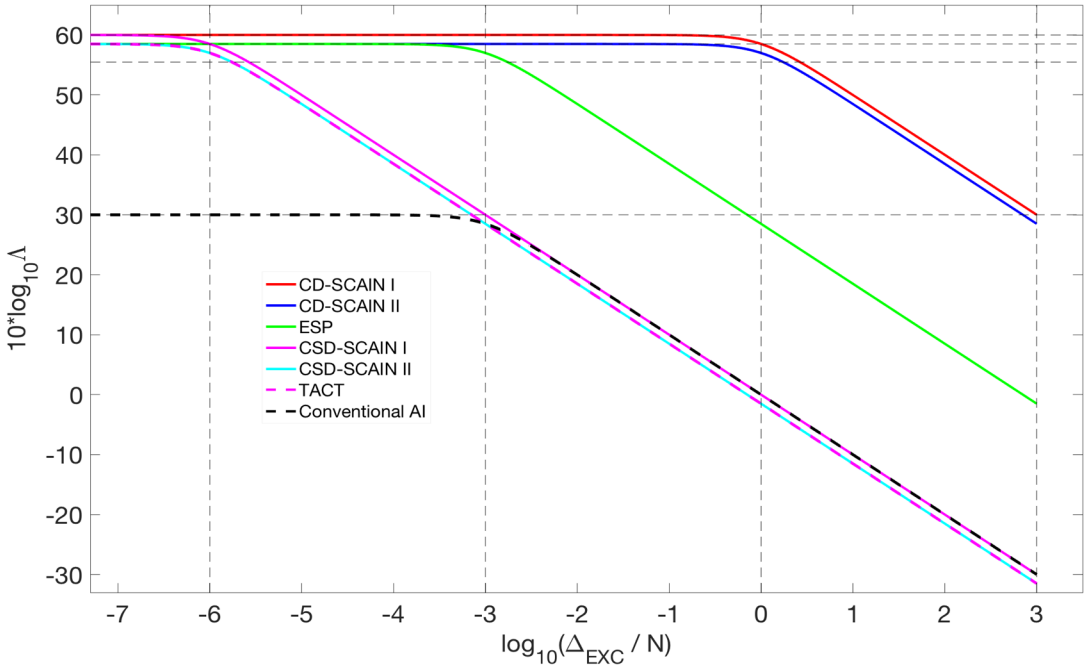

Figure 6.15. The sensitivity, Λ, as a function of excess noise (EN), ΔS_{EN}, for various protocols. For both CSD-SCAIN and CD-SCAIN, we have used two labels: I and II; I indicates the case when the parity of N is known, while II indicates the case where the signal is averaged over both parities.

than ESP (TACT). We also see that CSD-SCAIN is as sensitive to excess noise as TACT. Thus, in switching from collective state detection to conventional detection, the robustness of the SCAIN protocol to excess noise is improved by a factor of N. One can also define the range of usefulness of a protocol as the value of ΔS_{EN} for which the sensitivity drops to $\Lambda = \sqrt{N/2}$. By this measure, the usefulness of CD-SCAIN extends to $N^{3/2}$, while that for ESP extends only to N. Ref. [**78**] presents a protocol that also makes use of OAT critically tuned to the same degree as that employed by SCAIN. However, the usefulness of this also extends only to N.

6.5. Experimental Considerations for Realizing the SCAIN

In this section, we describe the experimental steps envisioned for realizing the SCAIN, and discuss potential limitations. It should be noted that the discussions in this section are also appliable to SCAC. The basic protocol is akin to that employed for the CRAIN, with the addition of auxiliary rotations, one axis twist (OAT) squeezing and collective state detection (CSD). In what follows, we first summarize briefly the experimental approach for OAT squeezing and CSD that are well-suited for the SCAIN. This is followed by a discussion of the complete protocol for the SCAIN. We discuss both Protocols A and B, but limit the description to the case of $\mu = \pi/2$. The case for $\mu < \pi/2$ can be easily inferred from this discussion.

There are several experimental schemes for realizing one-axis-twist squeezing [**15, 16, 22, 23, 24, 40, 88, 89, 90, 91**]. For concreteness, we consider here the approach based on cavity feedback dynamics [**15, 16, 22, 23, 24, 40**]. In this approach, a probe is passed through a cavity, at a frequency that is tuned halfway between the two legs of a Λ transition in which the spin-up and spin-down states are coupled to an intermediate state. The cavity is tuned to be below resonance for the probe. The energy levels of the spin-up and spin-down states are light shifted due to the probe, in opposite directions. The resulting dispersion shifts the cavity resonance frequency by an amount that is proportional to J_z, the z-component of the total spin for all atoms. The intra-cavity probe intensity changes linearly with this cavity shift, since it is on the side of the resonance, thus affecting the light-shifts. The net result is an energy shift for all the atoms that is proportional to the square of J_z, so that the interaction Hamiltonian can be expressed as $H_{OAT} = \hbar\chi J_z^2$, where χ is a parameter that

determines the strength of the squeezing process. Changing the sign of the cavity detuning reverses the sign of the Hamiltonian, thus producing unsqueezing.

The collective state detection technique is detailed in section IV of Ref. [**64**], where a null-detection scheme is employed to measure population of one of the extremal Dicke collective states. The probe is one of the two counter-propagating Raman beams, which induces Raman transitions within the atomic ensemble unless it is in the desired extremal collective state. As a result, there will be photons emitted corresponding to the other leg of the Raman transition. The probe and the emitted photons are combined and sent to a high speed detector, which produces a dc signal along with a beat signal. This beat signal is at the same frequency as that of the signal produced by the frequency synthesizer (FS) that drives the Acousto-Optic Modulator (AOM), for example, used to generate the beam that excites one leg of the Raman excitation from the beam that excites the other leg of the Raman excitation, but with a potential difference in phase. To extract the amplitude, the beat signal is bifurcated and one part is multiplied by the FS signal, while the other is multiplied by the FS signal phase shifted by 90 degrees. The signals are then squared before being recombined and sent through a low-pass filter (LPF) to derive a dc voltage. This dc voltage is proportional to the number of scattered photons. A lower limit (ideally zero) is set for the voltage reading, and any value recorded above it indicate the presence of emitted photons. If no photon is emitted, the voltage will be at or below the limit, indicating that the ensemble is in the desired extremal collective state; otherwise at least one photon will be emitted and the ensemble will be in a combination of other collective states. This process is then repeated many times for a given value of ϕ. The fraction of events where no photons are detected will correspond to the signal for this value of ϕ. This process is then repeated for several values of ϕ, producing the signal fringe.

For the complete SCAIN experiment, we assume that the source atoms, are caught in a magneto-optic trap (MOT), followed by polarization gradient cooling and evaporative cooling, to a temperature of about $0.5\,\mu$K, with a phase-space density less than what is required for Bose-Einstein Condensation (BEC). The atoms are then pushed out, forming a sequential beam of N atoms in each sequence. An initial (counter-propagating) Raman pulse, corresponding to a rotation of $\pi/2$ around the x-axis, splits each atom, originally in the spin-down state, into an equal super-position of spin-up and spin-down states. The atoms then pass through a transverse ring cavity set up for OAT squeezing. The squeezing process is carried out for a duration corresponding to $\mu = \pi/2$, followed by an auxiliary rotation (produced by another pair of Raman beams) by an angle of $\pi/2$ around the x-axis. This creates the SC state, as a superposition of two extremal Dicke collective states: one in which all atoms are in the spin-down state, and another in which all atoms are in the spin-up state. The two components in the SC state get spatially separated during the first dark zone evolution. This is followed by another Raman pulse which produces a rotation of π around the x-axis. This pulse redirects the velocities of the two components. After the second dark zone, another Raman pulse is applied for a duration that produces a rotation of $\pi/2$ around the x-axis. This is followed by an unsqueezing pulse, of duration corresponding to $\mu = -\pi/2$, which is produced by sending the atoms through a second transverse ring cavity, with a cavity detuning that is equal and opposite to the one applied in the first cavity. After the unsqueezing, the final $\pi/2$ rotation around the x-axis, produced by another Raman pulse, causes the two paths to interfere. The collective state detection process is then used to determine the population of the atoms in the collective state in which all the atoms in the spin-down state, representing the signal for the SCAIN, under Protocol A and the limiting case of $\mu = \pi/2$.

For implementing Protocol B, for $\mu = \pi/2$, the basic sequence is the same as what is described above, with the following modifications. Note that, in the sequence described above, there are five different pairs of Raman beams; three of these are used for the conventional pulse sequences necessary for a CRAIN, while the other two are used for auxiliary rotations. In the case of Protocol B, the auxiliary rotations are around the y-axis. The phase of the beat signal between the two frequencies employed for Raman excitation determines the axis of rotation. Thus, this phase for the two pairs of Raman beams used for the auxiliary rotations has to be shifted by 90 degrees compared to the same for the three pairs of Raman beams used for the CRAIN pulse sequence. To see how this phase shift can be produced, we note that (as also mentioned in the discussion for the CSD above) for each pair of Raman beams, we start with a laser beam at a frequency that excites one leg of the Λ transition. The second laser frequency, which excites the other leg of the Λ transition, is produced by shifting the frequency of a piece of the first laser beam by passing it through an AOM, for example. The frequency that drives the AOM is generated from an FS. Thus, to generate the phase shift needed for Protocol B, we lock the difference between the phase of the FS used for the auxiliary Raman beams and that of the FS used for the CRAIN Raman beams to a value of 90 degrees. As a result, the auxilary Raman beams will produce rotations of $\pi/2$ around the y-axis, as needed for Protocol B.

To elucidate potential practical limitations in implementing the SCAIN protocol experimentally, as envisioned above, consider first the situation where the OAT squeezing and unsqueezing processes are ideal. In that case, the relevant issues pertain to the potential imperfections in generating the ideal collective states. In references [**57**] and [**64**], we discussed the issues that are relevant in this context, and how these issues may limit the performance of the COSAIN. Essentially the same issues are expected to constrain the performance of

the SCAIN. In what follows, we summarize the findings of the analysis presented in these two references [**57, 64**], in the context of the SCAIN, using ^{87}Rb atoms for specificity. First, we noted that for a Raman excitation based atomic interferometer (such as the COSAIN and the SCAIN), the collective states must be defined in a manner so that the spin-down state represents the atom being in the ground state of the internal energy, and in a momentum eigenstate of the center-of-mass (COM) motion, and the spin-up state represents the atom being in a higher-energy but metastable internal state, and in another momentum eigenstate of the COM motion. Since the atom is in a wavepacket with respect to the COM motion, the spin-down state, for example, is in a superposition of momentum eigenstates. Similarly, the spin-up state is also in a superposition of momentum eigenstates, even if we assume that the two-photon recoil imparted by the Raman beams is exactly the same for each atom. In Section 4 of reference [**57**], we addressed this issue explicitly, and showed that if the effective Rabi frequency of the off-resonant Raman transition (i.e., the Raman Rabi frequency) is much larger than the Doppler shift due to the COM momentum of each of the constituent plane waves in the ground state wavepacket, then the description of the semi-classical collective states (which ignores the COM motion), as employed here and in virtually all descriptions of collective states in the literature, remains valid. For the temperature of 0.5 µK mentioned above for the SCAIN, it should easily be possible to realize an effective Rabi frequency large enough to satisfy this condition.

Second, we considered the effect of the variations in the intensity profiles of the laser beams, which in turn cause variations in the Raman Rabi frequency. The effect of this inhomogeneity can be mitigated by increasing the ratio, ρ, of the diameter of the Raman beams to the diameter of the atomic cloud. For $\rho = 10$, the upper bound of the useful value of N was found to be $\sim 1.2 \times 10^5$. Third, we considered the effect of the velocity distribution,

which causes variations in the two-photon detuning. We found that at a temperature of $0.5\,\mu$K, this inhomogeneity limits the useful value of N to $\sim 2 \times 10^4$. The useful value of N can, in principle, be increased further by using colder atoms, as long as the phase space density is kept below the value at which BEC occurs.

Fourth, we considered the effect of spontaneous emission, since there is a small fraction of atoms in the intermediate state during the application of the Raman pulses. A proper analysis of the effect of spontaneous emission would require the use of a density matrix based model in the basis of the collective states. Coherent excitation of the atoms only populates the $(N+1)$ symmetric collective states [**57, 59, 92**]. However, the total number of collective states, which include the asymmetric ones, is 2^N, the size of the Hilbert space for N two-level atoms [**57**]. All of these states must be taken into account when considering the effect of spontaenous emission, which can couple to both symmetric and asymmetric states. Thus, even for a modest number of N that would be relevant for a SCAIN, such an analysis is intractable (as also noted in the supplement of reference [**22**]). For large N, one must rely on experiments to determine the degree to which the generation and detection of the SC state would be affected by the spontaneous emission process during Raman excitations. However, it should be noted that the effect of spontaneous emission can be suppressed to a large degree by simply increasing the optical detuning while also increasing the laser power. This is the approach used, for example, in reducing the effect of radiation loss of atoms in a far-off resonant trap (FORT).

Finally, we considered the effect of the fluctuations in the value of N. In our discussion for the SCAIN above, we have already assumed an averaging over odd and even parities of atoms, for the case where atoms are released from a trap. In addition, one must consider the fact that the mean value of N itself is expected to fluctuate in this case. As we have shown

in reference [**64**], such a fluctuation would simply cause of the width of the fringes due to interference between the extremal collective state to deviate from the ideal value, which is a factor of N narrower than the fringes in a CRAIN. Thus, for example, a fluctuation in the value of N by 1% would cause an $\sim 1\%$ fluctuation in the value of the QFR^{-1}.

Consider next the challenge in implementing the idealized OAT process as envisioned above. In the experiments done to date, employing OAT squeezing, such as those in references [**15**] and [**23**], the typical maximum value of the squeezing parameter, μ, is ~ 0.01. To the best of our knowledge, the highest value of μ, ~ 0.0125, was observed in references [**15**]. For the protocol proposed here, the ideal value of μ that produces the Schroedinger Cat states is $\pi/2$. Under ideal conditions, this value can be achieved by increasing the duration of the squeezing pulse, or increasing its intensity, for example. However, because of the various non-idealities, as discussed in detail in several papers, including the supplement of reference [**22**], it is clear that, for the current experimental implementations, the quantum state after such a strong degree of squeezing interaction would be severely degraded. The non-idealities that degrade the quantum state of the ensemble include the effect of back-action due to the cavity decay, as well as due to spontaneous emission that causes spin-flips. As noted in reference [**22**], the effect of both of these non-idealities can be suppressed by increasing the cooperativity parameters for the cavity (e.g., by making the cavity mode small enough so that the vacuum Rabi frequency would be much stronger than both the cavity decay rate and the rate of spontaneous emission).

However, it should be noted that, for the OAT Squeezing based protocols that have been considered so far, the maximum useful squeezing is produced for very small values of μ, of the order of ~ 0.01 for $\sim$ half a million atoms. Because of other non-idealities, such as poor quantum efficiency of detection, the currently achieved values of squeezing are not limited by

the values of μ. Furthermore, under conventional protocols employing OAT Squeezing, the Hussimi quasi probability distribution begins to get distorted when μ is increased beyond ~ 0.01, and the magnitude of the normalized Bloch vector starts getting smaller than unity. In fact, the factor of improvement in sensitivity due to squeezing drops to unity and even less than unity for μ far below the value of $\pi/2$. As such, experimental efforts to date have been focused on eliminating these non-idealities, instead of constructing apparatuses that would increase the cooperativity parameter significantly, or exploring new schemes for OAT squeezing that would be more robust again dephasing processes.

An important point of reference [**74**] is to show that there is a regime of OAT squeezing (namely when $\mu = \pi/2$) that produces ideal quantum states, such as a superposition of two extremal Dicke collective states, without distortion and any reduction in the amplitude of the Bloch vector. Previously, such a state has only been demonstrated for very few ions (such as in reference [**93**]). For a very large value of N, the number of particles, generating such a state requires knowing the parity of N. Therefore, no previous study has been carried out to show how to construct a protocol under which the Heisenberg Limit (within a factor of $\sqrt{2}$) can be reached even when averaging over both parities of N. This is the main point of this paper. We believe that the results shown in reference [**74**] would identify the need for, and generate an interest in, developing improvements in experimental implementation of OAT squeezing in a manner that makes it possible to reach a value of $\mu = \pi/2$, without significant degradation of coherence.

6.6. Summary

In this chapter, we proposed a protocol that makes use of squeezing, rotation, inverse rotation and unsqueezing operations for implementing Schrödinger Cat Atomic Interferometers and Schrödinger Cat Atomic Clocks. The protocol can be combined with two detection schemes – collective state detection and conventional detection schemes. We presented the complete pulse sequence employed for the protocol, showed the full state evolutions using QPDs, plotted the signal fringes and measurement sensitivities for various parameters, and compared the results with their conventional counterparts. In particular, we showed that for both detection schemes, the signal fringe widths will be reduced by a factor of N and the measurement sensitivities will reach the Heisenberg Limit under optimial conditions. Furthermore, the protocol using conventional detection will also be more robust against excess noise, due to the increased noise of the signal. For more thorough discussions of CSD-SCAIN and CSD-SCAC, please refer to Ref. [**74**]; for more detailed dicussions of CD-SCAIN and CD-SCAC, please refer to Ref. [**75**].

References

[1] D Leibfried, M Barrett, T Schaetz, J Britton, J Chiaverini, W Itano, J Jost, C Langer, and D Wineland. Toward heisenberg-limited spectroscopy with multiparticle entangled states. *Science*, 304:1476–1478, 2004.

[2] M. W. Mitchell, J. S. Lundeen, and A. M. Steinberg. Super-resolving phase measurements with a multiphoton entangled state. *Nature*, 429:161–164, 2004.

[3] H. S. Eisenberg, J. F. Hodelin, G. Khoury, and D. Bouwmeester. Multiphoton path entanglement by nonlocal bunching. *Phys. Rev. Lett.*, 94:090502, Mar 2005.

[4] Tomohisa Nagata, Ryo Okamoto, Jeremy L. O'Brien, Keiji Sasaki, and Shigeki Takeuchi. Beating the standard quantum limit with four-entangled photons. *Science*, 316(5825):726–729, 2007.

[5] K. J. Resch, K. L. Pregnell, R. Prevedel, A. Gilchrist, G. J. Pryde, J. L. O'Brien, and A. G. White. Time-reversal and super-resolving phase measurements. *Phys. Rev. Lett.*, 98:223601, May 2007.

[6] S. Wildermuth, S. Hofferberth, I. Lesanovsky, S. Groth, P. KrÃŒger, J. Schmiedmayer, and I. Bar-Joseph. Sensing electric and magnetic fields with bose-einstein condensates. *Applied Physics Letters*, 88(26):264103, 2006.

[7] M. Vengalattore, J. M. Higbie, S. R. Leslie, J. Guzman, L. E. Sadler, and D. M. Stamper-Kurn. High-resolution magnetometry with a spinor bose-einstein condensate. *Phys. Rev. Lett.*, 98:200801, May 2007.

[8] N. Behbood, F. Martin Ciurana, G. Colangelo, M. Napolitano, M. W. Mitchell, and R. J. Sewell. Real-time vector field tracking with a cold-atom magnetometer. *Applied Physics Letters*, 102(17):173504, 2013.

[9] M. Koschorreck, M. Napolitano, B. Dubost, and M. W. Mitchell. High resolution magnetic vector-field imaging with cold atomic ensembles. *Applied Physics Letters*, 98(7):074101, 2011.

[10] B. Lücke, M. Scherer, J. Kruse, L. Pezzé, F. Deuretzbacher, P. Hyllus, O. Topic, J. Peise, W. Ertmer, J. Arlt, L. Santos, A. Smerzi, and C. Klempt. Twin matter waves for interferometry beyond the classical limit. *Science*, 334(6057):773–776, 2011.

[11] Helmut Strobel, Wolfgang Muessel, Daniel Linnemann, Tilman Zibold, David B. Hume, Luca Pezzè, Augusto Smerzi, and Markus K. Oberthaler. Fisher information and entanglement of non-gaussian spin states. *Science*, 345(6195):424–427, 2014.

[12] M. Kitagawa and M. Ueda. Squeezed spin states. *Phys. Rev. A*, 47:5138, 1993.

[13] D. J. Wineland, J. J. Bollinger, W. M. Itano, F. L. Moore, and D. J. Heinzen. Spin squeezing and reduced quantum noise in spectroscopy. *Phys.Rev.A*, 46:6797, 1992.

[14] D. J. Wineland, J. J. Bollinger, W. M. Itano, and D. J. Heinzen. Squeezed atomic states and projection noise in spectroscopy. *Phys. Rev. A*, 50:67, 1994.

[15] M. H. Schleier-Smith, I. D. Leroux, and V. Vuletić. Squeezing the collective spin of a dilute atomic ensemble by cavity feedback. *Phys. Rev. A*, 81:021804, 2010.

[16] I. D. Leroux, M. H. Schleier-Smith, and V. Vuletić. Implementation of cavity squeezing of a collective atomic spin. *Phys. Rev. Lett.*, 104:073602, 2010.

[17] A. Sørensen, L. M. Duan, J. I. Cirac, and P. Zoller. Many-particle entanglement with bose–einstein condensates. *Nature*, 409:63 EP –, 01 2001.

[18] Nick Bigelow. Squeezing entanglement. *Nature*, 409:27 EP –, 01 2001.

[19] O. Guehne and G. Tóth. Entanglement detection. *Phys. Rep.*, 474:1, 2009.

[20] Eugene S. Polzik. The squeeze goes on. *Nature*, 453:45 EP –, 04 2008.

[21] Alexander D. Cronin, Jörg Schmiedmayer, and David E. Pritchard. Optics and interferometry with atoms and molecules. *Rev. Mod. Phys.*, 81:1051–1129, Jul 2009.

[22] E. Davis, G. Bentsen, and M. Schleier-Smith. Approaching the heisenberg limit without single-particle detection. *Phys. Rev. Letts.*, 116:053601, 2016.

[23] O. Hosten, R. Krishnakumar, N. J. Engelsen, and M. A. Kasevich. Quantum phase magnification. *Science*, 352:1552, 2016.

[24] Onur Hosten, Nils J. Engelsen, Rajiv Krishnakumar, and Mark A. Kasevich. Measurement noise 100 times lower than the quantum-projection limit using entangled atoms. *Nature*, 529:505–507, 2016.

[25] Luigi Amico, Rosario Fazio, Andreas Osterloh, and Vlatko Vedral. Entanglement in many-body systems. *Rev. Mod. Phys.*, 80:517–576, May 2008.

[26] Ryszard Horodecki, Paweł Horodecki, Michał Horodecki, and Karol Horodecki. Quantum entanglement. *Rev. Mod. Phys.*, 81:865–942, Jun 2009.

[27] M.A. Nielsen and I.L. Chuang. *Quantum Computation and Quantum Information*. Cambridge University Press, Cambridge, England, 2000.

[28] J. Stolze and D. Suter. *Quantum Computing: A Short Course from Theory to Experiment*. Wiley-VCH Verlag, Weinheim, 2008.

[29] J. J . Bollinger, Wayne M. Itano, D. J. Wineland, and D. J. Heinzen. Optimal frequency measurements with maximally correlated states. *Phys. Rev. A*, 54:R4649–R4652, Dec 1996.

[30] Girish S. Agarwal and Marlan O. Scully. Ramsey spectroscopy with nonclassical light sources. *Phys. Rev. A*, 53:467–470, Jan 1996.

[31] P.R. Berman. *Atom Interferometry*. Academic Press, 1997.

[32] G. Xu and D. Heinzen. State-selective rabi and ramsey magnetic resonance line shapes. *Phys. Rev. A*, 59:R922, 1999.

[33] V. Meyer, M. A. Rowe, D. Kielpinski, C. A. Sackett, W. M. Itano, C. Monroe, and D. J. Wineland. Experimental demonstration of entanglement-enhanced rotation angle estimation using trapped ions. *Phys. Rev. Lett.*, 86:5870–5873, Jun 2001.

[34] Greg A. Smith, Souma Chaudhury, Andrew Silberfarb, Ivan H. Deutsch, and Poul S. Jessen. Continuous weak measurement and nonlinear dynamics in a cold spin ensemble. *Phys. Rev. Lett.*, 93:163602, Oct 2004.

[35] D. Döring, G. McDonald, J. E. Debs, C. Figl, P. A. Altin, H.-A. Bachor, N. P. Robins, and J. D. Close. Quantum-projection-noise-limited interferometry with coherent atoms in a ramsey-type setup. *Phys. Rev. A*, 81:043633, Apr 2010.

[36] J. Appel, P. J. Windpassinger, D. Oblak, U. B. Hoff, N. Kjærgaard, and E. S. Polzik. Mesoscopic atomic entanglement for precision measurements beyond the standard quantum limit. *Proceedings of the National Academy of Sciences*, 106(27):10960–10965, 2009.

[37] Daniel Oblak, Plamen G. Petrov, Carlos L. Garrido Alzar, Wolfgang Tittel, Anton K. Vershovski, Jens K. Mikkelsen, Jens L. Sørensen, and Eugene S. Polzik. Quantum-noise-limited interferometric measurement of atomic noise: Towards spin squeezing on the cs clock transition. *Phys. Rev. A*, 71:043807, Apr 2005.

[38] Anders Sørensen and Klaus Mølmer. Spin-spin interaction and spin squeezing in an optical lattice. *Phys. Rev. Lett.*, 83:2274–2277, Sep 1999.

[39] D Meiser, Jun Ye, and M J Holland. Spin squeezing in optical lattice clocks via lattice-based qnd measurements. *New Journal of Physics*, 10(7):073014, 2008.

[40] I. D. Leroux, M. H. Schleier-Smith, and V. Vuletić. Orientation-dependent entanglement lifetime in a squeezed atomic clock. *Phys. Rev. Lett.*, 104:250801, 2010.

[41] A. André, A. S. Sørensen, and M. D. Lukin. Stability of atomic clocks based on entangled atoms. *Physical Review Letters*, 92(23):230801, 06 2004.

[42] D.F. Walls and P. Zoller. Enhanced sensitivity of a gravitational-wave detector. *Phys. Lett. A*, 85:118, 1981.

[43] J. Dunningham and K. Burnett. Sub-shot-noise-limited measurements with bose-einstein condensates. *Phys. Rev. A*, 70:033601, 2004.

[44] K. Goda, O. Miyakawa, E. E. Mikhailov, S. Saraf, R. Adhikari, K. McKenzie, R. Ward, S. Vass, A. J. Weinstein, and N. Mavalvala. A quantum-enhanced prototype gravitational-wave detector. *Nature Physics*, 4:472, 03 2008.

[45] R. Shankar. *Principles of Quantum Mechanics*. Springer US, 2012.

[46] H. Metcalf and P. van der Straten. *Laser Cooling and Trapping*. Graduate Texts in Contemporary Physics. Springer New York, 2012.

[47] I. I. Rabi. Space quantization in a gyrating magnetic field. *Phys. Rev.*, 51:652–654, 1937.

[48] M.H. Mittleman. *Introduction to the Theory of Laser-Atom Interactions*. Plenum Press, New York, 1982.

[49] L. Allen and J. Eberly. *Optical Resonance and Two-Level Atoms*. Dover Books on Physics. Dover Publications, 2012.

[50] M. Sargent, M. Scully, and W. Lamb. *Laser Physics*. Advanced book program. Perseus Books Group, 1978.

[51] R. Feynman, F. Vernon, and R. Hellwarth. Geometrical representation of the schrödinger equation for solving master problems. *J. App. Phys.*, 28(49), 1957.

[52] C. Cohen-Tannoudji and In Balian, editors. *Atoms in Strong Resonant Fields*, Amsterdam, North Holland, 1977. Proceedings of Les Houches XXVII.

[53] P. R. Hemmer, M. S. Shahriar, V. D. Natoli, and S. Ezekiel. Ac stark shifts in a two-zone raman interaction. *J. Opt. Soc. Am. B*, 6:1519–1528, 1989.

[54] M. Kasevich and S. Chu. Atomic interferometry using stimulated raman transitions. *Phys. Rev. Lett.*, 67:181–184, 1991.

[55] Daniel A. Steck. *Rubidium 85 D Line Data*, December 2010.

[56] Alan Corney. *Atomic and Laser Spectroscopy*. Oxford, 1977.

[57] R. Sarkar, M. E. Kim, R. Fang, Y. Tu, and S. M. Shahriar. Effects of non-idealities and quantization of the center of mass motion on symmetric and asymmetric collective states in a collective state atomic interferometer. *Journal of Modern Optics*, 62:1253–1263, 2015.

[58] May E. Kim, Resham Sarkar, Renpeng Fang, and Selim M. Shahriar. n-atom collective state atomic clock with $\sqrt{N}$ fold increase in effective frequency and $\sqrt{N}$ fold reduction in fringe width. *Physical Review A*, 91(063629), 2015.

[59] R. H. Dicke. Coherence in spontaneous radiation processes. *Phys. Rev.*, 93:99–110, 1954.

[60] Resham Sarkar. *Schrödinger Cat State Atomic Interferometer with Heisenberg-Limited Sensitivity and Detection of Collective States*. PhD thesis, Northwestern University, December 2016.

[61] E. Brion, L. H. Pedersen, and K Mølmer. Adiabatic elimination in a lambda system. *J. Phys. A: Math. Theor.*, 40:1033, 2007.

[62] M. S. Shahriar, P. Pradhan, Y. Tan, M. Jheeta, J. Morzinski, and P. R. Hemmer. Demonstration of a continuously guided atomic interferometer by single-zone optical excitation. *Journal of the Optical Society of America B*, 22(7):1566–1570, 2005.

[63] C. J. Bordé. Atomic interferometry with internal state labelling. *Phys. Lett. A*, 140:10, 1989.

[64] R. Sarkar, M. E. Kim, R. Fang, and S. M. Shahriar. N-atom collective-state atomic interferometer with ultrahigh compton frequency and ultrashort de broglie wavelength, with $\sqrt{N}$ reduction in fringe width. *Phys. Rev. A*, 92(063612), 2016.

[65] May E. Kim. *Collective State Representation of Atoms in Quantum Computing and Precision Metrology*. PhD thesis, Northwestern University, December 2015.

[66] Jian Ma, Xiaoguang Wang, CP Sun, and Franco Nori. Quantum spin squeezing. *Physics Reports*, 509(2):89–166, 2011.

[67] A.O. Barut and L. Girardel. New coherent states associated with non-compact groups. *Comm. Math. Phys.*, 21:41, 1971.

[68] R. Gilmore. Geometry of symmetrized states. *Ann. Phys.*, 74:391, 1972.

[69] A.M. Perelomov. Coherent states for arbitrary lie group. *Comm. Math. Phys.*, 26:222, 1972.

[70] A.M. Perelomov. *Generalized Coherent States and their Applications*. Springer-Verlag, Berlin, 1986.

[71] W. M. Zhang, D. H. Feng, and R. Gilmore. Coherent states: theory and some applications. *Rev. Modern Phys.*, 62:867, 1990.

[72] L. Song, X. Wang, D. Yan, and Z. Zong. Spin squeezing properties in the quantum kicked top model. *J. Phys. B: At. Mol. Opt. Phys.*, 39:559, 2006.

[73] E. Schrödinger. Die gegenwärtige situation in der quantenmechanik. *Naturwissenschaften*, 23:807, 1935.

[74] R. Sarkar, R. Fang, and S. M. Shahriar. Ultra-high compton frequency, parity independent, mesoscopic schrödinger cat atom interferometer with heisenberg limited sensitivity. *https://arxiv.org/pdf/1701.01210.pdf*, 2017.

[75] R. Fang, R. Sarkar, and S. M. Shahriar. Enhancing sensitivity of an atom interferometer to the heisenberg limit using increased quantum noise. *https://arxiv.org/pdf/1707.08260.pdf*, 2017.

[76] G. B. Malykin. The sagnac effect: correct and incorrect explanations. *Physics-Uspekhi*, 43(12):1229–1252, 2000.

[77] E. J. Post. Sagnac effect. *Reviews of Modern Physics*, 39(2):475–493, 04 1967.

[78] Samuel P. Nolan, Stuart S. Szigeti, and Simon A. Haine. Optimal and robust quantum metrology using interaction-based readouts. *Physical Review Letters*, 119(19):193601–, 11 2017.

[79] W. M. Itano, J. C. Bergquist, J. J. Bollinger, J. M. Gilligan, D. J. Heinzen, F. L. Moore, M. G. Raizen, and D. J. Wineland. Quantum projection noise: Population fluctuations in two-level systems. *Physical Review A*, 47(5):3554–3570, 05 1993.

[80] Klaus Mølmer and Anders Sørensen. Multiparticle entanglement of hot trapped ions. *Physical Review Letters*, 82(9):1835–1838, 03 1999.

[81] D. Leibfried and D.J. Wineland. Efficient eigenvalue determination for arbitrary pauli products based on generalized spin-spin interactions. *https://arxiv.org/abs/1707.03889*, 2017.

[82] M. S. Shahriar, P. R. Hemmer, D. P. Katz, A. Lee, and M. G. Prentiss. Dark-state-based three-element vector model for the stimulated raman interaction. *Physical Review A*, 55(3):2272–2282, 03 1997.

[83] Kristian Helmerson and Li You. Creating massive entanglement of bose-einstein condensed atoms. *Physical Review Letters*, 87(17):170402–, 10 2001.

[84] Isabelle Bouchoule and Klaus Mølmer. Preparation of spin-squeezed atomic states by optical-phase-shift measurement. *Physical Review A*, 66(4):043811–, 10 2002.

[85] M. Zhang, Kristian Helmerson, and L. You. Entanglement and spin squeezing of bose-einstein-condensed atoms. *Physical Review A*, 68(4):043622–, 10 2003.

[86] Y. L. Zhang, C. L. Zou, X. B. Zou, L. Jiang, and G. C. Guo. Detuning-enhanced cavity spin squeezing. *Phys. Rev. A*, 91:033625, 2015.

[87] Michael Foss-Feig, Andrew J. Daley, James K. Thompson, and Ana Maria Rey. Steady-state many-body entanglement of hot reactive fermions. *Physical Review Letters*, 109(23):230501–, 12 2012.

[88] M. Takeuchi, S. Ichihara, T. Takano, M. Kumakura, T. Yabuzaki, and Y. Takahashi. Spin squeezing via one-axis twisting with coherent light. *Phys. Rev. Lett.*, 94:023003, 2005.

[89] Mingfeng Wang, Weizhi Qu, Pengxiong Li, Han Bao, Vladan Vuletić, and Yanhong Xiao. Two-axis-twisting spin squeezing by multipass quantum erasure. *Phys. Rev. A*, 96:013823, 2017.

[90] Y. C. Liu, Z. F. Xu, G. R. Jin, and L. You. Spin squeezing: Transforming one-axis twisting into two-axis twisting. *Phys. Rev. Lett.*, 107:013601, 2011.

[91] L. I. R. Gil, R. Mukherjee, E. M. Bridge, M. P. A. Jones, and T. Pohl. Spin squeezing in a rydberg lattice clock. *Phys. Rev. Lett.*, 112:103601, 2014.

[92] F. T. Arecchi, Eric Courtens, Robert Gilmore, and Harry Thomas. Atomic coherent states in quantum optics. *Physical Review A*, 6(6):2211–2237, 12 1972.

[93] Thomas Monz, Philipp Schindler, Julio T. Barreiro, Michael Chwalla, Daniel Nigg, William A. Coish, Maximilian Harlander, Wolfgang Hänsel, Markus Hennrich, and Rainer Blatt. 14-qubit entanglement: Creation and coherence. *Physical Review Letters*, 106(13):130506–, 03 2011.

[94] Vittorio Giovannetti, Seth Lloyd, and Lorenzo Maccone. Advances in quantum metrology. *Nature Photonics*, 5:222, 03 2011.

[95] Vittorio Giovannetti, Seth Lloyd, and Lorenzo Maccone. Quantum-enhanced measurements: Beating the standard quantum limit. *Science*, 306(5700):1330–1336, 2004.

[96] J. Kitching, S. Knappe, L. Liew, J. Moreland, H. G. Robinson, P. Schwindt, V. Shah, V. Gerginov, and L. Hollberg. Chip-scale atomic clocks at nist. Proc. 2005 NCSL Intnl. Symp., 2005.

[97] L. Essen and J. V. L. Parry. An atomic standard of frequency and time interval: A caesium resonator. *Nature*, 176(4476):280–282, 1955.

[98] D.B. Sullivan. Time and frequency measurement at nist: The first 100 years. pages 4–17. IEEE International Frequency Control Symposium, 2001.

[99] F. Walls and J. R. Vig. *IEEE Trans. Ultrason. Ferroelectr. Freq. Control*, volume 42. 1995.

[100] J. Jespersen and J. Fitz-Randolph. *From Sundials to Atomic Clocks*. National Institute of Standards and Technology, 1999.

[101] Andrew D. Ludlow, Martin M. Boyd, Jun Ye, E. Peik, and P.O. Schmidt. Optical atomic clocks. *REVIEWS OF MODERN PHYSICS*, 87(2):637, 2015.

[102] M. J. Martin, M. Bishof, M. D. Swallows, X. Zhang, C. Benko, J. von Stecher, A. V. Gorshkov, A. M. Rey, and J. Ye. A quantum many-body spin system in an optical lattice clock. *Science*, 341:632 – 636, 2013.

[103] C. Will. *Theory and experiment in gravitational physics*. Cambridge University Press, 1993.

[104] S. Bize, P. Laurent, M. Abgrall, H. Marion, I. Maksimovic, L. Cacciapuoti, J. Grunert, C. Vian, F. P. dos Santos, P. Rosenbusch, P. Lemonde, and G. Santarelli. Cold atom clocks and applications. *C.R. Phys.*, 5(8):829, 2004.

[105] R. Bonifacio, P. Schwendimann, and F. Haake. Quantum statistical theory of superradiance. i. *Phys. Rev. A*, 4:302–313, 1971.

APPENDIX A

Matlab Codes for Raman-Rabi Interactions

This appendix contains matlab codes for simulating the various Raman-Rabi interactions within a two-level (or three-level) atomic system, including Raman-Rabi oscillation, Raman frequency scanning and Ramsey frequency scanning. The last two also have variants for collective state detections.

A.1. Matlab Codes for Raman-Rabi oscillation

```
clc
clear
close all

Delta = (-200 : 0.01 : 200); % Laser detuning (kHz)
Omega = 30; % Rabi frequency (kHz)
Omega_g = sqrt(Delta.^2 + Omega.^2); % Generalized Rabi frequency (kHz)
T1 = pi/2/Omega; % pi/2 pulse time
T2 = 0*T1; % Dark zone time one (zero)
T3 = 2*T1; % Dark zone time two (five times of pi/2 pulse)

P2 = 4 * (Omega.^2./Omega_g.^2).*sin(Omega_g.*T1/2).^2.*(cos(Omega_g.*T1/2).*...
cos(Delta.*T2/2)-(Delta./Omega_g).*sin(Omega_g.*T1/2).*sin(Delta.*T2/2)).^2;
```

```
P3 = 4 * (Omega.^2./Omega_g.^2).*sin(Omega_g.*T1/2).^2.*(cos(Omega_g.*T1/2).*...
cos(Delta.*T3/2)-(Delta./Omega_g).*sin(Omega_g.*T1/2).*sin(Delta.*T3/2)).^2;


plot(Delta, P2, '-b')
hold on
plot(Delta, P3, '-m')
axis([-200,200,0,1])
xlabel('Laser detuning \delta (kHz)', 'FontSize', 20)
ylabel('Probability transfer (a.u.)', 'FontSize', 20)
title('Ramsey fringes for separated oscillating field experiment')
```

A.2. Matlab Codes for Raman Frequency Scanning

```
clc
clear
close all


delta = -100 : 0.1 : 100; % two-photon detuning (kHz)
I = 30; % laser intensity (mW/cm^2)
omega = 0.6264 * I; % Rman-Rabi frequency (kHz)
tao = 500 / omega; % pi-pulse time (us)
P = omega.^2 ./ (omega.^2 + delta.^2) .* (sin(2 * pi * sqrt(omega.^2 + delta.^2)
    * tao/1000/2)).^2; % population transfer


plot(delta, P, '-b', 'linewidth', 1);
```

```
xlabel('Two-photon detuning (kHz)', 'FontSize', 20)
ylabel('Probability transfer (a.u.)', 'FontSize', 20)
title('Raman frequency scanning', 'FontSize', 20)
```

A.3. Matlab Codes for Raman Frequency Scanning with Collective State Detection

```
clc
clear
close all

N = [1, 10, 100, 1000];      % Number of atoms
omega = 30;                  % Raman-Rabi frequency (kHz)
tao = 500 / omega;           % Pi-pulse time (us)
delta = -55 : 0.01 : 55;     % Laser detuning (kHz)
P = omega.^2 ./ (omega.^2 + delta.^2) .*(sin(2 * pi * sqrt(omega.^2 + delta.^2)
    * tao/1000/2)).^2; % population transfer

PN = zeros(length(N), length(delta));

for i = 1 : length(N)
    PN(i, :) = P.^N(i);
end

figure
```

```
plot(delta, PN(1, :), 'b-', 'linewidth', 2)
hold on
plot(delta, PN(2, :), 'r--', 'linewidth', 1)
hold on
plot(delta, PN(3, :), 'k-', 'linewidth', 1)
hold on
plot(delta, PN(4, :), 'm-.', 'linewidth', 1)
hold on
xlabel('Detuning (kHz)', 'FontSize', 20)
ylabel('Probability transfer (a.u.)', 'FontSize', 20)
legend(['N = ' num2str(N(1))], ['N = ' num2str(N(2))], ['N = ' num2str(N(3))],
    ['N = ' num2str(N(4))])
title('Raman frequency scanning', 'FontSize', 20)
```

A.4. Matlab Codes for Ramsey Frequency Scanning

```
clc
clear
close all

Delta = (-200 : 0.01 : 200); % Laser detuning (kHz)
Omega = 30; % Rabi frequency (kHz)
Omega_g = sqrt(Delta.^2 + Omega.^2); % Generalized Rabi frequency (kHz)
T1 = pi/2/Omega; % pi/2 pulse time
T2 = 0*T1; % Dark zone time one (zero)
```

```
T3 = 2*T1; % Dark zone time two (five times of pi/2 pulse)

P2 = 4 *
    (Omega.^2./Omega_g.^2).*sin(Omega_g.*T1/2).^2.*(cos(Omega_g.*T1/2).*cos(Delta.*T2/2)-...
(Delta./Omega_g).*sin(Omega_g.*T1/2).*sin(Delta.*T2/2)).^2;

P3 = 4 *
    (Omega.^2./Omega_g.^2).*sin(Omega_g.*T1/2).^2.*(cos(Omega_g.*T1/2).*cos(Delta.*T3/2)-...
(Delta./Omega_g).*sin(Omega_g.*T1/2).*sin(Delta.*T3/2)).^2;

plot(Delta, P2, '-b')
hold on
plot(Delta, P3, '-m')
axis([-200,200,0,1])
xlabel('Laser detuning \delta (kHz)', 'FontSize', 20)
ylabel('Probability transfer (a.u.)', 'FontSize', 20)
title('Ramsey fringes for separated oscillating field experiment')
```

A.5. Matlab Codes for Ramsey Frequency Scanning with Collective State Detection

```
clc
clear
close all
```

```
N = [1, 10, 100, 1000]; % Number of atoms

delta = (-14.5 : 0.01 : 14.5); % Laser detuning (kHz)

Omega = 30; % Rabi frequency (kHz)

Omega_g = sqrt(delta.^2 + Omega.^2); % Generalized Rabi frequency (kHz)

T1 = pi/2/Omega; % Pi/2 pulse time (ms)

T2 = 3 * T1; % Dark zone time (ms)


P = 4*(Omega.^2./Omega_g.^2).*sin(Omega_g.*T1/2).^2.*(cos(Omega_g.*T1/2).*...

cos(delta.*T2/2)-(delta./Omega_g).*sin(Omega_g.*T1/2).*sin(delta.*T2/2)).^2;


PN = zeros(length(N), length(delta));


for i = 1 : length(N)

    PN(i, :) = P.^N(i);

end


figure

plot(delta, PN(1, :), '-b', 'linewidth', 2)

hold on

plot(delta, PN(2, :), '--r', 'linewidth', 1)

hold on

plot(delta, PN(3, :), '-k', 'linewidth', 1)

hold on

plot(delta, PN(4, :), '-.m', 'linewidth', 1)

hold on
```

```
xlabel('f (kHz)', 'fontsize', 20)
ylabel('Probability transfer (a.u.)', 'fontsize', 20)
legend({['N = ' num2str(N(1))], ['N = ' num2str(N(2))], ['N = ' num2str(N(3))],
    ['N = ' num2str(N(4))]}, 'fontsize', 20)
set(gca, 'fontsize', 15)
title('Ramsey fringes for separated oscillating field experiment', 'fontsize',
    20)
```

APPENDIX B

Matlab Codes for Common Functions

This appendix contains the common functions used by both spin squeezing and SCAIN and SCAC.

B.1. *css*

```
%%%%%%%%%% Purpose of this script %%%%%%%%%%%%%%%%%%%%%%%%%%%%%%%%%%%%%%%%
%
% This script is used to compute the components of the coherent spin state
% (css) pointed at direction (theta, phi) in the basis of the Dicke states
% (aka symmetric collective states) using the following theoretical
% expression:
%
% <J, J - k | css(theta, phi)> = [cos(theta/2)]^N * sqrt[nchoosek(N, k)] *
%                                [exp(i*phi) * tan(theta/2)]^k
%
% To avoid overflow, we will convert factorial to logarithm of gamma functions:
%
% [cos(theta/2)]^N * sqrt[nchoosek(N, k)] * [exp(i*phi) * tan(theta/2)]^k
%  = exp{1/2 * [gammaln(N+1) - gammaln(k+1) - gammaln(N-k+1)] +
%          (N-k) * log(cos(theta/2)) + k * log(sin(theta/2)) + 1i * k * phi}
%
```

```
%%%%%%%%%%%%%% End of purpose %%%%%%%%%%%%%%%%%%%%%%%%%%%%%%%%%%%%%%%%%%%%%%%%

function css_wf = css(J, theta, phi)


N = 2 * J;
css_wf = zeros(N + 1, 1);


if theta == 0
    css_wf(1) = 1;


elseif theta == pi
    css_wf(N + 1) = 1;


else
    for i = 1 : numel(css_wf)
        k = i - 1;
        css_wf(i) = exp(1/2 * (gammaln(N + 1) - gammaln(k + 1) - gammaln(N - k +
            1)) + (N - k) * log(cos(theta/2)) + k * log(sin(theta/2)) + 1i * k *
            phi);
    end
end


end
```

B.2. J_-

```
%%%%%%%%%% Purpose of this script %%%%%%%%%%
%
% This script is used to compute the matrix elements of the lowering spin
% operator J_minus in the basis of the Dicke states
%
%%%%%%%%%%%%%% End of purpose %%%%%%%%%%%%%%

function Jminus = J_minus(J)

Jminus = zeros(2 * J + 1);

for i = 1 : 2 * J
    M = (J + 1) - i;
    Jminus(i + 1, i) = sqrt((J + M) * (J - M + 1));
end

end
```

B.3. J_+

```
%%%%%%%%%% Purpose of this script %%%%%%%%%%
%
% This script is used to compute the matrix elements of the lowering spin
% operator J_minus in the basis of the Dicke states
%
```

```
%%%%%%%%%%%%%% End of purpose %%%%%%%%%%%%%%

%%%%%%%%%% Purpose of this script %%%%%%%%%%
%
% This script is used to compute the matrix elements of the raising spin
% operator J_plus in the basis of the Dicke states
%
%%%%%%%%%%%%%% End of purpose %%%%%%%%%%%%%%

function Jplus = J_plus(J)

Jplus = zeros(2 * J + 1);

for i = 2 : 2 * J + 1
    M = (J + 1) - i;
    Jplus(i - 1, i) = sqrt((J - M) * (J + M + 1));
end

end
```

B.4. J_x

```
%%%%%%%%%% Purpose of this script %%%%%%%%%%
%
% This script is used to compute the matrix elements of the x-component of
```

```
% the spin operator J_x in the basis of the Dicke states
%
%%%%%%%%%%%%%% End of purpose %%%%%%%%%%%%%%

function Jx = J_x(J)

Jx = (J_plus(J) + J_minus(J)) / 2;

end
```

B.5. J_y

```
%%%%%%%%%%% Purpose of this script %%%%%%%%%%
%
% This script is used to compute the matrix elements of the y-component of
% the spin operator J_y in the basis of the Dicke states
%
%%%%%%%%%%%%%% End of purpose %%%%%%%%%%%%%%

function Jy = J_y(J)

Jy = (J_plus(J) - J_minus(J)) / (2 * 1i);

end
```

B.6. J_z

```
%%%%%%%%%% Purpose of this script %%%%%%%%%%
%
% This script is used to compute the matrix elements of the z-component of
% the spin operator J_z in the basis of the Dicke states
%
%%%%%%%%%%%%%% End of purpose %%%%%%%%%%%%%%

function Jz = J_z(J)

Jz = zeros(2 * J + 1);

for i = 1 : 2 * J + 1
    M = (J + 1) - i;
    Jz(i, i) = M;
end

end
```

B.7. nu_oat_x

```
%%%%%%%%%% Purpose of this script %%%%%%%%%%
%
% This script is used to compute the corrective rotation angle nu
% for x protocol.
```

```
%
% Here nu = pi/2 for all possible values of the squeezing parameters mu.
%
%%%%%%%%%%%%%% End of purpose %%%%%%%%%%%%%%

function nu = nu_oat_x(~, mu)

nu = repmat(pi/2, size(mu));

end
```

B.8. *nu_oat_y*

```
%%%%%%%%%% Purpose of this script %%%%%%%%%%
%
% This script is used to compute the corrective rotation angle nu for
% y-protocol using the formula given in the Kitagawa and Ueda paper.
%
% Here nu take different values for different squeezing parameters mu.
%
%%%%%%%%%%%%%% End of purpose %%%%%%%%%%%%%%

function nu = nu_oat_y(J, mu)

A = 1 - (cos(2*mu)).^(2*J-2);
```

```
B = 4 * sin(mu) .* (cos(mu)).^(2*J-2);


nu = zeros(size(mu));


for i = 1 : numel(nu)
    if mu(i) == 0
        nu(i) = -pi/2;
    elseif mu(i) == pi/2
        nu(i) = 0;
    else
        nu(i) = -1/2 * atan(B(i)./A(i));
    end
end


% nu = nu + pi/2; % For mu=pi/2, we need this to maximize variance of J_z


end
```

B.9. P_K

```
%%%%%%%%%% Purpose of this script %%%%%%%%%%
%
% This script is used to compute the matrix elements of the projection
% operator PK formed by the (N+1-K)-th basis vector in the basis
% of the Dicke states (symmetric collective states). The basis vectors are
```

```
% arranged as follows:
%
% |1> = |J, J>,
% |2> = |J, J-1>,
% |3> = |J, J-2>,
% ...
% |N+1> = |J, -J>,
%
% where N = 2 * J is the total number of elementary spins.
%
% P_K(J, K) = |N+1-K><N+1-K|.
%
% Note the Dicke states are also referred to as E0, E1, ..., EN, where
%
% E0 = |J, -J><J, -J| = P_K(J, 0),
% E1 = |J, -J+1><J, -J+1| = P_K(J, 1),
% ...
% EN = |J, J><J, J| = P_K(J, N).
%
%%%%%%%%%%%%%% End of purpose %%%%%%%%%%%%%%

function PK = P_K(J, K)

N = 2 * J;
PK = zeros(N + 1);
```

```
PK(N + 1 - K, N + 1 - K) = 1;

end
```

B.10. Ψ_0

```
%%%%%%%%%% Purpose of this script %%%%%%%%%%
%
% This script is used to generate the initial state vector which will
% be the (J + 1 - M)-th basis vector in the basis of the Dicke states.
%
% Note:
% 1. M = J, J-1, ..., -J;
% 2. The Dicke states are arranged as |J, J>, |J, J-1>, ..., |J, -J>.
% 3. For a general CSS state, use the css function to convert them into
% the basis above.
%
%%%%%%%%%%%%%% End of purpose %%%%%%%%%%%%%%

function Psi0 = Psi_0(J, M)

Psi0 = zeros(2 * J + 1, 1);
Psi0(J + 1 - M) = 1;

end
```

B.11. QPD

```
%%%%%%%%%% Purpose of this script %%%%%%%%%%%%%%%%%%%%%%%%%%%%%%%%
%
% This script is used to, given any state vector |Psi> represented in the
% basis of the Dicke states (aka symmetric collective states), plot its
% Husimi quasi-probability distribution (QPD) in terms of the coherent spin
% states (CSS), |theta, phi>.
%
%%%%%%%%%%%%% End of purpose %%%%%%%%%%%%%%%%%%%%%%%%%%%%%%%%%%%%%

function QPD(Psi)

[theta, phi] = meshgrid(0 : pi/100 : pi, -pi : pi/100 : pi); % the spherical
    coordinates
x = sin(theta).*cos(phi);                                    % Corresponding x
    coordinate
y = sin(theta).*sin(phi);                                    % Corresponding y
    coordinate
z = cos(theta);                                              % Corresponding z
    coordinate
[m, n] = size(x);                                            % Size of theta

P = zeros(m, n);                                             % Quasi-probability
    distribution
```

```
J = (numel(Psi) - 1) / 2;                                % Total spin quantum
    number

for i = 1 : m
    for j = 1 : n
        css_theta_phi = css(J, theta(i, j), phi(i, j));    % CSS in direction
            (theta, phi)
        P(i, j) = abs(css_theta_phi' * Psi).^2;            % |<theta,phi|Psi>|^2
    end
end

figure
mesh(x, y, z, P)
xlabel('X')
ylabel('Y')
zlabel('Z')
title('QPD in terms of X, Y and Z')
colormap parula
colorbar

end
```

B.12. *U_oat*

```
%%%%%%%%%% Purpose of this script %%%%%%%%%%
```

```
%
% This script is used to compute the matrix elements of the unitary
% transformation operator generated by one-axis twisting Hamiltonian for
% the spin squeezing in the basis of the Dicke states
%
%%%%%%%%%%%%%% End of purpose %%%%%%%%%%%%%%

function U = U_oat(J, mu)

Jz = J_z(J);
U = expm(-1i * mu * Jz^2);

end
```

B.13. *U_tact_y*

```
%%%%%%%%%% Purpose of this script %%%%%%%%%%
%
% This script is used to compute the matrix elements of the unitary
% transformation operator generated by two-axis counter twisting
% Hamiltonian for the spin squeezing in the basis of the Dicke states.
%
% The two twisting operators are (Jx + iJz) and (Jx - iJz).
%
%%%%%%%%%%%%%% End of purpose %%%%%%%%%%%%%%
```

```
function U = U_tact_y(J, mu)


Jx = J_x(J);

Jz = J_z(J);

Jp = Jx + 1i * Jz;

Jm = Jx - 1i * Jz;

U = expm(-mu/2 * (Jp^2 - Jm^2));


end
```

B.14. *U_tact_z*

```
%%%%%%%%%% Purpose of this script %%%%%%%%%%
%
% This script is used to compute the matrix elements of the unitary
% transformation operator generated by two-axis counter twisting
% Hamiltonian for the spin squeezing in the basis of the Dicke states
%
% The two twisting operators are (Jx + iJy) and (Jx - iJy).
%
%%%%%%%%%%%%%%% End of purpose %%%%%%%%%%%%%%%

function U = U_tact_z(J, mu)
```

```
Jp = J_plus(J);

Jm = J_minus(J);

U = expm(-mu/2 * (Jp^2 - Jm^2));


end
```

B.15. U_x

```
%%%%%%%%%% Purpose of this script %%%%%%%%%%

%

% This script is used to compute the matrix elements of the unitary

% transformation operator generated by rotating around the x-axis by

% an angle of theta in the basis of the Dicke states

%

%%%%%%%%%%%%%% End of purpose %%%%%%%%%%%%%%


function U = U_x(J, theta)


Jx = J_x(J);

U = expm(-1i * theta * Jx);


end
```

B.16. U_y

```
%%%%%%%%%% Purpose of this script %%%%%%%%%%
```

```
%
% This script is used to compute the matrix elements of the unitary
% transformation operator generated by rotating around the y-axis by
% an angle of theta in the basis of the Dicke states
%
%%%%%%%%%%%%%% End of purpose %%%%%%%%%%%%%%

function U = U_y(J, theta)

Jy = J_y(J);
U = expm(-1i * theta * Jy);

end
```

B.17. U_z

```
%%%%%%%%%% Purpose of this script %%%%%%%%%%
%
% This script is used to compute the matrix elements of the unitary
% transformation operator generated by rotating around the z-axis by
% an angle of theta in the basis of the Dicke states
%
%%%%%%%%%%%%%% End of purpose %%%%%%%%%%%%%%

function U = U_z(J, theta)
```

```
Jz = J_z(J);

U = expm(-1i * theta * Jz);


end
```

APPENDIX C

Matlab Codes for Spin Squeezing Effects

This appendix contains matlab codes for simulating the various results for OAT and TACT spin squeezing.

C.1. QPD for OAT

```
%%%%%%%%%% Purpose of this script %%%%%%%%%%
%
% This script is used to compute the squeezed spin state (SSS) for a given
% coherent spin states (CSS) using one-axis-twist (OAT) squeezing in the
% basis of the Dicke collective states, and plot it in terms of Husimi
% Quasiprobability Distribution (QPD).
%
%%%%%%%%%%%%%% End of purpose %%%%%%%%%%%%%%

%% The actual program starts here %%
clc
clear
close all

%% Timing the program %%
tic
```

```
%% Initial parameters %%
N = 40;                          % Total number of elementary spin (1/2-spin)
J = N/2;                         % Total spin of the system (spin-J system)

Jz = J_z(J);                     % Jz matrix form in the Dicke states
Jx = J_x(J);                     % Jx matrix form in the Dicke states
Jy = J_y(J);                     % Jy matrix form in the Dicke states
Jp = J_plus(J);                  % J+ matrix form in the Dicke states
Jm = J_minus(J);                 % J- matrix form in the Dicke states

mu = [0, 0.05, 0.1, 0.3];        % Squeezing parameters mu = chi*t
nu = nu_oat_y(J, mu);            % Corrective rotation angle rotated around
    y-axis

[theta, phi] = meshgrid(0 : pi/500 : pi, -pi : pi/250 : pi); % the spherical
    coordinates
x = sin(theta).*cos(phi);        % Corresponding x coordinate
y = sin(theta).*sin(phi);        % Corresponding y coordinate
z = cos(theta);                  % Corresponding z coordinate
[m, n] = size(theta);

Psi_i = Psi_0(J, -J);            % Initial state vector of the system (assumed
    all spin are down)
```

```
Ux = U_x(J, pi/2);                % Rotation around x axis for the two
    pi/2-pulse interaction zones
L = 2 * length(mu);               % Number of probabilities to plot
P_f = zeros(m, n, L);             % Final probability distribution


for l = 1 : length(mu)
    Uoat_p = U_oat(J, mu(l));     % Unitary transformation for doing one-axis
        twisting
    Uy_p = U_y(J, nu(l));         % Corrective rotation around y axis after
        squeezing

    % State vector evolution
    P = zeros(m, n, l);
    Psi_f = zeros(N + 1, 4);
    Psi_f(:, 1) = Psi_i;
    Psi_f(:, 2) = Ux * Psi_f(:, 1);
    Psi_f(:, 3) = Uoat_p * Psi_f(:, 2);
    Psi_f(:, 4) = Uy_p * Psi_f(:, 3);

    for i = 1 : m
        for j = 1 : n
            css_theta_phi = css(J, theta(i, j), phi(i, j)); % state vector of CSS
                in direction (theta, phi)
```

```
            for k = 1 : 4
                P(i, j, k) = abs(css_theta_phi' * Psi_f(:, k)).^2;
            end
        end
    end

    P_f(:, :, 2*l-1) = P(:, :, 3);
    P_f(:, :, 2*l) = P(:, :, 4);
end

% Plot the QPD
idx = [1 : 2 : L-1, 2 : 2 : L]; % Index for plotting

figure

for i = 1 : 8
    subplot(2, length(mu), i)
    mesh(x, y, z, P_f(:, :, idx(i)));
    view([180 0])
    colormap jet
    xlabel('X', 'fontsize', 15)
    ylabel('Y', 'fontsize', 15)
    zlabel('Z', 'fontsize', 15)
    set(gca, 'fontsize', 20)
end
```

```
%% Print the running time %%
toc
```

C.2. CPD for OAT

```
%%%%%%%%%% Purpose of this script %%%%%%%%%%
%
% This script is used to compute the squeezed spin state (SSS) for a given
% coherent spin states (CSS) using one-axis-twist (OAT) squeezing in the
% basis of the Dicke collective states, and plot it in terms of
% Collective-state Quasiprobability Distribution (CPD).
%
%%%%%%%%%%%%%% End of purpose %%%%%%%%%%%%%%

%% The actual program starts here %%
clc
clear
close all

%% Timing the program %%
tic

%% Initial parameters %%
N = 40;                          % Total number of elementary spin (1/2-spin)
```

```
J = N/2;                          % Total spin of the system (spin-J system)

Jz = J_z(J);                      % Jz matrix form in the Dicke states
Jx = J_x(J);                      % Jx matrix form in the Dicke states
Jy = J_y(J);                      % Jy matrix form in the Dicke states
Jp = J_plus(J);                   % J+ matrix form in the Dicke states
Jm = J_minus(J);                  % J- matrix form in the Dicke states
P0 = P_K(J, 0);                   % P0 matrix form in the Dicke states
PN = P_K(J, N);                   % PN matrix form in the Dicke states

mu = [0, 0.1, 0.2, 0.6, pi]/2;        % Squeezing parameters
nu = nu_oat_y(J, mu);             % Corrective rotation angle rotated around
    y-axis

Psi_i = Psi_0(J, -J);             % Initial state vector of the system (assumed
    all spin are down)
Ux = U_x(J, pi/2);                % Rotation around x axis for the two
    pi/2-pulse interaction zones
Psi_y = Ux * Psi_i;               % State vector after the first pi/2-pulse

L = 2 * length(mu);               % Number of probabilities to plot
P_f = zeros(N + 1, L);            % Final probability distribution

for l = 1 : length(mu)
```

```
    Uoat_p = U_oat(J, mu(l));      % Unitary transformation for doing one-axis
        twisting

    if mu(l) == pi/2
        Uy_p = U_x(J, pi/2);       % Corrective rotation around x axis after
            squeezing
    else
        Uy_p = U_y(J, nu(l));      % Corrective rotation around y axis after
            squeezing
    end

    P_f(:, 2*l-1) = Uoat_p * Psi_y;
    P_f(:, 2*l) = Uy_p * P_f(:, 2*l-1);
end

% Plot the CPD
idx = [1 : 2 : L-1, 2 : 2 : L]; % Index for plotting
xlimits = [-J, J];
ylimits = [0, 0.5];

figure

for i = 1 : L
    subplot(2, length(mu), i)
    bar(-J : J, abs(P_f(:, idx(i))).^2, 'b')
```

```
    hold on
    plot(-J : J, abs(P_f(:, idx(i))).^2, 'r-', 'Linewidth', 2)
    xlabel('M', 'FontSize', 15)
    ylabel('P', 'FontSize', 15)
    if i == L
        xlim(xlimits)
    else
        xlim(xlimits*3/4)
    end
    ylim(ylimits)
end

figure

for i = 1 : length(mu)
    subplot(1, length(mu), i)
    bar(-J : J, abs(P_f(:, idx(i + length(mu)))).^2, 'b')
    hold on
    plot(-J : J, abs(P_f(:, idx(i + length(mu)))).^2, 'r-', 'linewidth', 2)
    xlabel('M', 'fontsize', 15)
    ylabel('P', 'fontsize', 15)
    set(gca, 'fontsize', 20)
    if i == length(mu)
        xlim(xlimits)
    else
```

```
        xlim(xlimits*3/4)
    end
    ylim(ylimits)
end

%% Print the running time %%
toc
```

C.3. ξ_{KU} for OAT

```
%%%%%%%%%% Purpose of this script %%%%%%%%%%
%
% This script is used to compute the spin-squeezing parameter Xi_KU
% for different squeezing parameters mu.
%
%%%%%%%%%%%%%% End of purpose %%%%%%%%%%%%%%

%% The actual program starts here %%
clc
clear
close all

%% Timing the program %%
tic
```

```
%% Initial parameters %%
N = 40;                              % Total number of elementary spin (1/2-spin)
J = N/2;                             % Total spin of the system (spin-J system)
mu = 0 : pi/100000 : pi/2;             % Squeezing parameters
A = 1 - (cos(2*mu)).^(N-2);          % Parameter A
B = 4 * sin(mu) .* (cos(mu)).^(N-2); % Parameter B

xi_KU = (1 + 1/2 * (J - 1/2) * (A - sqrt(A.^2 + B.^2))); % Spin-squeezing
    parameter proposed by Kitagawa and Ueda

figure
plot(mu, xi_KU, '-b', 'linewidth', 2)
xlabel('\mu', 'fontsize', 15)
ylabel('\xi_{KU}', 'fontsize', 15)
set(gca, 'fontsize', 25)
xlim([0, pi/2])

%% Print the running time %%
toc
```

C.4. Enhancement for OAT

```
%%%%%%%%%%%%%%%% Purpose of this script %%%%%%%%%%%%%%%%%%%
%
% This script is used to compute the enhancement of OAT spin squeezing,
```

```
% which is defined as -10*log(Xi_KU), where Xi_KU is the spin squeezing
% parameter for OAT. The final answer will be in unit of dB.
%
%%%%%%%%%%%%%%%%% End of purpose %%%%%%%%%%%%%%%%%%%%

%% The actual program starts here %%
clc
clear
close all

%%
tic

%% Computing S_var
mu = 0 : pi/1000000 : pi/5000;
N = [10, 100, 1000, 10000, 100000, 500000, 1000000];
S_var = zeros(length(N), length(mu));

for i = 1 : length(N)
    A = 1 - (cos(2 * mu)).^(N(i) - 2);
    B = 4 * sin(mu) .* (cos(mu)).^(N(i) - 2);
    Q = 1 + (N(i) - 1) / 4 .* (A - sqrt(A.^2 + B.^2));
    S_var(i, :) = -10 * log10(Q);
end
```

```
% Plot separately
for i = 1 : length(N)
    figure
    plot(mu, S_var(i, :), 'b-', 'linewidth', 3)
    xlabel('\mu', 'fontsize', 30)
    ylabel('S_{var}', 'fontsize', 30)
    title(['N = ' num2str(N(i))])
    set(gca, 'fontsize', 15)
end

%% Plot together
figure

plot(mu, S_var(1, :), 'b-', 'linewidth', 3)
hold on
plot(mu, S_var(2, :), 'r-', 'linewidth', 3)
hold on
plot(mu, S_var(3, :), 'y-', 'linewidth', 3)
hold on
plot(mu, S_var(4, :), 'k-', 'linewidth', 3)
hold on
plot(mu, S_var(5, :), 'c-', 'linewidth', 3)
hold on
plot(mu, S_var(6, :), 'g-', 'linewidth', 3)
hold on
```

```
plot(mu, S_var(7, :), 'm-', 'linewidth', 3)


xlabel('\mu', 'fontsize', 30)
ylabel('S_{var}', 'fontsize', 30)
legend(['N = ' num2str(N(1))], ['N = ' num2str(N(2))], ['N = ' num2str(N(3))],
    ['N = ' num2str(N(4))], ...
       ['N = ' num2str(N(5))], ['N = ' num2str(N(6))], ['N = ' num2str(N(7))])
legend(['N = ' num2str(N(1))], ['N = ' num2str(N(2))])
title('S_{var} vs. \mu')
set(gca, 'fontsize', 15)
ax = gca; ax.XAxis.Exponent = 0;


%%
toc
```

C.5. QPD for TACT

```
%%%%%%%%%% Purpose of this script %%%%%%%%%%
%
% This script is used to compute the squeezed spin state (SSS) for a given
% coherent spin states (CSS) using two-axis-counter-twist (TACT) squeezing
% in the basis of the Dicke collective states, and plot it in terms of
% Husimi Quasiprobability Distribution (QPD).
%
%%%%%%%%%%%%%% End of purpose %%%%%%%%%%%%%%
```

```
%% The actual program starts here %%
clc
clear
close all

%% Timing the program %%
tic

%% Initial parameters %%
N = 40;                             % Total number of elementary spin (1/2-spin)
J = N/2;                            % Total spin of the system (spin-J system)

Jz = J_z(J);                        % Jz matrix form in the Dicke states
Jx = J_x(J);                        % Jx matrix form in the Dicke states
Jy = J_y(J);                        % Jy matrix form in the Dicke states
Jp = J_plus(J);                     % J+ matrix form in the Dicke states
Jm = J_minus(J);                    % J- matrix form in the Dicke states

mu = [0, 0.025, 0.05, 0.075];       % Squeezing parameters mu = chi*t
nu = nu_oat_y(J, mu);               % Corrective rotation angle rotated around
    y-axis

[theta, phi] = meshgrid(0 : pi/500 : pi, -pi : pi/250 : pi); % the spherical
    coordinates
```

```
x = sin(theta).*cos(phi);          % Corresponding x coordinate
y = sin(theta).*sin(phi);          % Corresponding y coordinate
z = cos(theta);                    % Corresponding z coordinate
[m, n] = size(theta);

Psi_i = Psi_0(J, -J);              % Initial state vector of the system (assumed
    all spin are down)
Ux = U_x(J, pi/2);                 % Rotation around x axis for the two
    pi/2-pulse interaction zones
L = length(mu);                    % Number of squeezing parameters mu
P_f = zeros(m, n, L);              % Final probability distribution

for l = 1 : L
    Uoat_p = U_tact_y(J, mu(l));     % Unitary transformation for doing one-axis
        twisting

    % State vector evolution
    P = zeros(m, n, 3);
    Psi_f = zeros(N + 1, 3);
    Psi_f(:, 1) = Psi_i;
    Psi_f(:, 2) = Ux * Psi_f(:, 1);
    Psi_f(:, 3) = Uoat_p * Psi_f(:, 2);

    for i = 1 : m
        for j = 1 : n
```

```
            css_theta_phi = css(J, theta(i, j), phi(i, j)); % state vector of CSS
                in direction (theta, phi)

            for k = 1 : 3
                P(i, j, k) = abs(css_theta_phi' * Psi_f(:, k)).^2;
            end
        end
    end

    P_f(:, :, l) = P(:, :, 3);
end

% Plot the QPD
figure

for i = 1 : L
    subplot(1, L, i)
    mesh(x, y, z, P_f(:, :, i));
    view([180 0])
    colormap jet
    xlabel('X', 'fontsize', 15)
    ylabel('Y', 'fontsize', 15)
    zlabel('Z', 'fontsize', 15)
    set(gca, 'fontsize', 20)
end
```

```
%% Print the running time %%

toc
```

APPENDIX D

Matlab Codes for SCAIN and SCAC

This appendix contains matlab codes for simulating the various results for SCAIN and SCAC, including QPD evolution, CPD evolution, frequency scanning, and QFR and QFF calculations. Here I'm only showing codes for X-protocol, which can be modified to account for Y-protocol.

D.1. QPD for SCAIN Using X-Protocol

```
%%%%%%%%%% Purpose of this script %%%%%%%%%%%%%%%%%%
%
% This script is used to compute the state vector evolutioins of
% atomic interferometers with x-protocol spin squeezing (SS) in the basis of the
% Dicke states (aka symmetric collective states) for even or odd number of
% atoms. The state vector is then projected onto the coherent spin states (CSS).
%
%%%%%%%%%%%%%% End of purpose %%%%%%%%%%%%%%%%%%

%% The actual program starts here %%
clc
clear
close all
```

```
%% Timing the program %%
tic

%% Initial parameters %%
N = 100;                          % Total number of elementary spin (1/2-spin)
J = N/2;                          % Total spin of the system (spin-J system)

Jz = J_z(J);                      % Jz matrix form in the Dicke states
Jx = J_x(J);                      % Jx matrix form in the Dicke states
Jy = J_y(J);                      % Jy matrix form in the Dicke states
Jp = J_plus(J);                   % J+ matrix form in the Dicke states
Jm = J_minus(J);                  % J- matrix form in the Dicke states
P0 = P_K(J, 0);                   % P0 matrix form in the Dicke states
PN = P_K(J, N);                   % PN matrix form in the Dicke states

alpha1 = pi/2/N;                    % Dark zone phase shift (angle rotated
    around z-axis)
beta1 = pi/2;                     % Interaction zone width for pi/2-pulses
beta2 = pi;                       % Interaction zone width for pi-pulses
mu = pi/2;                        % Squeezing parameters
nu = nu_oat_x(J, mu);             % Corrective rotation angle rotated around
    x-axis
CRS = -1;                         % Corrective rotation sign
```

```
[theta, phi] = meshgrid(0 : pi/500 : pi, -pi : pi/250 : pi); % the spherical
    coordinates
x = sin(theta).*cos(phi);          % Corresponding x coordinate
y = sin(theta).*sin(phi);          % Corresponding y coordinate
z = cos(theta);                    % Corresponding z coordinate
[m, n] = size(theta);

%% Initial state vector and operators for spin squeezing %%
Psi_i = Psi_0(J, -J);              % Initial state vector of the system (assumed
    all spin are down)
Ux = U_x(J, beta1);                % Rotation around x axis for the two
    pi/2-pulse interaction zones
Uoat_p = U_oat(J, mu);             % Unitary transformation for doing one-axis
    twisting
Ux_p = U_x(J, nu);                 % Corrective rotation around x axis after
    squeezing
Uz_p = U_z(J, alpha1/2);           % Rotation around z axis in the first dark zone
Ux_pi = U_x(J, beta2);             % Rotation around x axis for the pi-pulse
    interaction zone
Uz_m = U_z(J, -alpha1/2);          % Rotation around z axis in the second dark
    zone
Ux_m = U_x(J, nu * CRS);           % Corrective rotation around x axis before
    undoing squeezing
Uoat_m = U_oat(J, -mu);            % Unitary transformation for undoing one-axis
    twisting
```

```
%% State vector evolution %%
d = 10;
P = zeros(m, n, d);
Psi_f = zeros(N + 1, d);
Psi_f(:, 1) = Psi_i;
Psi_f(:, 2) = Ux * Psi_f(:, 1);
Psi_f(:, 3) = Uoat_p * Psi_f(:, 2);
Psi_f(:, 4) = Ux_p * Psi_f(:, 3);
Psi_f(:, 5) = Uz_p * Psi_f(:, 4);
Psi_f(:, 6) = Ux_pi * Psi_f(:, 5);
Psi_f(:, 7) = Uz_m * Psi_f(:, 6);
Psi_f(:, 8) = Ux_m * Psi_f(:, 7);
Psi_f(:, 9) = Uoat_m * Psi_f(:, 8);
Psi_f(:, 10) = Ux * Psi_f(:, 9);

for i = 1 : m
    for j = 1 : n
        css_theta_phi = css(J, theta(i, j), phi(i, j)); % state vector of CSS in
            direction (theta, phi)

        for k = 1 : d
            P(i, j, k) = abs(css_theta_phi' * Psi_f(:, k)).^2;
        end
    end
```

```
end

%% Plot the probabilities %%
x_axis = -1 : 1/1000 : 1; % auxiliary line
y_axis = -1 : 1/1000 : 1; % auxiliary line
z_axis = -1 : 1/1000 : 1; % auxiliary line
px = cos(pi * x_axis);   % auxiliary circle
py = sin(pi * x_axis);   % auxiliary circle

if rem(N, 2) == 0
    AZ = [185, 185, 95, 185, 185, 185, 185, 95, 95, 185]; % Pespective view
        azimuthal angle -- Even N
else
    AZ = [185, 185, 185, 185, 185, 185, 185, 95, 95, 95]; % Pespective view
        azimuthal angle -- Odd N
end

EL = [-5, -5, -5, -5, -5, -5, -5, -5, -5, -5];   % Pespective view elevation angle

for k = 1 : d
    % PLot as a function of theta & phi
    figure
    mesh(theta/pi, phi/(2*pi), P(:, :, k))
    xlabel('$\frac{\theta}{\pi}$', 'Interpreter', 'latex', 'FontSize', 15)
    ylabel('$\frac{\phi}{2\pi}$', 'Interpreter', 'latex', 'FontSize', 15)
```

```
zlabel('P')
title(['Husimi quasi-probability distribution in terms of \theta and \phi --
    Squeezing with y-protocol and N = '...
        num2str(N) ' and CRS = ' num2str(CRS) ' and \mu = ' num2str(mu/pi)
            '*\pi'])


% PLot as a function of x & y & z
figure
mesh(x, y, z, P(:, :, k))
xlabel('X')
ylabel('Y')
zlabel('Z')
title(['Husimi quasi-probability distribution in terms of x, y and z --
    Squeezing with x-protocol and N = '...
        num2str(N) ' and CRS = ' num2str(CRS) ' and \mu = ' num2str(mu/pi)
            '*\pi'])
colormap cool
colorbar

% PLot as a function of x & y & z with auxiliary lines
figure
plot3(px, py, zeros(1, numel(px)), 'k', 'linewidth', 2) % circle perp to z
hold on
plot3(zeros(1, numel(px)), px, py, 'k', 'linewidth', 2) % circle perp to x
```

```
    hold on
    plot3(px, zeros(1, numel(px)), py, 'k', 'linewidth', 2) % circle perp to y
    hold on
    plot3(x_axis, zeros(1, numel(x_axis)), zeros(1, numel(x_axis)), 'k',
        'linewidth', 2) % draws x-axis
    hold on
    plot3(zeros(1, numel(y_axis)), y_axis, zeros(1, numel(y_axis)), 'k',
        'linewidth', 2) % draws y-axis
    hold on
    plot3(zeros(1, numel(z_axis)), zeros(1, numel(z_axis)), z_axis, 'k',
        'linewidth', 2) % draws z-axis
    hold on

    sf = surf(x, y, z, P(:, :, k));
    alpha(sf, 0.9) % make sure this function is not shadowed by user-defined
        variables
    shading interp;
    axis off;
    colormap cool
    view(AZ(k), EL(k))
end

%% Print the running time %%
toc
```

D.2. CPD for SCAIN Using X-Protocol

```
%%%%%%%%%% Purpose of this script %%%%%%%%%%%%%%%%%
%
% This script is used to compute the state vector evolutioins of
% atomic interferometers with x-protocol spin squeezing (SS) in the basis of the
% Dicke states (aka symmetric collective states) for even or odd number of
% atoms. The state vector is then projected onto the Dicke states to plot the
% population distribution on each symmetric collective state.
%
%%%%%%%%%%%%%% End of purpose %%%%%%%%%%%%%%%%%%

%% The actual program starts here %%
clc
clear
close all

%% Timing the program %%
tic

%% Initial parameters %%
N = 41;                             % Total number of elementary spin (1/2-spin)
J = N/2;                            % Total spin of the system (spin-J system)

Jz = J_z(J);                        % Jz matrix form in the Dicke states
Jx = J_x(J);                        % Jx matrix form in the Dicke states
```

```
Jy = J_y(J);                        % Jy matrix form in the Dicke states
Jp = J_plus(J);                     % J+ matrix form in the Dicke states
Jm = J_minus(J);                    % J- matrix form in the Dicke states
P0 = P_K(J, 0);                     % P0 matrix form in the Dicke states
PN = P_K(J, N);                     % PN matrix form in the Dicke states

if rem(N, 2) == 0
    alpha = pi/2/N;                 % Dark zone phase shift (angle rotated around
        z-axis) -- even N
else
    alpha = pi/4;                   % Dark zone phase shift (angle rotated around
        z-axis) -- odd N
end

beta1 = pi/2;                       % Interaction zone width for pi/2-pulses
beta2 = pi;                         % Interaction zone width for pi-pulses
mu = pi/2;                          % Squeezing parameters
nu = nu_oat_x(J, mu);               % Corrective rotation angle rotated around
    x-axis
CRS = -1;                           % Corrective rotation sign

%% Initial state vector and operators for spin squeezing %%
Psi_i = Psi_0(J, -J);               % Initial state vector of the system (assumed
    all spin are down)
```

```
Ux = U_x(J, beta1);                % Rotation around x axis for the two
    pi/2-pulse interaction zones
Uoat_p = U_oat(J, mu);             % Unitary transformation for doing one-axis
    twisting
Ux_p = U_x(J, nu);                 % Corrective rotation around x axis after
    squeezing
Uz_p = U_z(J, alpha/2);            % Rotation around z axis in the first dark zone
Ux_pi = U_x(J, beta2);             % Rotation around x axis for the pi-pulse
    interaction zone
Uz_m = U_z(J, -alpha/2);           % Rotation around z axis in the second dark
    zone
Ux_m = U_x(J, nu * CRS);           % Corrective rotation around x axis before
    undoing squeezing
Uoat_m = U_oat(J, -mu);            % Unitary transformation for undoing one-axis
    twisting

%% State vector evolution %%
d = 10;
Psi_f = zeros(N + 1, d);
Psi_f(:, 1) = Psi_i;
Psi_f(:, 2) = Ux * Psi_f(:, 1);
Psi_f(:, 3) = Uoat_p * Psi_f(:, 2);
Psi_f(:, 4) = Ux_p * Psi_f(:, 3);
Psi_f(:, 5) = Uz_p * Psi_f(:, 4);
Psi_f(:, 6) = Ux_pi * Psi_f(:, 5);
```

```
Psi_f(:, 7) = Uz_m * Psi_f(:, 6);
Psi_f(:, 8) = Ux_m * Psi_f(:, 7);
Psi_f(:, 9) = Uoat_m * Psi_f(:, 8);
Psi_f(:, 10) = Ux * Psi_f(:, 9);

%% Plot the probabilities %%
x_pos = -4;       % Position of x label
x_lower = -2;     % Lower limit of x axis
x_upper = N + 2;  % Upper limit of x axis

% Plot in subplots
if N == 100
    y_upper = [1.1, 0.1, 0.6, 0.2, 0.6];
elseif N == 101
    y_upper = [1.1, 0.1, 0.2, 0.08, 0.16];
elseif N == 40
    y_upper = [1.1, 0.2, 0.6, 0.3, 0.6];
elseif N == 41
    y_upper = [1.1, 0.2, 0.3, 0.15, 0.2];
else
    y_upper = [1.1, 1.1, 1.1, 1.1, 1.1];
end

Psi_index = [1, 2, 4, 8, 10];
```

```
for k = 1 : 5
    subplot(5, 1, k)
    plot(N : -1 : 0, abs(Psi_f(:, Psi_index(k))).^2, 'b-', 'Linewidth', 2)
    set(gca, 'xdir', 'reverse')
    xlabel('n', 'FontSize', 15, 'Position', [x_pos, 0, 0])
    ylabel('|E_n|^2', 'FontSize', 13)
    xlim([x_lower, x_upper])
    ylim([0, y_upper(k)])
end

% Plot separately
for k = 1 : d
    figure
    plot(N : -1 : 0, abs(Psi_f(:, k)).^2, 'b-', 'Linewidth', 2)
    set(gca, 'xdir', 'reverse')
    xlabel('n', 'FontSize', 15, 'Position', [x_pos, 0, 0])
    ylabel('|E_n|^2', 'FontSize', 13)
    xlim([x_lower, x_upper])
    title(['Collective state population distribution -- Squeezing with x-protocol
        and N = '...
            num2str(N) ' and CRS = ' num2str(CRS) ' and \mu = ' num2str(mu/pi)
                '*\pi'])
end

%% Print the running time %%
```

```
toc
```

D.3. Frequency Scanning for SCAIN Using X-Protocol

```
%%%%%%%%%% Purpose of this script %%%%%%%%%%
%
% This script is used to compute the frequency scanning (FS) results of
% atomic interferometer with x-protocol spin squeezing (SS) in the basis of the
% Dicke states (aka symmetric collective states) and compare the cases of
% even and odd number of atoms with fixed squeezing parameters and CRS.
%
%%%%%%%%%%%%%% End of purpose %%%%%%%%%%%%%%

%% The actual program starts here %%
clc
clear
close all

%% Timing the program %%
tic

%% Initial parameters %%
n = 200;                                    % Base number of elementary spin
    (1/2-spin)
```

```
N = n : n + 1;                          % Total number of elementary spin
    (1/2-spin)

max = 10 * pi/n;                        % Maximum plottable value of dark
    zone phase shift
step = pi/10/n;                         % Step value for dark zone phase shift
phi = -max : step : max;                % Dark zone phase shift (angle rotated
    around z-axis)
theta1 = pi/2;                          % Angle rotated around x-axis for
    pi/2-pulse
theta2 = pi;                            % Angle rotated around x-axis for
    pi-pulse
mu = pi/2;                              % Squeezing parameters
CRS = 1;                                % Corrective rotation sign

P_E0 = zeros(numel(mu), numel(phi), numel(N)); % P_E0, probability in |E0>, as a
    function of phi and mu, with squeezing
P_1 = zeros(numel(mu), numel(phi), numel(N)); % P_1, probability in |1> (spin
    down) , as a function of phi and mu, with squeezing
P_z = zeros(numel(mu), numel(phi), numel(N)); % P_z, average value of Jz
    operator, as a function of phi and mu, with squeezing

P_E00 = zeros(1, numel(phi), numel(N));     % P_E00, probability in |E0> , as a
    function of phi, without squeezing
```

```
P_10 = zeros(1, numel(phi), numel(N));     % P_10, probability in |1> (spin
    down), as a function of phi, without squeezing
P_z0 = zeros(1, numel(phi), numel(N));     % P_z0, average value of Jz operator,
    as a function of phi, without squeezing


for k = 1 : numel(N)
    %% Initial parameters for each case %%
    J = N(k)/2;                            % Total spin of the system (spin-J
        system)
    Jz = J_z(J);                           % Jz matrix form in the Dicke states
    Jx = J_x(J);                           % Jx matrix form in the Dicke states
    Jy = J_y(J);                           % Jy matrix form in the Dicke states
    Jp = J_plus(J);                        % J+ matrix form in the Dicke states
    Jm = J_minus(J);                       % J- matrix form in the Dicke states
    P0 = P_K(J, 0);                        % P0 matrix form in the Dicke states
    PN = P_K(J, N(k));                     % PN matrix form in the Dicke states
    Psi_i = Psi_0(J, -J);                  % Initial state vector of the system
        (assumed all spin are down)
    Ux = U_x(J, theta1);                   % Rotation around x axis in the two
        pi/2-pulse interaction zones
    Ux_pi = U_x(J, theta2);                % Rotation around x axis in the
        pi-pulse interaction zone
    nu = nu_oat_x(J, mu);                  % Corrective rotation angle rotated
        around x-axis
```

```
%% Computation for collective atomic interometer with spin-squeezing %%
for i = 1 : numel(mu)
    Uoat_p = U_oat(J, mu(i));           % Unitary transformation for doing
        one-axis twisting
    Uoat_m = U_oat(J, -mu(i));          % Unitary transformation for undoing
        one-axis twisting
    Ux_p = U_x(J, nu(i));               % Corrective rotation around x axis
        after squeezing
    Ux_m = U_x(J, nu(i) * CRS);         % Corrective rotation around x axis
        before undoing squeezing

    for j = 1 : numel(phi)
        Uz_p = U_z(J, phi(j)/2);        % Rotation around z axis in the first
            dark zone
        Uz_m = U_z(J, -phi(j)/2);       % Rotation around z axis in the
            second dark zone
        Psi_f = Ux * Uoat_m * Ux_m * Uz_m * Ux_pi * Uz_p * Ux_p * Uoat_p * Ux
            * Psi_i; % Final state vector with x-protocol
        P_E0(i, j, k) = abs(Psi_f' * P0 * Psi_f);
        P_1(i, j, k) = abs(J - Psi_f' * Jz * Psi_f) / N(k);
        P_z(i, j, k) = real(Psi_f' * Jz * Psi_f);
    end
end

%% Computation for collective atomic interometer without spin-squeezing %%
```

```
    for i = 1 : numel(phi)
        Uz_p = U_z(J, phi(i)/2);            % Rotation around z axis in the first
            dark zone
        Uz_m = U_z(J, -phi(i)/2);           % Rotation around z axis in the
            second dark zone
        Psi_f = Ux * Uz_m * Ux_pi * Uz_p * Ux * Psi_i;
        P_E00(1, i, k) = abs(Psi_f' * P0 * Psi_f);
        P_10(1, i, k) = abs(J - Psi_f' * Jz * Psi_f) / N(k);
        P_z0(1, i, k) = real(Psi_f' * Jz * Psi_f);
    end
end

%% Plot the probabilities %%
for i = 1 : numel(mu)
    figure      % PLot P_E0
    plot(phi/(2*pi), P_E0(i, :, 1), 'r-', 'Linewidth', 3)
    hold on
    plot(phi/(2*pi), P_E0(i, :, 2), 'b-', 'Linewidth', 3)
    hold on
    plot(phi/(2*pi), (P_E0(i, :, 1) + P_E0(i, :, 2))/2, 'k:', 'Linewidth', 2)
    hold on
    plot(phi/(2*pi), P_E00(1, :, 1), 'r--', 'Linewidth', 2)
    hold on
    plot(phi/(2*pi), P_E00(1, :, 2), 'b--', 'Linewidth', 2)
```

```
xlabel('$\frac{\phi}{2\pi}$', 'Interpreter', 'latex', 'FontSize', 20,
    'Position', [-4, 0, 0])
ylabel('P_{E0}', 'FontSize', 15)
xlim([-0.025, 0.025])
ylim([-0.05, 1])
set(gca, 'fontsize', 25)
legend(['Squeezed with N = ' num2str(N(1))], ['Squeezed with N = '
    num2str(N(2))], 'Squeezed average', ...
       ['No squeezing with N = ' num2str(N(1))], ['No squeezing with N = '
          num2str(N(2))])
title('Collective state detection', 'FontSize', 15)
suptitle(['FS -- Squeezing with x-protocol and CRS = ' num2str(CRS) ' and \mu
    = ' num2str(mu(i)/pi) '*\pi']);


figure          % PLot P_1
plot(phi/(2*pi), P_1(i, :, 1), 'r-', 'Linewidth', 2)
hold on
plot(phi/(2*pi), P_1(i, :, 2), 'b-', 'Linewidth', 2)
hold on
plot(phi/(2*pi), (P_1(i, :, 1) + P_1(i, :, 2))/2, 'k:', 'Linewidth', 2)
hold on
plot(phi/(2*pi), P_10(1, :, 1), 'r--', 'Linewidth', 2)
hold on
plot(phi/(2*pi), P_10(1, :, 2), 'b--', 'Linewidth', 2)
xlabel('$\frac{\phi}{2\pi}$', 'Interpreter', 'latex', 'FontSize', 10)
```

```
ylabel('P_1', 'FontSize', 15)
ylim([0, 1])
legend(['Squeezed with N = ' num2str(N(1))], ['Squeezed with N = '
    num2str(N(2))], 'Squeezed average', ...
       ['No squeezing with N = ' num2str(N(1))], ['No squeezing with N = '
          num2str(N(2))])
title('Conventional detection', 'FontSize', 15)
suptitle(['FS -- Squeezing with x-protocol and CRS = ' num2str(CRS) ' and \mu
    = ' num2str(mu(i)/pi) '*\pi']);

figure          % PLot P_z
plot(phi/(2*pi), P_z(i, :, 1), 'r-', 'Linewidth', 2)
hold on
plot(phi/(2*pi), P_z(i, :, 2), 'b-', 'Linewidth', 2)
hold on
plot(phi/(2*pi), (P_z(i, :, 1) + P_z(i, :, 2))/2, 'k:', 'Linewidth', 2)
hold on
plot(phi/(2*pi), P_z0(1, :, 1), 'r--', 'Linewidth', 2)
hold on
plot(phi/(2*pi), P_z0(1, :, 2), 'b--', 'Linewidth', 2)
xlabel('$\frac{\phi}{2\pi}$', 'Interpreter', 'latex', 'FontSize', 10)
ylabel('P_z', 'FontSize', 15)
ylim([-J, J])
legend(['Squeezed with N = ' num2str(N(1))], ['Squeezed with N = '
    num2str(N(2))], 'Squeezed average', ...
```

```
        ['No squeezing with N = ' num2str(N(1))], ['No squeezing with N = '
            num2str(N(2))])
    title('Conventional detection', 'FontSize', 15)
    suptitle(['FS -- Squeezing with x-protocol and CRS = ' num2str(CRS) ' and \mu
        = ' num2str(mu(i)/pi) '*\pi']);
end

%% Print the running time %%
toc
```

D.4. QFR for SCAIN Using X-Protocol

```
%%%%%%%%%% Purpose of this script %%%%%%%%%%
%
% This script is used to compute the quantum frequency fluctuation (QFF)
% for atomic interferometer with x-protocol spin squeezing (SS) in the basis of
    the
% Dicke states (aka symmetric collective states) and compare the cases of
% even and odd number of atoms
%
%%%%%%%%%%%%%% End of purpose %%%%%%%%%%%%%%

%% The actual program starts here %%
clc
clear
```

```
close all

%% Timing the program %%
tic

%% Initial parameters %%
n = 100;                                    % Base number of elementary
    spin (1/2-spin)
N = n : n + 1;                              % Total number of elementary
    spin (1/2-spin)
step = 1e-8;                                % Step value for dark zone
    phase shift
max = 1e-4;                                 % Maximum plottable value of
    dark zone phase shift
min = max - step;                           % Minimum plottable value of
    dark zone phase shift
phi = [min, max];                           % Dark zone phase shift
    (angle rotated around z-axis)
theta1 = pi/2;                              % Angle rotated around
    x-axis for pi/2-pulse
theta2 = pi;                                % Angle rotated around
    x-axis for pi-pulse
mu = 0 : pi/400 : pi/2;                     % Squeezing parameters
CRS = 1;                                    % Corrective rotation sign
```

```
QFR_inv_P_E0 = zeros(numel(mu), numel(phi), numel(N)); % Inverse of QFR for
    collective state detection
QFR_inv_P_Jz = zeros(numel(mu), numel(phi), numel(N)); % Inverse of QFR for
    conventional detection

HL_inv = zeros(numel(N), 1);                          % Inverse of QFR in the
    Heisenberg limit (HL)
SQL_inv = zeros(numel(N), 1);                         % Inverse of QFR in the
    standard quantum limit (SQL)
QFR_inv_HL = zeros(numel(mu), 2);                     % Inverse of QFR in the
    Heisenberg limit (HL)
QFR_inv_SQL = zeros(numel(mu), 2);                    % Inverse of QFR in the
    standard quantum limit (SQL)

P_E0 = zeros(numel(phi), 2);                          % P_E0, probability in |E0>
    with squeezing
P_E0_2 = zeros(numel(phi), 2);                        % (P_E0)^2
P_Jz = zeros(numel(phi), 2);                          % P_Jz, average value of Jz
    with squeezing
P_Jz_2 = zeros(numel(phi), 2);                        % (P_Jz)^2

for k = 1 : numel(N)
    %% Initial parameters for each case %%
    J = N(k)/2;                                       % Total spin of the system
        (spin-J system)
```

```
Jz = J_z(J);                                % Jz matrix form in the
    Dicke states
Jx = J_x(J);                                % Jx matrix form in the
    Dicke states
Jy = J_y(J);                                % Jy matrix form in the
    Dicke states
Jp = J_plus(J);                             % J+ matrix form in the
    Dicke states
Jm = J_minus(J);                            % J- matrix form in the
    Dicke states
P0 = P_K(J, 0);                             % P0 matrix form in the
    Dicke states
PN = P_K(J, N(k));                          % PN matrix form in the
    Dicke states
Psi_i = Psi_0(J, -J);                       % Initial state vector
    (assumed all spin are down)
Ux = U_x(J, theta1);                        % Rotation around x axis in
    the two pi/2-pulse interaction zones
Ux_pi = U_x(J, theta2);                     % Rotation around x axis in
    the pi-pulse interaction zone
nu = nu_oat_x(J, mu);                       % Corrective rotation angle
    rotated around x-axis

HL_inv(k) = N(k);                           % Inverse of QFR in the
    Heisenberg limit (HL)
```

```
SQL_inv(k) = HL_inv(k) / sqrt(N(k));            % Inverse of QFR in the
    standard quantum limit (SQL)
QFR_inv_HL(:, k) = repmat(HL_inv(k), numel(mu), 1); % Inverse of QFR in the
    Heisenberg limit (HL)
QFR_inv_SQL(:, k) = repmat(SQL_inv(k), numel(mu), 1); % Inverse of QFR in the
    standard quantum limit (SQL)

%% Computation for collective atomic clock with spin-squeezing %%
for i = 1 : numel(mu)
    Uoat_p = U_oat(J, mu(i));                   % Unitary transformation for
        doing one-axis twisting
    Uoat_m = U_oat(J, -mu(i));                  % Unitary transformation for
        undoing one-axis twisting
    Ux_p = U_x(J, nu(i));                       % Corrective rotation around
        x axis after squeezing
    Ux_m = U_x(J, nu(i) * CRS);                 % Corrective rotation around
        x axis before undoing squeezing

    for j = 1 : numel(phi)
        Uz_p = U_z(J, phi(j)/2);                % Rotation around z axis in
            the first dark zone
        Uz_m = U_z(J, -phi(j)/2);               % Rotation around z axis in
            the second dark zone
        Psi_f = Ux * Uoat_m * Ux_m * Uz_m * Ux_pi * Uz_p * Ux_p * Uoat_p * Ux
            * Psi_i; % Final state vector with x-protocol
```

```
            P_E0(j, k) = abs(Psi_f' * P0 * Psi_f);
            P_E0_2(j, k) = abs(Psi_f' * P0 * P0 * Psi_f);

            P_Jz(j, k) = abs(Psi_f' * Jz * Psi_f);
            P_Jz_2(j, k) = abs(Psi_f' * Jz * Jz * Psi_f);

            Delta_P_E0 = sqrt(abs(P_E0_2(j, k) - P_E0(j, k).^2));
            Delta_P_Jz = sqrt(abs(P_Jz_2(j, k) - P_Jz(j, k).^2));

            Partial_P_E0 = 0;
            Partial_P_Jz = 0;

            if j > 1
                Partial_P_E0 = abs(P_E0(j, k) - P_E0(j - 1, k)) / step;
                Partial_P_Jz = abs(P_Jz(j, k) - P_Jz(j - 1, k)) / step;
            end

            QFR_inv_P_E0(i, j, k) = Partial_P_E0 / Delta_P_E0;
            QFR_inv_P_Jz(i, j, k) = Partial_P_Jz / Delta_P_Jz;
        end
    end
end

%% Plot inverse of QFF vs. squeezing parameter mu %%
```

```
point = numel(phi);            % The point to take the QFF of the dark zone phase
    shift

% Plot in subplots
subplot(1, 3, 1)      % Plot QFR_inv for conventional detection but different N
plot(mu/pi, QFR_inv_P_Jz(:, point, 1)/HL_inv(1), 'r-', 'Linewidth', 2)
hold on
plot(mu/pi, QFR_inv_P_Jz(:, point, 2)/HL_inv(2), 'b--', 'Linewidth', 2)
hold on
plot(mu/pi, QFR_inv_HL(:, 1)/HL_inv(1), 'k-', 'Linewidth', 2)
hold on
plot(mu/pi, QFR_inv_SQL(:, 1)/HL_inv(1), 'k:', 'Linewidth', 2)
legend({['N = ' num2str(N(1))], ['N = ' num2str(N(2))], 'HL', 'SQL'},
    'FontSize', 12)
legend('boxoff')
xlabel('\mu/\pi', 'FontSize', 15)
ylabel('QFR^{-1}/QFR^{-1}_{HL}', 'FontSize', 10)
ylim([0, 1.2])
title('Atomic State Detection', 'FontSize', 15)

subplot(1, 3, 2)      % Plot QFR_inv for even N but different detection schemes
plot(mu/pi, QFR_inv_P_Jz(:, point, 1)/HL_inv(1), 'r-', 'Linewidth', 2)
hold on
plot(mu/pi, QFR_inv_P_E0(:, point, 1)/HL_inv(1), 'b--', 'Linewidth', 2)
hold on
```

```
plot(mu/pi, QFR_inv_HL(:, 1)/HL_inv(1), 'k-', 'Linewidth', 2)    % Normaized HL
hold on
plot(mu/pi, QFR_inv_SQL(:, 1)/HL_inv(1), 'k:', 'Linewidth', 2)   % Normaized SQL
legend({'Atomic State Det', 'Collective State Det', 'HL', 'SQL'}, 'FontSize', 12)
legend('boxoff')
xlabel('\mu/\pi', 'FontSize', 15)
ylabel('QFR^{-1}/QFR^{-1}_{HL}', 'FontSize', 10)
ylim([0, 1.2])
title(['N = ' num2str(N(1))], 'FontSize', 15)

subplot(1, 3, 3)      % Plot QFR_inv for odd N but different detection schemes
plot(mu/pi, QFR_inv_P_Jz(:, point, 2)/HL_inv(2), 'r-', 'Linewidth', 2)
hold on
plot(mu/pi, QFR_inv_P_E0(:, point, 2)/HL_inv(2), 'b--', 'Linewidth', 2)
hold on
plot(mu/pi, QFR_inv_HL(:, 1)/HL_inv(1), 'k-', 'Linewidth', 2)    % Normaized HL
hold on
plot(mu/pi, QFR_inv_SQL(:, 1)/HL_inv(1), 'k:', 'Linewidth', 2)   % Normaized SQL
legend({'Atomic State Det', 'Collective State Det', 'HL', 'SQL'}, 'FontSize', 12)
legend('boxoff')
xlabel('\mu/\pi', 'FontSize', 15)
ylabel('QFR^{-1}/QFR^{-1}_{HL}', 'FontSize', 10)
ylim([0, 1.2])
title(['N = ' num2str(N(2))], 'FontSize', 15)
```

```
% Plot separately
figure      % Plot QFR_inv for collective state detection but different N
plot(mu/pi, QFR_inv_P_E0(:, point, 1)/HL_inv(1), 'r-', 'Linewidth', 2)
hold on
plot(mu/pi, QFR_inv_P_E0(:, point, 2)/HL_inv(2), 'b--', 'Linewidth', 2)
hold on
plot(mu/pi, QFR_inv_HL(:, 1)/HL_inv(1), 'k-', 'Linewidth', 2)    % Normaized HL
hold on
plot(mu/pi, QFR_inv_SQL(:, 1)/HL_inv(1), 'k:', 'Linewidth', 2)   % Normaized SQL
legend(['N = ' num2str(N(1))], ['N = ' num2str(N(2))], 'HL', 'SQL')
xlabel('$\frac{\mu}{\pi}$', 'Interpreter', 'latex', 'FontSize', 15)
ylabel('QFR^{-1}/QFR^{-1}_{HL}', 'FontSize', 10)
ylim([0, 1.2])
title('Collective state detection -- QFR^{-1}/QFR^{-1}_{HL} vs. \mu',
    'FontSize', 12)
suptitle(['QFR -- Squeezing with x-protocol and CRS = ' num2str(CRS)]);

figure        % Plot QFR_inv for conventional detection but different N
plot(mu/pi, QFR_inv_P_Jz(:, point, 1)/HL_inv(1), 'r-', 'Linewidth', 2)
hold on
plot(mu/pi, QFR_inv_P_Jz(:, point, 2)/HL_inv(2), 'b--', 'Linewidth', 2)
hold on
plot(mu/pi, QFR_inv_HL(:, 1)/HL_inv(1), 'k-', 'Linewidth', 2)
hold on
plot(mu/pi, QFR_inv_SQL(:, 1)/HL_inv(1), 'k:', 'Linewidth', 2)
```

```
legend(['N = ' num2str(N(1))], ['N = ' num2str(N(2))], 'HL', 'SQL')
xlabel('$\frac{\mu}{\pi}$', 'Interpreter', 'latex', 'FontSize', 15)
ylabel('QFR^{-1}/QFR^{-1}_{HL}', 'FontSize', 10)
ylim([0, 1.2])
title('Atomic state detection -- QFR^{-1}/QFR^{-1}_{HL} vs. \mu', 'FontSize', 12)
suptitle(['QFR -- Squeezing with x-protocol and CRS = ' num2str(CRS)]);

figure      % Plot QFR_inv for even N but different detection schemes
plot(mu/pi, QFR_inv_P_Jz(:, point, 1)/HL_inv(1), 'r-', 'Linewidth', 2)
hold on
plot(mu/pi, QFR_inv_P_E0(:, point, 1)/HL_inv(1), 'b--', 'Linewidth', 2)
hold on
plot(mu/pi, QFR_inv_HL(:, 1)/HL_inv(1), 'k-', 'Linewidth', 2)    % Normaized HL
hold on
plot(mu/pi, QFR_inv_SQL(:, 1)/HL_inv(1), 'k:', 'Linewidth', 2)   % Normaized SQL
legend('Atomic state detection', 'Collective state detection', 'HL', 'SQL')
xlabel('$\frac{\mu}{\pi}$', 'Interpreter', 'latex', 'FontSize', 15)
ylabel('QFR^{-1}/QFR^{-1}_{HL}', 'FontSize', 10)
ylim([0, 1.2])
title(['N = ' num2str(N(1)) ' -- QFR^{-1}/QFR^{-1}_{HL} vs. \mu'], 'FontSize',
    12)
suptitle(['QFR -- Squeezing with x-protocol and CRS = ' num2str(CRS)]);

figure      % Plot QFR_inv for odd N but different detection schemes
plot(mu/pi, QFR_inv_P_Jz(:, point, 2)/HL_inv(2), 'r-', 'Linewidth', 2)
```

```
hold on
plot(mu/pi, QFR_inv_P_E0(:, point, 2)/HL_inv(2), 'b--', 'Linewidth', 2)
hold on
plot(mu/pi, QFR_inv_HL(:, 1)/HL_inv(1), 'k-', 'Linewidth', 2)    % Normaized HL
hold on
plot(mu/pi, QFR_inv_SQL(:, 1)/HL_inv(1), 'k:', 'Linewidth', 2)   % Normaized SQL
legend('Atomic state detection', 'Collective state detection', 'HL', 'SQL')
xlabel('$\frac{\mu}{\pi}$', 'Interpreter', 'latex', 'FontSize', 15)
ylabel('QFR^{-1}/QFR^{-1}_{HL}', 'FontSize', 10)
ylim([0, 1.2])
title(['N = ' num2str(N(2)) ' -- QFR^{-1}/QFR^{-1}_{HL} vs. \mu'], 'FontSize',
    12)
suptitle(['QFR -- Squeezing with x-protocol and CRS = ' num2str(CRS)]);

%% Print the running time %%
toc
```

D.5. QPD for SCAC Using X-Protocol

```
%%%%%%%%%% Purpose of this script %%%%%%%%%%
%
% This script is used to compute the state vector evolutioins of
% atomic clocks with x-protocol spin squeezing (SS) in the basis of the
% Dicke states (aka symmetric collective states) for even or odd number of
% atoms. The state vector is then projected onto the coherent spin states (CSS).
```

```
%
%%%%%%%%%%%%%% End of purpose %%%%%%%%%%%%%%

%% The actual program starts here %%
clc
clear
close all

%% Timing the program %%
tic

%% Initial parameters %%
N = 40;                          % Total number of elementary spin (1/2-spin)
J = N/2;                         % Total spin of the system (spin-J system)

Jz = J_z(J);                     % Jz matrix form in the Dicke states
Jx = J_x(J);                     % Jx matrix form in the Dicke states
Jy = J_y(J);                     % Jy matrix form in the Dicke states
Jp = J_plus(J);                  % J+ matrix form in the Dicke states
Jm = J_minus(J);                 % J- matrix form in the Dicke states
P0 = P_K(J, 0);                  % P0 matrix form in the Dicke states
PN = P_K(J, N);                  % PN matrix form in the Dicke states

alpha1 = pi/2/N;                 % Dark zone phase shift (angle rotated around
    z-axis)
```

```
beta = pi/2;                        % Interaction zone pulse width for pi/2 pulse
mu = pi/2;                          % Squeezing parameters
nu = nu_oat_x(J, mu);               % Corrective rotation angle rotated around
    x-axis
CRS = -1;                           % Corrective rotation sign

[theta, phi] = meshgrid(0 : pi/500 : pi, -pi : pi/250 : pi); % the spherical
    coordinates
x = sin(theta).*cos(phi);           % Corresponding x coordinate
y = sin(theta).*sin(phi);           % Corresponding y coordinate
z = cos(theta);                     % Corresponding z coordinate
[m, n] = size(theta);

%% Initial state vector and operators for spin squeezing %%
Psi_i = Psi_0(J, -J);               % Initial state vector of the system (assumed
    all spin are down)
Ux = U_x(J, beta);                  % Rotation around x axis in the two
    interaction zones
Uoat_p = U_oat(J, mu);              % Unitary transformation for doing one-axis
    twisting
Ux_p = U_x(J, nu);                  % Corrective rotation around x axis after
    squeezing
Uz = U_z(J, alpha1);                % Rotation around z axis in the dark zone
Ux_m = U_x(J, nu * CRS);            % Corrective rotation around x axis before
    undoing squeezing
```

```
Uoat_m = U_oat(J, -mu);           % Unitary transformation for undoing one-axis
    twisting

%% State vector evolution %%
d = 8;
P = zeros(m, n, d);
Psi_f = zeros(N + 1, d);
Psi_f(:, 1) = Psi_i;
Psi_f(:, 2) = Ux * Psi_f(:, 1);
Psi_f(:, 3) = Uoat_p * Psi_f(:, 2);
Psi_f(:, 4) = Ux_p * Psi_f(:, 3);
Psi_f(:, 5) = Uz * Psi_f(:, 4);
Psi_f(:, 6) = Ux_m * Psi_f(:, 5);
Psi_f(:, 7) = Uoat_m * Psi_f(:, 6);
Psi_f(:, 8) = Ux * Psi_f(:, 7);

for i = 1 : m
    for j = 1 : n
        css_theta_phi = css(J, theta(i, j), phi(i, j)); % state vector of CSS in
            direction (theta, phi)

        for k = 1 : d
            P(i, j, k) = abs(css_theta_phi' * Psi_f(:, k)).^2;
        end
    end
```

```
end

%% Plot the probabilities %%
x_axis = -1 : 1/1000 : 1; % auxiliary line
y_axis = -1 : 1/1000 : 1; % auxiliary line
z_axis = -1 : 1/1000 : 1; % auxiliary line
px = cos(pi * x_axis);   % auxiliary circle
py = sin(pi * x_axis);   % auxiliary circle

if rem(N, 2) == 0
    AZ = [185, 185, 95, 185, 185, 95, 95, 185]; % Pespective view azimuthal angle
        -- Even N
else
    AZ = [185, 185, 185, 185, 185, 95, 185, 185]; % Pespective view azimuthal
        angle -- Odd N
end

EL = [-5, -5, -5, -5, -5, -5, -5, -5];   % Pespective view elevation angle

for k = 1 : d
    % PLot as a function of theta & phi
    figure
    mesh(theta/pi, phi/(2*pi), P(:, :, k))
    xlabel('$\frac{\theta}{\pi}$', 'Interpreter', 'latex', 'FontSize', 15)
    ylabel('$\frac{\phi}{2\pi}$', 'Interpreter', 'latex', 'FontSize', 15)
```

```
zlabel('P')
title(['Husimi quasi-probability distribution in terms of \theta and \phi --
    Squeezing with y-protocol and N = '...
        num2str(N) ' and CRS = ' num2str(CRS) ' and \mu = ' num2str(mu/pi)
            '*\pi'])

% PLot as a function of x & y & z
figure
mesh(x, y, z, P(:, :, k))
xlabel('X')
ylabel('Y')
zlabel('Z')
title(['Husimi quasi-probability distribution in terms of x, y and z --
    Squeezing with x-protocol and N = '...
        num2str(N) ' and CRS = ' num2str(CRS) ' and \mu = ' num2str(mu/pi)
            '*\pi'])
colormap cool
colorbar

% PLot as a function of x & y & z with auxiliary lines
figure
plot3(px, py, zeros(1, numel(px)), 'k', 'linewidth', 2) % circle perp to z
hold on
plot3(zeros(1, numel(px)), px, py, 'k', 'linewidth', 2) % circle perp to x
hold on
```

```
    plot3(px, zeros(1, numel(px)), py, 'k', 'linewidth', 2) % circle perp to y
    hold on
    plot3(x_axis, zeros(1, numel(x_axis)), zeros(1, numel(x_axis)), 'k',
        'linewidth', 2) % draws x-axis
    hold on
    plot3(zeros(1, numel(y_axis)), y_axis, zeros(1, numel(y_axis)), 'k',
        'linewidth', 2) % draws y-axis
    hold on
    plot3(zeros(1, numel(z_axis)), zeros(1, numel(z_axis)), z_axis, 'k',
        'linewidth', 2) % draws z-axis
    hold on

    sf = surf(x, y, z, P(:, :, k));
    alpha(sf, 0.9) % make sure this function is not shadowed by user-defined
        variables
    shading interp;
    axis off;
    colormap cool
    view(AZ(k), EL(k))
end

%% Print the running time %%
toc
```

```
%%%%%%%%%% Purpose of this script %%%%%%%%%%
%
% This script is used to compute the state vector evolutioins of
% atomic clocks with x-protocol spin squeezing (SS) in the basis of the
% Dicke states (aka symmetric collective states) for even or odd number of
% atoms. The state vector is then projected onto the Dicke states to plot the
% population distribution on each symmetric collective state.
%
%%%%%%%%%%%%%% End of purpose %%%%%%%%%%%%%%

%% The actual program starts here %%
clc
clear
close all

%% Timing the program %%
tic

%% Initial parameters %%
N = 40;                          % Total number of elementary spin (1/2-spin)
J = N/2;                          % Total spin of the system (spin-J system)

Jz = J_z(J);                      % Jz matrix form in the Dicke states
Jx = J_x(J);                      % Jx matrix form in the Dicke states
Jy = J_y(J);                      % Jy matrix form in the Dicke states
```

```
Jp = J_plus(J);                    % J+ matrix form in the Dicke states
Jm = J_minus(J);                   % J- matrix form in the Dicke states
P0 = P_K(J, 0);                    % P0 matrix form in the Dicke states
PN = P_K(J, N);                    % PN matrix form in the Dicke states

if rem(N, 2) == 0
    alpha = pi/2/N;                % Dark zone phase shift (angle rotated around
        z-axis) -- even N
else
    alpha = pi/4;                  % Dark zone phase shift (angle rotated around
        z-axis) -- odd N
end

beta = pi/2;                       % Interaction zone width for pi/2-pulses
mu = pi/2;                         % Squeezing parameters
nu = nu_oat_x(J, mu);              % Corrective rotation angle rotated around
    x-axis
CRS = -1;                          % Corrective rotation sign

%% Initial state vector and operators for spin squeezing %%
Psi_i = Psi_0(J, -J);              % Initial state vector of the system (assumed
    all spin are down)
Ux = U_x(J, beta);                 % Rotation around x axis for the two
    pi/2-pulse interaction zones
```

```
Uoat_p = U_oat(J, mu);            % Unitary transformation for doing one-axis
    twisting
Ux_p = U_x(J, nu);                % Corrective rotation around x axis after
    squeezing
Uz = U_z(J, alpha);               % Rotation around z axis in the dark zone
Ux_m = U_x(J, nu * CRS);          % Corrective rotation around x axis before
    undoing squeezing
Uoat_m = U_oat(J, -mu);           % Unitary transformation for undoing one-axis
    twisting

%% State vector evolution %%
d = 8;
Psi_f = zeros(N + 1, d);
Psi_f(:, 1) = Psi_i;
Psi_f(:, 2) = Ux * Psi_f(:, 1);
Psi_f(:, 3) = Uoat_p * Psi_f(:, 2);
Psi_f(:, 4) = Ux_p * Psi_f(:, 3);
Psi_f(:, 5) = Uz * Psi_f(:, 4);
Psi_f(:, 6) = Ux_m * Psi_f(:, 5);
Psi_f(:, 7) = Uoat_m * Psi_f(:, 6);
Psi_f(:, 8) = Ux * Psi_f(:, 7);

%% Plot the probabilities %%
x_pos = -4;       % Position of x label
x_lower = -2;     % Lower limit of x axis
```

```
x_upper = N + 2;  % Upper limit of x axis

% Plot in subplots
if N == 100
    y_upper = [1.1, 0.1, 0.6, 0.2, 0.6];
elseif N == 101
    y_upper = [1.1, 0.1, 0.2, 0.08, 0.16];
elseif N == 40
    y_upper = [1.1, 0.2, 0.6, 0.3, 0.6];
elseif N == 41
    y_upper = [1.1, 0.2, 0.3, 0.15, 0.2];
else
    y_upper = [1.1, 1.1, 1.1, 1.1, 1.1];
end

Psi_index = [1, 2, 4, 6, 8];

for k = 1 : 5
    subplot(5, 1, k)
    plot(N : -1 : 0, abs(Psi_f(:, Psi_index(k))).^2, 'b-', 'Linewidth', 2)
    set(gca, 'xdir', 'reverse')
    xlabel('n', 'FontSize', 15, 'Position', [x_pos, 0, 0])
    ylabel('P(E_n)', 'FontSize', 13)
    xlim([x_lower, x_upper])
    ylim([0, y_upper(k)])
```

```
end

% Plot separately
for k = 1 : d
    figure
    plot(N : -1 : 0, abs(Psi_f(:, k)).^2, 'b-', 'Linewidth', 2)
    set(gca, 'xdir', 'reverse')
    xlabel('n', 'FontSize', 15, 'Position', [x_pos, 0, 0])
    ylabel('P(E_n)', 'FontSize', 13)
    xlim([x_lower, x_upper])
    title(['Collective state population distribution -- Squeezing with x-protocol
        and N = '...
            num2str(N) ' and CRS = ' num2str(CRS) ' and \mu = ' num2str(mu/pi)
                '*\pi'])
end

%% Print the running time %%
toc
```

D.7. Frequency Scanning for SCAC Using X-Protocol

```
%%%%%%%%%% Purpose of this script %%%%%%%%%%
%
% This script is used to compute the frequency scanning (FS) results of
% atomic clocks with x-protocol spin squeezing (SS) in the basis of the
```

```
% Dicke states (aka symmetric collective states) and compare the cases of
% even and odd number of atoms
%
%%%%%%%%%%%%%% End of purpose %%%%%%%%%%%%%%

%% The actual program starts here %%
clc
clear
close all

%% Timing the program %%
tic

%% Initial parameters %%
n = 100;                                % Base number of elementary spin
    (1/2-spin)
N = n : n + 1;                          % Total number of elementary spin
    (1/2-spin)

max = 10 * pi/n;                        % Maximum plottable value of dark
    zone phase shift
step = pi/2000;                         % Step value for dark zone phase shift
phi = -max : step : max;                % Dark zone phase shift (angle
    rotated around z-axis)
```

```
theta = pi/2;                                % Interaction zone pulse width. For
    Pi/2 pulse, theta = pi/2
mu = pi/2;                                   % Squeezing parameters
CRS = 1;                                     % Corrective rotation sign

P_EN = zeros(numel(mu), numel(phi), numel(N)); % P_EN, probability in |EN> with
    squeezing
P_2 = zeros(numel(mu), numel(phi), numel(N)); % P_2, probability in |2>
    (spin-up) with squeezing
P_z = zeros(numel(mu), numel(phi), numel(N)); % P_z, average value of Jz, as a
    function of phi and mu, with squeezing

P_EN0 = zeros(1, numel(phi), numel(N));     % P_EN0, probability in |EN> without
    squeezing
P_20 = zeros(1, numel(phi), numel(N));      % P_20, probability in |2> (spin-up)
    without squeezing
P_z0 = zeros(1, numel(phi), numel(N));      % P_z0, average value of Jz, as a
    function of phi, without squeezing


for k = 1 : numel(N)
    %% Initial parameters for each case %%
    J = N(k)/2;                              % Total spin of the system (spin-J
        system)
    Jz = J_z(J);                             % Jz matrix form in the Dicke states
```

```
Jx = J_x(J);                          % Jx matrix form in the Dicke states
Jy = J_y(J);                          % Jy matrix form in the Dicke states
Jp = J_plus(J);                       % J+ matrix form in the Dicke states
Jm = J_minus(J);                      % J- matrix form in the Dicke states
P0 = P_K(J, 0);                       % P0 matrix form in the Dicke states
PN = P_K(J, N(k));                    % PN matrix form in the Dicke states
Psi_i = Psi_0(J, -J);                 % Initial state vector of the system
    (assumed all spin are down)
Ux = U_x(J, theta);                   % Rotation around x axis in the two
    interaction zones
nu = nu_oat_x(J, mu);                 % Corrective rotation angle around
    x-axis

%% Computation for collective atomic clock with spin-squeezing %%
for i = 1 : numel(mu)
    Uoat_p = U_oat(J, mu(i));         % Unitary transformation for doing
        one-axis twisting
    Uoat_m = U_oat(J, -mu(i));        % Unitary transformation for undoing
        one-axis twisting
    Ux_p = U_x(J, nu(i));             % Corrective rotation around x axis
        after squeezing
    Ux_m = U_x(J, nu(i) * CRS);       % Corrective rotation around x axis
        before undoing squeezing

    for j = 1 : numel(phi)
```

```
            Uz = U_z(J, phi(j));              % Rotation around z axis in the dark
                zone
            Psi_f = Ux * Uoat_m * Ux_m * Uz * Ux_p * Uoat_p * Ux * Psi_i; % Final
                state vector with x-protocol
            P_EN(i, j, k) = abs(Psi_f' * PN * Psi_f);
            P_2(i, j, k) = abs(J + Psi_f' * Jz * Psi_f) / N(k);
            P_z(i, j, k) = real(Psi_f' * Jz * Psi_f);
        end
    end

    %% Computation for collective atomic clock without spin-squeezing %%
    for i = 1 : numel(phi)
        Uz = U_z(J, phi(i));                  % Rotation around z axis in the dark
            zone
        Psi_f = Ux * Uz * Ux * Psi_i;         % Final state vector without squeezing
        P_EN0(i, k) = abs(Psi_f' * PN * Psi_f);
        P_20(i, k) = abs(J + Psi_f' * Jz * Psi_f) / N(k);
        P_z0(i, k) = real(Psi_f' * Jz * Psi_f);
    end
end

%% Plot the probabilities %%
for i = 1 : numel(mu)
    figure     % PLot P_EN
    plot(phi/(2*pi), P_EN(i, :, 1), 'b-', 'Linewidth', 2)
```

```
hold on
plot(phi/(2*pi), P_EN(i, :, 2), 'r-', 'Linewidth', 2)
hold on
plot(phi/(2*pi), (P_EN(i, :, 1) + P_EN(i, :, 2))/2, 'k:', 'Linewidth', 2)
hold on
plot(phi/(2*pi), P_EN0(:, 1), 'b:', 'Linewidth', 2)
hold on
plot(phi/(2*pi), P_EN0(:, 2), 'r:', 'Linewidth', 2)
xlabel('$\frac{\phi}{2\pi}$', 'Interpreter', 'latex', 'FontSize', 15)
ylabel('P_{EN}', 'FontSize', 15)
ylim([0, 1])
legend(['Squeezed with N = ' num2str(N(1))], ['Squeezed with N = '
    num2str(N(2))], 'Squeezed average', ...
       ['No squeezing with N = ' num2str(N(1))], ['No squeezing with N = '
          num2str(N(2))])
title('Collective state detection', 'FontSize', 15)
suptitle(['FS -- Squeezing with x-protocol and CRS = ' num2str(CRS) ' and \mu
    = ' num2str(mu(i)/pi) '*\pi']);

figure     % PLot P_2
plot(phi/(2*pi), P_2(i, :, 1), 'b-', 'Linewidth', 2)
hold on
plot(phi/(2*pi), P_2(i, :, 2), 'r-', 'Linewidth', 2)
hold on
plot(phi/(2*pi), (P_2(i, :, 1) + P_2(i, :, 2))/2, 'k:', 'Linewidth', 2)
```

```
hold on
plot(phi/(2*pi), P_20(:, 1), 'b:', 'Linewidth', 2)
hold on
plot(phi/(2*pi), P_20(:, 2), 'r:', 'Linewidth', 2)
xlabel('$\frac{\phi}{2\pi}$', 'Interpreter', 'latex', 'FontSize', 15)
ylabel('P_2', 'FontSize', 15)
ylim([0, 1])
legend(['Squeezed with N = ' num2str(N(1))], ['Squeezed with N = '
    num2str(N(2))], 'Squeezed average', ...
       ['No squeezing with N = ' num2str(N(1))], ['No squeezing with N = '
          num2str(N(2))])
title('Conventional detection', 'FontSize', 15)
suptitle(['FS -- Squeezing with x-protocol and CRS = ' num2str(CRS) ' and \mu
    = ' num2str(mu(i)/pi) '*\pi']);

figure     % PLot P_z
plot(phi/(2*pi), P_z(i, :, 1), 'b-', 'Linewidth', 2)
hold on
plot(phi/(2*pi), P_z(i, :, 2), 'r-', 'Linewidth', 2)
hold on
plot(phi/(2*pi), (P_z(i, :, 1) + P_z(i, :, 2))/2, 'k:', 'Linewidth', 2)
hold on
plot(phi/(2*pi), P_z0(:, 1), 'b:', 'Linewidth', 2)
hold on
plot(phi/(2*pi), P_z0(:, 2), 'r:', 'Linewidth', 2)
```

```
    xlabel('$\frac{\phi}{2\pi}$', 'Interpreter', 'latex', 'FontSize', 15)
    ylabel('P_z', 'FontSize', 15)
    ylim([-J, J])
    legend(['Squeezed with N = ' num2str(N(1))], ['Squeezed with N = '
        num2str(N(2))], 'Squeezed average', ...
           ['No squeezing with N = ' num2str(N(1))], ['No squeezing with N = '
               num2str(N(2))])
    title('Conventional detection', 'FontSize', 15)
    suptitle(['FS -- Squeezing with x-protocol and CRS = ' num2str(CRS) ' and \mu
        = ' num2str(mu(i)/pi) '*\pi']);
end

%% Print the running time %%
toc
```

D.8. QFF for SCAC Using X-Protocol

```
%%%%%%%%%% Purpose of this script %%%%%%%%%%
%
% This script is used to compute the quantum frequency fluctuation (QFF)
% for atomic clocks with x-protocol spin squeezing (SS) in the basis of the
% Dicke states (aka symmetric collective states) and compare the cases of
% even and odd number of atoms
%
%%%%%%%%%%%%%%% End of purpose %%%%%%%%%%%%%%%
```

```
%% The actual program starts here %%
clc
clear
close all

%% Timing the program %%
tic

%% Initial parameters %%
n = 40;                                          % Base number of elementary
    spin (1/2-spin)
N = n : n + 1;                                   % Total number of elementary
    spin (1/2-spin)
step = 1e-8;                                     % Step value for dark zone
    phase shift
max = 1e-4;                                      % Maximum plottable value of
    dark zone phase shift
min = max - step;                                % Minimum plottable value of
    dark zone phase shift
phi = [min, max];                                % Dark zone phase shift
    (angle rotated around z-axis)
theta = pi/2;                                    % Interaction zone pulse
    width. Here theta = pi/2
mu = 0 : pi/400 : pi/2;                          % Squeezing parameters
```

```
CRS = 1;                                        % Corrective rotation sign

HL_inv = zeros(numel(N), 1);                    % Inverse of QFF in the
    Heisenberg limit (HL) -- single value
SQL_inv = zeros(numel(N), 1);                   % Inverse of QFF in the
    standard quantum limit (SQL) -- single value
QFF_inv_HL = zeros(numel(mu), 2);               % Inverse of QFF in the
    Heisenberg limit (HL)
QFF_inv_SQL = zeros(numel(mu), 2);              % Inverse of QFF in the
    standard quantum limit (SQL)

QFF_inv_P_EN = zeros(numel(mu), numel(phi), numel(N)); % Inverse of QFF for
    collective state detection
QFF_inv_P_Jz = zeros(numel(mu), numel(phi), numel(N)); % Inverse of QFF for
    conventional detection
QFF_inv_P_SU = zeros(numel(mu), numel(phi), numel(N)); % Inverse of QFF for
    SU-protocol

P_EN = zeros(numel(phi), 2);                    % P_EN, probability in |EN>
    with squeezing
P_EN_2 = zeros(numel(phi), 2);                  % (P_EN)^2
P_Jz = zeros(numel(phi), 2);                    % P_Jz, average value of Jz
    with squeezing
P_Jz_2 = zeros(numel(phi), 2);                  % (P_Jz)^2
```

```
P_SU = zeros(numel(phi), 2);                    % P_SU, average value of Jy
    with squeezing for the SU protocol
P_SU_2 = zeros(numel(phi), 2);                  % (P_SU)^2

for k = 1 : numel(N)
    %% Initial parameters for each case %%
    J = N(k)/2;                                 % Total spin of the system
        (spin-J system)
    Jz = J_z(J);                                % Jz matrix form in the
        Dicke states
    Jx = J_x(J);                                % Jx matrix form in the
        Dicke states
    Jy = J_y(J);                                % Jy matrix form in the
        Dicke states
    Jp = J_plus(J);                             % J+ matrix form in the
        Dicke states
    Jm = J_minus(J);                            % J- matrix form in the
        Dicke states
    P0 = P_K(J, 0);                             % P0 matrix form in the
        Dicke states
    PN = P_K(J, N(k));                          % PN matrix form in the
        Dicke states
    Psi_i = Psi_0(J, -J);                       % Initial state vector
        (assumed all spin are down)
```

```
Psi_i_SU = css(J, pi/2, 0);                          % Initial state vector for
    SU-protocol: CSS |+x>
Ux = U_x(J, theta);                                  % Rotation around x axis in
    the two interaction zones
nu = nu_oat_x(J, mu);                                % Corrective rotation angle
    rotated around x-axis

HL_inv(k) = N(k);                                    % Inverse of QFF in the
    Heisenberg limit (HL)
SQL_inv(k) = HL_inv(k) / sqrt(N(k));                 % Inverse of QFF in the
    standard quantum limit (SQL)
QFF_inv_HL(:, k) = repmat(HL_inv(k), numel(mu), 1); % Inverse of QFF in the
    Heisenberg limit (HL)
QFF_inv_SQL(:, k) = repmat(SQL_inv(k), numel(mu), 1); % Inverse of QFF in the
    standard quantum limit (SQL)

%% Computation for collective atomic clock with spin-squeezing %%
for i = 1 : numel(mu)
    Uoat_p = U_oat(J, mu(i));                        % Unitary transformation for
        doing one-axis twisting
    Uoat_m = U_oat(J, -mu(i));                       % Unitary transformation for
        undoing one-axis twisting
    Ux_p = U_x(J, nu(i));                            % Corrective rotation around
        x axis after squeezing
```

```
Ux_m = U_x(J, nu(i) * CRS);                    % Corrective rotation around
    x axis before undoing squeezing

for j = 1 : numel(phi)
    Uz = U_z(J, phi(j));                       % Rotation around z axis in
        the dark zone
    Psi_f = Ux * Uoat_m * Ux_m * Uz * Ux_p * Uoat_p * Ux * Psi_i; % Final
        state vector with x-protocol

    P_EN(j, k) = abs(Psi_f' * PN * Psi_f);
    P_EN_2(j, k) = abs(Psi_f' * PN * PN * Psi_f);

    P_Jz(j, k) = abs(Psi_f' * Jz * Psi_f);
    P_Jz_2(j, k) = abs(Psi_f' * Jz * Jz * Psi_f);

    Delta_P_EN = sqrt(abs(P_EN_2(j, k) - P_EN(j, k).^2));
    Delta_P_Jz = sqrt(abs(P_Jz_2(j, k) - P_Jz(j, k).^2));

    Partial_P_EN = 0;
    Partial_P_Jz = 0;

    if j > 1
        Partial_P_EN = abs(P_EN(j, k) - P_EN(j - 1, k)) / step;
        Partial_P_Jz = abs(P_Jz(j, k) - P_Jz(j - 1, k)) / step;
    end
```

```
            QFF_inv_P_EN(i, j, k) = Partial_P_EN / Delta_P_EN;
            QFF_inv_P_Jz(i, j, k) = Partial_P_Jz / Delta_P_Jz;

            % SU-protocol
            Uy = U_y(J, phi(j));                        % Rotation around y axis for
                SU-protocol
            Psi_f_SU = Uoat_m * Uy * Uoat_p * Psi_i_SU; % Final state vector with
                SU-protocol
            P_SU(j, k) = abs(Psi_f_SU' * Jy * Psi_f_SU);
            P_SU_2(j, k) = abs(Psi_f_SU' * Jy * Jy * Psi_f_SU);
            Delta_P_SU = sqrt(abs(P_SU_2(j, k) - P_SU(j, k).^2));
            Partial_P_SU = 0;

            if j > 1
                Partial_P_SU = abs(P_SU(j, k) - P_SU(j - 1, k)) / step;
            end

            QFF_inv_P_SU(i, j, k) = Partial_P_SU / Delta_P_SU;
        end
    end
end

%% Plot inverse of QFF vs. squeezing parameter mu %%
```

```
point = numel(phi);            % The point to take the QFF of the dark zone phase
    shift

%Plot in subplots
subplot(1, 2, 1)      % Plot QFF_inv for even N but different detection schemes
plot(mu/pi, QFF_inv_P_Jz(:, point, 1)/HL_inv(1), 'r-', 'Linewidth', 2)
hold on
plot(mu/pi, QFF_inv_P_EN(:, point, 1)/HL_inv(1), 'b--', 'Linewidth', 2)
hold on
plot(mu/pi, QFF_inv_P_SU(:, point, 1)/HL_inv(1), 'g-', 'Linewidth', 2)
hold on
plot(mu/pi, QFF_inv_HL(:, 1)/HL_inv(1), 'k-', 'Linewidth', 2)    % Normaized HL
hold on
plot(mu/pi, QFF_inv_SQL(:, 1)/HL_inv(1), 'k:', 'Linewidth', 2)   % Normaized SQL
legend({'Atomic State Det', 'Collective State Det', 'SU Protocol', 'HL', 'SQL'},
    'FontSize', 14)
legend('boxoff')
xlabel('\mu/\pi', 'FontSize', 15)
ylabel('QFF^{-1}/QFF^{-1}_{HL}', 'FontSize', 10)
ylim([0, 1.2])
title(['N = ' num2str(N(1))], 'FontSize', 15)

subplot(1, 2, 2)      % Plot QFF_inv for odd N but different detection schemes
plot(mu/pi, QFF_inv_P_Jz(:, point, 2)/HL_inv(2), 'r-', 'Linewidth', 2)
hold on
```

```
plot(mu/pi, QFF_inv_P_EN(:, point, 2)/HL_inv(2), 'b--', 'Linewidth', 2)
hold on
plot(mu/pi, QFF_inv_P_SU(:, point, 2)/HL_inv(2), 'g-', 'Linewidth', 2)
hold on
plot(mu/pi, QFF_inv_HL(:, 1)/HL_inv(1), 'k-', 'Linewidth', 2)    % Normaized HL
hold on
plot(mu/pi, QFF_inv_SQL(:, 1)/HL_inv(1), 'k:', 'Linewidth', 2)   % Normaized SQL
legend({'Atomic State Det', 'Collective State Det', 'SU Protocol', 'HL', 'SQL'},
    'FontSize', 14)
legend('boxoff')
xlabel('\mu/\pi', 'FontSize', 15)
ylabel('QFF^{-1}/QFF^{-1}_{HL}', 'FontSize', 10)
ylim([0, 1.2])
title(['N = ' num2str(N(2))], 'FontSize', 15)

% Plot separately
figure        % Plot QFF_inv for collective state detection but different N
plot(mu/pi, QFF_inv_P_EN(:, point, 1)/HL_inv(1), 'r-', 'Linewidth', 2)
hold on
plot(mu/pi, QFF_inv_P_EN(:, point, 2)/HL_inv(2), 'b:', 'Linewidth', 2)
hold on
plot(mu/pi, QFF_inv_HL(:, 1)/HL_inv(1), 'k-', 'Linewidth', 2) % Normalized HL
hold on
plot(mu/pi, QFF_inv_SQL(:, 1)/HL_inv(1), 'k:', 'Linewidth', 2) % Normalized SQL
legend(['N = ' num2str(N(1))], ['N = ' num2str(N(2))], 'HL', 'SQL')
```

```
xlabel('$\frac{\mu}{\pi}$', 'Interpreter', 'latex', 'FontSize', 15)
ylabel('QFF^{-1}/QFF^{-1}_{HL}', 'FontSize', 10)
ylim([0, 1.2])
title('Collective state detection -- QFF^{-1}/QFF^{-1}_{HL} vs. \mu',
    'FontSize', 15)
suptitle(['QFF -- Squeezing with x-protocol and CRS = ' num2str(CRS)]);

figure     % Plot QFF_inv for conventional detection but different N
plot(mu/pi, QFF_inv_P_Jz(:, point, 1)/HL_inv(1), 'r-', 'Linewidth', 2)
hold on
plot(mu/pi, QFF_inv_P_Jz(:, point, 2)/HL_inv(2), 'b:', 'Linewidth', 2)
hold on
plot(mu/pi, QFF_inv_HL(:, 1)/HL_inv(1), 'k-', 'Linewidth', 2)
hold on
plot(mu/pi, QFF_inv_SQL(:, 1)/HL_inv(1), 'k:', 'Linewidth', 2)
legend(['N = ' num2str(N(1))], ['N = ' num2str(N(2))], 'HL', 'SQL')
xlabel('$\frac{\mu}{\pi}$', 'Interpreter', 'latex', 'FontSize', 15)
ylabel('QFF^{-1}/QFF^{-1}_{HL}', 'FontSize', 10)
ylim([0, 1.2])
title('Conventional detection -- QFF^{-1}/QFF^{-1}_{HL} vs. \mu', 'FontSize', 15)
suptitle(['QFF -- Squeezing with x-protocol and CRS = ' num2str(CRS)]);

figure         % Plot QFF_inv for even N but different detection schemes
plot(mu/pi, QFF_inv_P_Jz(:, point, 1)/HL_inv(1), 'r-', 'Linewidth', 2)
hold on
```

```
plot(mu/pi, QFF_inv_P_EN(:, point, 1)/HL_inv(1), 'b--', 'Linewidth', 2)
hold on
plot(mu/pi, QFF_inv_HL(:, 1)/HL_inv(1), 'k-', 'Linewidth', 2) % Normalized HL
hold on
plot(mu/pi, QFF_inv_SQL(:, 1)/HL_inv(1), 'k:', 'Linewidth', 2) % Normalized SQL
legend('Conventional detection', 'Collective state detection', 'HL', 'SQL')
xlabel('$\frac{\mu}{\pi}$', 'Interpreter', 'latex', 'FontSize', 15)
ylabel('QFF^{-1}/QFF^{-1}_{HL}', 'FontSize', 10)
ylim([0, 1.2])
title(['N = ' num2str(N(1)) ' -- QFF^{-1}/QFF^{-1}_{HL} vs. \mu'], 'FontSize',
    15)
suptitle(['QFF -- Squeezing with x-protocol and CRS = ' num2str(CRS)]);

figure     % Plot QFF_inv for odd N but different detection schemes
plot(mu/pi, QFF_inv_P_Jz(:, point, 2)/HL_inv(1), 'r-', 'Linewidth', 2)
hold on
plot(mu/pi, QFF_inv_P_EN(:, point, 2)/HL_inv(2), 'b:', 'Linewidth', 2)
hold on
plot(mu/pi, QFF_inv_HL(:, 1)/HL_inv(1), 'k-', 'Linewidth', 2)
hold on
plot(mu/pi, QFF_inv_SQL(:, 1)/HL_inv(1), 'k:', 'Linewidth', 2)
legend('Conventional detection', 'Collective state detection', 'HL', 'SQL')
xlabel('$\frac{\mu}{\pi}$', 'Interpreter', 'latex', 'FontSize', 15)
ylabel('QFF^{-1}/QFF^{-1}_{HL}', 'FontSize', 10)
ylim([0, 1.2])
```

```
title(['N = ' num2str(N(2)) ' -- QFF^{-1}/QFF^{-1}_{HL} vs. \mu'], 'FontSize',
    15)
suptitle(['QFF -- Squeezing with x-protocol and CRS = ' num2str(CRS)]);

%% Print the running time %%
toc
```